BEHAVIOR OF REINFORCED CONCRETE BEAM-COLUMN RETROFITTED WITH COMPOSITE WRAPPING SYSTEMS

PRELIMINARY REPORT

Prepared By

Omar Chaallal, Ph.D., P.E., and

Mohsen A. Shahawy, Ph.D., P.E.

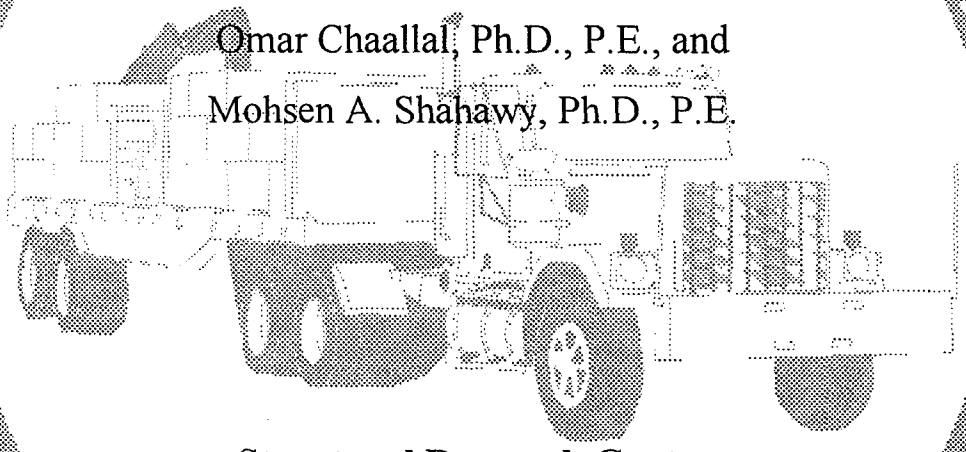

Structural Research Center

Florida Department Of Transportation

2007 E. Paul Dirac Drive

Tallahassee, Florida 32310

May 1999

ABSTRACT

In recent years much research has been carried out on numerous aspects related to use of composite materials for structural rehabilitation and strengthening. The confinement of concrete columns with composite sheets and straps is among the research topics considered. However, most of the research work was undertaken on small cylinders and on cylindrical reinforced concrete (RC) columns mainly subjected to axial loading. No research has been reported dealing with rectangular RC columns retrofitted with composite wrapping and subjected to a combined axial compression - bending moment condition.

The main objectives of this study are as follows :(i) Carry out a comprehensive state-of-the art review on the behavior of RC columns confined with external jacketing; (ii) Investigate the behavior of carbon-wrapped rectangular concrete beam-columns when subjected to eccentric loadings; and (iii) Provide guidelines for the design of carbon-wrapped rectangular concrete beam-columns subjected to a combined axial force-flexural moment.

Six series are performed in this study. Each series is made of a RC column without carbon fiber reinforced plastic (CFRP) jacket as a control specimen and a RC column retrofitted with CFRP jacket. The six series correspond to the following load eccentricities 0" (i.e., concentric loading), 3" (7.5 mm), 6" (15 mm), 12" (300 mm), 16" (400 mm), and pure bending (i.e., an eccentricity approaching infinity). The test specimens, which have corbels at the ends, have an 8" x 14" (200 x 350 mm) rectangular cross section and a total length of 140" (3500 mm). The length between corbels is 7' (2100 mm). They were made of an ordinary 3,000 psi concrete.

The CFRP jacketing improved the uniaxial capacity of the beam-columns; the maximum gain achieved was slightly below 30%. However, it enhanced significantly the flexural capacity of the beam-columns where a gain of more than 100% was observed. While the source of increase in pure flexure was mainly attributed to the longitudinal weaves of the CFRP fabric, the contribution of the transverse weaves within the compression controlled zone increased with increasing axial load to become predominant in pure compression. Finally, within the conditions and the limits of this study, the proposed design procedure based on the stress of confined concrete in the compression zone compared reasonably well with experimental results. The confined stress was calculated using the bi-linear stress-strain model developed specifically for FRP wrapped columns in conjunction with an effective confinement ratio that takes into account the rectangular shape of the beam-columns.

The following recommendations can be formulated for considerations in further studies: (a) the effect of concrete strength on the beam-column behavior should be undertaken. Therefore, a research study, similar to the present study as far as the procedure and the parameters are concerned, but with a concrete strength of 6,000 psi is suggested; (b)the experimental stress-strain behavior of rectangular specimens wrapped with FRP material and subjected to an axial load should be determined. In particular, the following parameters are of interest: the aspect ratio, the radius of the section corner and the concrete strength.

TABLE OF CONTENTS

LIST OF FIGURES

ECCENTRICITY= 6"

ECCENTRICITY = 12"

ECCENTRICITY = 16"

PURE BENDING

LIST OF TABLES

CHAPTER

IINTRODUCTION

This chapter introduces the report. It states the problem and poses the objectives of the study. It also presents the outline of the present report.

1.1 Problem Statement

Many countries around the world and the United States, in particular, have tremendous needs to repair and strengthen their existing infrastructure. Large numbers of existing structures are deteriorating due to various problems related to marine environment, extensive use of deicing salts, increase of number of trucks, increase of allowable weight of load bearing trucks, and under design of old structures.

In recent years much research has been carried out on numerous aspects related to use of composite materials for structural rehabilitation and strengthening. The confinement of concrete columns with composite sheets and straps is among the research topics considered. However, most of the research work was undertaken on small cylinders and on cylindrical reinforced concrete (RC) columns mainly subjected to axial loading. Cantilever cylindrical columns subjected to cyclic horizontal loading were also considered in seismic regions. No research has been reported dealing with rectangular RC columns retrofitted with composite wrapping and subjected to a combined axial compression - bending moment condition.

1.2 Research Objectives

This project is intended to examine several aspects in the use of fiber reinforced plastic (FRP) laminates for strengthening rectangular RC columns subjected to combined axial compression and bending moment conditions.

The objectives of this study are as follows

1. Carry out a comprehensive state-of-the art review on the behavior of RC columns confined with external jacketing.
2. Design and carry out an experimental study on the behavior of rectangular RC columns confined with externally bonded CFRP laminates.
3. Investigate the behavior of carbon-wrapped rectangular concrete beam-columns when subjected to eccentric loadings.
4. Provide guidelines for the design of carbon-wrapped rectangular concrete beamcolumns subjected to a combined axial force-flexural moment.

1.3 Report Outline

This report consists of three parts:

- *Part I : Review of the state of the art,* includes chapter 2 and chapter 3. Chapter 2 provides a review of the relevant literature, while chapter 3 presents a review of the relevant models used for confined concrete.
- *Part 11: Test program and procedure,* is contained in chapter 4. The latter describes the specimens, the materials, as well as the instrumentation used and presents the testing procedure and the experimental program.
- *I'art III : Presentation and analysis of the results,* is covered by chapter 5 (Presentation of the results), chapter 6 (Analysis of the results) and Chapter 7 (Design considerations of wrapped beam-columns).

Chapter 8 summarizes the conclusions and discusses various recommendations.

PART I

REVIEW OF THE STATE OF THE ART

CHAPTER 2

REVIEW OF RESEARCH FINDINGS

This part of the study will focus on the literature review of recent research findings, in particular, those related to wrapping techniques applied to RC columns.

2.1 Research Findings Related to Columns

The desire to increase the axial capacity of RC columns is not a new idea. Already in 1903, Considere performed triaxial tests on 3.15" *x* 11.8" mortar cylinders and showed that a constant confining lateral pressure applied to concrete cylinders can substantially increase its compressive strength. He proposed a relationship to predict the compressive . strength of confined concrete that was later adapted to concrete by Richart et al. (1928). This pioneering work was then continued by other researchers (Balmer 1949, Chinn and Zimmerman 1965, Newman and Newman 1972). In columns, this confining pressure can be provided by using steel tube (Klnppel and Goder 1957, Gardner and Jacobson 1967), steel stirrups of various forms (Richart et al. 1929, Iyengar et al. 1972 Ahmad and Shah 1982), or,by wrapping and bonding FRP composite sheets or straps on the surface of the columns, Numerous simple models are now available that adequately describe the behavior of columns confined using steel tube and steel hoops and stirrups (Knowles and Park 1969 and 1970, Sheikh 1982, Sheikh and Uzumuri 1980, Mander et al. 1988, and Saatcioglu and Razvi 1992). These models were adapted and are implemented in most modern codes and standards such as ACI, CSA, and CEB. However, models dealing with RC columns wrapped with composite materials are very few and do not cover all geometries and loading conditions. Besides, most of these models were originally developed for steel and, therefore, fail to take the inherent linear behavior of FRP properties into consideration.

FRP composites have been used for confinement of concrete since the early 1980's, although using commercially available plastic pipes (PVC) filled with concrete was already suggested in the late 1970's (Kurt 1978).

Fardis and Khalili (1981) conducted uniaxial compression tests on 3" x 6" and 4" x 8" concrete cylinders wrapped with different types of CFRP fabrics and reported enhanced strength and ductility due to confinement. They later (Fardis and Khalili 1982) proposed an analytical hyperbolic model for the compressive strength of confined concrete.

Katsumata et al. (1988) presented results of an experimental investigation on the seismic behavior of columns retrofitted with carbon fiber reinforced plastic (CFRP). Ten 1/4 scale column models, having a 200 x 200 mm square section and rounded corners, were tested. Two series of tests were considered and targeted to investigate the efficiency of the interface between the concrete and CFRP material. In the first series, an isolant was applied between concrete and the composite material whereas in the second series the composite material was directly bonded to concrete with epoxy. The following observations were drawn from tests:

- The ultimate displacement as well as energy dissipation capacity increased linearly with the amount of CFRP wrapping.
- The seismic resistance of columns strengthened with CFRP approached that of RC columns with helical steel stirrups.
- Given the amount of CFRP wrapping, the ultimate displacement achieved by both series was very similar.

In an attempt to make the confinement model proposed by Ahmed and Shah (1982), usable for concrete confined by FRP spirals, Ahmed et al., (1991) carried out axial compression tests on 33 - 4" x 8" concrete cylinders confined with GFRP spirals and proposed an expression for the peak stress and peak strain of confined concrete.

Priestley et al. (1992) investigated the use of fiberglass/epoxy jackets to enhance both flexure and shear performance of bridge columns located in seismic areas. They first presented simple design models developed earlier (Priestley 1991, Priestley and Sieble 1991) for ductility and shear enhancements. Seven RC bridge columns were retrofitted with fiberglass/epoxy jackets and tested to validate the models. Three (3) columns were strengthened in the plastic hinge region and tested in flexure, whereas the four (4) remaining columns were strengthened and subjected to double bending. The experimental results showed that properly designed composite jackets can inhibit lap-splice failures in hinge regions and provide sufficient shear strength to columns with shear strength deficiency to ensure ductile flexural response.

Saadatmanesh et al. (1994) conducted a parametric analytical study on the behavior of circular and rectangular columns strengthened with external composite procured E-glass or carbon thin straps. They used the confinement model of Mander et al. (1988). Four parameters were considered: the concrete strength, the FRP strap thickness, the strap spacings, and the material of the straps.

Nanni and Bradford (1995) investigated the behavior of 6" x 12" concrete cylinders confined by three types of fiber-wraps: pretensioned braided aramid cables, procured hybrid glass-aramid shells, and glass filament-winding. For the first series, they tested 16 specimens with variable diameter and spacing of the cables. Four specimens were tested in the second 'series, and 15 in the third series. The cylinders of the third series were made with a central rod, which was then placed on a filament-winding machine, and wrapped with 1, 2, 4, or 8 plies of E-glass fibers and vinylester resin (or polyester for some of the specimens). The strength of concrete core was reported as: 5.2, 6.6 and 5.3 ksi for the three series, respectively. They concluded that the stress-strain response of FRP-encased concrete, in general, could be modeled by a simple bilinear curve with a bend-over point at the peak stress of unconfined concrete, which corresponds to a strain of 0.003. They, however, did not develop a confinement model. Test results were also compared with the confinement models by Mander et al. (1988) and Fardis and

Khalili (1982), both of which grossly underestimated the ultimate strain of encased concrete, but compared reasonably well for strength of confined concrete.

Mirmiran and Shahawy (1995) proposed a concrete-filled FRP tube (CFFT), in which the tube acts as a form-work for the encased concrete, hoop and longitudinal reinforcement, and corrosion-resistant casing for the concrete. The CFFT was proposed for bridge columns as well as for pile splicing. The Florida Department of Transportation (FDOT) sponsored a series of projects in order to investigate the behavior of the proposed CFFT. Several parameters were considered in these studies, e.g. the type of loading, the cross-section, the bond, and the length effect.

Kargahi (1995) investigated the strength of CFFT under uniaxial compression. A total of 12 cylindrical specimens were tested, 9 CFFTs and three 6" x 12" plain concrete cylinders. Filament-wound E-glass/polyester tubes were used, with a winding angle of 75° with respect to the longitudinal axis of the tube. Three different tube thicknesses were included, namely, 0.074", 0.13" and 0.237". An enhancement in the concrete strength, in the order of 2.5 to 3.5 times the unconfined strength, was reported. The author also performed a series of split-cylinder tests, in order to investigate the improvement of the tensile strength of the FRP-confined concrete. It was concluded that the FRP tube improves the behavior of the concrete section in tension by containing the cracked concrete rather than confining it. A parametric study was also performed on the effect of ply thickness, winding angle, and the composite action on confined strength of the column. The analysis was based on the confinement model of Mander et al. (1988). It was concluded that the thickness of the tube increases the pure axial strength. The presence of full composite action does not significantly improve the axial capacity of the column but rather the flexural capacity. Moreover, an increase in the fiber winding angle will decrease the pure axial strength. The pure flexural capacity is maximum at a winding angle of ± 45°.

Sherer (1996) extended the study by Kargahi and investigated the shape of the stress-strain curve and also the dilatancy properties of the same type of tubes under the same type of loading. He further studied the cost optimization of the proposed composite structure.

The bond effect was investigated by Mastrapa (1997). He tested thirty-two 6"x 12" composite cylinders, half of which were wrapped in 1, 3, 5, or 7 layers of S-glass fabric, while for the other half concrete of the same batch was poured in tubes made of the same S-glass fabric and with the same number of layers. Tests were done in two series. In Series 1, multi-layer jackets were made layer-by-layer with a splice of about 17% o of the perimeter of the cylinders, while in Series 2, the jacket was made of a continuous wrap of the fabric with an overlap of about 32% of the perimeter of the cylinder. The average unconfined strength of concrete for specimens of Series 1 was 5.4 ksi. The hoop strength and modulus of the FRP jacket were 85 ksi and 2,984 ksi, respectively. It was concluded that the effect of construction bond on axially loaded confined concrete is not significant.

Pico (1997) tested a total of nine 6"x6"x 12" square concrete-filled FRP tubes under axial compression, in order to study the effect of the CFFT cross section. No bond was provided between the concrete core and the FRP tube. A marginal increase instrength was observed independent of the jacket thickness. The over-riding parameter in controlling the confinement was shown to be the product of the corner radius and the confining pressure.

El Echary (1997) evaluated the effects of length-to-diameter (L/D) and diameterto-thickness (D/t) ratios on the behavior of the CFFT. A total of 24 circular CFFTs (Di.., = 5.71 ") with three different tube thicknesses (6, 10, and 14 layers) and four different lengths (12", 18", 24" and 30") were tested. No buckling was observed during the tests. The analysis of the test results indicated that the maximum eccentricity was within 10-12% of the section width. The reduction in strength was not significant. It was concluded that up to a ratio L/D of 5: 1, slenderness effects are negligible.

Picher et al. (1996) examined the effect of the orientation of the confining fibers on the behavior of concrete cylinders wrapped with CFRP composite material. They also evaluated the application of the method to short columns having rectangular and square sections. Twenty-seven short columns in total were wrapped with CFRP material with different fiber orientations, as follows: fifteen 152 x 304 mm - cylinders, eight 152 x 152 x 500 mm square and four 152 x 203 x 500 mm (a x b x h) rectangular prisms. The following observations were reached:

- Confining the cylinders with CFRP greatly improved ductility and compression strength.
- The method can be efficiently applied to prismatic sections, provided the corners are rounded off prior to application of CFRP composite material. The compression capacity enhancement can reach 20% for square sections.
- The variation of wrapping orientation demonstrated that although axial stiffness decreases with an increase of the angle of orientation, ductility remained constant.
- No improvement in failure mode by varying orientations of the confinement was observed.

Saadatmenash et al. (1996) studied the seismic behavior of reinforced concrete columns designed according to standards earlier than 1971, and retrofitted with unidirectional confining resin-impregnated GFRP straps. Ten 1/5 scale column models, 5 'circular and 5 rectangular, were tested. The following parameters were studied: (a) the section form (circular and rectangular); (b) the longitudinal steel content; (c) the steel detailing in the plastic hinge zone; and (d) the confinement type (active or passive). The circular models were 305 mm in diameter, whereas the rectangular models had a section of 241 x 368 mm. The models were retrofitted using resin-impregnated glass-fiber reinforced plastic straps over a length of 635 mm above foundation level (hinge region). They were then submitted to a horizontal cyclic loading, in addition to a statically applied compression. Results show that retrofitting with GFRP straps greatly improved the ductility of columns. It also inhibited buckling of longitudinal reinforcement within the

hinge region, as well as bond failure in lapped starter bars. The following observations were also made:

. Bridge columns having lap-spliced bars in the potential plastic hinge region and that were built before the new seismic design codes failed prematurely at relatively low ductility levels ranging from 1.2 to 1.5.

. The use of continuous longitudinal bars through a potential plastic hinge improve column-behavior by inhibiting bond failure. Column failure in this case is due to the buckling of longitudinal bars because of insufficient lateral confinement in the plastic hinge region.

. Retrofitting RC columns with external FRP confinement showed significant enhancement in both flexure and ductility. Stable hysteresis loops up to a ductility factor of 6 were achieved with no significant degradation due to anchorage or buckling problems.

. The improvement achieved by active confinement retrofit scheme, as compared to passive, did not seem to justify the additional cost associated with the active retrofit scheme.

Xiao et al. (1996) presented results of an experimental study on three ½ scale bridge column models (610 mm-diameter and 2440 mm-height). The study was aimed to validate the effectiveness of a prefabricated GFRP composite wrapping system. The models simulated the columns of the I-10 Santa Monica Freeway/Fairfax, Washington Under Crossing, which collapsed in the 1994 Northridge Earthquake. The new system utilizes a series of prefabricated glass fiber reinforced composite cylindrical shells with slits. When a column is retrofitted, the shells are opened and clamped around the column in sequences and glued together to form a continuous jacket. The column models were subjected to horizontal cyclic loading in addition to an' axial compression simulating gravity load. Following results were drawn from the study:

. The "as built" model column developed unstable hysteresis loops and degraded rapidly before yielding was achieved, due to longitudinal reinforcement splice anchorage failure.

. Compared to the "as built" model, the seismic behavior of the retrofitted models was considerable enhanced as the hysteresis loops were very stable up to a displacement ductility of 5.7.

. Repairing the "as built" model resulted in an increase to its load carrying capacity approximately equal to the first yield strength of the virgin sections. The repaired model showed a stable hysteresis loop up to a ductility factor of 4.0, after which it degraded gradually to 50% of maximum capacity at a ductility factor of 8.

. A rational retrofit design of bridge columns with lap-spliced longitudinal bars should take into account deteriorating (bond slip) of retrofitted columns. The authors suggested an analytical model for that purpose. The model is based on the moment-curvature analysis taking into consideration the bond slips at the lap-spliced starter bars by varying the plastic hinge length Lp in function of steel stress f,.

$$Lp = 0.08h + 0.15d_b,f_s \qquad \text{for "as built" (without jacket)} \quad (2.1)$$

$$Lp = g + 0.30d_b,f_3 \qquad \text{for retrofitted (with jacket)} \quad (2.2)$$

where h = column height, db, = diameter of longitudinal bar, g = gap provided at the lower bottom of the jacket. In the lap-splice region, the stresses in the starter bars are transferred to the longitudinal column bars through a series of bond links, which are distributed through a length L_b:

$$L_b = L_S - 0.15\ d_b,f_s \quad (2.3)$$

where L_g = length of lap-splices. The bond stress in the bond links are expressed by τ_b - s_b relation (τ_b = bond stress and s_b = corresponding slip), and the equilibrium condition between bond and tensile force in the bar, is used as a criterion to determine the bond slip of an arbitrary starter bar.

Restrepol and DeVino (1996) proposed analytical expressions based on Mander's model for the determination of the capacity of axially loaded reinforced concrete columns which are confined by a combination of steel hoops and composite jackets externally applied on the perimeter of the columns. The paper develops equations that can be used to determine the axial compressive load carrying capacity of reinforced concrete rectangular columns, with externally bonded FRP. The equations take into account the confinement effect due to both steel and FRP jacket.

Bavarian et al. (1996) investigated the effects of externally wrapping concrete cylinders with composite materials. Three sizes of cylinder: 3" x 6", 4" x 8", and 6" x 12"; two types of composite material: S-glass and Kevlar-29, were considered. It was found that the ultimate stress and strain respectively doubled and tripled when using 4 layers of S-glass and 4 layers of Kevlar-29.

Monti and Spoelstra (1997) proposed a confinement model for circular columns wrapped with fiber-reinforced plastics. The procedure is basically the same as the model by Ahmad and Shah (1982). For a certain axial strain $E_{c;}$, a value f,; is assumed. The axial stress f; is then calculated using the confinement model of Mander et al. (1988) as an active confinement model. The lateral strain E_r is then calculated using the expression developed by Pantazopoulou (1995). Knowing E_r and the constitutive relationship of the jacket, a new value of f_r is calculated and compared with the previous value. The procedure is repeated until f_r converges to a stable value.

Lavergne and Labossiere (1997) carried out an experimental investigation on two 300 x 2150 mm circular column models strengthened with externally applied composite wrapping. Three tests were undertaken on these 2 specimens. The first model (F) was first tested without composite wrapping as a reference behavior. It was then repaired using a unidirectional CFRP wrapping (F*) around the potential plastic hinge region and tested. The second model (D) was strengthened with CFRP in the same manner as F* but was not load-tested prior to strengthening. All models were subjected to horizontal

reversal loading while maintaining a constant axial compression load. The following observations were made:

. Columns with lap-splices in the hinge regions and designed according to old standards (20 years and more) failed at a low ductility factor of 1.5, due to bond failure between the lapped starter bars, to lack of transverse reinforcement and insufficient development length of longitudinal bars.

. RC columns externally retrofitted with CFRP in the hinge region showed a slight increase in strength, but a very significant improvement in ductility with very stable loops up to a ductility factor of 8.0.

. Concrete columns with initial damage, retrofitted with CFRP wrapping in the hinge region, exceeded its initial strength and became much more ductile.

. The application of one layer fibers in the vertical direction did not enhance the flexural strength of the column but seem to inhibit the development of horizontal cracking in the composite straps until failure.

Haroun et al. (1997) reported results of experimental cyclic tests on bridge columns retrofitted by CFRP composite jackets. Six half-scale circular columns were considered to evaluate lap-splice enhancement in flexure and confinement enhancement in shear as follows: Three 610 x 3430 mm with a lap-splice length of 380 mm were retrofitted with hand-laid CFRP sheets, whereas the other three columns, 610 x 2440 mm, had continuous longitudinal bars and'were retrofitted with machine wound CFRP strands. All specimens were subjected to cyclic horizontal loading, while maintaining a constant axial compression load. The control columns (i.e., with CFRP wrapping) with and without lap-splices developed a maximum ductility of 1.5 and 2.0, respectively, whereas the corresponding retrofitted specimens developed a maximum ductility of 6 and 10 with very stable hysteresis loops. Results also showed that lateral stiffness of columns were not altered with CFRP wrapping, and therefore the dynamic properties of bridges will not be altered when using this method of strengthening and repair.

Seible (1997) presented design equations for columns retrofitted with FRP composite in seismic regions. He considered the following aspects; (a) shear, (b) flexural hinge confinement, and (c) lap-splice clamping. These equations were validated by experimental tests and will be presented in Chapter 3.

Benzoni et al. (1997) reported results of two full-size bridge circular columns. The first column, as built, was aimed at evaluating the conventional shear design as affected by size effects. The second column, repaired with CFRP jacketing, was aimed to investigating the effectiveness of jacketing as a repair technique for full-size columns. It was found that for "as built" columns, the shear design equations provided a generally conservative prediction of the shear capacity. The UCSD design models were found to predict very well the maximum lateral force. The repaired model exceeded expected performance. Peak strength was more than 45% than in the "as built" and exceeded nominal flexural strength by 20%. This indicates that column with extensive shear failure and degraded strength can be satisfactorily repaired to adequate stiffness and full strength characteristics.

Hosotani et al. (1997) studied the confinement effect of concrete cylinders by carbon fiber sheets (CFS) for seismic strengthening. They conducted a series of compressive loading test on 600 x 200mm concrete cylinders (10 circular and 12 square) to investigate the stress-strain relation under confinement by CFS. The parameters considered in the tests were the shape of the specimen, the content and the type of CFS (normal and high elastic modulus). Three series of specimens were considered: (a) N-series (cylinders without confinement), (b) S-series (cylinders confined by the CFS with normal elastic modulus - 230GPa), and (c) H-series (cylinders confined by the CFS with high elastic modulus - 392MPa). All the specimens were loaded in axial direction under the displacement control with a loading rate of 0.2 mm/min. The following conclusions were dawn from the test results:

1. At a carbon ratio in the range of 0.05 to 0.15%, the peak axial stress of concrete, f_{cc}, and the axial strain of concrete corresponding to the peak stress, ε_{cc}, do not increase as the carbon fiber ratio increases, and are almost independent of the cross sectional shape of specimens. However, the deteriorating rate of the axial concrete stress after the peak stress decreases and the axial strain of concrete at rupture of the CFS increases as the carbon fiber ratio increases.

2. At a carbon ratio greater than about 1%, the axial stress of concrete continues to increase with a change of gradient at an axial concrete strain of 3,000 to 3,500 με until failure of CFS.

3. The circumferential strain of the CFS at the peak axial stress of concrete, ε_{cft}, is 1,100 to 2,500με for a carbon fiber ratio of 0.056 to 0.16%, while the circumferential strain of the CFS where the gradient changes from the initial value to the second gradient, ε_{cft} is 1,800 to 1,900με for a carbon fiber ratio of 1.336%; thus, ε_{cfs} is quite close to ε_{cft}.

Miyauchi and al. (1997) performed uniaxial compression tests on concrete columns reinforced with carbon fiber sheet (CFS) to estimate the strengthening effects. They took into account the compressive strength of the concrete (30 and 50 MPa), the number of layers of CFS (1, 2 and 3 layers) and the dimensions of the column ((~10 x 20cm and X15 x 30cm). Test results show that: (a) the compressive strength of the concrete strengthened with CFS is enhanced in proportion to the number of layers of CFS, but not the compressive strength of the plain concrete and the' dimensions of the specimens; (b) the axial strain at maximum stress of the concrete strengthened with CFS exponentially extends with the number of layers of CFS and is influenced by the compressive strength of plain concrete. Based on these results, a stress-strain relationship, consisting of a parabola and a straight line tangent to the parabola, for the strengthened concrete is proposed and used to perform a time history response analysis for existing bridge piers strengthened with CFS and subjected to earthquake motion. The analytical results show that existing piers strengthened with 2 layers of CFS would be able to withstand an earthquake equal in intensity to the Southern Hyogo Prefecture Earthquake.

Watanabe et al. (1997) investigated experimentally and analytically the confinement effect of FRP sheets on the strength and ductility of concrete cylinders subjected to a uniaxial compression. Plain concrete cylinder specimens with dimensions of (~ 100 x 200mm retrofitted with FRP sheets were tested under a uniaxial compression. Variables selected for the test and analysis include the type and the number of FRP sheets. Carbon fiber reinforced plastic (CFRP), high stiffness carbon fiber reinforced plastic (HCFRP) and aramid fiber reinforced plastic (AFRP) were used and the number of FRP sheet layers varied from 1 to 4. The analytical procedure used considered a nonlinear 3Dimensional FEM, which implements Endochronic theory. Comparison of test results with those obtained by the analytical study showed good agreements and the following conclusions were drawn:

. A nonlinear 3-dimensonal finite element procedure, which implemented the Endochronic theory proposed by Bazant, can be applicable to predict responses of concrete cylinders under a uniaxial compression.

. The proposed FE analysis procedure can simulate the confinement effect of FRP sheets on the strength and ductility of concrete cylinders under a uniaxial compression.

. If FRP sheets are used to improve the strength and the ductility of concrete cylinder, then the relationship between the Young's modulus and the confinement effect of FRP sheets need to be clarified.

. Compressive strength of concrete cylinders retrofitted with the sheets linearly increased with an increase in the number of plies.

Nagasaka et al. (1997) conducted an experimental study to evaluate the strengthening effect of aramid fiber tapes on existing reinforced concrete columns with poor shear capacity. Nine square RC columns specimens, with cross section of 30x30 cm and 110 cm in clear length, were subjected to repeated cyclic reversals of lateral load under a constant vertical load. The rotation at both ends of columns was restrained. The columns were strengthened by fiber tapes spirally wounded around them with epoxy resin. Two columns were pre-damaged and the cracks grouted with epoxy resin before strengthening. The test variables considered during these tests were : (a) the type of fiber

tape (aramid and carbon fibers), (b) spacing patterns in spirally winding (1.0, 0.5 and 0 times the width of the tape) and (c) hoop reinforcement ratios (0.13 and 0.30%). The analysis of the test results showed that

. The increment of shear capacity obtained by winding the aramid fiber tape about 0.1% in tape ratio around the column with a hoop ratio of 0.13% was equivalent to that of the increase of hoop ratio by 0.17%.

. The shear capacity of the column increased with an increase in the amount of fiber tape, but not linearly.

. The difference in the types of aramid fiber tape did not significantly affect the strengthening effect on the shear capacity. However, the effectiveness of the aramid fiber tapes was slightly inferior to that of the carbon fiber tape.

. The tape winding of pre-damaged columns, after cracks were grouted with epoxy resin, showed practically the same effectiveness as that of the undamaged columns.

Kataoka and al. (1997) studied the ductility improvement of RC columns wrapped with continuous fiber sheets. In order to investigate the restoring strength characteristics of RC columns wrapped by sheets empirically and to propose an evaluation method of strutural performance of RC columns wrapped with sheets, Kataoka et al. conducted an experimental program consisting of 3 series of tests:

(a) The objective of the first series was to evaluate the shear strengthening! effect of sheets. A total of 15 RC 300 x 300mm square columns with 1 IOOmm clear span length were tested under anti-symmetrical moment condition with constant axial force (cyclic loading controlled by deflection angle). The main parameters selected for this test were the amount of sheets, the type of sheets and the amount of hoops. Four (4) specimens were conventional RC columns (without wrapping sheets), 10 specimens were sheet-RC columns (wrapped by sheets), and one column was wrapped with sheets after shear failure had occurred, without repair of shear cracks.

(b) The objective of the second series of test was to evaluate the post yielding ductility of RC members wrapped with sheets. A total of 9 RC 300x300mm square columns with clear span length of 900mm were tested. The load was applied similarly to the first series. The main parameters selected for the test were the amount of sheets and the amount of hoops. One specimen was standard column (with 0.13% shear reinforcement ratio and without wrapping sheets), 2 specimens were conventional RC columns (without wrapping sheets); and 6 specimens were sheet-RC columns (wrapped by sheets).

(c) The objective of the third series of test was to investigate the axial compressive behavior of columns wrapped with sheets, empirically. A total of 10 specimens were tested. The dimensions of the columns were the same as those of the second series. The main parameters selected for the test were the amount of sheets and the amount of hoops. One specimen was standard, one was conventional RC column, and 8 were sheet-RC columns. In this last series, two types of tests were carried out : one was normal monotonic axial compression test and the other was axial compression test to investigate the axial compression capacity of the columns which had already failed under lateral loading in the second series.

From the test results over the three series of test, the following conclusions were achieved: (i) the sheet-wrapping method can enhance the seismic behavior, the capacity as well as the ductility, of existing RC columns; (ii) structural performance of RC columns wrapped with sheets can generally be evaluated using the effective shear reinforcement ratio $Ep_{,,} = p_{H,} + (f6_{,,}/ G W_{Y)}\ fP_{W}$, where: p_w = shear reinforcement ratio of hoops, $fp_{,,}$ _ shear reinforcement ratio of sheets, a. = yield strength of hoops,$fv_{,,}$ = tensile strength of . sheets.

Sirbu et al. (1997) conducted an experimental program to assess the seismic resistance of reinforced concrete piers retrofitted with carbon fiber sheets (CFS). A RC pier often encountered in Japan has been chosen as a model for this study. Two 1/5 scaled down models, representing square RC piers with strong footing ensemble, were fabricated

measured and the confining effects examined for 5 different bond lengths and 3 wrapping techniques. The confinement due to the CFRP sheet suppressed brittle side splitting failure and increased both the bond strength and the slip capacity of the embedded deformed steel bar. On layer of CFRP sheet increased the bond strength by a factor of 1.8 on average. Finally, the last series of test was conducted on 3 beam specimens (200 x 300 x 1300mm) to examine the confining effects on a structural member. One beam was not confined and served as reference beam while the remaining two were half and fully confined respectively. The confinement due to CFRP sheet suppressed the brittle bond splitting observed in the reference beam and increased the load carrying capacities. However, the expected load carrying capacity of the half confined specimen was not reached due to the failure of lapping of the CFRP sheet.

Kanatharana and Lu (1998) studied the behavior of FRP-reinforced concrete columns under uniaxial compression. Two types of FRP tubes were used in this study; namely the filament-wound FRP (FFRP) and the pultruded FRP (PFRP) tubes. The FFRP has continuous glass fibers winding at 53° and 127° from its circumference, whereas the PFRP has continuous fibers running along its axis. Based on the results obtained from FRP tube tests, 3 configurations of FRP incorporated concrete were selected: Type A configuration simulating a situation similar to a concrete-filled steel tube; Type B configuration simulating a condition similar to an ordinary spiral reinforced concrete column; Type C configuration combining type A and B type configurations. The experimental results showed that significant increases in concrete ductility and FRP strength occurred in all the FFRP specimens but not in the PFRP specimens. Detailed examination revealed that the inclined orientations of the glass fibers provide the FFRP with a circumferential strength necessary for confining concrete, which in turn restrains the FFRP from local instability, and enables strength and ductility gains in the FFRP specimens.

Harmon et al. (1998) investigated the behavior and the failure modes of confined concrete subjected to cyclic loading. Composite tubes, 51 mm in diameter and 102 mm long, were fabricated by filament winding, then filled with concrete. The resulting confined cylinders were loaded in uniaxial compression for up to 10,000 cycles. Variables included amplitude, range, fiber type (carbon and glass) and fiber to concrete volume ratio (0, 2, 4 and 6%). The authors reached the following conclusions:

Cyclic loading increased axial, radial and volume strains for a given range and amplitude. Monotonic loading following cyclic loading rejoined the monotonic stress strain relationship unless failure occurs first. Cyclic loading at a given amplitude is equivalent to preloading to a higher load which depends on the amplitude, range and number of cycles, followed by unloading to the given amplitude.

Failure occurred when the circumferential strain in the wrap exceeded the strain capacity of the fiber. The critical threshold can be crossed either by monotonic loading or by cycling loading. Under cyclic loading, the load at failure may be much lower than under monotonic loading. Some evidence suggested that the critical strain threshold may be reduced due to cyclic loading.

Radial strain tended to stabilize with increasing number of cycles for high wrap stiffness.

Void compaction increased with load level and decreased with concrete strength and wrap stiffness. Shear slip and void compaction were closely related.

. A reasonable cyclic model for failure and stress-strain behavior can be constructed from a monotonic model and models for the increase in radial strain, the increase in void compaction and the reduction in the critical threshold level with number of cycles.

Harries et al. (1998) presented the results of an extensive experimental investigation on the axial behavior of reinforced concrete columns retrofit with FRPC jackets. Initially, 152 x 610 mm plain concrete cylinders and 152 x 152 x 610 mm square concrete prisms having FRPC jackets were tested under monotonically increasing concentric axial compression. These tests were aimed at addressing some of the issues raised in previous studies.

Following these tests, 8 full-scale, 508mm diameter circular and 457mm square reinforced concrete columns confined with external FRPC jackets were tested under monotonically increasing concentric axial compression. Reinforcing details of the columns were typical of those designed prior to 1971. In these tests, 3 different FRPC materials were used:(a) A stitched multi-directional E-Glass fabric with 50% of the fibers oriented at 0° with respect to the circumferential direction of the column and 25% of the fibers oriented at each of ± 45°; (b) A women unidirectional E-Glass fabric oriented in the circumferential direction of the column; and (c) A unidirectional carbon fiber tow sheet oriented in the circumferential direction of the column. The results of this study showed that external FRPC jackets retrofits increase axial force capacity and axial deformation capacity and suggested that practical retrofit measures will provide confinement equivalent to that provided by closely spaced, well detailed, conventional transverse reinforcement. The stiffness of the applied FRPC jacket was found to be the key parameter in the design of external jacket retrofits. The results of this study suggested that there was no significant scale effect where jackets with similar confinement capacity were provided.

2.2 Research Findings Related to Beam-Columns

Obviously most of research work has been devoted to beam-columns confined by lateral steel reinforcement or steel tubes. Sheikh and Yeh (1986 and 1992) showed that the confinement provided by lateral steel reinforcement, while it greatly improves ductility, it does not enhance the strength. They therefore modified the confinement model proposed by Sheikh and Uzumbri (1980) to take the strain gradient into consideration and used a modified concrete compression block to calculate the flexural capacity of confined sections.

Ziara et al. (1995) investigated the effect of confinement provided by stirrups in the compression zone. They carried out tests on under-reinforced and over-reinforced beams in flexure and concluded that over-reinforced beams with confinement can be designed to fail in ductile manner and develop their full flexural capacity.

Chai et al. (1991) carried out tests on 0.4-scale columns retrofitted with steel jackets. The specimens included models designed with the pre - 1971 reinforcement detailing. A gap of 1/4" was left between the column surface and the jacket, to be pressure injected with water/cement grout. The authors concluded that the confinement provided by the steel jacket could contain the concrete cover from spalling and thereby bond failure of longitudinal reinforcement is eliminated. The confinement also achieved a ductile mode of failure with improved energy dissipation capability.

Prion and Boehme (1994) studied the behavior of concrete filled steel tubes. They tested 26 circular steel tubes with a 6" outside diameter, under different load combinations ranging from pure axial compression, through various combinations of axial-flexure, topure flexure. They reported that the beam-column specimens failed by tension failure of the steel tube accompanied by buckling of the steel in the compression zone. Significant slippage between steel and concrete was observed in pure flexure tests. It was also noticed that the secondary moments, due to the P-Δ effects, constituted 20% of the total ultimate moment. This was a result of the large deformations prior to failure.

Fardis and Khalili (1981 and 1982) tested a concrete-filled FRP box in pure flexure. The cross-section of the box was 3" wide and 6" deep with a total length of 48". The bottom, sides, and ends of the FRP box consisted of two layers of 24 oz. fiberglass bi-directional woven roving. In addition, reinforcing unidirectional plies were provided at the bottom. After pouring concrete in the FRP box, the top and the sides were covered with two layers of 10 oz. fiberglass cloth. Five specimens with different number of reinforcing layers were tested under four point flexure loading. No mechanical interlocking was provided between concrete and FRP, which caused some slippage during tests. The failure was mainly due to crushing of the concrete followed by bursting of the FRP layers in the compression zone. They also tested four reinforced concrete beams with different reinforcement ratios for comparison.

Nanni and Norris (1995) performed a series of flexural and axial-flexural tests on circular and rectangular FRP-wrapped reinforced concrete beams. They tested 19 circular 6" diameter and 7 rectangular (6" x 8") specimens. Two types of FRP jackets were used; braided aramid/epoxy shells. The specimens were 60" long and were loaded under cyclic flexure. The concentric axial loads on some of the specimens was applied via prestressing bars. It was concluded that the FRP jacketing increased the ductility of the specimens in comparison to typical unconfined beams. This was more apparent for specimens with higher axial loads.

Carbrera (1996) conducted two series of tests on short square concrete filled FRP tube in pure flexure. The first series consisted of eight 6" x 6" x 22" concrete beams, 6 of which were encased in fiberglass tubes, and 2 were control specimens. The beams were loaded to failure under a four-point loading test. Test results indicated that while the shear strength of the beams was increased by up to 1333 percent, excessive slippage at the concrete jacket interface inhibited development of full shear strength by the jacket. A second series of tests was conducted with shear connectors on all interior faces of the FRP tube. Results of these tests demonstrated that slippage was completely arrested by the shear connectors. The FRP tube was able to increase the shear strength beyond the flexural capacity of the members. She also conducted a study on the seismic performance of concrete-filled FRP tube based on a cyclic stress-strain model.

CHAPTER 3

REVIEW OF PROPOSED MATHEMATICAL MODELS AND DESIGN EQUATIONS

This chapter presents the evolution of the proposed mathematical models and design equations for confined columns and cylinders.

3.1 Active Confinement (Triaxial tests)

Table 3.1 summarizes the different models proposed for tri-axially stressed concrete.

3.2 Passive Confinement Using Lateral Steel Reinforcement

From the 80's, numerous research studies have dealt with the behavior of concrete columns of various strengths, passively confined using different configurations of steel reinforcing cages. The general formulae relating the axial compressive stress at failure f, to effective confining pressure f_2 proposed are presented in Table 3.2.

Table 3.1- Proposed Models for Tri-axially Stressed Concrete

Authors	Models	Comments
Considere (1903)	$f, = k_1 f'_c + 4.8 f_2$ (3.1)	$1.0 \leq k_1 \leq 1.5$ f, =axial comp. stress f_2 =lateral pressure f, = comp. Strength of unconfined concrete
	$f_1 = f'_c + k_c f_2$ (3.2)	
Richart et al. (1928)	$k_c = 4.1$ (3.3)	
Chinn and Zimmerman (1965)	$k_c = 3.65 f_2^{-0.117}$ (f_2 in ksi) (3.4)	
Newman & Newman (1972)	$k_c = 3.7\left(\frac{f_2}{f_c'}\right)^{-14}$ (3.5)	
Saatcioglu and Razvi (1992)	$k_c = 4.825 f_2^{-17}$ (f_2 in ksi) 3.6)	

Table 3.2 - Models for Passive Confinement by Lateral Steel Reinforcement

Authors	Models	Comments
General formula	$f_, = f'_c + 4.1\, f_2$ (3.7)	Same as active confinement
Richart et al. (1929)	$f_2 = \frac{2 f_{sy} d_s}{D}$ (3.8)	f_{sy} = steel yield stress d_s = diameter of confining spirals D = inside diameter of column.
Iyengar et al. (1972)	$f_2 = \frac{2 A_{sp} f_{sy}}{D S_{sp}}$ (3.9)	A_{sp}, S_{sp}= cross section and pitch of spiral
Ahmad and Shah (1982a)	$f_, = f'_c + 4.256\, f_2$ (for $f_2 \le 0.679\, f'_c$) (3. 10a) $f_l = 1.776\, f'_c + 3.117\, f_2$ (for $f_2 > 0.679\, f'_c$) (3. 10b)	
Mander et al. (1988)	$f_c = \frac{f'_{cc} x r}{r - 1 + x}$ (3.11) $x = \frac{\in_c}{\in_{cc}}$ (3.12) $\in_{cc} = \in_{co} \left[1 + 5 \left[\frac{f'_{cc}}{f'_{co}} - 1 \right] \right]$ (3.13) $r = \frac{E_c}{E_c - E_{\sec}}$ (3.14) $E_{\sec} = \frac{f'_{cc}}{\in_{cc}}$ (3.15) $f'_{cc} = f'_{co} [1.254 + 2.254] \sqrt{1 + \frac{7.94 f'_1}{f'_{co}}} - 2 \frac{f'_1}{f'_{co}}$ (3.16) $f'_1 = f_1 k_e$ (3.17) $k_e = \frac{A_e}{A_{cc}}$ (3.18)	(1) Based on work of several other research works (Popovics1973; Richart et al. 1928; Scott et al. 1982, etc.) (2) The model assumes a constant confining pressure throughout the loading history and is insensitive to variation of the ratio of concrete.

3.3 Passive Confinement Using Steel Tubes

In parallel to these studies on the confinement using steel cages, other studies were carried out where the confinement was provided by thin walled steel tube. These studies were conveniently summarized by Knowles and Park (1969) who suggested the following design formulae that were adapted by many modern codes and standards, for the compressive strength of concrete filled steel tubes. The compressive strength of a concrete filled steel tube is made of the strengths of concrete and of the steel tube, modified by correction factors i and i'. These factors reflect the effects of the slenderness of the columns, as well as the steel tube thickness compared to the column diameter. That is:

$$Crc = \tau C_r + \tau' C_r^{'} \tag{3.19}$$

$$C'_r = 0.85 \phi_c f_c^{'} A_c \lambda_c^{-2} \left[\sqrt{1 + 0.25 \lambda_{-2}^{-4} - 0.5 \lambda_c^{-2}} \right] \tag{3.20}$$

$$\lambda_c = \frac{kl}{r_c} \sqrt{\frac{f_c^{'}}{\pi^2 E_c}} \tag{3.21}$$

and where r_c = radius of gyration of concrete; E_c = modulus of elasticity of concrete including long-term effects; k = factor reflecting column-end conditions; 1 = length of column; f_c' = compression strength of concrete; ϕ_c, ϕ_s = resistance factors for concrete and steel, respectively; A_c, A_s = section area of concrete and steel, respectively.

The correction factors τ and τ' can be assumed equal to 1.0 (no confinement) if the section of the steel tube is rectangular or if the length of the column (L) is greater than 25 times its diameter D (i.e., L/D>25). Note that confinement enhances the compressive strength of concrete but decreases that of the steel envelope due to the biaxial state of loading. Therefore, $\tau' \geq 1.0$ and $\tau \leq 1.0$. These correction factors can be derived from:

$$\tau = \frac{1}{\sqrt{1+\rho+\rho^2}} \le 1 \qquad \tau' = 1 + \left(\frac{25\rho^2\tau}{D/t}\right)\left(\frac{F_y}{0.85f_c'}\right) \ge 1 \qquad (3.22)$$

with

$$\rho = 0.02(25 - \frac{l}{D}) \qquad (3.23)$$

where D = diameter of the column, and t = thickness of steel tube.

3.4 Available Models for FRP Wrapped Columns

It is observed that most existing empirical models were developed for concrete confined with steel tube. These models are based on an elastic perfectly plastic behavior of the steel tube and consider, therefore, the confining pressure constant after concrete has reached its compressive strength. While this may be true for steel tube confined concrete, it may not hold for FRP confined concrete where the confining pressure increases with loading up to failure since FRP composites behave linearly up to rupture, as seen in Figure 3.1. Table 3.3 summarizes the confinement models for FRP wrapped circular columns.

Table 3.3 - Confinement models for FRP Wrapped Columns

Authors	Models	Comments
Fardis and Khalili (1981)	$f_c = \dfrac{E_c \varepsilon_c}{l + \varepsilon_c \left[\dfrac{E_c}{f'_{cc}} - \dfrac{1}{\varepsilon_{cc}} \right]}$ $\varepsilon_{cc} = 0.002 + 0.001 \dfrac{E_j t_j}{D f'_c}$	E_j, t_j = modulus of elasticity and thickness of FRP jacket. E_c = initial tangent modulus of concrete.
Ahmad et al. (1991)	$f'_{cc} = f'_c \left[1 + \dfrac{k}{4^{nSsp}} \right]$ (3.26) $\varepsilon_{cc} = \varepsilon_{co} \left[1 + \dfrac{k}{4^{nSsp}} \right]$ (3.27)	k and n are functions of f_C S_P = spacing of FRP spirals.
Monti and Spoe Istra (1997)	$\varepsilon_r = 0.5 \beta \dfrac{E_c - E_{\sec}}{E_{\sec}}$ (3.28) $E_{\sec} = f_c / \varepsilon_c$ $\beta = -\dfrac{V_p^3 v_c}{3}$ $v_c = 3.22 \dfrac{W_o - 0.364 \alpha_x}{1 + 3.22 W_o}$ $v_c = \dfrac{1.031 Wo}{0.194 + W_o}$	Basically the same as the model by Ahmad and Shah(1982) V_P = volume fraction of paste in concrete V_c = natural capillary porosity of paste w_o = water-cement ratio a_x = degree of hydration
Samaan, Mirmiran and Shahawy(1998)	(a) Model for the axial strains(see Fig. 3.2) $v_c = \dfrac{(E_1 - E_2)\varepsilon_c}{\left[1 + \left(\dfrac{(E_1 - E_2)\varepsilon_c}{f_o} \right)^n \right]^{\frac{1}{n}}} + E_2 \varepsilon_c$ (3.29) $f'_{cu} = f'_c + 3.38 f_{r7}^{0.7}$	• See definitions of f~, E,, E_2, E_c, f_o, f in Fig. 3.2. • f, E_j and tensile strength, modules of elasticity and thickness of FRP wrap.

Authors	Models	Comments
	$f_r = \frac{2 f_j t_j}{D}$ (3.31) $E_1 = 47.586\sqrt{1.000 f'_c}$ (3.32) $E_2 = 52.4111 f'_c 0.2 + 1.3456 \frac{E_j t_j}{D}$ (3.33) $f_o = 0.872 f'_c + 0.371 f_r + 0.908$ (3.34) $\varepsilon_{cu} = \frac{f'_{ju} - f_o}{E_2}$ (3.35) (b) Model for lateral strains (see Fig. 3.3) $f_c = \frac{(E_{lr} - E_{2r})\varepsilon_r}{\left[1 + \left(\frac{(E_1 r - E_{2r})\varepsilon_r}{f_{or}}\right)^{nr}\right]^{\frac{1}{nr}}} + E_{2r}\varepsilon_r$ (3.36) $E_{lr} = \frac{E_1}{V}$ (3.37) $\mu = -\frac{d\varepsilon_r}{de_c}$ (3.38) $\mu_u = -0.187 Ln\left(\frac{2E_j t_j}{f'_c D}\right) + 0.881$ (3.39) $E_{2r} = \frac{E_2}{\mu_u}$ (3.41) $n_r = \frac{n}{\mu_n}$ (3.31) $f_{or} = 0.636 f' + 0.233 f_r + 0.661$ (3.42) $\varepsilon_{ru} = \frac{f'_{ju} - f_{or}}{E_{2r}}$ (3.43)	• D = diameter of column • n = curve shape parameter (n = 1.5 for circular). • r denotes lateral (radial) direction • v = Poisson's ratio • p = dilation rate • p = ultimate radial strain

$$f_t = \frac{As \cdot fsy}{\left[\frac{p}{2n} + 2\left(d_b + cc\right)\right] L_s} \tag{3.47}$$

It is seen from Eq. (3.47) that the thickness is proportional to D and inversely proportioned to E_j.

3.4.3 Design for Flexural Hinge Confinement

For circular columns, the required jacket thickness can be expressed as

$$t^c j = 0.09 \frac{D\left(\varepsilon c_{ju} - 0.004\right) f'_{cc}}{\phi_f \cdot f_{ju} \cdot \varepsilon_{ju}} \tag{3.48}$$

where f_{cc} is the confined concrete compression strength which depends on the effective lateral confining stress and the nominal concrete strength and can be conservatively taken as 1.5 f_c, for most retrofit designs, f_{ju} and ϵ_{ju} are the strength and deformation capacity of the composite jacket in the hoop direction, ϕ_f is a flexural capacity reduction factor (typically taken as 0.9), ϵ_{cu} is the ultimate concrete strain which depends on the level of confinement provided by the composite jacket.

The buckling of longitudinal bars in the plastic zone, which can develop particularly in slender columns where (M/(VD)>4), can be prevented. This would result in a jacket thickness in the form of (Priestley et al. 1996)

$$t^b j - \frac{D}{Ej} \times C_b \tag{3.49}$$

The above equations were provided for circular columns and originated from the radial pressure forces. For rectangular sections, an oval jacket can be provided and an equivalent D_e assumed (average principal radii). In the case of the rectangular sections, it was found that for columns with a side aspect ratio of depth/width < 1.5 and columns with depth in the loading direction of 0.75 or less, rectangular composite jackets with twice the theoretical thickness derived from an equivalent circular column (D_c) would be adequate to achieve the design target ductility level.

3.4.4 Thickness Design Considerations

Priestley et al. (1997) computed and compared the required thickness of FRP jacket using composite materials in Table 3.4. As can be seen in this table, the jacket thicknesses for shear and lap-splice clamping are rather based on the modulus of the jacket in the hoop direction which favors higher modulus materials, whereas the flexural plastic hinge confinement can also efficiently be achieved with a lower modulus and higher strain capacity material.

Table 3.4 - Comparison of Hypothetical Jacket Thickness (Seible and1997)

System	Mechanical Characteristics	Normalized Jacket Thickness			
		Shear strength	Plastic hinge confinement	Anti-bar buckling	Lap splice Clamping
	Design Relationships	$t_j^{\nu} - \frac{1}{E_j D} \times C_{\nu}$	$t_j^{\nu} - \frac{D}{f_{ju} Eju} \times C_c$	$t_j b - \frac{D}{E_j} \times cb$	$t_j s - \frac{D}{E_j} \times c_s$
System A	E = 124 GPa f = 1380 MPa ϵ = 1%	1	1	1	1
System B	E = 76 GPa f= 1380 MPa ϵ = 1.5%	16	7	16	16
System C	E = 124 GPa f = 1380 MPa ϵ = 1%	60	9	60	60

1 MPa =0.145 ksi, 1 GPa = 145 ksi

PART II

TESTING PROGRAM AND PROCEDURE

CHAPTER 4

EXPERIMENTAL PROGRAM

This chapter presents the experimental program. It gives details of the specimens, the material used, the instrumentation as well as the testing procedures.

4.1 Description of Specimens

The test specimens (see Fig. 4.1) chosen for the study have an 8" x 14" (200 x 350 mm) rectangular cross section and a total length of 140" (3500 mm). The length between corbels is 7'(2100 mm). Since large applied loads are expected to be required for failure of several specimens, large corbels or "feet" were designed in which a single load source could be used and applied eccentrically on the corbel thus simulating the combined stress effects in columns. Note, however, that for pure flexure and pure compression conditions, four specimens each [j](one control and three wrapped) were cast as simple rectangular beams (total length = 140" for pure flexure and 84" for pure compression) with no corbels. The total length of each corbel is 28" (700 mm), with a total height also of 28". Steel reinforcement details of the specimens are presented in Figure 4.1. Primary internal reinforcement consists of 2 layers of grade 60 #6 (ϕ = 19 mm) bars, the first layer having d' = 2" (50 mm), while the second layer has d = 12" (300 mm). Shear stirrups, consisting of grade 60 closed #3 (ϕ = 9.5 m) bars, are spaced evenly though the effective length at a spacing of 4" (100 mm).

4.4 Testing Procedure and Program

Six series of at least three tests are performed in this study. Each series is made of a RC column without CFRP jacket as a control specimen and a RC column retrofitted with CFRP jacket. The six series correspond to the following load eccentricities 0" (i.e., concentric loading), 3" (7.5 mm), 6" (15 mm), 12" (300 mm), 16" (400 mm), and pure bending (i.e., an eccentricity approaching infinity**).**

The test program of the different series is presented in Table 4.4. Note that the specimens were labeled as follows:

BC-XLY-EZ,

where: X, Y, and Z are all numeric values.

BC stands for "Beam Column" project.

XLY stands for "X" number of carbon "L"ayers with a concrete strength of "Y"ksi.

EZ stands for "E"ccentricity of "Z" inches.

4.5 Load Capacity Prediction of Specimens

4.5.1 Specimens With No Wrap

In the general case where columns are subjected to a combined axial compressionbending moment, the nominal load capacity varies as the applied moment (that is, the load eccentricity) varies. Although it is possible to derive equations to evaluate the strength of columns subjected to combined bending and axial loads, the equations are tedious to use. For this reason, interaction diagrams for columns are generally computed by assuming a series of strain distributions, each corresponding to a particular point on the interaction diagram, and computing the corresponding values of P and M (see Fig. 4.3).

(i) With reference to Fig. 4.3 the nominal concentric load capacity, P,,, of a RC column is given by ACI Code as follows:

$$P_n = 0.85 f'_c \left(A_g - A_{st}\right) + A_{st} f_y \qquad (4.1)$$

where f, = compression strength of concrete; A_g = total gross area of concrete section; A_{sp} = total steel area ($A_{SS} = A_S + A's$), and f_y = yield stress of steel reinforcement

Noting that:

f_y = 60 ksi

A_{st} = 1.76 in.' (4#6)

f ' = 3000-psi

A_g = 112 $in.^2$

and using Eq. (4.1), the nominal concentric load P_n follows:

P_n = 0.85 x 3000 (1.2 - 1.76) + (1.76 x 6000)

P_n = 281,112 + 105,600

P_n = 387 kips

Therefore, with reference to Fig. 4.3, point A is given by:

P_n = 387 kips and M„ = 0

(ii) The balanced point C can be calculated as follows with reference to strain distributions:

d = 12 in.

$$c_b = \frac{8700}{870000 + f_y} d = 7.1in$$

$$\varepsilon_s = \frac{0.003(7.1-2)}{7.1} = 0.00215 \triangleright \varepsilon_y \Rightarrow f'_s = f_y = 60ksi$$

M_{nb}= 0.85 f'c ba (ÿ - $\frac{9}{2}$) + A_s'f_y (ÿ-d') - $A_S f_y$ (d - ÿ)

with ÿ = h/2 = 7" , it follows:

P_{nb} = 122.6 kip, M_{nb} = 1018 kip-in, and e_b = 8.3"

Table 4.1 - Concrete Mix Design (per cubic yard)

Water	313 lbs (142 kg)
Cement	4601bs (209 kg)
Coarse aggregate (1)	17721bs (804 kg)
Fine aggregate	16601bs (754 kg)
W/C Ratio	0.68

(1) 3/4" maximum aggregate size, river rock

Table 4.2 - Concrete Average Strength of Different Pours

Pour No.	Compressive Strength ksi (MPa)
1	3.1 (21.4)
2	3.2 (22.0)
3	3.0 (20.0)
4	4.6 (30.6)
5	5.4 (36.0)

Table 4.3 - Material Properties of Carbon

Description	Manufacturer's data(1)	FDOT's suggested values (2)
Tensile Strength	530 ksi (3.65 GPa)	330 ksi (2.27 GPa)
Tensile Modulus of Elasticity	33500 ksi (231 GPa)	12000 ksi (82.6 GPa)
Ultimate Tensile Elongation	1.4%	1.4
Filament Diameter	7 m	7 m
Filaments/ am	12000	12000
Thickness of layer		0.02 in. (0.5)

(1) Reported for the carbon fabric only (11 yarns/inch, 70 x 10.50/yam)
(2) Based on split-disk tests and finite element analysis by Tom Beitelman of FDOT.

Table 4.4 - Test Program

SERIES	SPECIMEN NO.	CRFP LAYERS	ECCENTRICITY (INCH.)	POUR NO.	COMMENTS
1 -	BC-OL3-EO	0	0	2	
	BC-OL3-EO	0	0	3	no corbels (84")
	BC-2L3-EO	2 Layers	0	2	
	BC-2L3-EO1	2 Layers	0	4	no corbels (84")
	BC-2L3-EO2	2 Layers	0	4	no corbels (84")
	BC-2L3-EO3	2 Layers	0	4	no corbels (84")
2	BC-OL3-E3	0	3	1	
	BC-2L3-E3-1	2 Layers	3	1	
	BC-2L3-E3-2	2 Layers	3	5	
3	BC-OL3-E6	0	6	1	
	BC-2L3-E6-1	2 Layers	6	1	
	BC-2L3-E6-2	2 Layers	6	5	
4	BC-OL3-E12	0	12	2	
	BC-2L3-E12-1	2 Layers	12	2	
	BC-2L3-E12-2	2 Layers	12	5	
	BC-2L3-E12RL	2 Layers	12	1	
5	BC-OL3-16	0	16	3	
	BC-2L3-16-1	2 Layers	16	2	
	BC-2L3-16-2	2 Layers	16	5	
6'	BC-OL3-FL	0	PB(1)	3	no corbels (140")
	BC-2L3-FL-1	2 Layers	PB(1)	3	no corbels (140")
	BC-2L3-FL-2	2 Layers	PB(1)	3	no corbels (140")
	BC-2L3-FL-3	2 Layers	PBM	3	no corbels (140")
	BC-2L3-FL(corbel)	2 Layers	PBM	3	with corbels

Note: 0) PB = Pure Bending

CHAPTER 5

PRESENTATION OF THE RESULTS

This chapter presents the experimental results of all the series mainly in terms of load or moment. versus mid-span deflections, secondary moments and strain distribution.

The maximum experimental values obtained from tests for all series are summarized in Table 5.1. The table gives the maximum axial load, as well as the primary, secondary, and total moments attained, the maximum deflection at mid-span, the maximum tensile, compressive and transverse (when available) strains, the maximum curvature and curvature ductility at mid-span and the modes of failure. Some of the experimental values were not reported in the table due to malfunction of some of the instruments during testing.

5.1 Series One: Concentric Load

The results of specimens tested with concentric loads (that is specimens labeled BC-OL3EO and BC-2L3EO) are presented in Fig. 5.1 to Fig. 5.5. Figure 5.1 shows the curves presenting the load versus deflection at different locations along the beam column. It is seen that the maximum deflections attained by the specimens were respectively 0.016 in. and 0.038 in. for unwrapped and wrapped specimens. Note however that Specimen BC-21-3-130 (see Table 5.1) underwent excessive deflection (0.26 in.) due to initial misalignment. These deflections obviously generate secondary moments, as presented in Fig. 5.2. It is observed that the secondary moment in control specimens (BC-01-3130) reached 6 kip-in which represents 0.81 % of ultimate moment in pure flexure, whereas it reached 3.8 % of ultimate moment in specimens with 2 layers.

Fig. 5.3 presents the strain distribution across the beam-column depth at midspan, for different loading levels. It is seen that in all specimens, the strain distribution across the beam-column depth at mid-span was fairly uniform. However, this feature was not observed in the specimen that underwent excessive deflection, that is BC-21_3ISO (see Fig. 5.3c). The latter experienced significant strain gradients across the section due to secondary moments, particularly at higher loadings. This specimen failed prematurely since its maximum strain at the center (around 960με) was well below the ultimate strain. The maximum strain reached in control specimen approached 1800με indicating that the maximum load attained (i.e., 422 kips) approached the capacity of the beam-column.

The longitudinal compressive strain distributions along beam-column length for different loading levels are displayed in Fig. 5.4 for specimens BC-OL3EO and BC2L3EO only as no readings were performed on the other specimens. It is observed that the strains are fairly uniform along the beam-column. In specimen BC-2L3EO (Fig. 5.4b), strain readings on short (compression) sides (SS) are greater than those on long tension) sides (LS), due to secondary moments, as already pointed out earlier.

Fig. 5.5 presents the load versus transverse surface strain at mid-span of wrapped specimens BC-2L3EO and specimen BC-OL3EO (with no corbels). It is observed that in control specimen with no corbels (Fig. 5.5b) the transverse strains at the different sides of the beam-column were quite different and depended on the magnitude of the axial compressive strain. They were higher in the 14 inch-top side which was more compressed (From LVDT readings). It attained 480με at maximum load. The opposite 14 inch-side experienced a maximum strain less than 200με at maximum compressive load. the transverse strains at the 8 inch-sides were around 310με and 240με. In the specimen that experienced excessive secondary moment (see Fig.5.5c) the transverse strains were also different at different sides, depending on the compressive train. At maximum compressive load, the maximum transverse strain at the 8 inch-side was around 280με, whereas it was 220με at the 14 inch-side. This

would correspond to transverse stresses of 1820 psi and 1430 psi, respectively. The wrapped specimens with no corbels which were subjected to almost perfect concentric loading (and hence similar compressive strains at all column faces), experienced similar transverse strains at all faces (see Figs. 5.5d to f), around 500 to 600με:

5.2 Series 2: 3-inch Eccentricity

The results of specimens tested with 3-inch eccentric compressive load (that is specimens labeled BC-OL3E3 and BC-2L3E3) are presented in Fig. 5.6 to Fig. 5.9. Figure 5.6 presents the primary, the secondary and the total moment versus the midspan deflection. Note that the readings of mid-span deflection were not available due to malfunction of the transducer. It is seen that the secondary moment increased almost linearly to reach 21 % of the total moment at ultimate load for BC-2L3E3.

The strain distribution across the beam-column depth at mid-span for selected total applied moments up to ultimate are displayed in Fig. 5.7. It is seen that the compressive strain attained 2698με for specimen BC-OL3E3 and 4036με for BC2L3E3. Note that the neutral axis of the wrapped specimen was slightly deeper (from compression face) than the unwrapped specimen.

The longitudinal compressive strain distributions along beam length for different loading levels are presented in Fig. 5.8. It is observed that the strains are fairly uniform particularly in the zone between corbels and for low to moderate loadings.

Fig. 5.9 presents the applied total moment versus the transverse surface strain around the mid-span section of specimens BC-2L3E3 (no transverse strain readings are available for BC-OL3E3). It is observed that the east side, that is the 8-inch Compression face experienced the highest transverse strain (around 1600με, that is a transverse tensile stress of 10,400 psi), whereas in the 8-inch tension face (west side), no transverse strain was observed.

The transverse strain in top and bottom sides (14-inch faces) attained 1504E and 350,ue,that is an average strain of 250413. Note that the strain gauges were glued at face centers, which were in compression (see strain distribution across depth, Fig. 5.7).

5.3 Series 3: 6-inch Eccentricity

The results of specimens tested with 6-inch eccentric compressive load (that is specimens labeled BC-OL3E6 and BC-2L3E6) are presented in Fig. 5.10 to Fig. 5.13. Figure 5.10 presents the primary, the secondary and the total moment versus the mid-span deflection. It is seen that the secondary moment increased almost linearly to reach 12 % and 15 % of the total moment at ultimate load for BC-OL3E6 and BC-2L3E6, respectively. Note that the maximum mid-span deflection of specimen BC-OL3E6 was low as the specimen failed prematurely (see Table 5.1).

The strain distributions across the beam-column depth at mid-span for selected total applied moments are displayed in Fig. 5.11. It is seen that compressive strain attained 1600με for specimen BC-OL3E6 and 4300με for BC-2L3E6. Note that the neutral axis of unwrapped specimen was around 7 inches compared to 8 inches (from compression face) for wrapped specimen.

The longitudinal compressive strain distributions along beam-column length for different loading levels are presented in Fig. 5.12. It is observed that the strains are fairly uniform particularly in the cental zone away from corbels and for low to moderate loadings. The non-uniformity of strains in tension face in unwrapped specimen is due to cracking.

Fig. 5.13 presents the applied total moment versus the transverse surface strain around the mid-span section of specimen BC-21_3136 (no transverse strain readings are available for control unwrapped specimen BC-OL3136). It is observed that the east side, that is the 8-inch compression face experienced the highest transverse strain (around

3600με corresponding to a transverse tensile stress of 23,400 psi), whereas in the 8-inch tension face (west side) no transverse strain was observed.

The transverse strains in top and bottom sides (14-inch face) were small, less than 100με. Note that the strain gauges were glued at the centers of the specimen faces, which were close to neutral axis but in compression (see strain distribution across the depth, Fig. 5.7).

5.4 Series 4: 12-inch Eccentricity

The results of specimens tested under 12-inch eccentric compressive load (that is specimens labeled BC-OL3E12, BC-OL3E12-RL2, and BC-2L3E12) are presented in Fig. 5.14 to Fig. 5.17. Note that specimen BC-OL3E12-RL2 is BC-OL3-E12 that was repaired with 2 layers of CFRP after it has been tested. Fig. 5.14 presents the primary, the secondary and the total applied moment versus the mid-span deflection. It is seen that the secondary moment increased almost linearly to reach 10.9% , 10.8 %, and 9.7% of the total moment at ultimate load for BC-OL3E12, BC-OL3E12-RL2, and BC-2L3E12, respectively.

The strain distributions across the beam-column depth at mid-span for selected total applied moments are displayed in Fig. 5.15. It is seen that the compressive strain attained 2637με and 6790με for specimens BC-OL3E12, BC-OL3E12-RL2, and 4800με for BC-2L3E12. Note that the neutral axis of the unwrapped specimen was around 5.5 in. (from compression face) compared to 7 in. for the wrapped specimens.

The longitudinal compressive and tensile strain distribution along the column-beam length for different loading levels are presented in Fig. 5.16. It is observed that the strains are fairly uniform along the beam-column, particularly in the central zone and for low to moderate loads. The non-uniformity of strains in tension face in unwrapped specimen is due to cracking.

Fig. 5.17 presents the applied total moment versus the transverse surface strain around the mid-span section of specimen BC-0L3E12-RL2 and BC-2L3E12-2 (no transverse strain readings were made for BC-OL3E12 and BC-ZL3E12-1). Again, it is observed that the East side, that is the 8-inch compression face experienced the highest transverse strain (around 5,600με corresponding to a transverse tensile stress of 36,400 psi), whereas in the 8-inch tension face (West side), no transverse strain was observed. Practically no transverse strains were read in top and bottom sides (14-inch faces) as the neutral axis coincided with the location of the strain gauges.

5.5 Series 5: 16-inch Eccentricity

The results of specimens tested under 16-inch eccentric compressive load (that is specimens labeled BC-0L3E16 and BC-2L3E16) are presented in Fig. 5.18 to Fig. 5.21. Figure 5.18 presents the primary, the secondary and the total applied moment versus the mid-span deflection. It is seen that the secondary moment increased almost linearly to reach 8 % and 9 % of the total applied moment at ultimate load for BCOL3E16 and BC-2L3E16, respectively.

The strain distributions across the beam-column depth at mid-span for selected total applied moments are displayed in Fig. 5.19. It is seen that the compressive strain attained ? 2790με for specimen BC-0L3E16 and 4200με for BC-2L3E16. Note that the neutral axis of unwrapped specimen was around ? 4.5 inches from compression face compared to 5.2 inches for wrapped specimens.

The longitudinal compressive strain distributions along beam length for different loading levels are presented in Fig. 5.20. It is observed that the strains are fairly uniform, particularly at the central zone and for low to moderate loads. Obviously at a higher applied load, cracks develop, which explains some of the high strain readings. Fig. 5.21 presents the applied total moment versus the transverse surface strain around the mid-span section of specimens BC-0L3E16 and BC-2L3E16. It is observed

in the wrapped specimen (BC-2L3E16) that the East side, that is the 8-inch compression face, experienced the highest transverse strain (around 3200AE, that is a transverse tensile stress of 20,800 psi), whereas in the 8-inch tension face (West side), no transverse strain is observed. The transverse strains in top and bottom sides (14inch face) were practically equal to zero, the location of the surface strain gauges being close to the neutral axis (see strain distribution across the depth, Fig. 5.19).

5.6 Series 6: Pure Flexure

The results of specimens tested in four-point flexure with no axial load (that is specimens labeled BC-OL3-FL, BC-2L3-FL (with corbels), BC-2L3-FL1, BC-2L3-FL2 and BC-2L3-FL3) are presented in Fig. 5.22 to Fig. 5.24. Note that BC-2L3-FL was a specimen with corbels, whereas specimens BC-OL3-FL, BC-2L3-FL1, BC-2L3-FL2 and BC-2L3-FL3 were simple rectangular beams with no corbels spanning 132" (total length =140").

Fig. 5.22 presents the applied moment versus the mid-span deflection. It is seen that the moment corresponding to first cracking is 140 kip-in for unwrapped and around 160 kip-in for wrapped specimens, whereas the moment at yield of steel is respectively around 600 kip-in and 700 to800 kip-in. It is seen that the post yielding moment-deflection curve of the wrapped specimens is consistently linear.

The strain distribution across the beam depth at mid-span for selected applied moments are displayed in Fig. 5.23. It is seen that the compressive strain attained 4059 με in BC-OL3-FL, 5,000gG in BC-2L3 -FL (corbel), and 2,200με in average in BC-21_3-FLI, 2 and 3. The neutral axis at yielding of steel is seen to be equal to 2.5inches from compression face for BC-OL3-FL, whereas it is 5 inches and 4.5 inches in average for BC-2L3-FL(corbel), and BC-2L3-FL1, 2, and 3, respectively.

Fig. 5.24 shows the applied moment versus the longitudinal strains at different locations of mid-span section. The cracking and the yielding moment can clearly be identified in these curves. Fig. 5.25 presents the curves of the applied moment versus the transverse strain on the compression face of mid-span section. It is observed that the transverse train attained 1,600με for the unwrapped specimen and over 900με in average in wrapped specimens.

Table 5.1 Maximum Experimental Results (f_c = 3 ksi)

Specimen	Pmax	Moment			Midspan	Microstrain (Max)			n.a depth	Curvature					Failure mode
		primary	secondary	total	Deflection	compression	tension	Transverse	at yield	maudmun	confluncond	yield	ductility	confluncof	
	kip	kip.in	kip.in	kip.in	in.										
1	2	3	4	5	6		8	9	10	11	12	13	14	15	16
BCOL-EO	378	0	6	6	0.016	-1751	-1246	NA	NA	-	-	na	na	-	Crushing of concrete at end (premature failure)
BGoL-EO(no comb.)	422	0	4.6	4.6	0.011	-1652	-1379	NA	NA	-	-	na	na	-	fc=4.6 ksi, Crushing of concrete near cfrp capping
BC2L-EO	380	0	90	90	0.237	-958	-1533	NA	NA	-	-	na	na	-	Busting of concrete at a comer at end (premature failure)
BC-2L-EOI(no comb.)	488	0	7.3	7.3	0.015	-1627	-1324	NA	NA	-	-	na	na	-	fc=4.6 ksi,Bursting and fracture of cfrp on comers due to compression
BC2L-EO2(- cab.)	520	0	19.8	19.8	0.038	-1986	-1862	NA	NA	-	-	na	na	-	fc=4.6 ksi. Bursting and fracture of chp on comers due to compression
BG2L-03(w comb.)	542	0	4.9	4.9	0.009	-2077	-1503	NA	NA		-	na	na	-	fc=4.6 ksi, Bursting and fracture of o on comers due to c sion
BCOL-E3	276	829	-	829	-	-2698	791	NA	10	249		1000	0.25		Crushing of concrete in compression
BC-2L-E3-1	300	901	238	1139	0.79	-4036.	1418	1630	8.7	390	1.56	606	0.64	2.58	Bursting of concrete at a comer in compression
BC-2L-E3-2	423	1268	235	1503	0.56	-3839	1744	2066	0	0	0.00	0	0.00	0.00	fc=5.4ksi, Tensin fracture of frp followed b bursting in compression at comer
BCOL-E6	160	959	133	1092	0.833	-1598	1601	NA	7	229		400	0.57		Premature failure at corbels
BC-2L-E6-1	186	1071	184	1255	1.31	-4265	2650	3300	7.6	494	2.16	455	1.09	1.90	Bursting of concrete at a toner in compression
BC-2L-E6-2	235	1413	215	1628	0.843	-4676	8095	1131	7.6	912	1.85	455	2.01	1.85	fc=5.4ksi, Tensin fracture of followed b bursting in compression at comer
BCOL-E12	69.6	835	102	937	1.46	-2637	4097	NA	5.5	481		308	1.56		Crushing of concrete in compression
BC-2L-E12-1	99	1193	128	1321	1.286	-4796	4397	NA	7.4	657	1.37	435	1.51	0.97	Bursting of concrete at a toner in compression
BC-2L-E12-2	120	1448	177	1625	1.61	-4861	12636	1891	6	1250	1.90	333	3.75	2.48	fc=5.4ksi, Tensin fracture of imp (no bursting in compression)
BC-2L-E12R	102	1213	147	1360	1.443	-6787	5506	5600	6.5	878	1.83	364	2.41	1.54	Bursting of concrete at a comer in compression
8COL-E16	54	864	74	938	1.37	-2790	5598	NA	4.6	599		270	2.22		fc=4.6 kst, Crushing of concrete in compression
BC-2t.-E16-11	80	1280	129	1409	1.616	-4190	6378	3200	5.2	755	1.26	294	2.57	1.16	Bursting of concrete at a toner in compression followed by rupture of CFRP In tension
BG2L-E16-2	79	1264	109	1374	1.39	-2722	7646	706	5.8	741	0.98	323	2.30	0.89	fc=5.4ksi, Tensin fracture of no bursting in compression)
BCOL-FL	0	741	0	**741**	1.69	-4059	28000	NA	2.5	2290		211	10.88		Crushing of concrete in compression
BC-2L-FL-1	0	1039	0	1039	1.28	-2776	11462	806	4	1017	0.44	250	4.07	0.37	Tension Failure at Bottom and Buckling at Compression Face
BC-2L-FL-2	0	1142	0	1142	1.63	-1348	12589	858	4	996	0.43	250	3.98	0.37	Tension Failure at Bottom and Bucking at compression Face
8C-2L-FL-3	0	1028	0	1028	1.26	-2500	9000	1270	4.7	821	0.36	274	3.00	0.28	Tension Failure at Bottom and Budding at Compression Face
BC-2L-FL(corbel)	0	1175	0	1175	1.35	-5000	11681	NA	5	1192	0.52	286	4.17	0.38	Bursting of concrete at a comer in compression followed by rupture of CFRP In tension

compared. Note that, except for pure bending conditions, the maximum curvature and the curvature ductility in wrapped specimens are greater than those of corresponding unwrapped specimens.

The maximum moment capacity in pure flexure achieved by the wrapped specimens was 1175 kip-in, that is 59 % increase with respect to unwrapped specimens. The maximum secondary moment due to the so-called P-Delta effect varied from 7.9 % to 12.2 % for unwrapped and from 9.2 % to 21 % for wrapped specimens, with respect to the total applied moment. Typical views of the beam-columns after tests are presented in Fig. 6.1. It was observed that the wrapped specimens subjected to an axial load in addition to flexure ruptured by bursting of corners at the compressive face accompanied by tension fracture of CFRP fabric in the tension face (see Fig. 6.1). The wrapped specimen under pure flexure failed by rupture of the CFRP wrap at the tension face and buckling at the compression face.

In the following sections the behavior of wrapped specimens will be presented, analyzed and compared to control specimens mainly in terms of the applied moment versus the mid-span deflection, the longitudinal strain distribution at mid-span, the maximum transverse strain behavior at mid-span and the ductility enhancement achieved by the CFRP wrapping. Design considerations and interaction diagrams of CFRP wrapped beam-columns will be discussed in the next chapter.

6.2 Applied Moment versus Mid-span Deflection Behavior

Representative curves of applied total moment versus midspan deflection are presented in Fig. 6.2. Typically, the unwrapped specimens featured a higher initial slope compared to wrapped specimens. However, this is reversed as the load progressed, the lower the eccentricity the higher the applied moment at which the reversal occurred. This is attributed to the fact that at the initial stage of loading the outer CFRP shells, which possess a lower modulus of elasticity than that of steel, were engaged before the longitudinal steel reinforcement in wrapped specimens, compared to control specimens

where the steel contributed earlier. For flexure controlled conditions, the strengthened beam-columns exhibited a higher flexural stiffness compared to control specimens. This difference in stiffness increased with increasing eccentricity. This can be attributed to the fact that as the eccentricity increased, the control specimens featured more cracks which obviously affected the flexural stiffness, compared to wrapped specimens where the *effect* of concrete cracking was minimal.

The total moment corresponding to first cracking varied from 130 kip-in to 150 kip-in for unwrapped specimens. This is slightly higher than the theoretical value as per the ACI code, which is equal to 108 kip-in. The cracked moment was not apparent from the curves of wrapped specimens, although a slight change in the slope at roughly 140 kip-in was noticed in the specimen subjected to pure flexure.

Yielding of steel, which is characterized by the change of the post-crack slope, is clearly apparent in wrapped specimens although more evident in control specimens. However, in wrapped specimens yielding occurred at a higher applied moment and a higher mid-span deflection than in control specimens (see Fig. 6.2). This is attributed to the retention of composite action in the tension face which lowered the neutral axis and to the confining effect which allowed the concrete in compression to achieve a higher strain (see strain distributions in Fig. 6.4). This resulted in a higher curvature and hence a greater displacement at yielding of steel. The branch corresponding to post yielding of steel is seen to be quasi-linear ascending in wrapped and perfectly plastic in control specimens. In wrapped specimens under pure bending, the slope of this branch is 30% that of the pre-yielding branch. However, this value is expected to increase with the modulus of elasticity and the number of layers of the FRP wrap.

Generally, wrapped specimens achieved higher moment capacities than control specimens, although the difference in moment capacities decreased as the axial load increased. This feature can also be seen from the experimental interaction diagrams presented later in Fig. 7.2. The wrapped beam-columns also exhibited substantially large

deflections beyond yielding stress of steel. However, given the applied moment, they showed reduced deflections and thereby increased serviceability.

The effect of the load eccentricity on the behavior of wrapped specimens is seen in Fig. 6.3, which presents the curves of applied moment versus mid-span deflection of specimens with eccentricities of 3" (75 mm), 6" (150 mm), 12" (300 mm), and infinity
(pure flexure). The following observations can be reported:

(a) The flexural stiffness, characterized by the slope of the curve, increased as the eccentricity decreased. The stiffness enhancement due to axially applied load. This enhancement was more effective when the location of applied load was closer to the center of the specimen cross-section.

(b) Given the applied moment, the specimens with lower eccentricities featured less displacement.

(c) The lower the eccentricity, the higher the moment and the corresponding displacement at which yielding of steel occurred.

6.3 Strain Distribution at Mid-span Section

The strain distributions across the beam-column depth at mid-span for selected total applied moments are displayed in Fig. 6.4. The strain distribution is seen to be essentially linear up to rupture for both wrapped and unwrapped specimens. The increase; in the compressive strain due to the confinement effect varied from 49.6 % to 166 %'. It was more pronounced for specimens governed by flexure. Given the eccentricity, the neutral axis depth from compression face of wrapped specimens was smaller than that of corresponding control specimens. Also, the neutral axis depth decreased as the eccentricity increased. However, this increase was slightly and consistently more pronounced in control specimens.

The superior maximum compressive strain achieved by wrapped compared to unwrapped specimens; is clear from the figures. This is attributed to the confinement effect of the CFRP jacket in the compression zone. As the eccentricity increased the

maximum tensile strain also increased thereby engaging more efficiently the CFRP weaves in the longitudinal direction. This efficiency is optimized in pure flexure where rupture occurred by failure of the CFRP material at a tensile strain approaching 12600ge.

6.4 Curvature and Ductility

-Fig. 6.5 presents the behavior of the maximum curvature and the curvature ductility with increasing axial load in specimens under combined conditions. As expected the maximum curvature as well as the ductility decreased as the axial load increased for both wrapped and unwrapped specimens. Given the axial load, the curvature and the ductility achieved by the wrapped specimens were consistently superior to those of corresponding control specimens. This feature was more pronounced for lower axial loads. This enhancement in deformation capabilities was attributed to the confinement provided by the CFRP jacket, which resulted in higher stain capacities.

6.5 Transverse Strain at Mid-span

Fig. 6.6 shows typical curves representing the applied total moment versus the transverse surface strain around the mid-span section of wrapped specimens where readings were available. It is observed that the transverse strain is present in the compression zone from the early stage of loading. The confinement provided by the wrap, which is directly related to the transverse strain (the higher the transverse strain, the greater the confining pressure), was engaged earlier in the loading for specimens with smaller eccentricities (the smaller the eccentricity the earlier this engagement). This is due to the fact that these beam-columns have a greater cross-section area under compression since their neutral axis is deeper and are obviously subjected to a higher applied load for a given moment.

The 8-inch compression face experienced the highest transverse strain, whereas in the 8-inch tension face, no transverse strain was observed. It was also noted that the 63

transverse strain increased as the compressive longitudinal strain increased (see Fig. 6.4, strain distribution across the mid-span depth). The large transverse strains developed at the compression face after the confinement is engaged indicate significant expansion of the cover concrete. The strains increased as the displacement increased even though the applied load was essentially constant.

Since the strain gauges were glued at the face centers, the magnitude of the transverse strains in the 14-inch faces depends whether the center of the faces were in tension or in compression. Here it was also observed that the higher the compressive strain in the center of the face (see the strain distribution across the depth, Fig. 6.4), the greater the transverse strain. Therefore, when the longitudinal strains were tensile, the transverse strains were equal to zero, as clearly illustrated in the case of pure flexure.

CHAPTER 7

DESIGN CONSIDERATIONS OF WRAPPED BEAM-COLUMNS

This chapter provides preliminary recommendations as far as the design of FRP retrofitted beam-columns subjected to flexure in addition to an axial compressive load.

7.1 Design Philosophy

From experimental results it was observed that the concrete in the compression zone of wrapped beam-columns is effectively confined since the CFRP wrap achieved compressive strains varying between 4000 and 6000με with an average strain around 5000με. The transverse strains attained on the compression face of the retrofitted specimens are another indication of the confinement effectiveness of the wraps.

One way of calculating the capacity of RC beam-columns wrapped with FRP and subjected to a combined axial force-bending moment, is by considering this improved ultimate compressive strain to calculate the ultimate stress of confined concrete in compression using a reliable stress-strain model. This way of doing has already been used by other researchers to calculate the moment capacity of wrapped sections with conjunction of the Mander stress-strain model (Mander et al. 1988) for confined concrete (e.g. Xiao et al. 1996).

However Mander's model, although widely used for steel- and FRP jacketed RC columns, was originally developed for conventional RC columns. It is therefore based on an elastic perfectly plastic behavior of the jacket and hence considers the confining pressure constant after concrete has reached its compressive strength. While this may be representative for steel jacketed columns, it does not hold for FRP jacketed columns.

7.2 Stress-Strain Model

In this study the analytical bilinear stress-strain model developed specially for RC columns wrapped with FRP jackets (Mirmiran and Shahawy 1997) is used to calculate the compressive strength of confined concrete, whereas the maximum strain is taken as 0.005 as confirmed by the experimental data obtained in this study. According to the model, the confined strength of concrete, f_{cc}, can be computed from:

$$f_{cc} = f_c : +3.38 f_r^{O.7} \qquad (7.1)$$

where f, is the compressive strength of unconfined concrete and f, is the confinement pressure. It must be noted that recent experimental studies (e.g. Harries et al. 1996)
showed that the stress-strain curve describing FRP jacketed RC columns are also bilinear and very similar in shape to circular columns.

The model expressed by Eq. (7.1) was derived on the basis of experiments performed on circular columns. However, while all of the section is fully confined in a circular column, considerable dilation of the section is required before the flat sides of the wraps are engaged in the confinement of a rectangular column. Due to the relatively small strain capacity of the CFRP fabric, the wrap will typically rupture at its comers before the sides of the wrap can develop any significant confinement. This type of failure has been observed in many of the tested specimens as will be reported later. In addition and contrary to a circular column, the lateral confining pressure differs in the two axes in a rectangular column. Clearly, this should be reflected in the calculation of the confining pressure in the interim of reliable experimentally - based models for rectangular columns.

One way of adjusting the confining pressure is by using an effective confinement ratio based on the shape of the section and defined as the area of effectively confined concrete over the gross-sectional area (see Fig. 7.1). For a rectangular column the lateral confining stresses induced by the jacket in the x and y directions, $f_{r,x}$ and $f_{r,y}$, are:

$$f_{r,x} = P_{j,x}\, k_e\, f_j \tag{7.2}$$

$$f_{r,y} = P_{j,y}\, k_e\, f_j \tag{7.3}$$

where k_e is the effective confinement ratio given by:

$$k_e = A_e / A_{ce} \tag{7.4}$$

where A_e and A_{ce} are respectively the effectively confined and concrete core areas, given by (see Fig. 10 for definitions):

$$A_e = t_x\, t_y - ((w_x^2 + w_y^2)/3) - A_S \tag{7.5}$$

and

$$A_{ee} = A_e - A_S \tag{7.6}$$

with $w_x = t_x - 2r$ and $w_y = t_y - 2r$. The section area ratios of FRP wraps $p_{j,x}$ and $p_{j,y}$ are given by:

$$P_{j,x} = 2\, t_j / t_x \tag{7.7}$$

$$P_{j,y} = 2\, t_j / t_y \tag{7.8}$$

where t_j is the thickness of the wrap. The average jacket stress f_j when the peak axial load is attained can be calculated as:

$$f = E_j\, \epsilon_{j,experimental} \tag{7.9}$$

where E_j and $E\epsilon_{j,experimental}$ are the modulus of elasticity of FRP wrap (see Table 4.3) and the average experimental transverse strain, which was found to be 0.003 in this study. Recentstudies (Restrepol and DeVino 1996) reported values of ϵ_j of the order of 0.005.

Given the geometrical properties of the wrapped specimens considered in this study, the following values were obtained: $p_{j,x}$ = 1.0 %, $p_{j,y}$ = 0.57 %, w_x = 6 in., w_y = 12 in., A_e = 50.24 in.^{2}, A_{CC} = 110.24 in .^{2}, k_e = 0.46, f_j = 22 ksi, and $f_{r,max}$ = 90 psi. This resulted in f_{cc} = 3.7 ksi. Note that the value of the effective confinement ratio obtained in this study (k_e = 0.46) compares quite well with the empirical value of 0.5 suggested by other researchers (e.g. Seible 1997) for rectangular sections having an aspect ratio below 1.5.

7.3 Interaction Diagram

The points defining the experimental maximum values of axial compression and corresponding maximum bending moment are plotted in Fig. 7.2 in terms of the ratios P_n/P_o. and M_n/M_o for both wrapped and unwrapped specimens along with the corresponding theoretical interaction diagrams, for comparison. Note that P_o and M_o are the experimental axial force and corresponding bending moment capacity. The theoretical values of wrapped beam-columns were calculated as for control specimens but with maximum stress and ultimate strain pertaining to confined concrete. The ultimate strain of the CFRP fabric was taken as ϵ_j=12000$\mu\epsilon$, as confirmed by experimental evidence described earlier.

With reference to Fig. 7.2, the following observations can be made:

(a) For control specimens the experimental and theoretical results were very close.

(b) For wrapped specimens, the experimental results were consistently greater and compared reasonably well with the theoretical values. Therefore, within the conditions and the limits of this study, the proposed design procedure was safe and adequate.

(c) In wrapped specimens, the point corresponding to the balanced condition moved slightly downwards with respect to that of unwrapped specimens.

(d) The CFRP jacketing improved the uniaxial capacity of the beam-columns; the maximum gain achieved was slightly below 30%. However it enhanced significantly the flexural capacity of the beam-columns since a gain of more than 54% and 74% was observed under pure flexure and under combined conditions, respectively.

(e) The source of increase in pure flexure is mainly attributed to the longitudinal weaves of the CFRP fabric. However, above the balanced condition the contribution of the transverse weaves increased with increasing axial load to become predominant in pure compression while that of the longitudinal weaves attenuated.

CHAPTER 8

CONCLUSIONS AND RECOMAMNDATIONS

This chapter presents the conclusions reached in this study. It also provides some recommendations for further studies.

8.1 Conclusions

The results of an experimental investigation on the performance of reinforced concrete rectangular beam- columns strengthened with externally applied bi-directional carbon fiber reinforced plastic material were presented. Results showed that the strength capacity of beam-columns improved significantly as a result of the combined action of the longitudinal and the transverse weaves of the bi-directional composite fabric. The longitudinal CFRP elements contributed mostly to flexural capacity, whereas the transverse elements enhanced the compressive capacity of the compression zone through confinement action. A design procedure of such elements was also suggested.

The following conclusions can be drawn from the study:

1. The CFRP jacketing improved the uniaxial capacity of the beam-columns; the maximum gain achieved was slightly below 30%. However, it enhanced significantly the flexural capacity of the beam-columns where a gain of more than 54% was observed in pure flexure. Under combined conditions, that gain reached 70%. While the source of increase in pure flexure was mainly attributed to the longitudinal weaves of the CFRP fabric, the contribution of the transverse weaves within the compression controlled zone increased with increasing axial load to become predominant in pure compression.

2. The increase in the compressive strain due to the confinement effect varied from 49.6 % to 166 %. It was more pronounced for specimens governed by flexure.

3. Given the axial load, the curvature and the ductility achieved by the wrapped specimens were consistently superior to those of corresponding control specimens. This feature was more pronounced for lower axial loads.

4. Yielding of steel in wrapped specimens generally occurred at a higher applied moment and a higher mid-span deflection than in control specimens.

5. The transverse confinement was engaged in the compression zone from the early stage of loading.

6. Finally, within the conditions and the limits of this study, the proposed design procedure based on the stress of confined concrete in the compression zone compared reasonably well with experimental results. The confined stress was calculated using the bilinear stress-strain model developed specifically for FRP wrapped columns in conjunction with an effective confinement ratio that takes into account the rectangular shape of the beam-columns.

8.2 Recommendations

The following recommendations can be formulated for considerations in further studies.

(a) The effect of concrete strength on the beam-column behavior should be undertaken. Therefore, a research study, similar to the present study as far as the procedure and the parameters are concerned, but with a concrete strength of 6000 psi is suggested.

(b) The experimental stress-strain behavior of rectangular specimens wrapped with FRP material and subjected to an axial load should be determined. In particular, the following parameters are of interest: the aspect ratio, the radius of the section corner and the concrete strength.

Chai, Y.H., Priestly, M.J.N., and Seible, F. (1991). *"Seismic retrofit of circular bridge columns for enhanced flexural performance".* ACI Struct. J., 88 (5), 572-584.

Chinn, J., and Zimmerman, R.M. (1965). *"Behavior of plain concrete under various triaxial compression loading conditions".* Technical Report No. WLTR-64-163, Air Force Weapons Laboratory, NM.

Considere, A. (1903). *"Resistance d la compression du beton acme et du beton frette".* G6nie Civil.

El Echary, H., (1997). *"Length effect on concrete filled FRP tubes using acoustic emission". MS* thesis, University of Central Florida, Orlando, FL.

Fardis, M.N., and Khalili, H.H. (1982). *"FRP-encased concrete as a structural material".* Mag. of Concrete Research., 34 (121), 191-201.

Fardis, M.N., and Khalili, H.H. (1981). *"Concrete encased in fiberglass-reinforced plastic".* ACI J., 78 (6), 440-446.

Gardner, N. J., and Jacobson, E. R. (1967). *"Structural behavior of concrete filled steel tubes".* ACI J., 64 (7), 404-413.

Harmon, T. G., Gould, P. L., Wang, E. and Ramakrishnan, S., (1998), *"Behavior of Confined Concrete Under Cyclic Loading, "* Proceedings of the Second International on Composites in Infrastructures, ICCI'98, H. Saadatmanesh and M.R. Ehsani, Editors, Tucson, Arizona, pp. 398-409.

Haroun, M.A., Feng, M.Q., Bhatia, H., Sultant, M., Hoshijima, T., Kobatake, Y., (1997), *"Testing Bridge Columns Enhanced by Fiber Composite Jackets, "* Recent Advances in Bridge Engineering: Advanced Rehabilitation, Durable Materials,

Nondestructive Evaluation and Management, Urs Meier and Raimondo Better, Editors, pp. 143-141.

Harries, K.A., Kestner, J., Pessiki, S., Sause, R., and Ricles, J., (1998), *"Axial Behavior of Reinforced Concrete Columns Retrofit with FRPC Jackets,"* Proceedings of the First International Using Composites in Infrastructure, ICCI `98, H. Saadatmanesh and M._ R. Ehsani, Editors, Tucson, Arizona, pp. 411-425.

Hosotani, M., Kawashima, K. and Hoshikima, J., (1997), "A *study on Confinement Effect of Concrete Cylinders by Carbon Fiber Sheets,"* Non metallic (FRP) Reinforcement for Concrete Structures, Proceedings of the Third International Symposium, Vol. 1, Sapporo, Japan, pp. 209-216.

Iyengar, K.T.S.R., Desayi, R., and Reddy, K.N. (1970). *"Stress-strain characteristics of concrete confined in steel binders'.* Magazine of Concrete Research (London), 22 (72), 173-184.

Kanatharana, J. and Lu, L.-W., (1998), *"Strength and Ductility of Concrete Columns Reinforced with FRP Tubes, "* Proceedings of the Second International on Composites in Infrastructure, ICCI `98, H. 'Saadatmanesh and M. R. Ehsani, Editors, Tucson, Arizona, pp. 370-384.

Kataoka, T. et al. (1997), *"Ductility of Retrofitted RC Columns with Continuous Fiber Sheets,"* Non metallic (FRP) Reinforcement for Concrete Structures, Proceedings of the Third International Symposium, Vol. 1, Sapporo, Japan, pp.547-554.

Katsumata, H., et al., (1998), "A *Study with Carbon Fiber for Earthquake-Resistant Capacity of Existing Reinforced Concrete Column, "* Proceedings of the Ninth Conference on Earthquake Engineering, Tokyo, Japan, Vol 7, pp. 517-522.

Katsumata, H., and Kobatake, Y., (1997), *"Retrofit of Existing Reinforced Concrete Columns Using Carbon Fibers, "* Non metallic (FRP) Reinforcement for Concrete Structures, Proceedings of the Second International Symposium, Vol. 1, Sapporo, Japan, pp. 555-570.

Kl6ppel, Von K., and Goder, W. (1957). *"Traglastversuche mit ausbetonierten Stahlroren and Aufstellyung einer Bemessungsformel".* Der Stahlbau (Berlin), 26 (1).

Knowles, B. R., and Park, R., (1970), *"Axial Load Design for Concrete Filled Steel Tubes, "* Journal of the Structural Division, Proceedings of the American Society of Civil Engineers, Vol. 96, ST10, pp. 2125-2153.

Kono, S. Inazumi, M. and Kaku, T., (1998), *"Evaluation of Confining Effects of CRFP Sheets on Reinforced Concrete members,"* Proceedings of the Second International on Composites in Infrastructure, ICCI `98, H. Saadatmanesh and M. R. Ehsani, Editors, Tucson, Arizona, pp. 343-355.

Lavergne, S., Labossiere, P., (1997), *"Experimental Study of Concrete Columns Confined by a Composite Jackets Under Combined Axial and Flexural Load, "* Annual Congress of the CSCE, Vol. 6, Edited by K. W. Neale, P. Labossiere et G. McClure, Sherbrooke, Quebec, pp. 11-20.

Mander, J. B., Priestely, M.J.N., and Park, R., (1984), *"Seismic Design of Bridge Piers, "* Research Report No. 84-2, University of Canterbury, New Zealand.

Mander, J.B., Priestley, M.J.N., and Park, R., (1988), *"Theoretical Stress-Strain Model for Confined Concrete,, "* Journal of Structural Engineering, ASCE, Vol. 114, No. 8, pp. 1804-1826.

Mirmiran, A., Kargahi, M., Samaan, M., and Shahawy, M.., (1996), *"Composite FRP - Concrete Column with Bi-Directional External Reinforcement, "* Proceedings of the First International Conference on Composites in Infrastructure, ICCI `96, H. Saadatmenash and M.R. Ehsani, Editors, Tucson, Arizona, pp. 903-916.

Mirmiran, A., and Shahawy, M., (1997), *"Behavior of Concrete Columns Confined with Fiber Composites",* Journal of Structural Engineering, ASCE, Vol. 123, pp. 583590.

Miyaushi, K., Nishibayashi, S. and Inoue, S., (1997), *"Estimation of Strengthening Effects with Carbon Fiber Sheet for Concrete column, "* Non metallic (FRP) Reinforcement for Concrete Structures, Proceedings of the Third International Symposium, Vol. 1, Sapporo, Japan, pp.217-232.

Monti, G., and Spoelstra, M. R. (1997). *"Fiber-section analysis of RC bridge piers retrofitted with FRP jackets "*. Proc. Structures Congress XV Building to Last, ASCE, Portland, OR., 884-888.

Nagasaka, T., Okamoto, T. and Tanigaki, M. (1997), *"Shear Strengthening effectiveness of Aramid Fiber Tapes on Existing R/C Columns, "* Non metallic (FRP) Reinforcement for Concrete Structures, Proceedings of the Third International Symposium, Vol. 1, Sapporo, Japan, pp. 539-546.

Nanni, A., and Bradford, N.M. (1995). *"FRP jacketed concrete under uniaxial compression"*. Constr. & Bldg. Mater., 9 (2), 115-124.

Nanni, A., and Norris, M. (1995).*"FRP jacketed concrete under flexure and combined flexure-compression "*. Constr. & Bldg. Mater., 9 (5), 273-281.

Newman, R., and Newman, J.B. *(1971). "Failure theories and design criteria for plain concrete".* Proc. Int. Civil Engr. Mater. Conf. on Struct., Solid Mech. And Engr. Design, Wiley Interscience, New York, NY, *936, 936-995.*

Pantazopoulou, S.J. *(1995). "Role of expansion on mechanical behavior of concrete".* J. Struct. Engr., ASCE, *121 (12), 1795-1805.*

Park, R., Priestley, M.J.N., *Gill, W., (1982), "Ductility of Square-Confined Concrete Columns, "* Journal of Structural Engineering, ASCE, *108(ST4), 929-950.*

Picher, F., Rochetter, P. and Labossie re, p. *(1996), "Confinement of Concrete Cylinders with CFRP, "* Proceedings of the First International Conference on Composites in Infrastructure, *ICCI `96,* Edited by Saadatmanesh and Ehsani, Tucson, Arizona, pp. *829-841.*

Pico, O. (1997). "Confinement effectiveness of square FRP tubes in hybrid columns". MS thesis, University of Central Florida, Orlando, FL.

Popovics, S., (1973), "Numerical Approach to the Complete Stress-Strain Curves for Concrete, " Cement and Concrete Research, Vol. *3,* No. *5, pp. 583-599.*

Priestley, M.J. N., Seible, F., and Alvi, *G. M., (1996), "Seismic Design and Retrofit* of *Bridges, "* John Wiley and Sons, Inc., p. *686.*

Priestley, M.J. N., Seible, F., Fyfe, E., *(1992), "Column Seismic Retrofit Using Fiberglass/Epoxy Jackets, "* First International Conference, Advanced Composite Materials for Bridges and Structures. K. W. Neale et P. Labossiere, Editors, pp. *287298.*

Priestley, M.J.N., (1991), *"Seismic Assessment of Exsting Concrete Bridges, "* In Seismic Assessment and Retrofit of Bridges, University of California, San Diego, Structural Systems Research Project Report No. SSRP 91-03, July 1991, pp. 84-149.

Priestley, M.J.N., (1991), *"Design of Retrofit Measure for Concrete Bridges, "* In Seismic Assessment and Retrofit of Bridges, University of California, San Diego, Structural Systems Research Report No. SSRP 91-03, July 1991, pp. 197-250.

Prion, H.G.L., and Boehme, J. (1994). *"Beam-column behavior of steel tubes filled with high strength concrete".* Canadian J. Civil Engr., 21 (2), 207-218.

Restrepol, III. I., and DeVino, B., (1996), *"Enhancement of the Axial Load Carrying Capacity of Reinforced Concrete Columns by Means of Fiberglass-Epoxy Jackets, "* Advanced Composite Materials in Bridges and Structures, Second International Conference, Canadian Society of Engineering, M.M. El-Badry, Editor, pp. 547-553.

Richart, F. E. , Brandtzaeg, A., and Brown, R. L. , *(1928), "Study of the Failure of Concrete under Combined Compressive Stresses, "* Bulletin 185, University of Illinois Engineering Experiment Station, Urbana, IL.

Richart, F. E. , Brandtzaeg, A., and Brown, R. L. (1929). *"Failure of Plain and Spirally Reinforced Concrete in Compression ".* Engineering Experiment Station Bulletin No. 190., University of Illinois, Urbana, IL.

Saadatmanesh M., Ehsani, M.R., Limin Jin, (1996), *"Behavior of Concrete Retrofitted with Fiber Composite Straps Under Cyclic Loading".* Fiber Composites Infrastructure. Proceedings of the First International Conference on Composites in Infrastructures, ICCI `96, H. Saadatmanesh and M.R. Ehsani, Editors, Tucson, Arizona, U.S.A., pp. 842-856. ,

Saadatmanesh, H., Ehsani, M. R. and Li, M.W. (1994). *"Strength and Ductility of Concrete Columns Externally Reinforced with Fiber Composite Straps". ACI* Struct. J., 91 (4), 434-447.

Saatcioglu, M., Razvi, S. R. (1992), *"Strength and Ductility of Confined Concrete, "* Journal of Structural Engineering, 118(6), 1590-1607.

Samaan, M., Mirmiran, A., and Shahawy, M., (1998), *"Modeling of Concrete Confined by Fiber Composites",* J. Struct. Engrg., ASCE (in Press).

Scherer, M.E. (1996). *"Design optimization and behavior of concrete filled FRP tubes".*MS thesis, University of Central Florida, Orlando, FL.

Scott, B.D., Park, R., and Priestley, M.J.N., (1982), *"Stress-Strain Behavior of Concrete Confined by Overlapping Hopps at Low and High Strain Rates, "* ACI Structural Journal, Vol. 79, No. 1, pp. 13-27.

Seible, F., (1997), *"Bridge Pier Rehabilitation with Continuous Carbon Fiber Wraps, "* Recent Advances in Bridge Engineering: Advanced Rehabilitation, Durable Materials, Nondestructive Evaluation and Management, Urs Meier and Raimondo Betti, Editors, Proceedings of the U.S./Canada/Europe Workshop on Bridge Engineering, Zurich 1415, July, pp 59-66.

Sheikh, S. A., (1982), "A *Comparative Study of Confinement Models, "* American Concrete Institute Journal, 79(4), 296-306.

Sheikh, S.A., and Uzumeri, S.M., (1980), *"Strength and Ductility of Tied Concrete Columns, "* Journal of Structural Division, ASCE, Vol. 106, No. 5, pp. 1079-1102.

Sheikh, S.A., and Yeh, C. (1986). *"Flexural behavior of confined concrete columns".* ACI J., 83 (3), 389-404.

Sheikh, S.A., and Yeh, C. (1992). *"Analytical moment-curvature relations for tied concrete columns".* J. Of Struct. Engr., ASCE, 118 (2), 529-544.

Sirbu, G. and al. (1997), *"Seismic Resistance of Reinforced Concrete Pier with Carbon Fiber Sheet Retrofitting, "* Non metallic (FRP) Reinforcement for Concrete Structures, Proceedings of the Third International Symposium, Vol. 1, Sapporo, Japan, pp.571578.

Watanabe, K., and al. (1997), *"Confinement Effect of FRP Sheet on Strength and Ductility of Concrete Cylinders Under Uniaxial Compression,"* Non metallic (FRP) Reinforcement for Concrete Structures, Proceedings of the Third International Symposium, Vol. 1, Sapporo, Japan, pp.233-238.

Xiao, Y., Martin, G. R., Yin, Z., Ma, R., (1996), *"Seismic Retrofit of Existing Reinforced Concrete Bridge Columns Using a Prefabricated Composite Wrapping System. "* Proceedings of the First International Conference on Composites in Infrastructure, ICCI `96, H. Saadatmanesh and M.R. Ehsani, Editors, Tucson, Arizona, U.S.A., pp. 903-916.

Ziara, M.M., Haldane, D., and Kuttab, A.S. (1995). *"Flexural behavior of beams with confinement".* ACI Struct. J., 92 (1), 103-114.

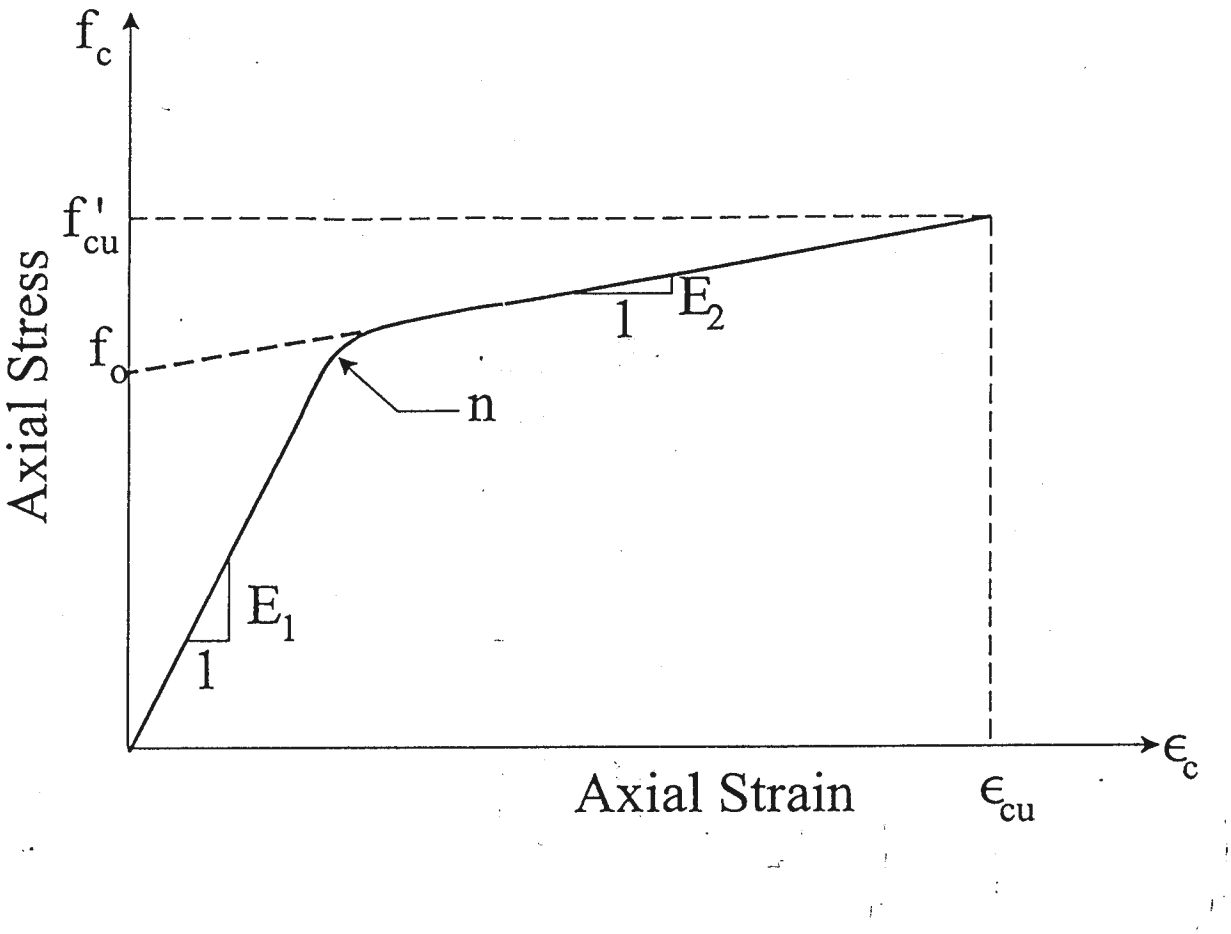

Fig. 3.1 Parameters of the Confinement Model for Wrapped Circular Columns

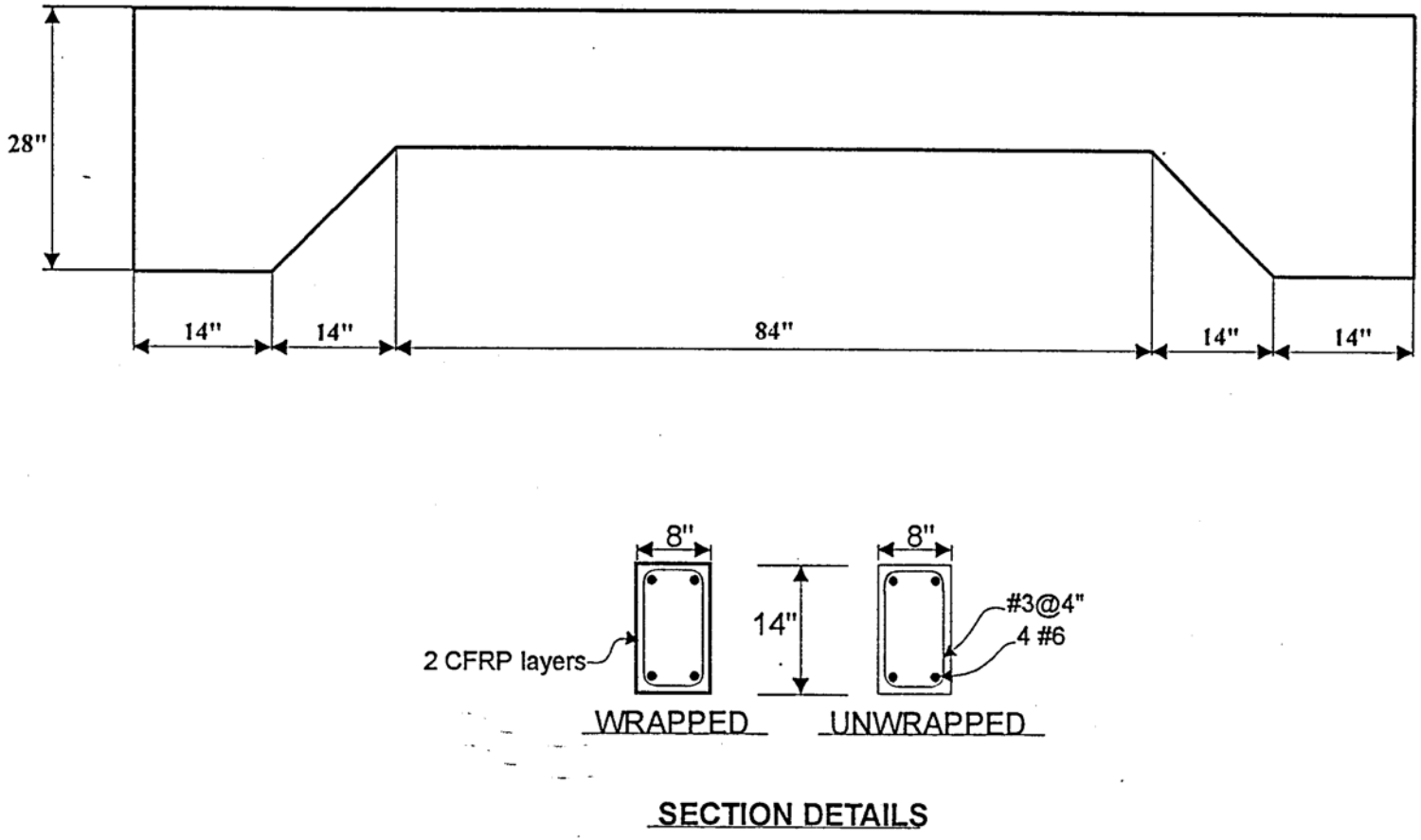

Fig. 4.1(a) Details of Specimen with Corbels

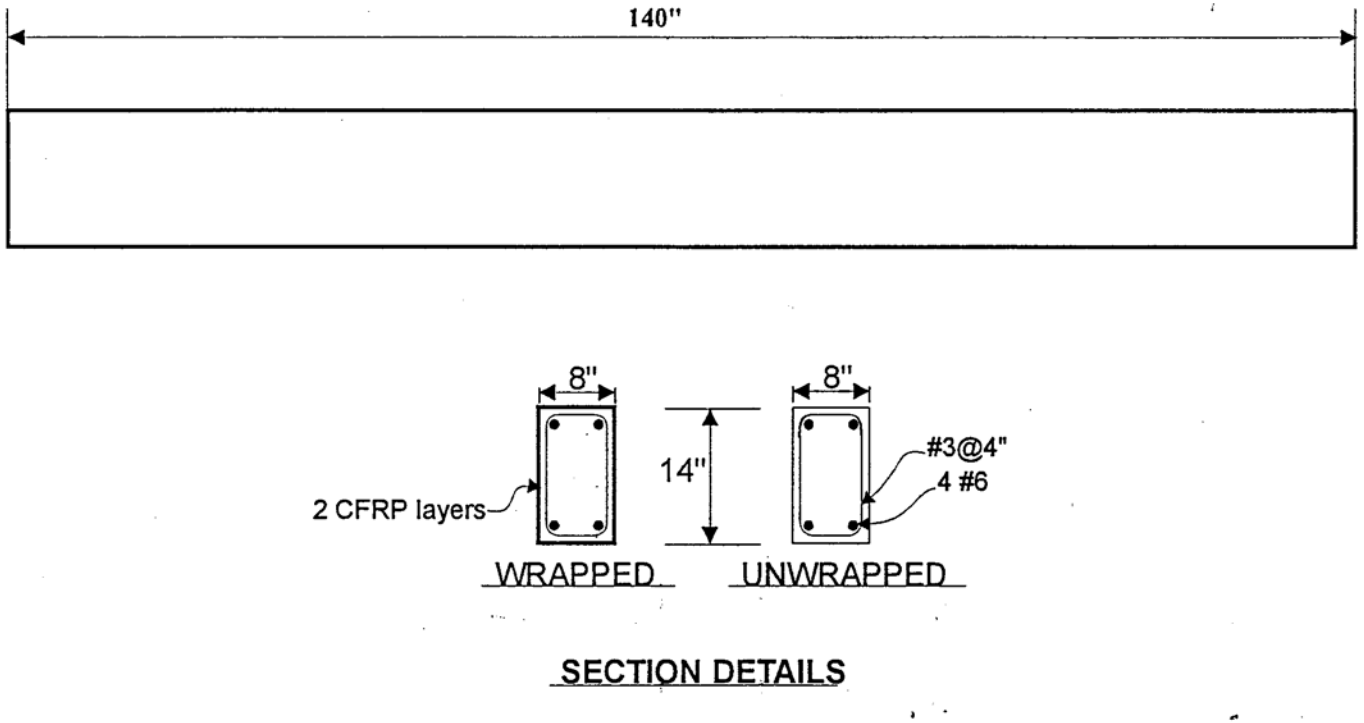

Figure 4.1 (b) Details of Specimen Without Corbels For Flexure

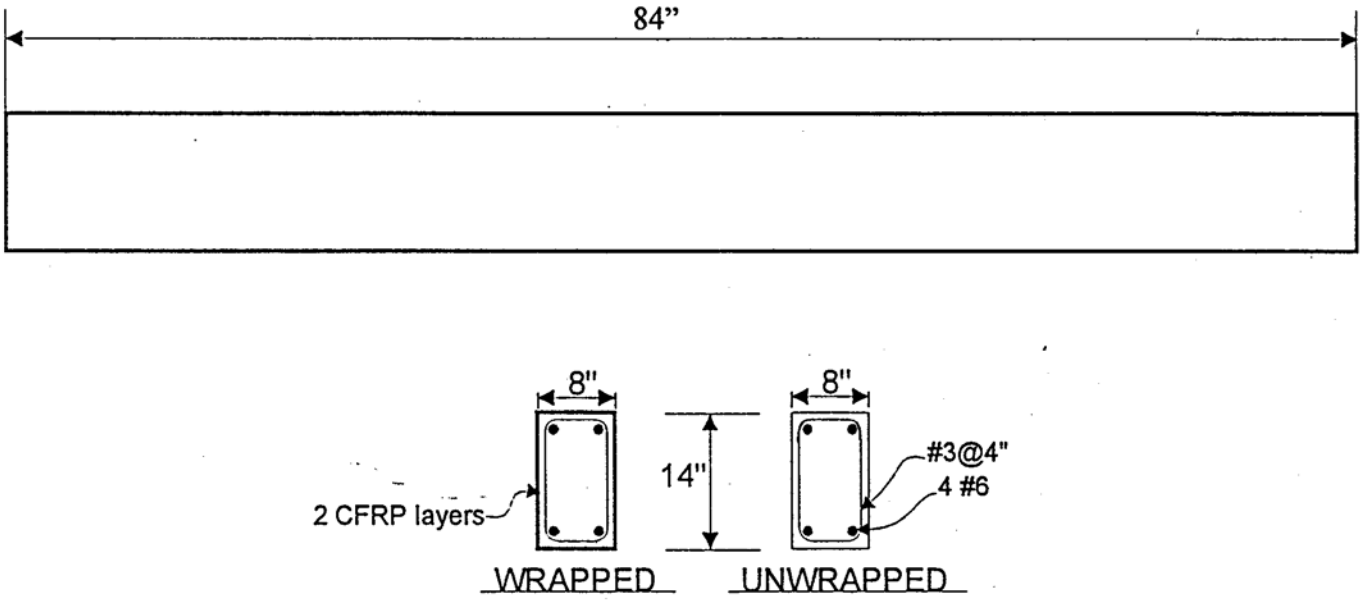

Figure 4.1 (c) Details of Specimen Without Corbels For Pure Compression

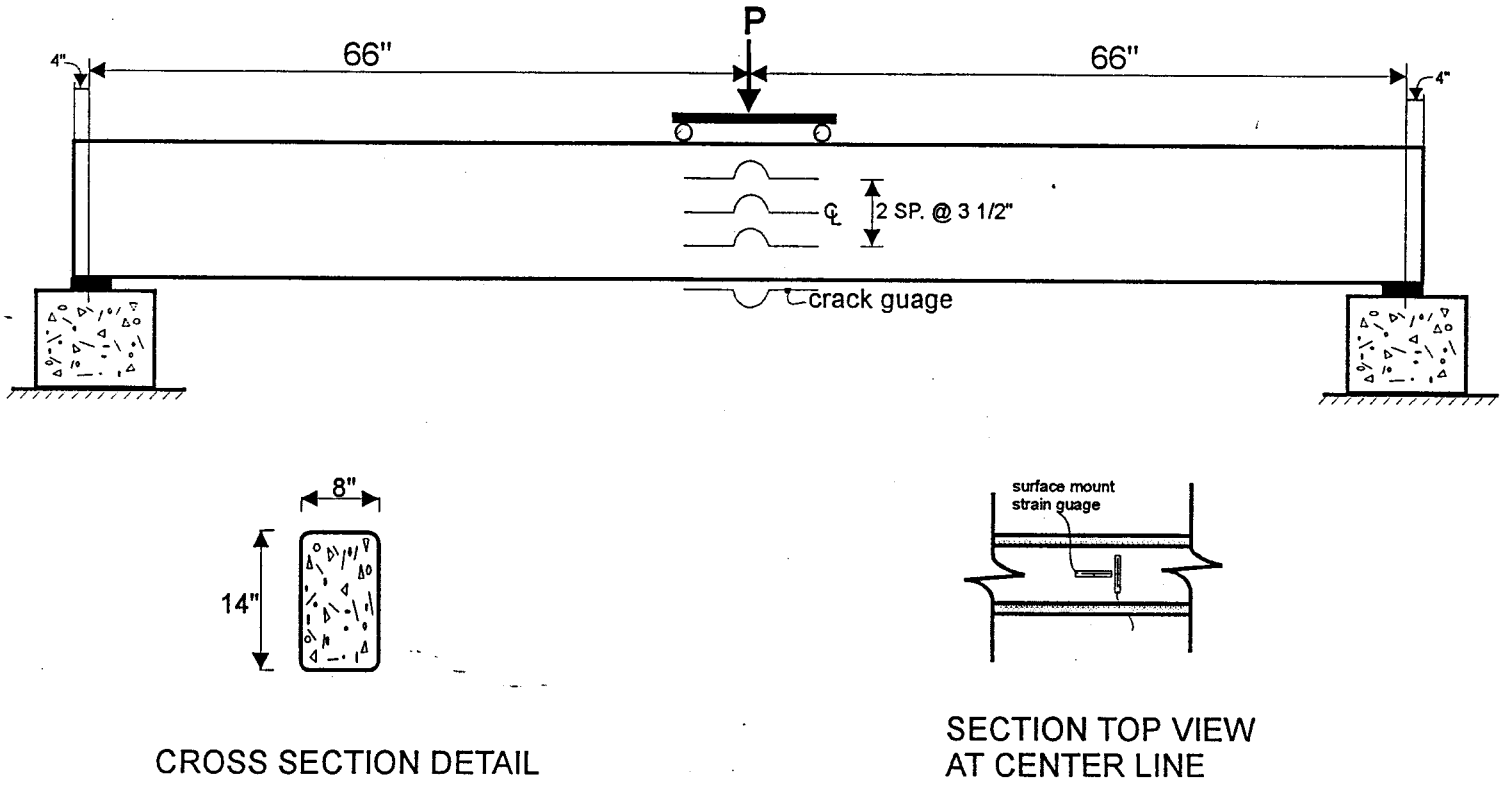

Fig. 4.2(a) Instrumentation Details of Specimen Without Corbels

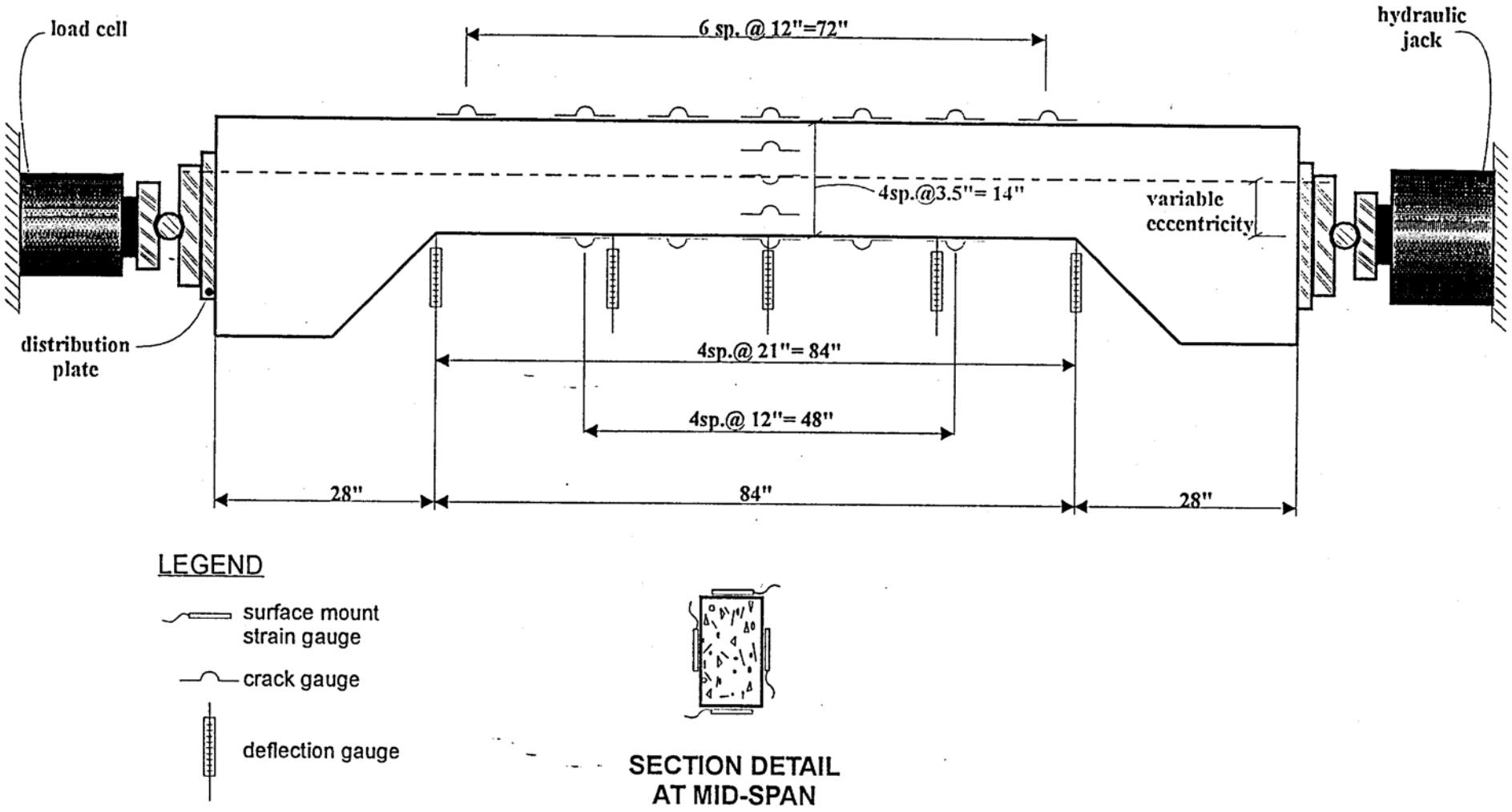

Fig. 4.2(b) Instrumentation Details of Specimen With Corbels

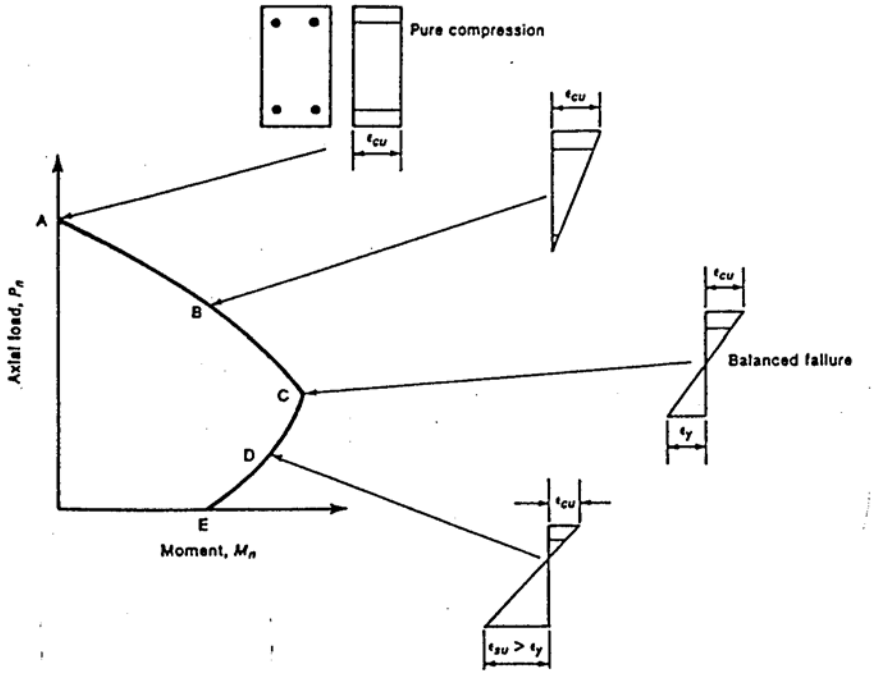

Fig. 4.3 Strain Distributions Corresponding to Points on Interaction Diagram

(Fig. 5.1a) Load vs. Deflection Along Beam Length

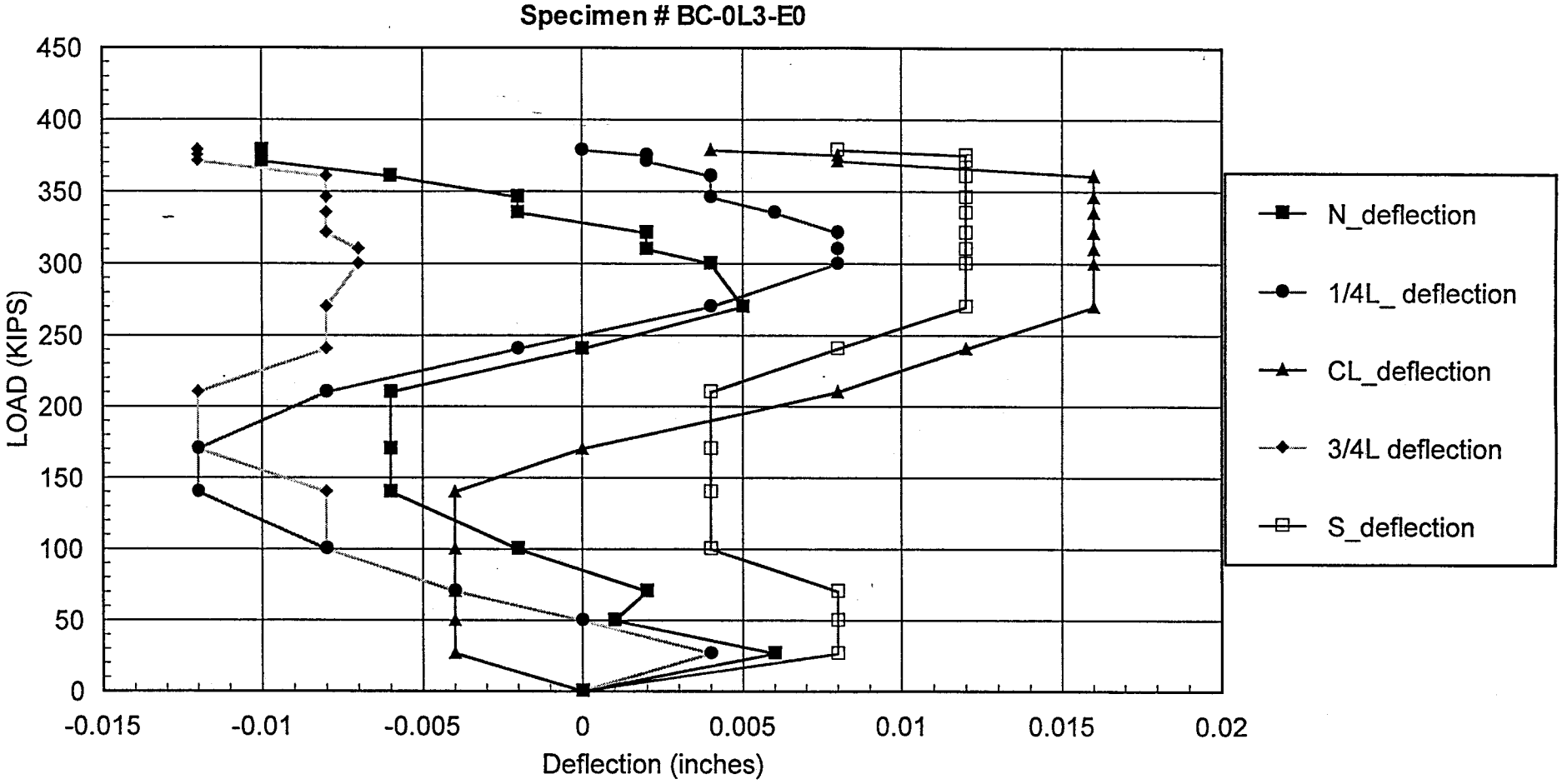

(Fig. 5.1b) Moment VS. CL- Deflection

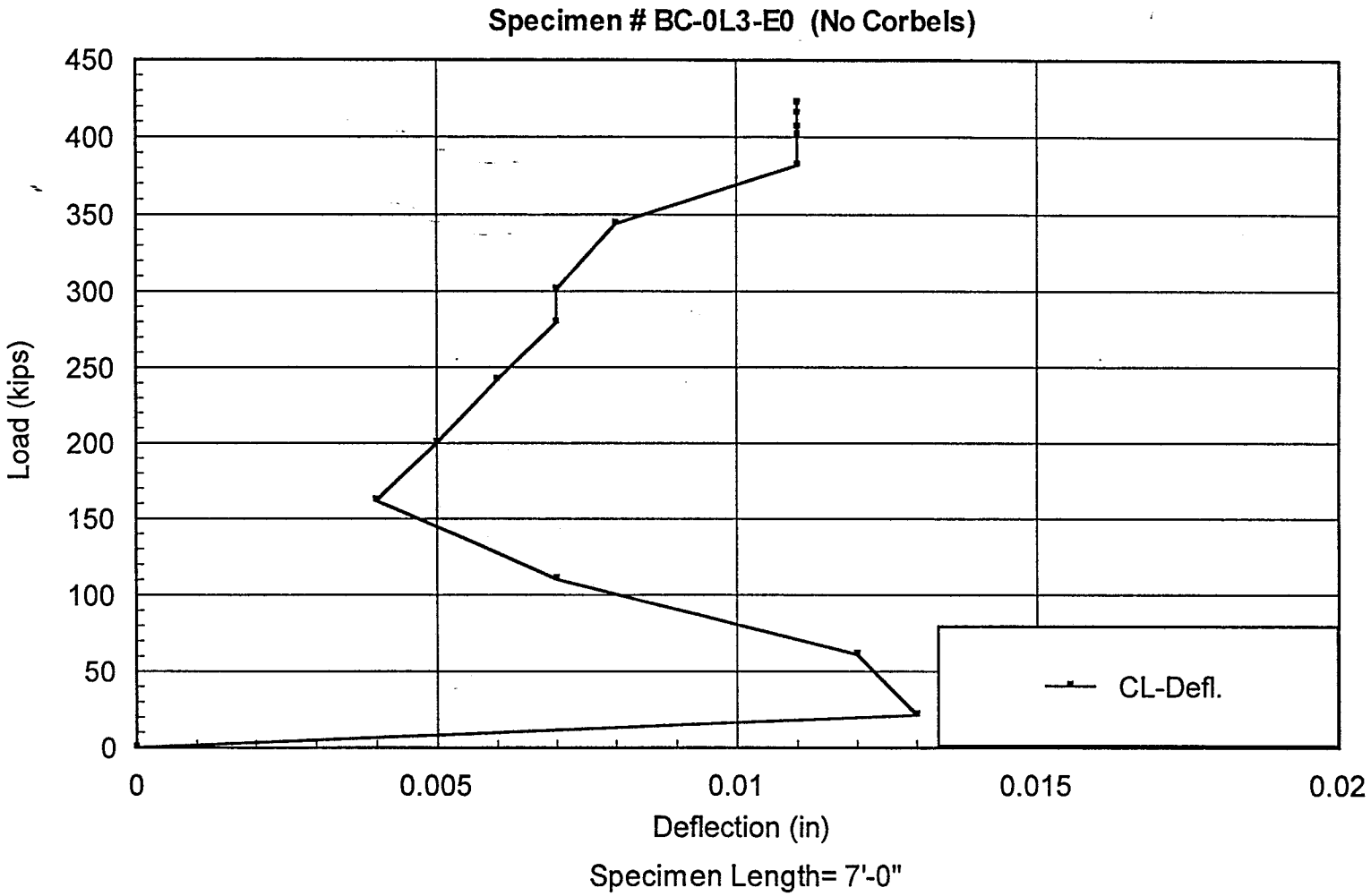

(Fig. 5.1c) Load vs. Deflection Along Beam Length

Specimen # BC-2L3-E0

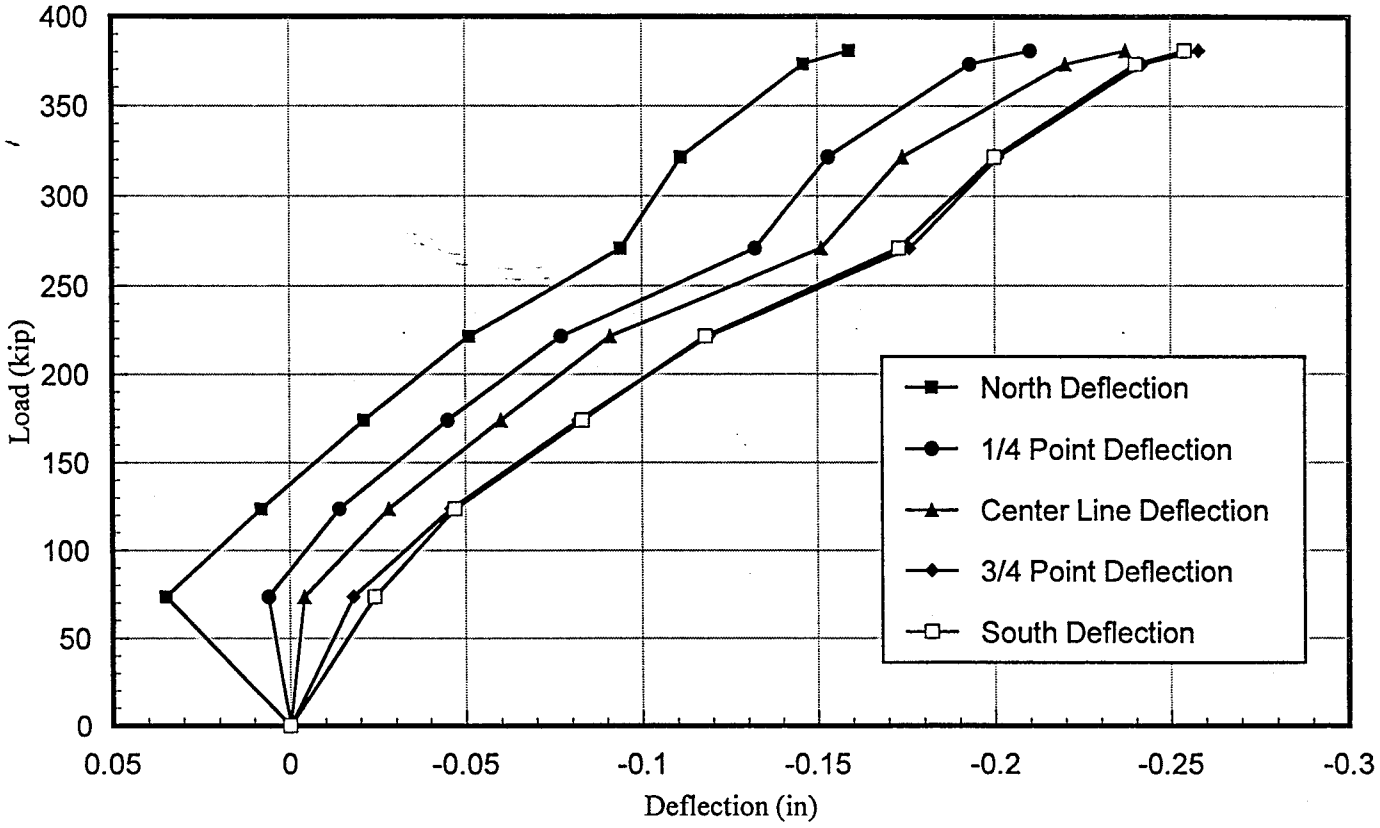

(Fig. 5.1d) Load VS CL-Deflection

Specimen # BC-2L3-E01 (No Corbels)

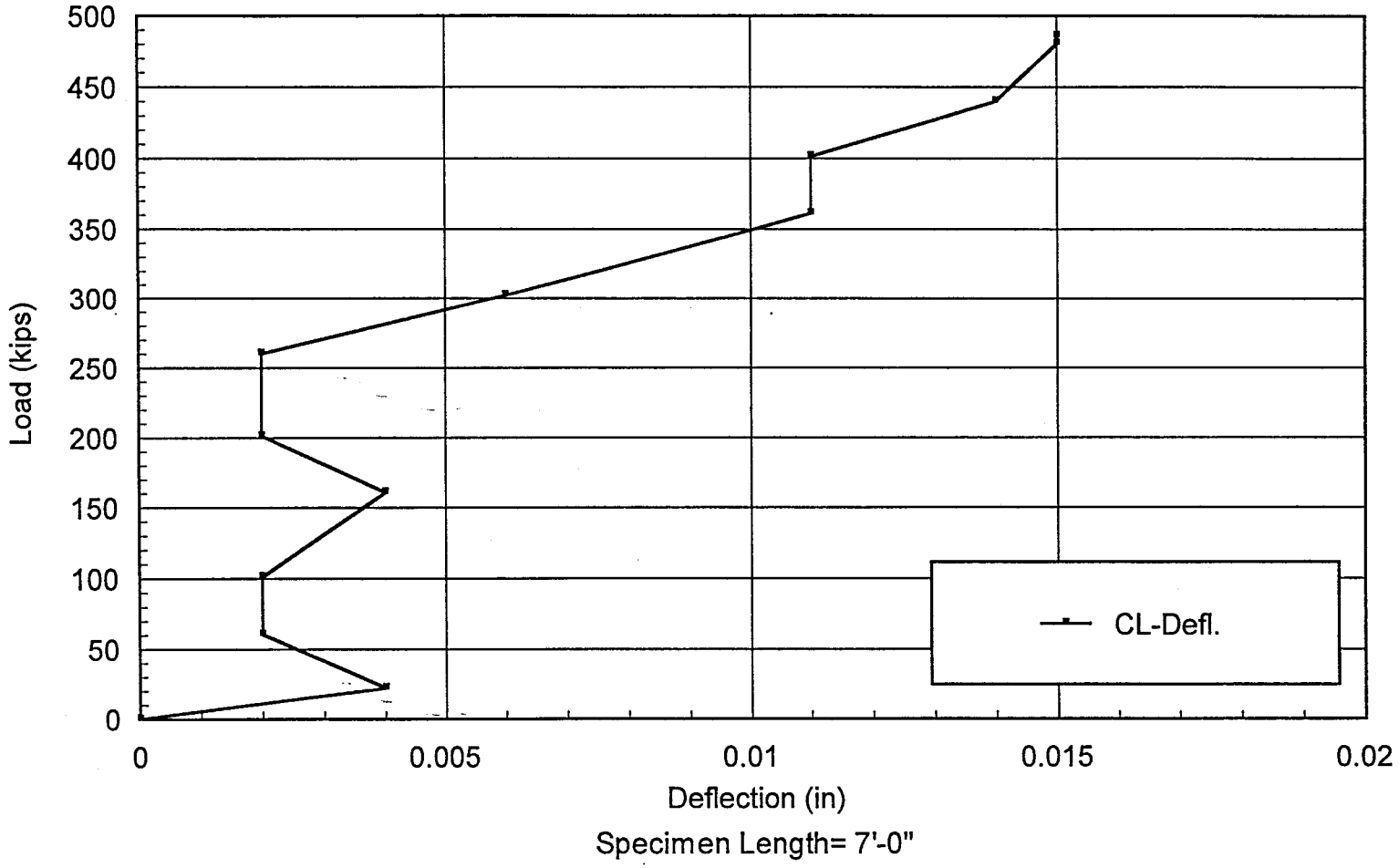

Specimen Length= 7'-0"

(Fig. 5.1e) Load VS. CL-Deflection

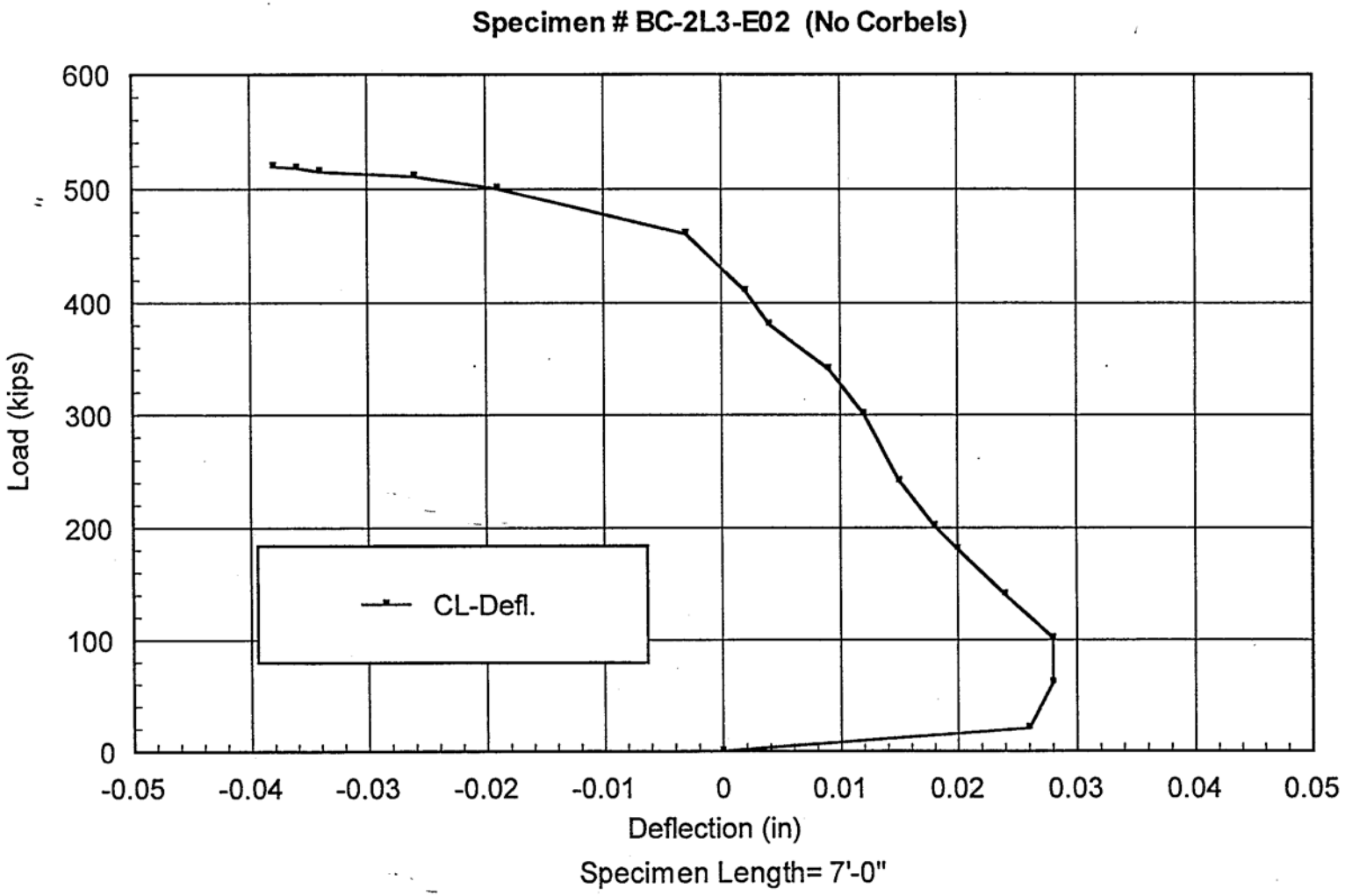

(Fig. 5.1f) Load VS. CL-Deflection

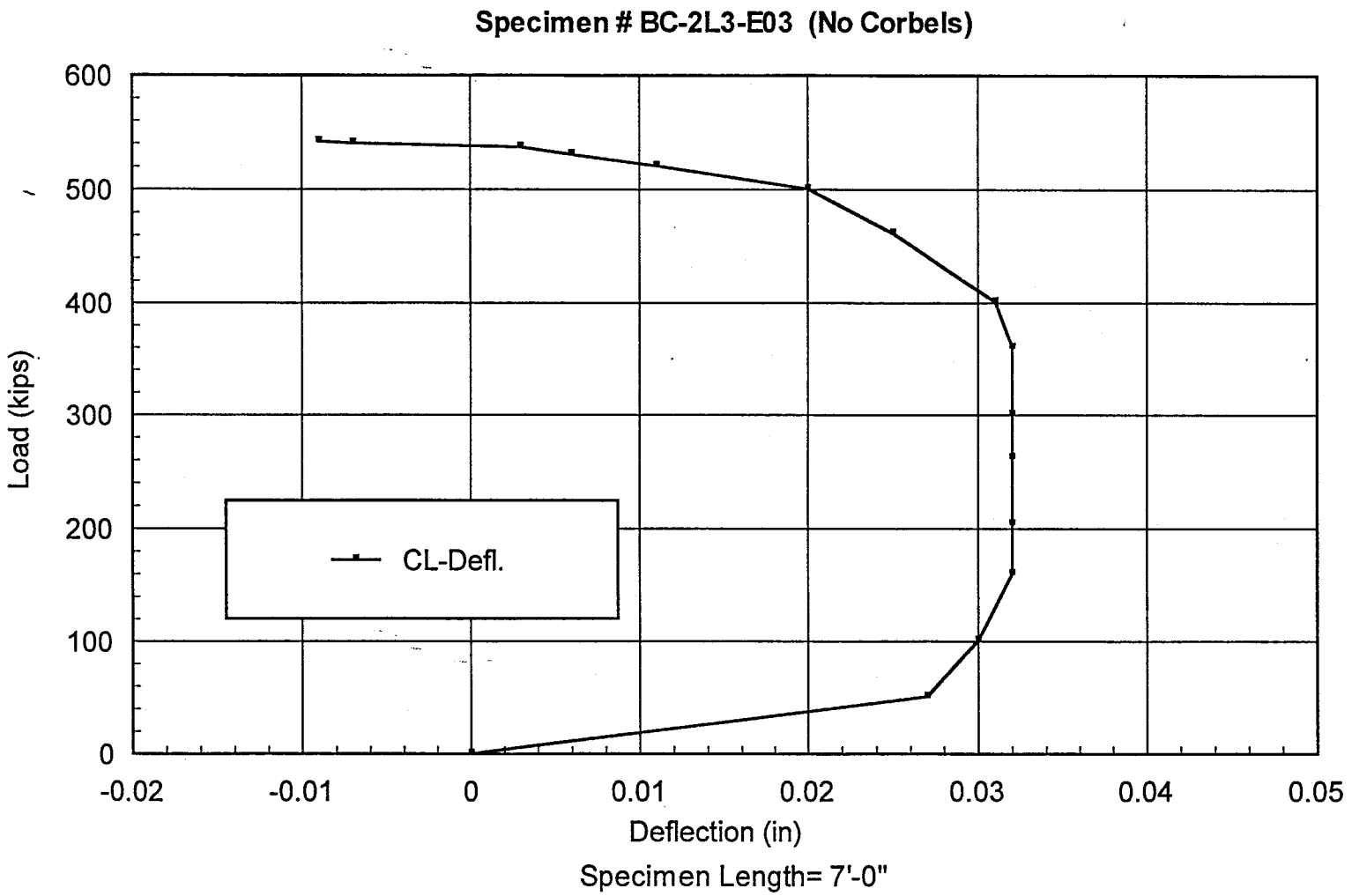

(Fig. 5.2a) Secondary Moment vs center line deflection

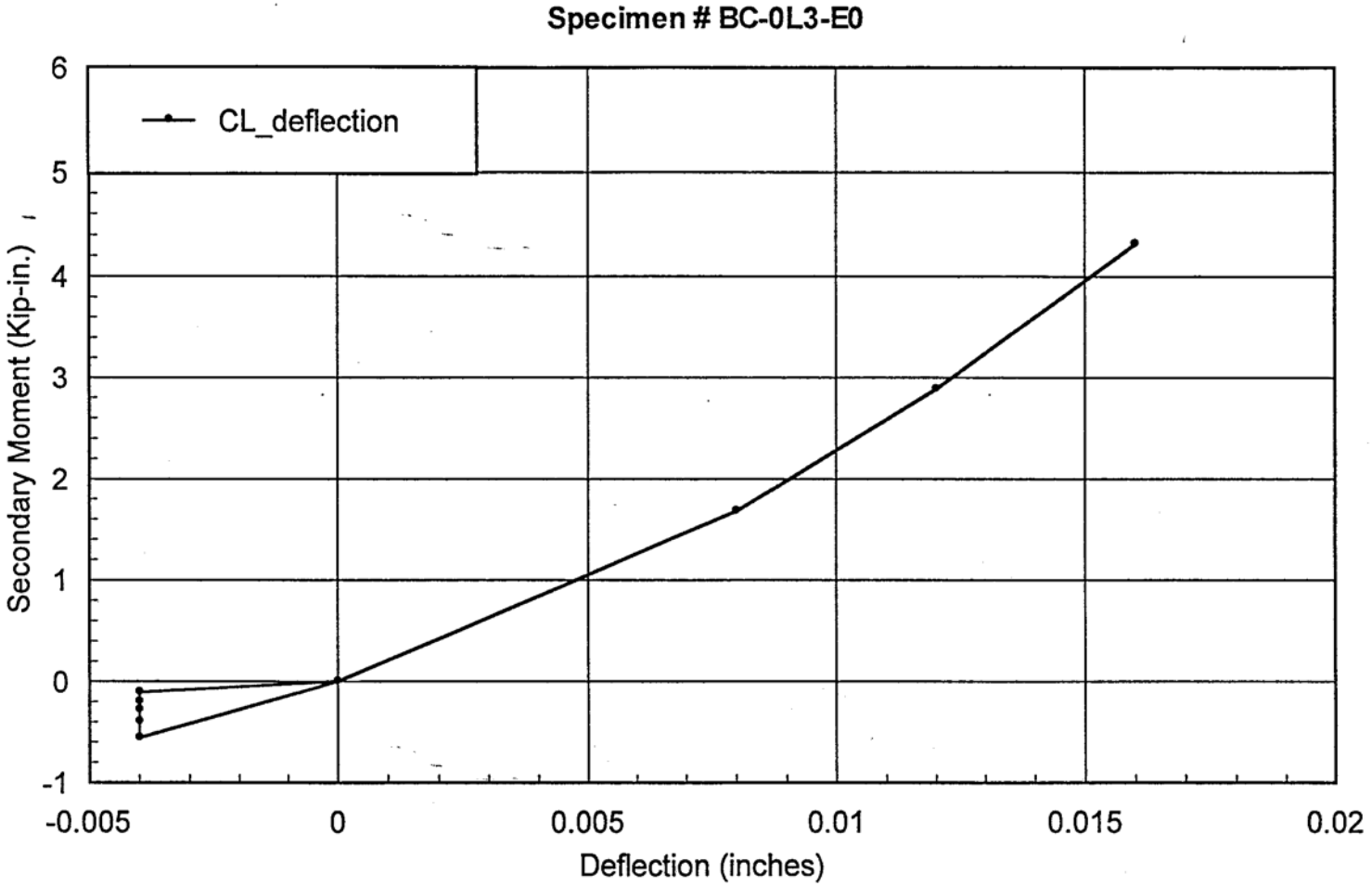

(Fig. 5.2b) Secondary Moment VS. Center Line Deflection

Specimen #BC-0L3-E0(No Corbels)

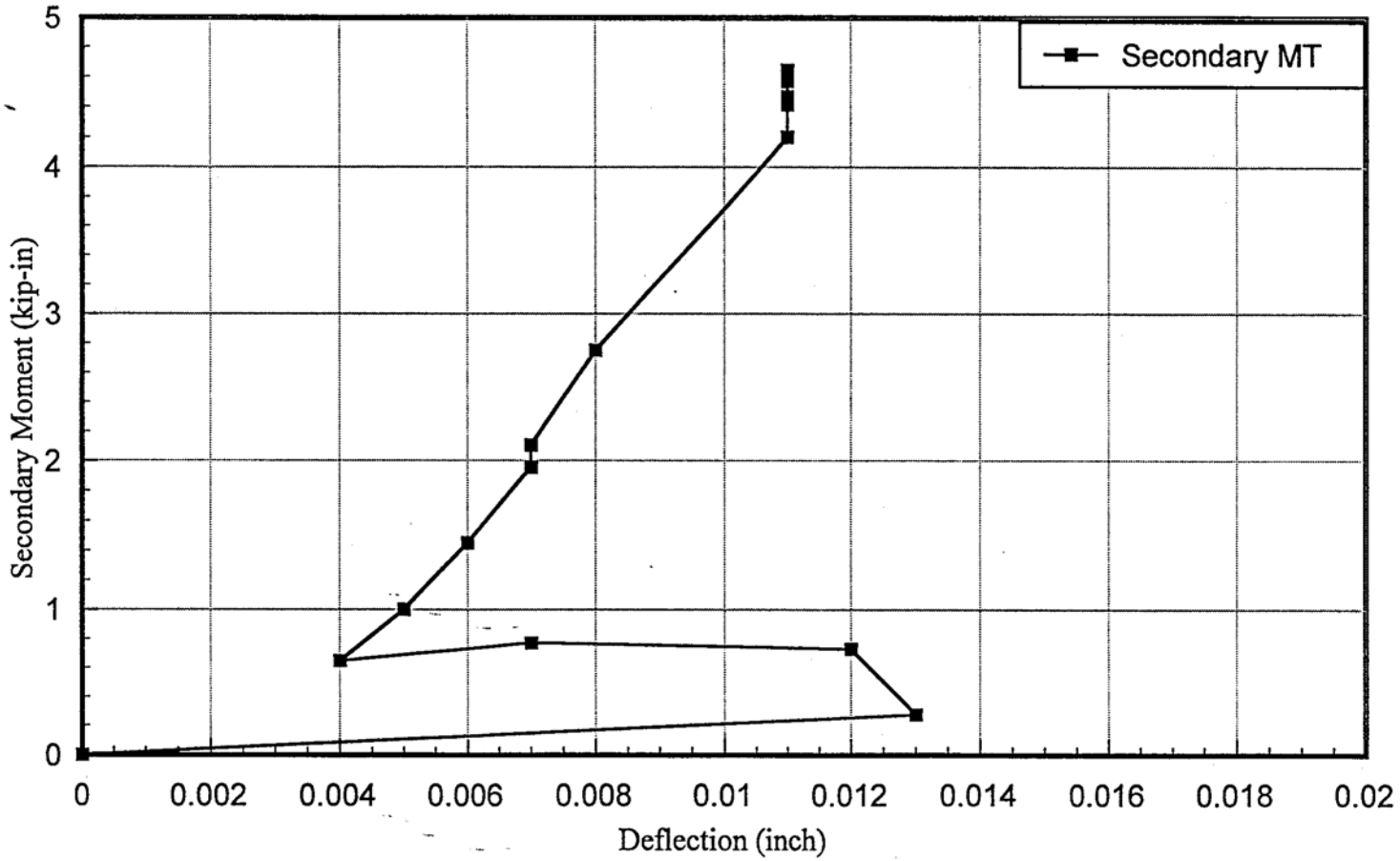

(Fig. 5.2c) Secondary Moment VS. Center Line Deflection

Specimen #BC-2L3-E0

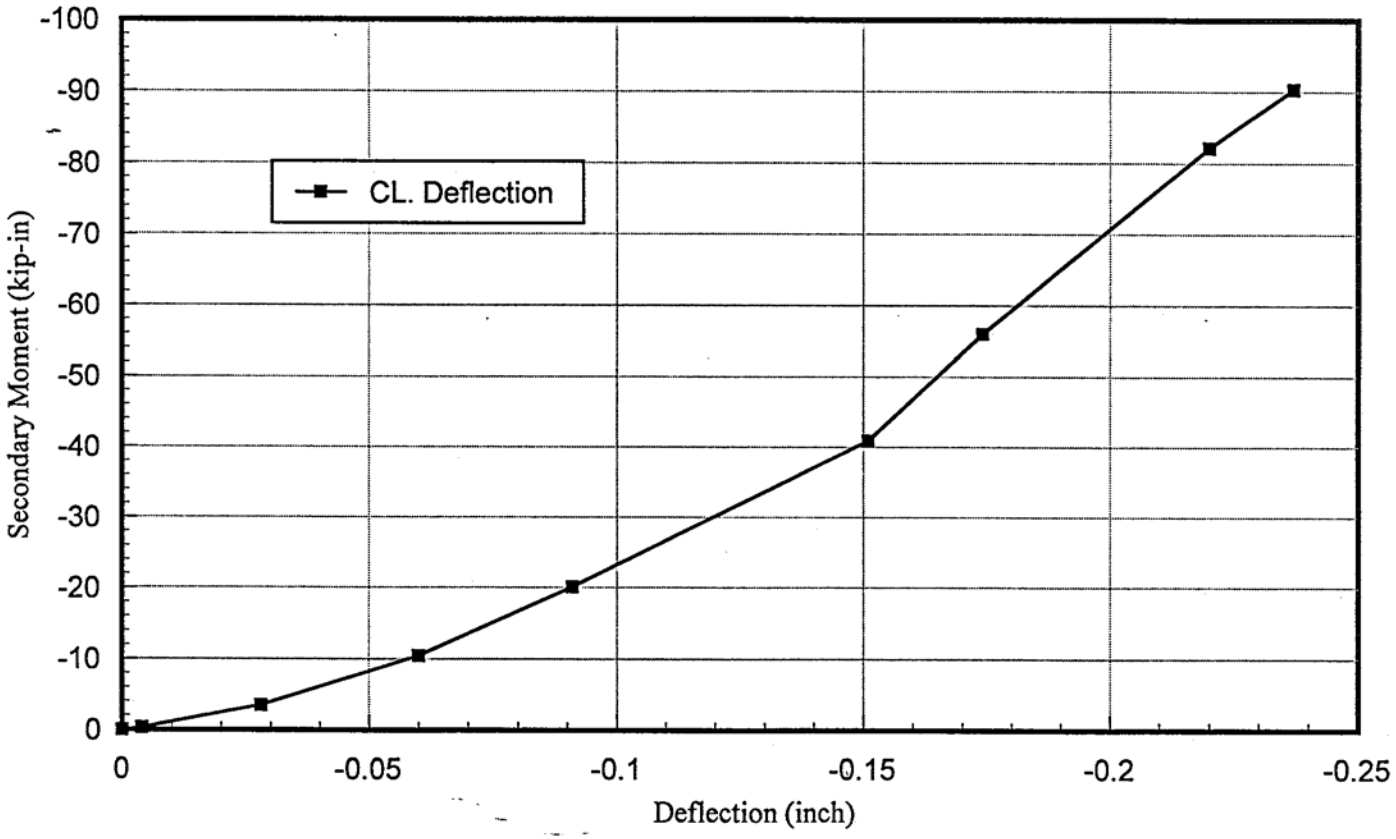

(Fig. 5.2d) Secondary Moment VS. Center Line Deflection

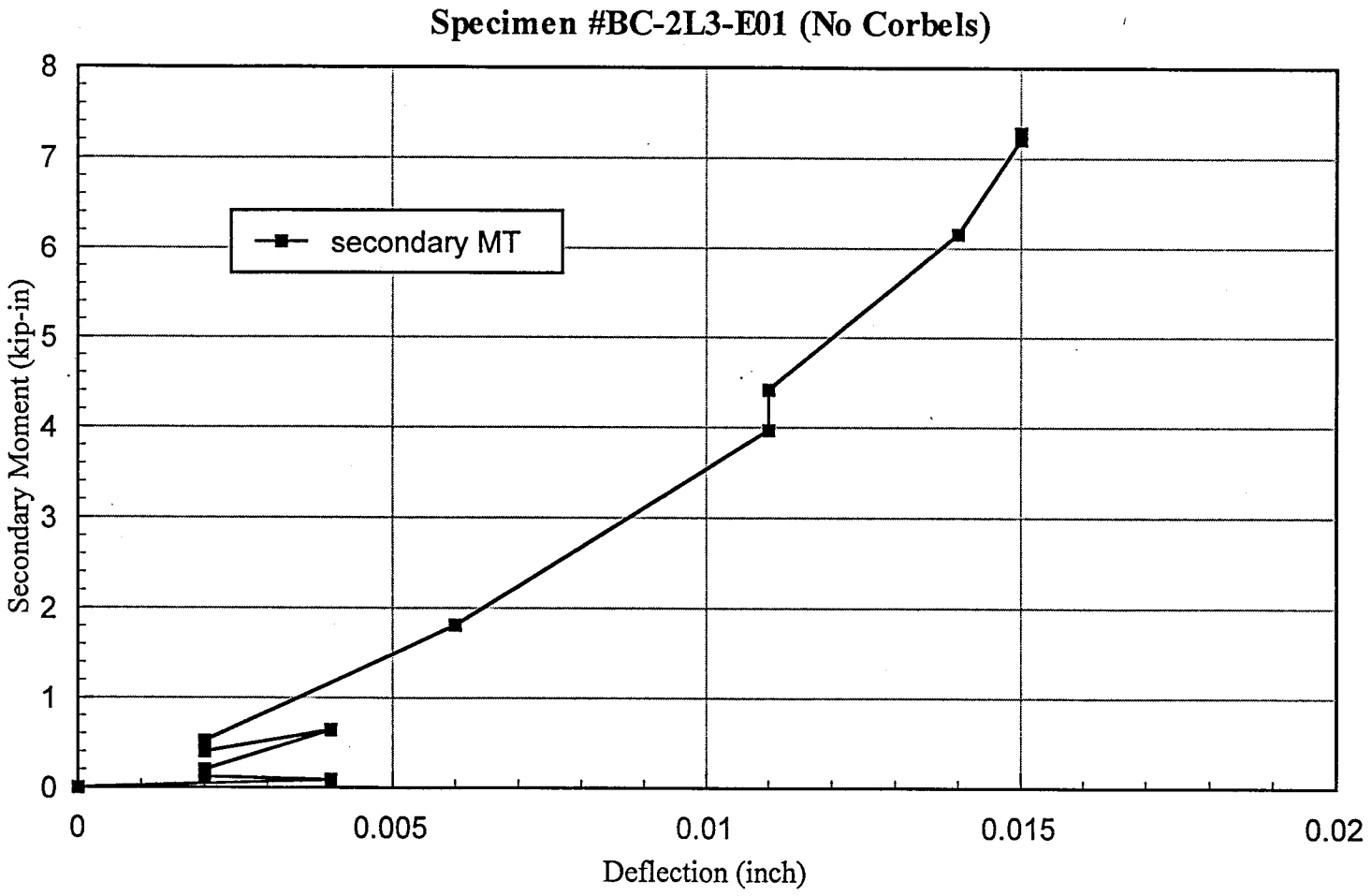

(Fig. 5.2e) Secondary Moment VS. Center Line Deflection

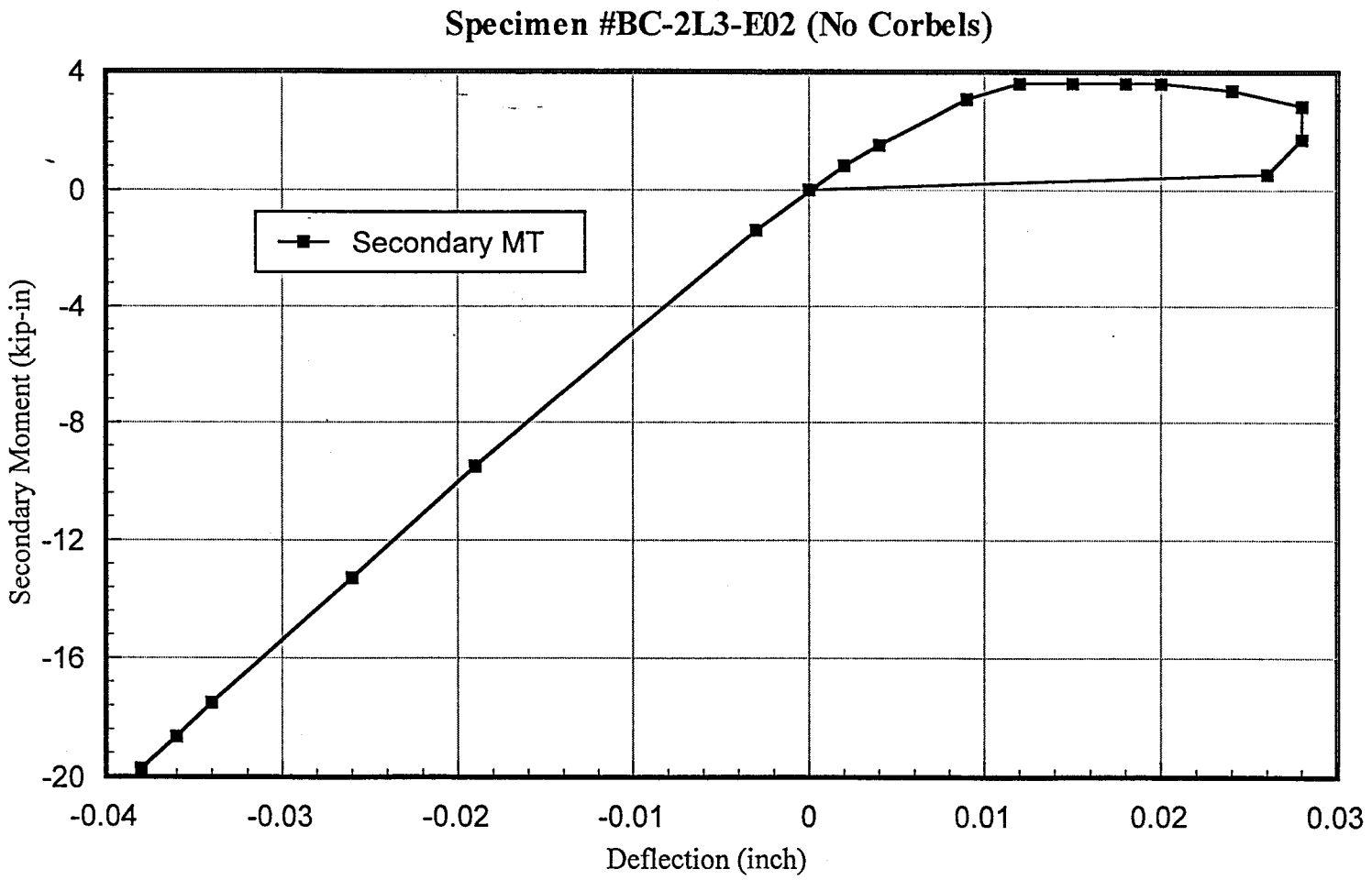

(Fig. 5.2f) Secondary Moment VS. Center Line Deflection

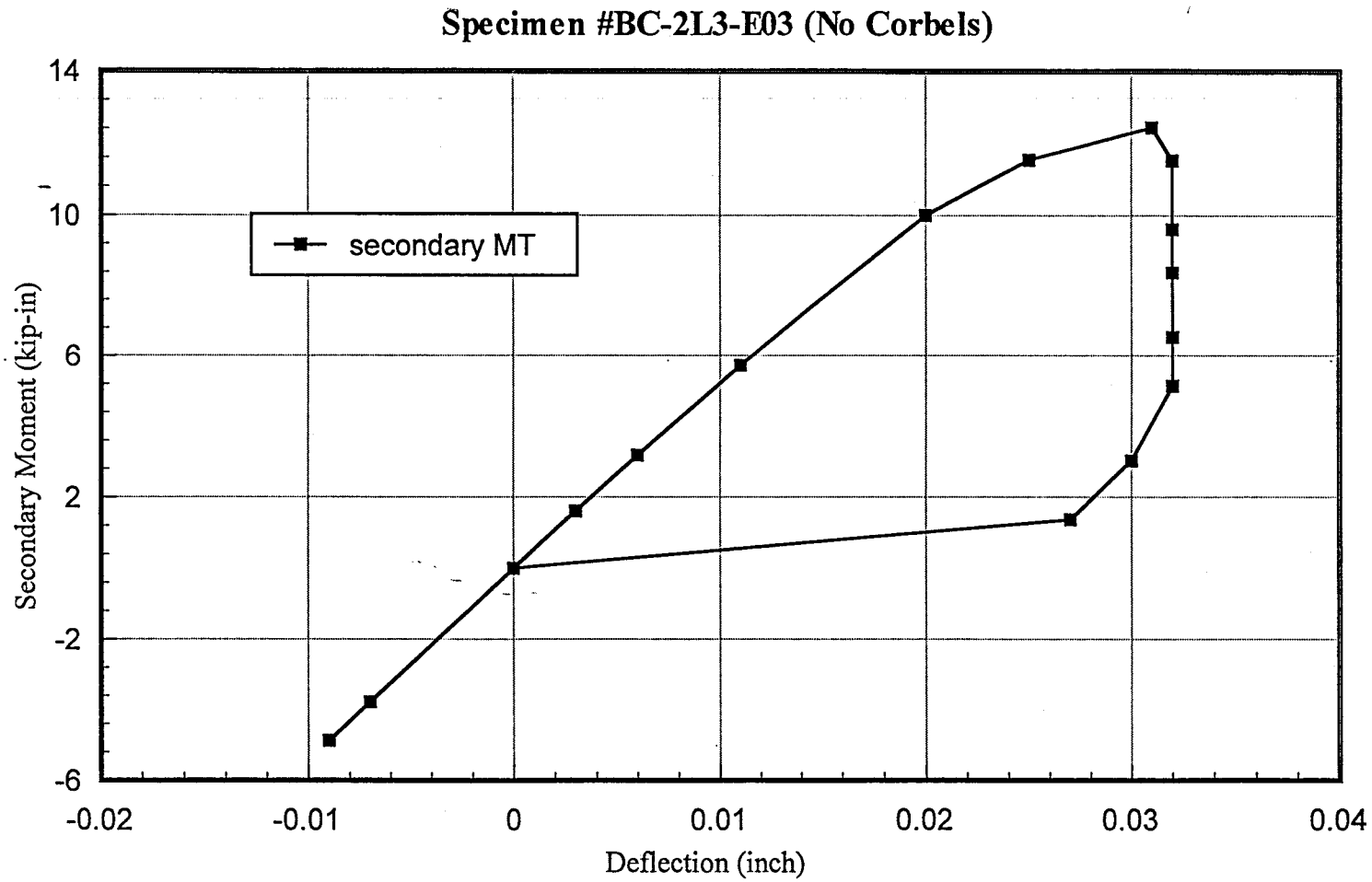

(Fig. 5.3a) Center Line Strain Distribution

Specimen # BC-0L3-E0

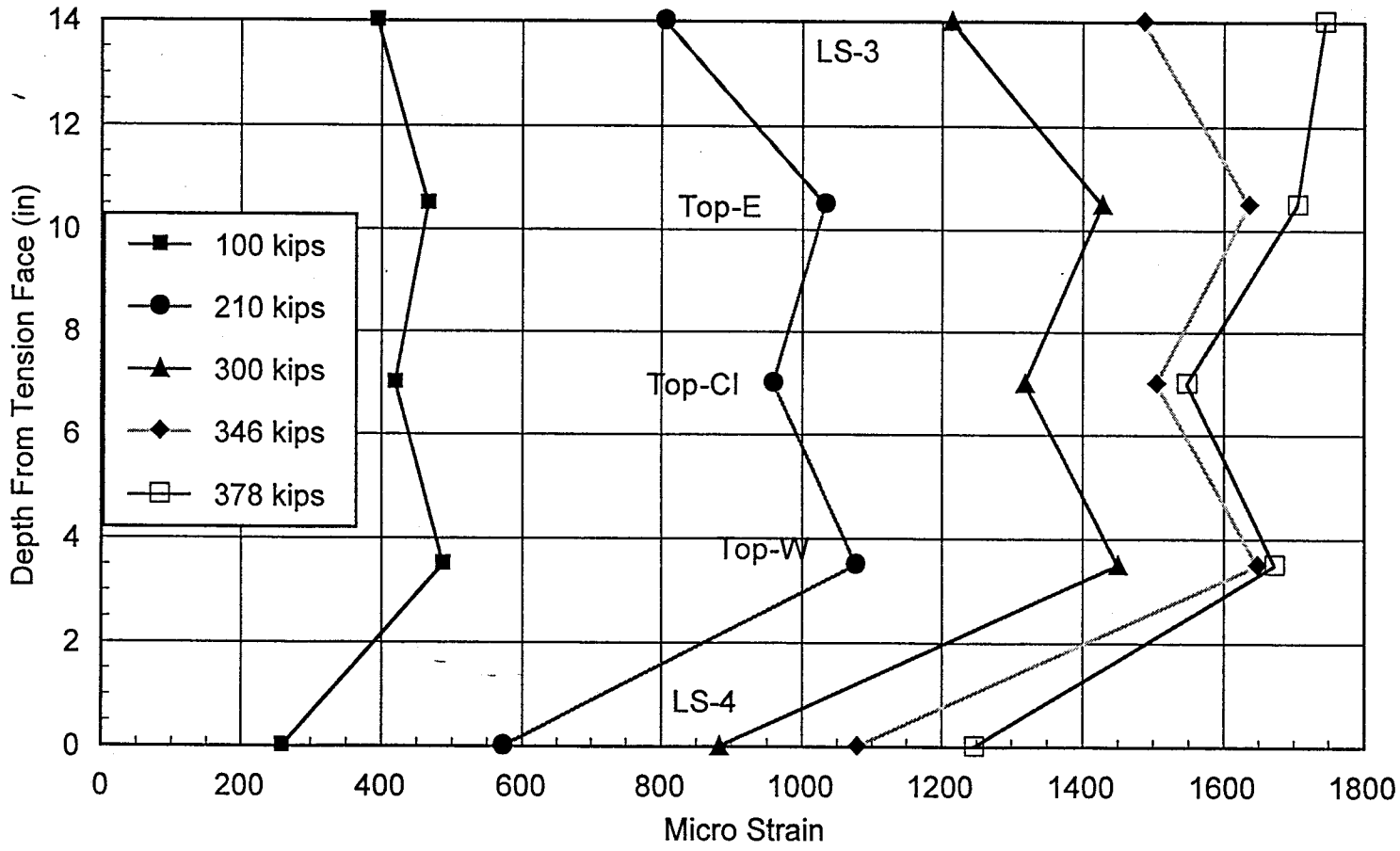

(Fig. 5.3b) Center Line Strain Distribution

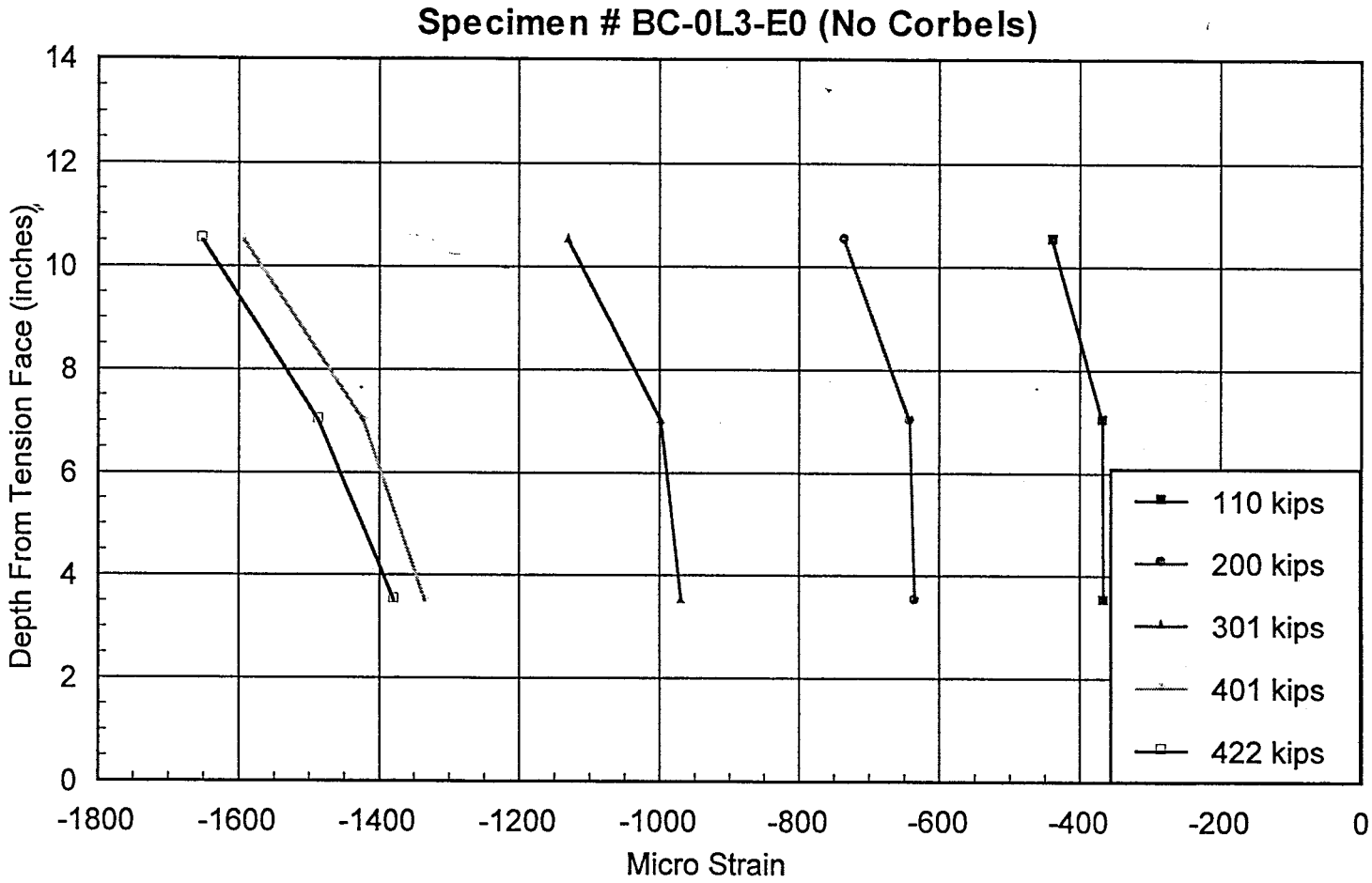

(Fig. 5.3c) Centerline Strain Distribution

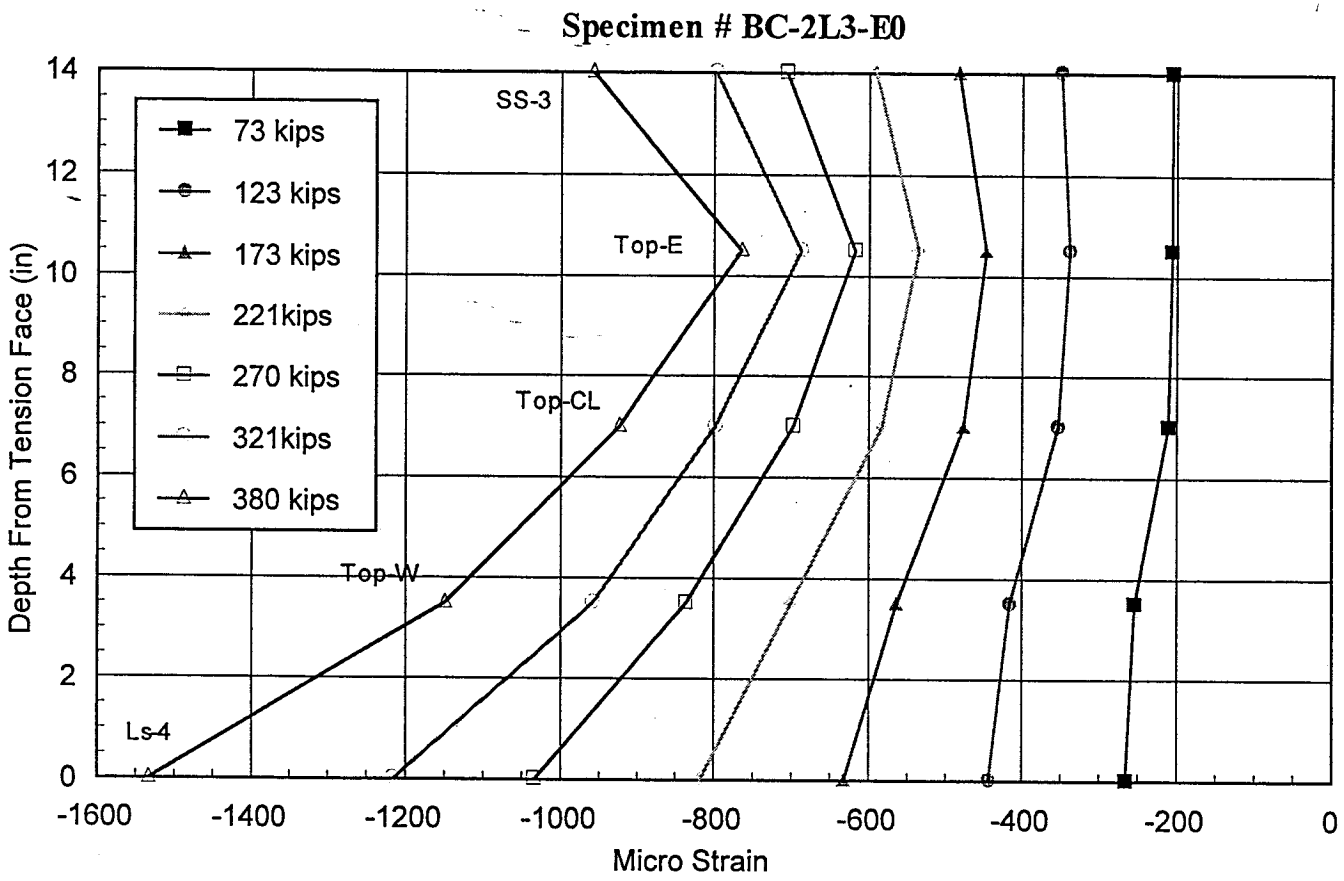

(Fig.5.3d) Center Line Strain Distribution

Specimen # BC-2L3-E01 (No Corbels)

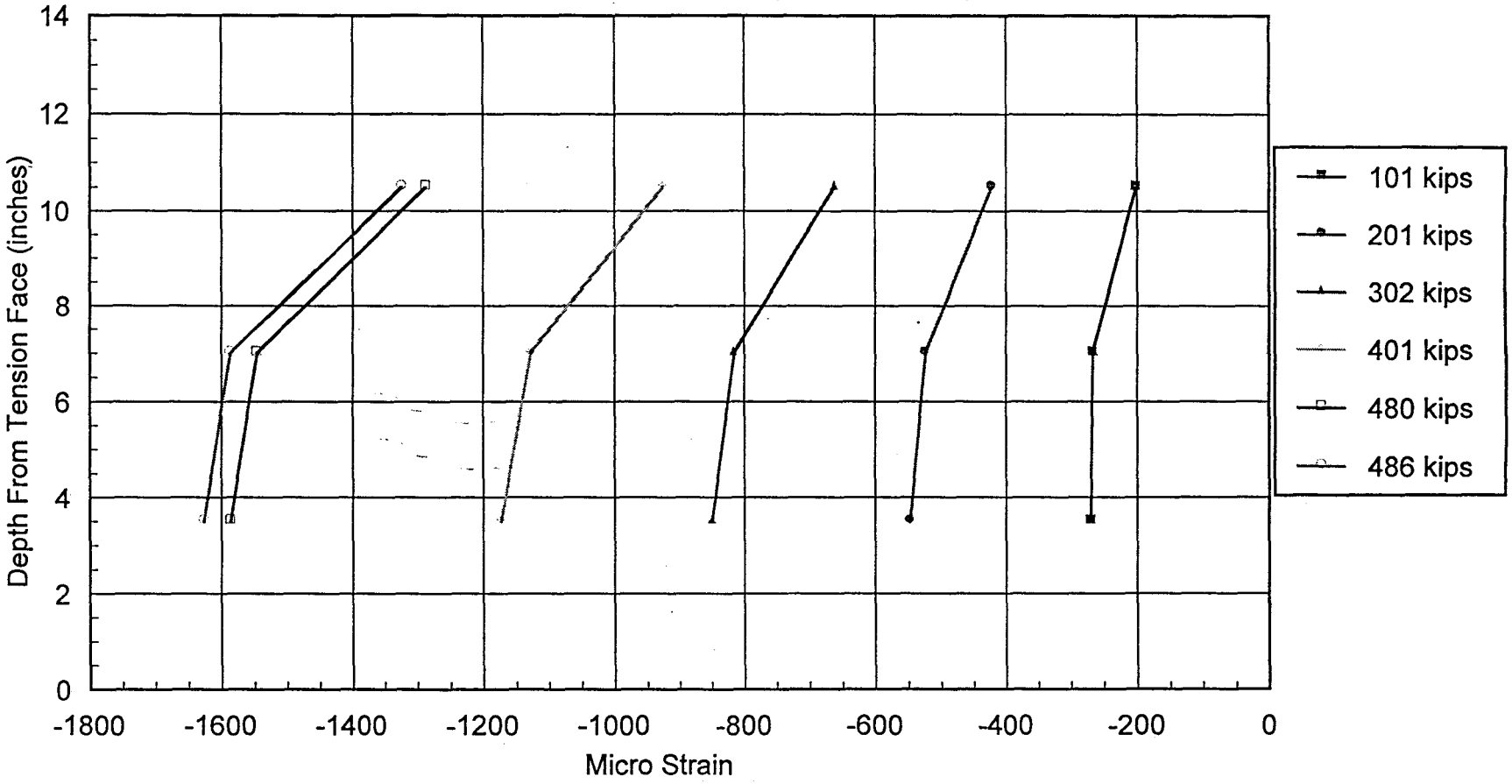

(Fig. 5.3e) Center Line Strain Distribution

Specimen # BC-2L3-E02 (No Corbels)

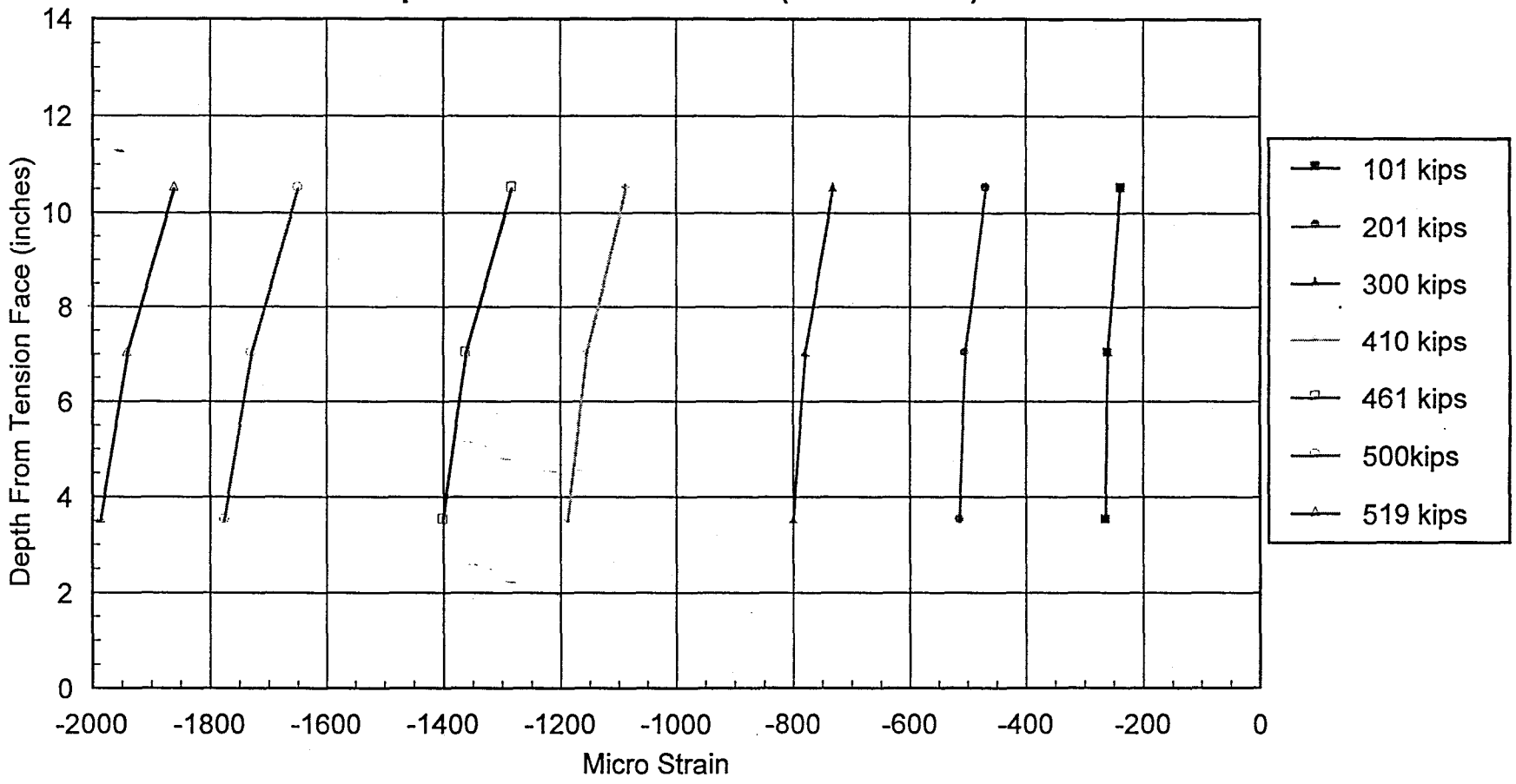

(Fig. 5.3f) Center Line Strain Distribution

Specimen # BC-2L3-E03 (No Corbels)

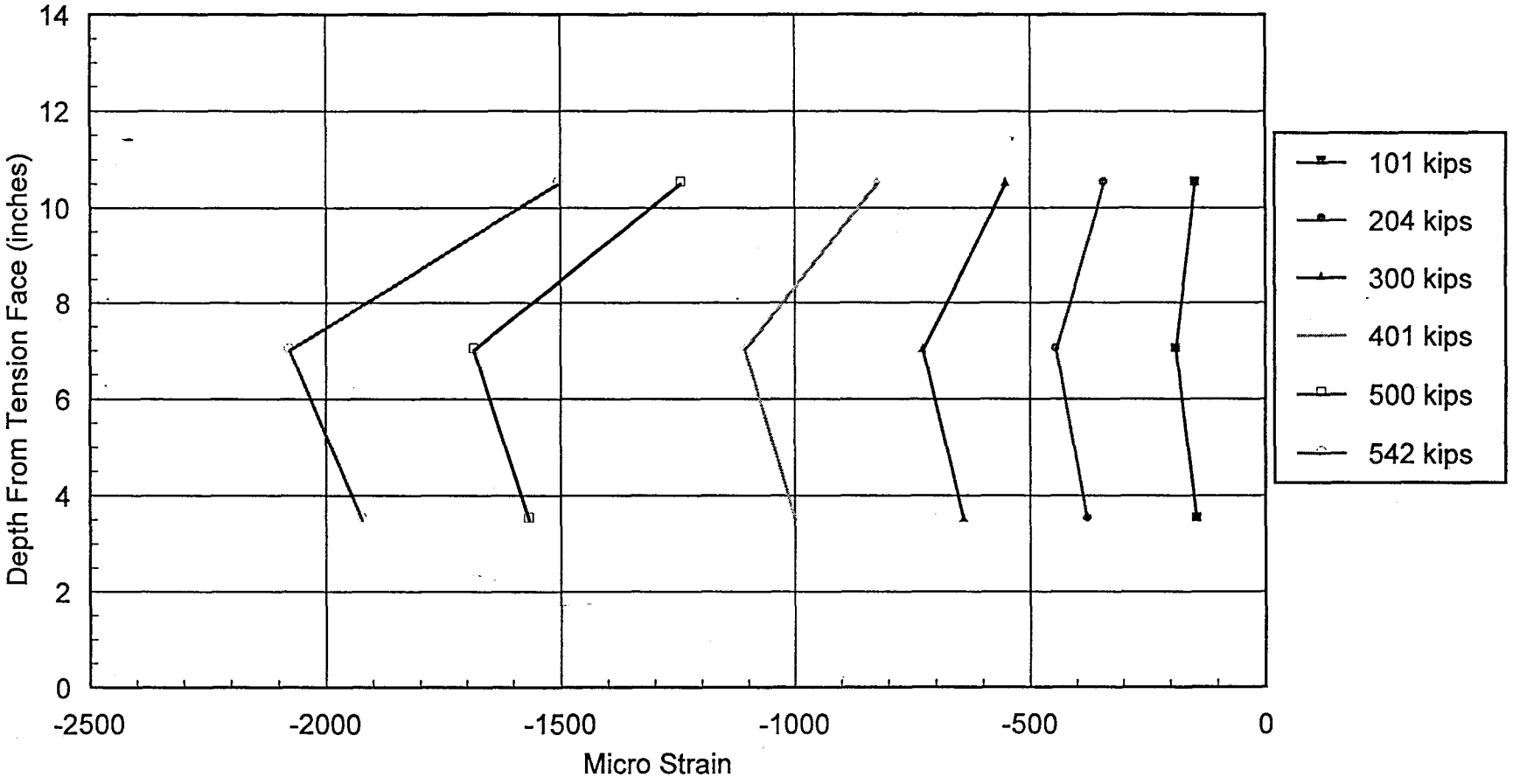

(fIG. 5.4a) LONGITUDINAL COMPRESSIVE STRAIN DISTRIBUTION ALONG BEAM LENGTH

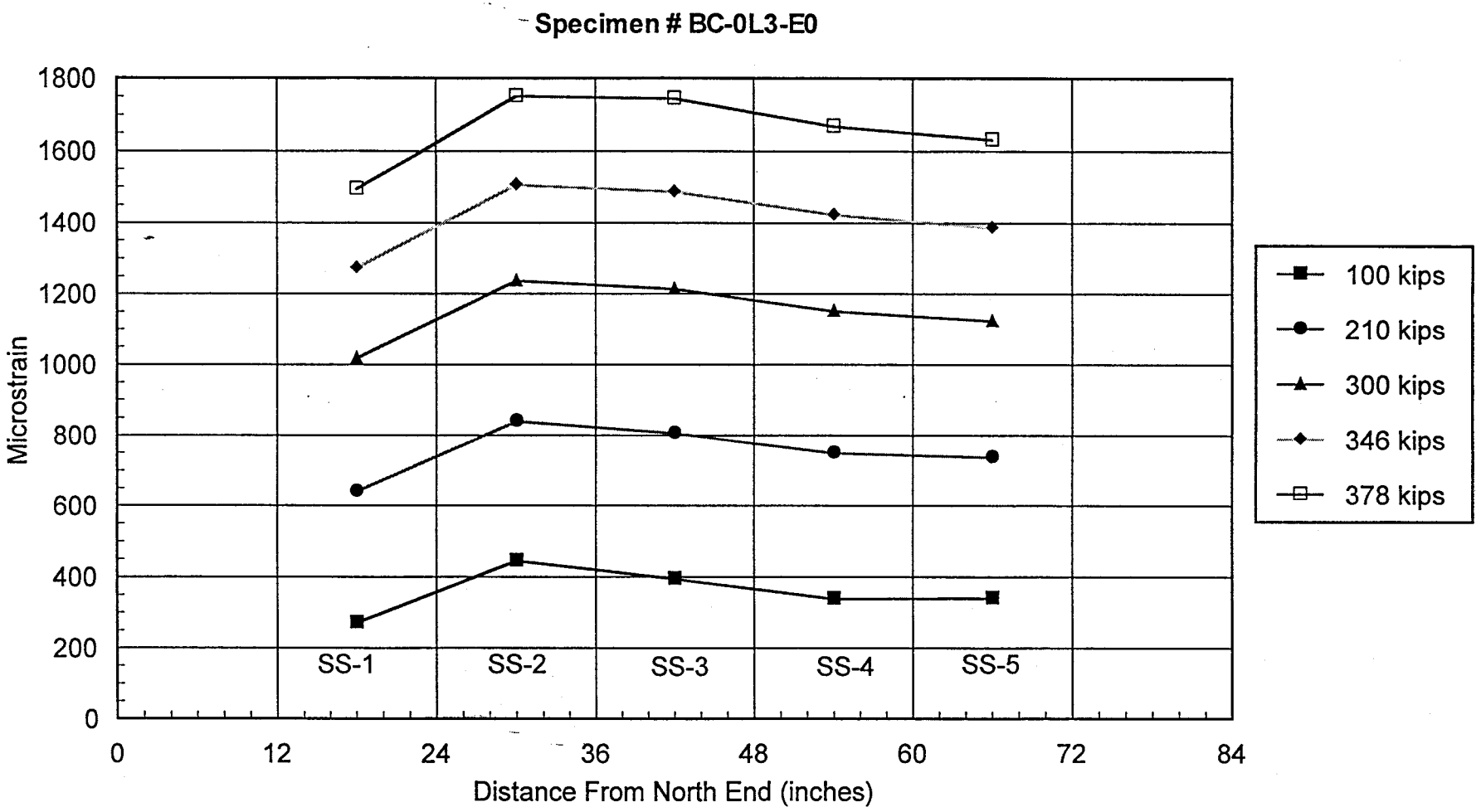

(Fig. 5.4a) LONGITUDINAL TENSION STRAIN DISTRIBUTION ALONG BEAM LENGTH

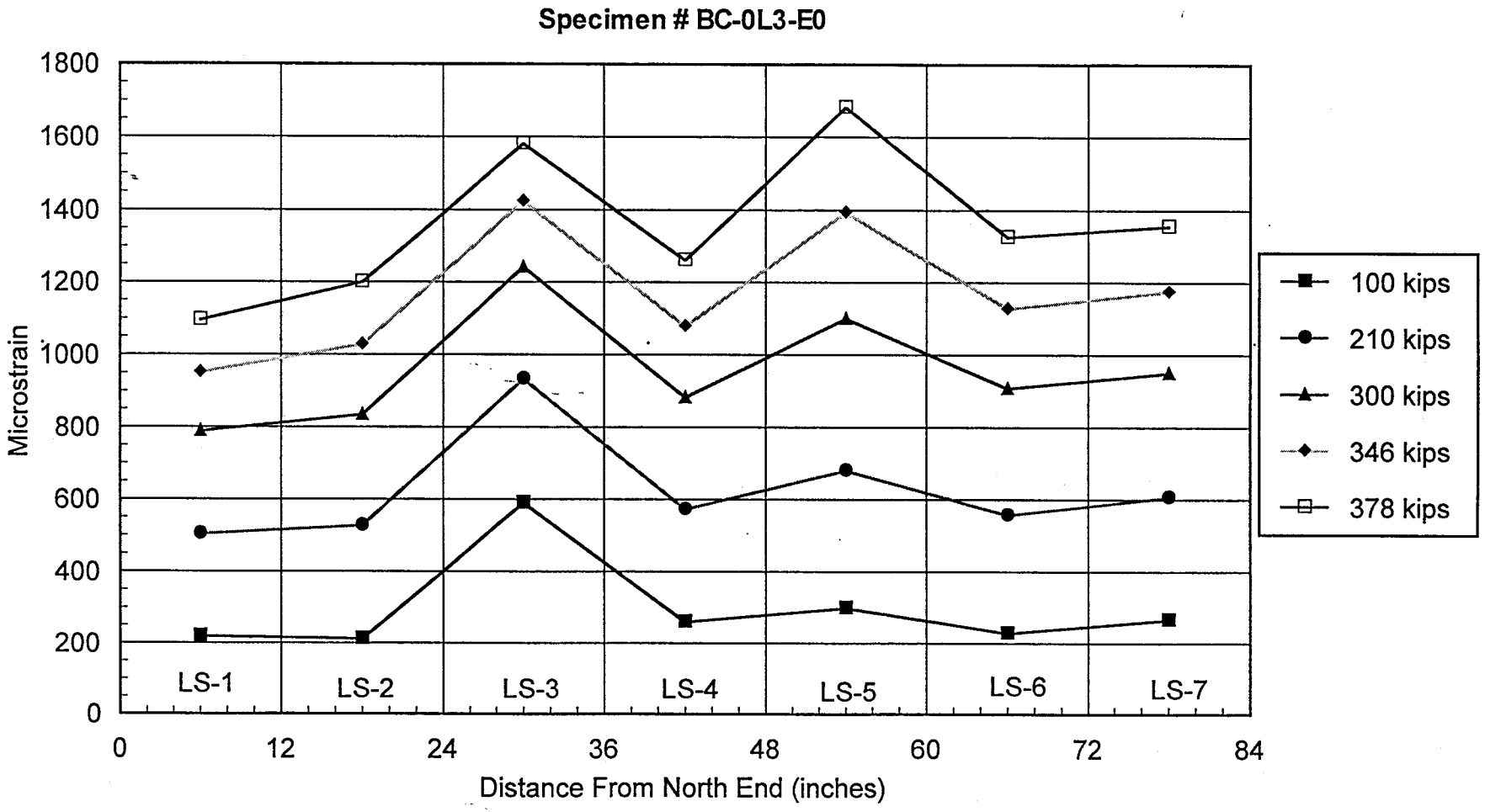

(Fig. 5.4b) Longitudinal Compressive Strain Distribution Along Beam Length

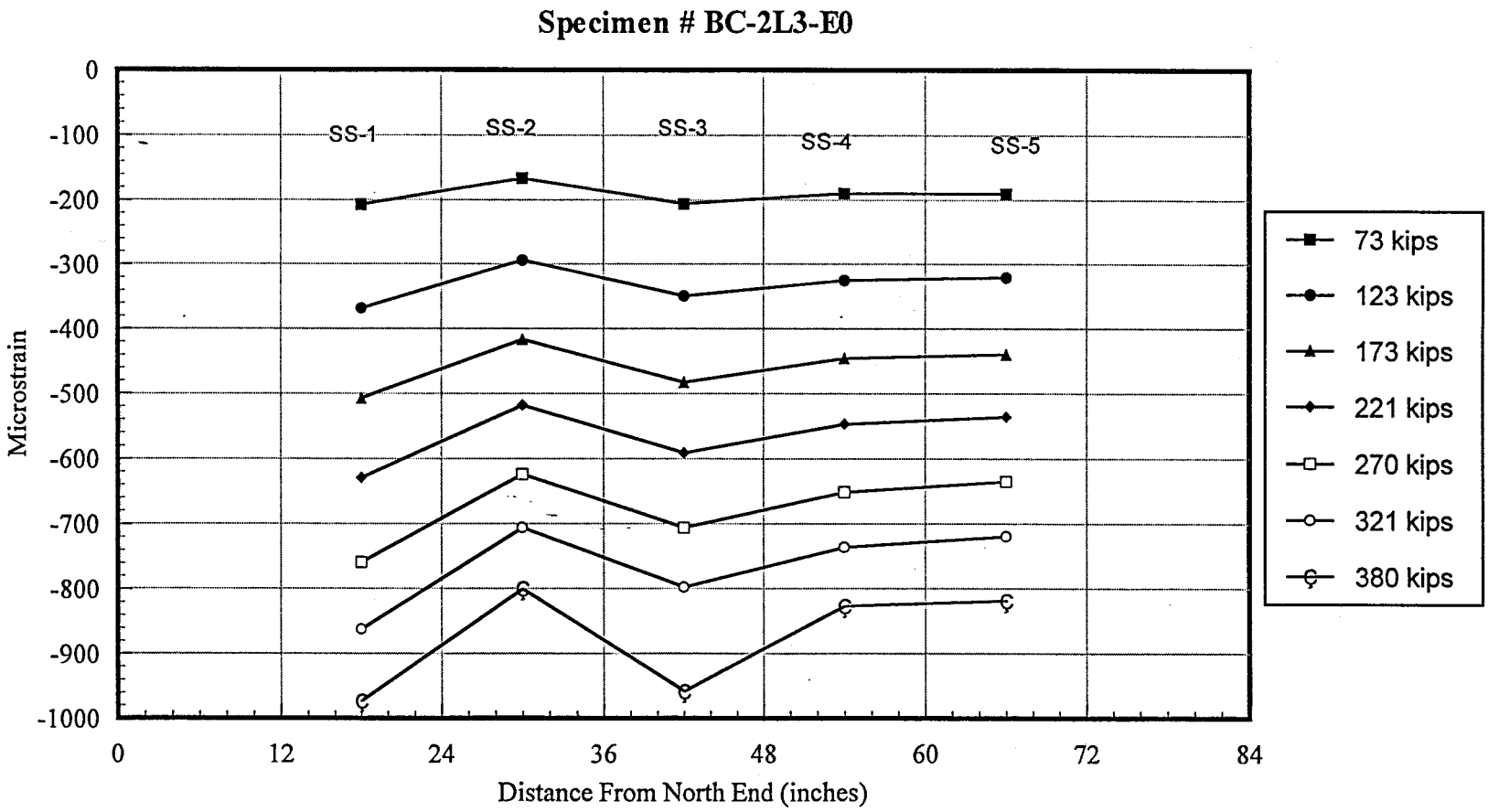

(Fig. 5.4b) Longitudinal Tension Strain Distribution Along Beam Length

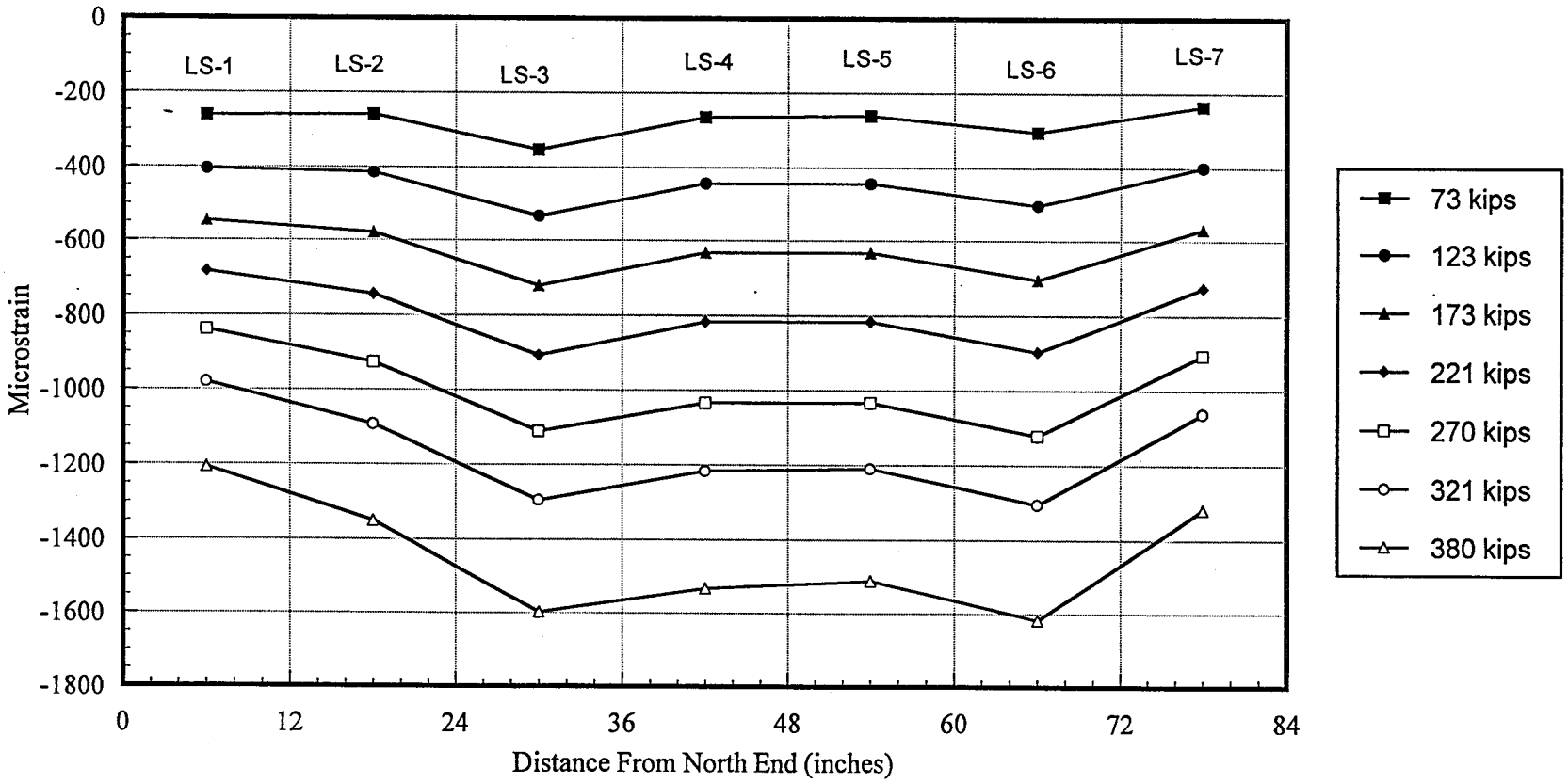

(Fig. 5.5a) Load vs. Transverse Surface Strain At Center Line

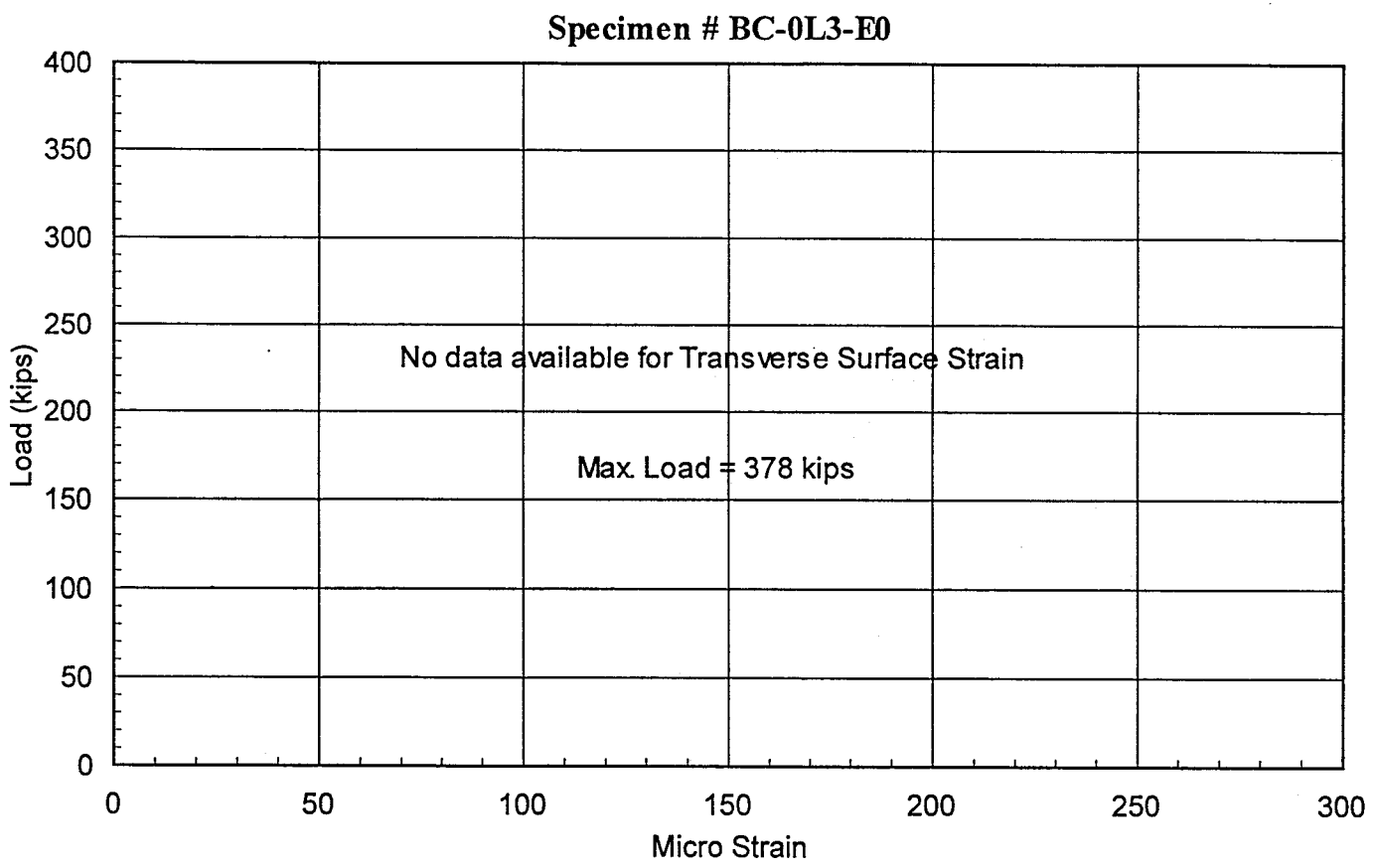

(Fig. 5.5b) Load VS.Transverse Surface Strain At Midspan

Specimen # BC-0L3-E0 (No Corbels)

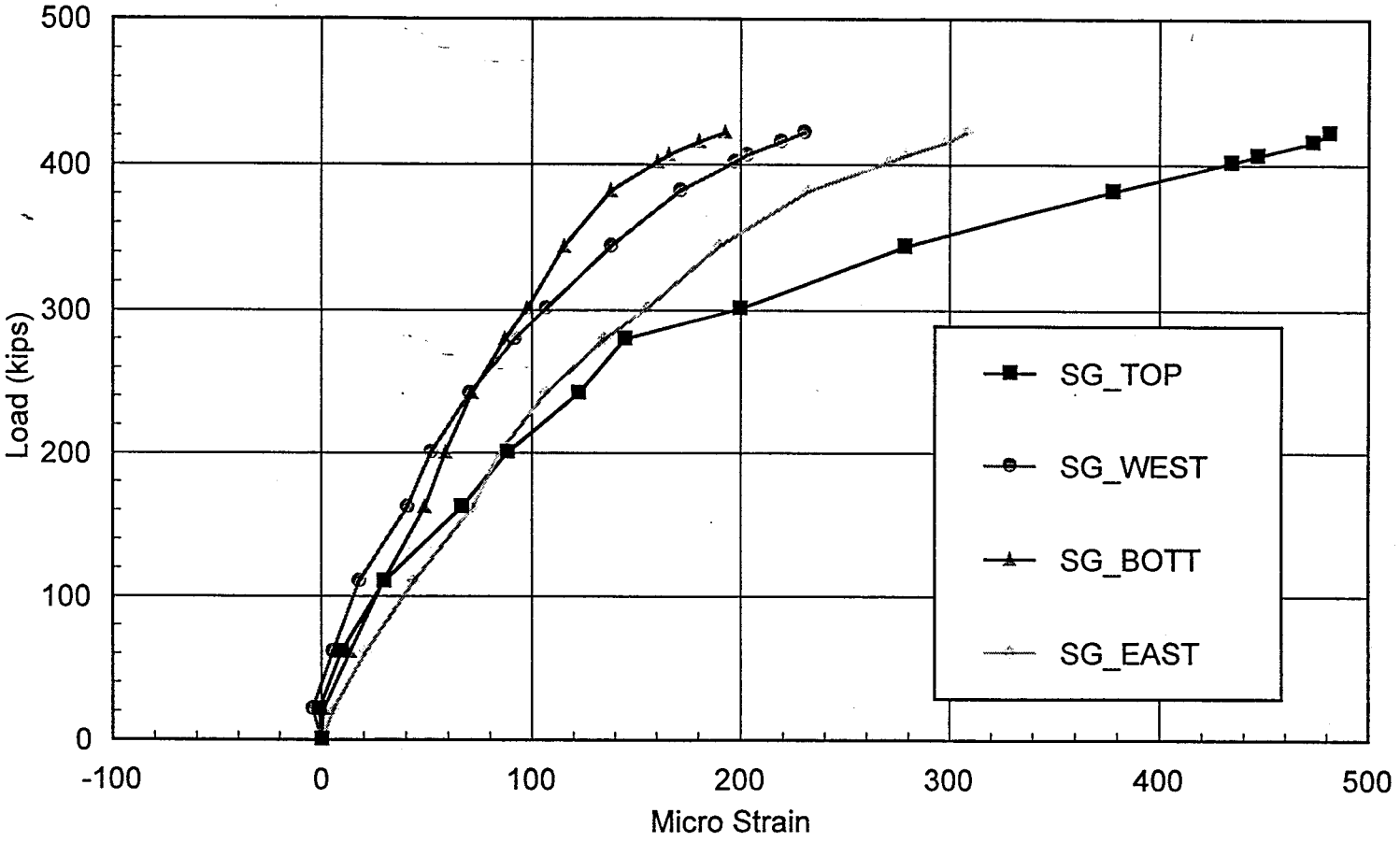

(Fig. 5.5c) Load vs. Transverse Surface Strain Around Beam Center Line

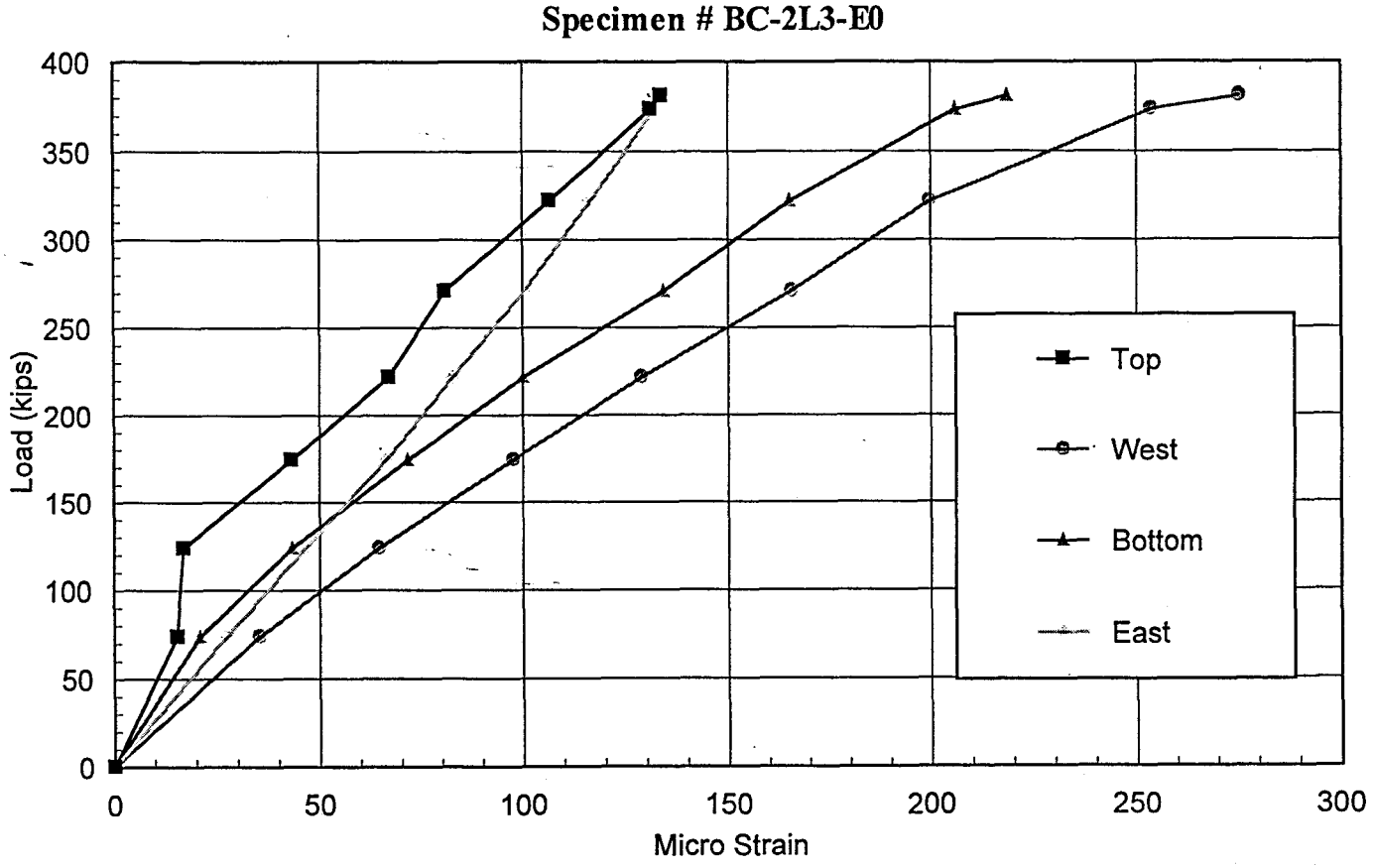

(Fig. 5.5d) Load VS.Transverse Surface Strain At Midspan

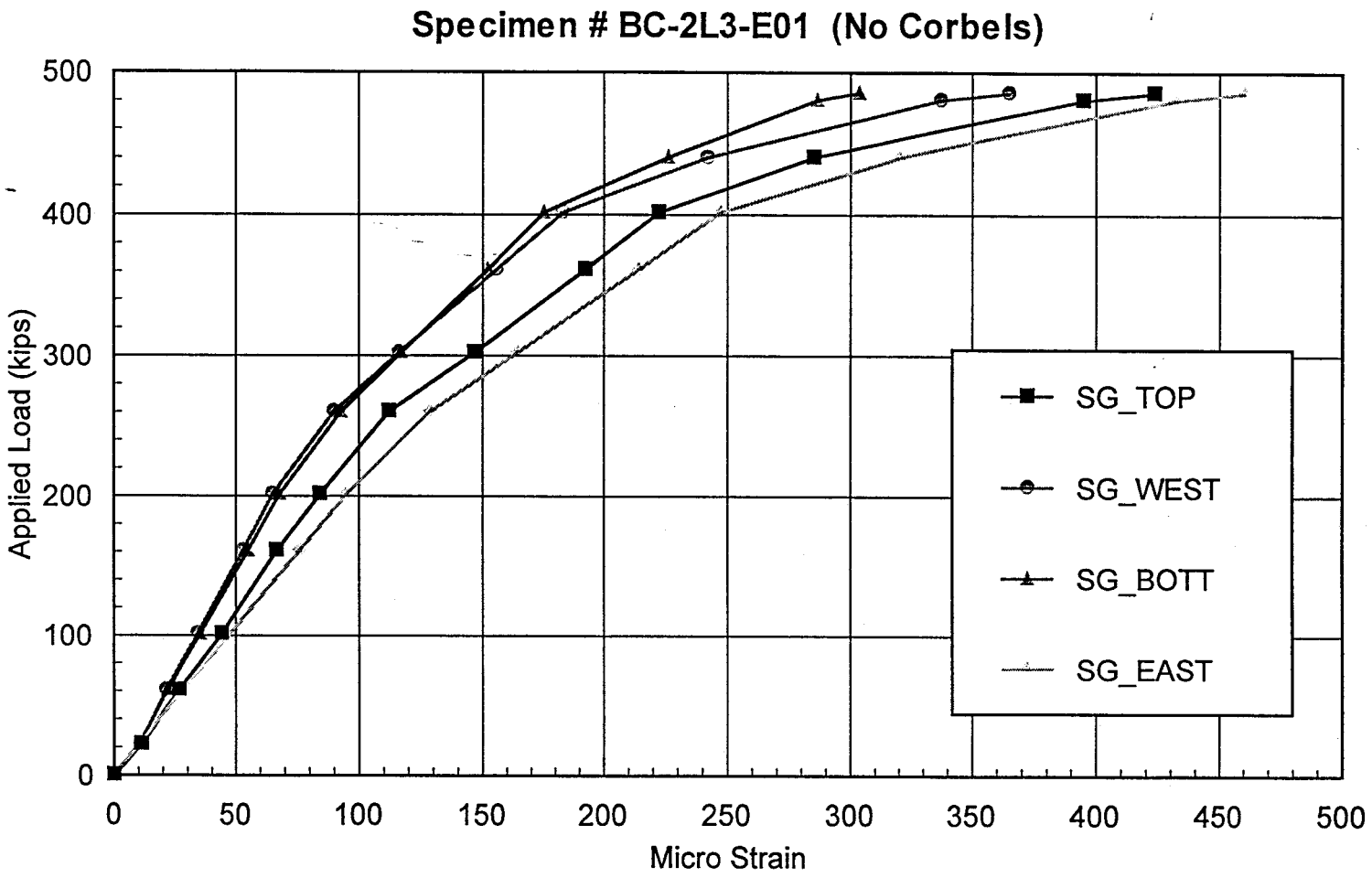

(Fig. 5.5e) Load VS.Transverse Surface Strain At Midspan

Specimen # BC-2L3-E02 (No Corbels)

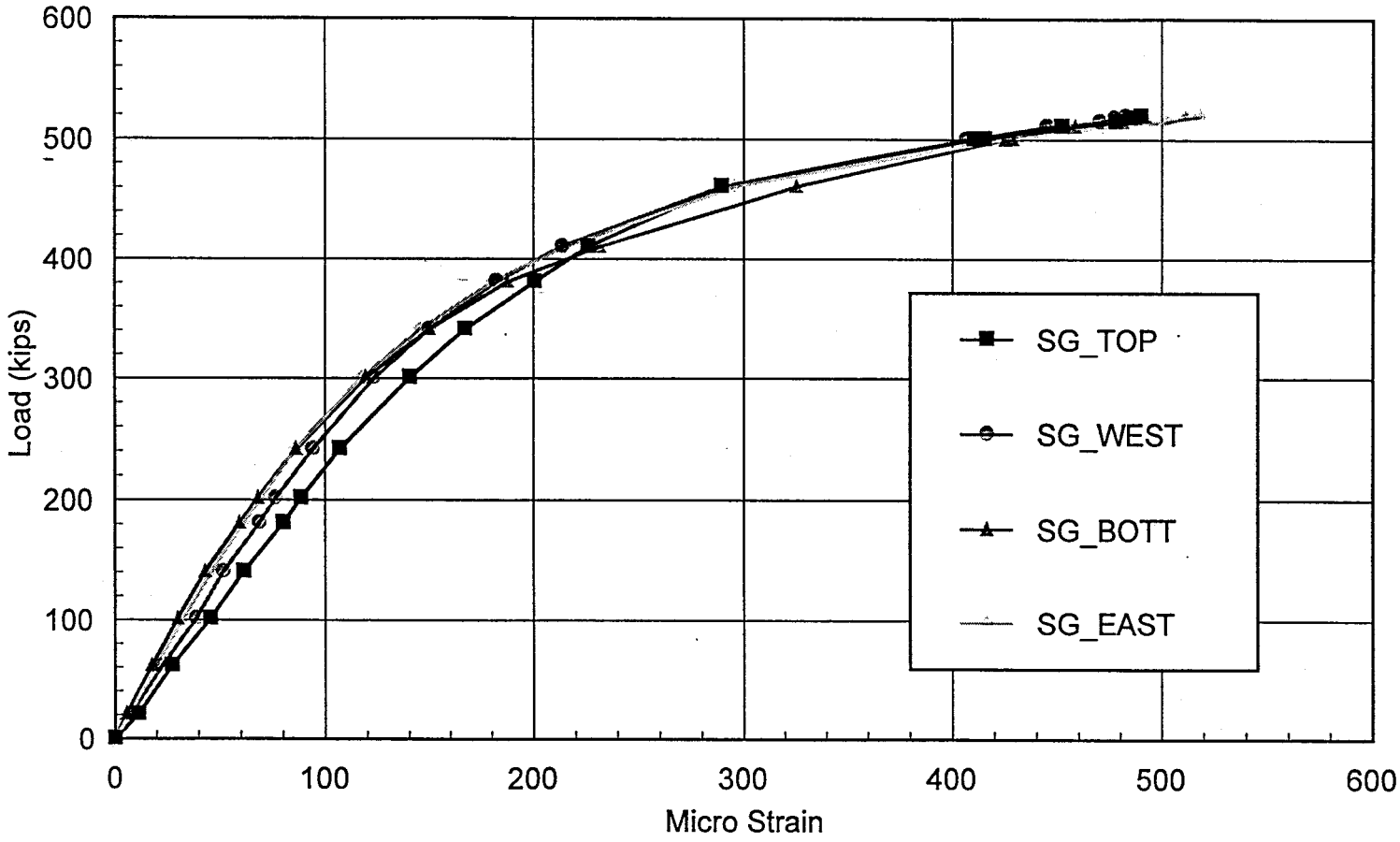

(Fig. 5.5f) Load VS.Transverse Surface Strain At Midspan

Specimen # BC-2L3-E03 (No Corbels)

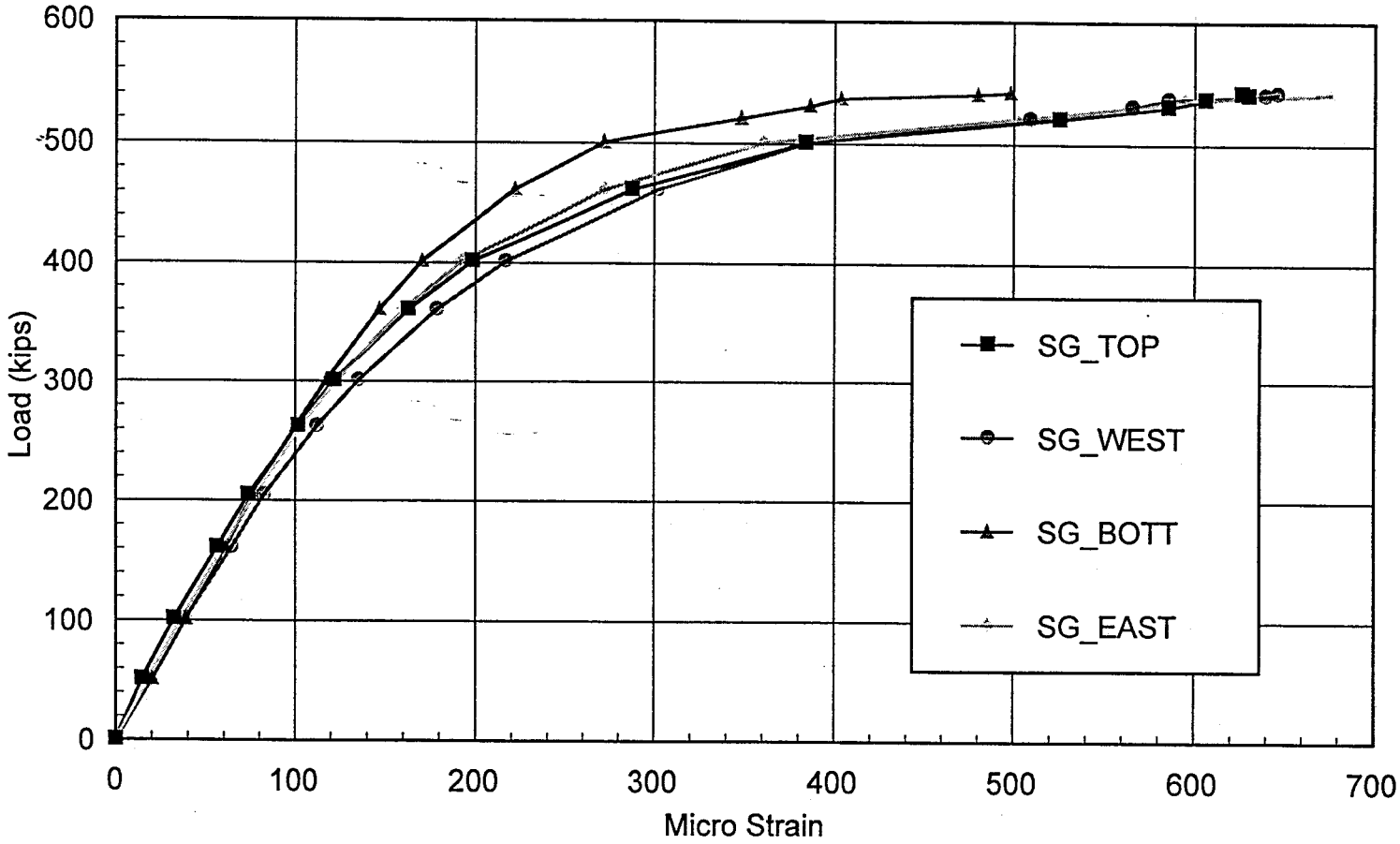

(Fig. 5.6b) Moment VS. Deflection At Center Line

Specimen #BC-2L3-E3-1

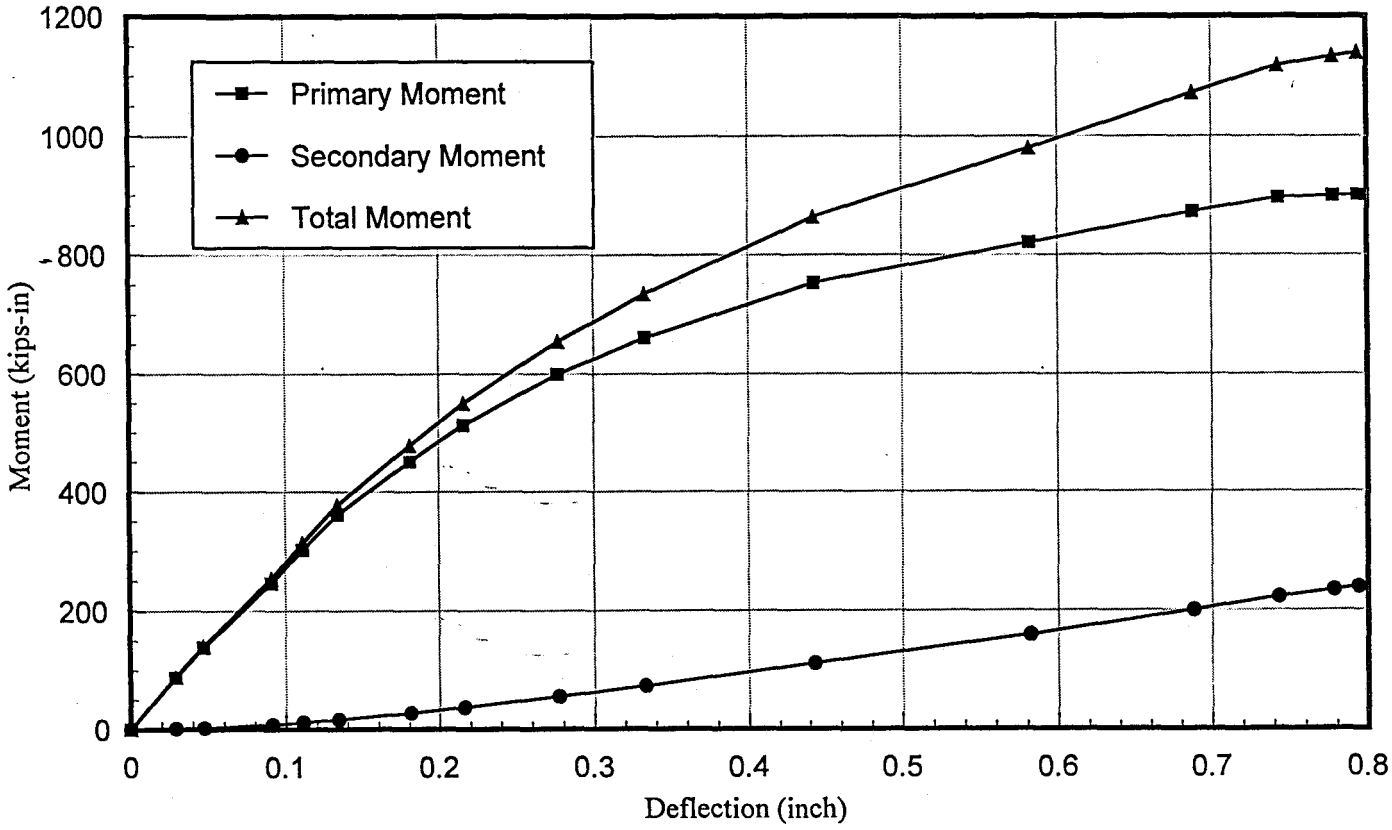

(Fig 5.8a) Longitudinal Compressive Strain Distribution Along Beam Length

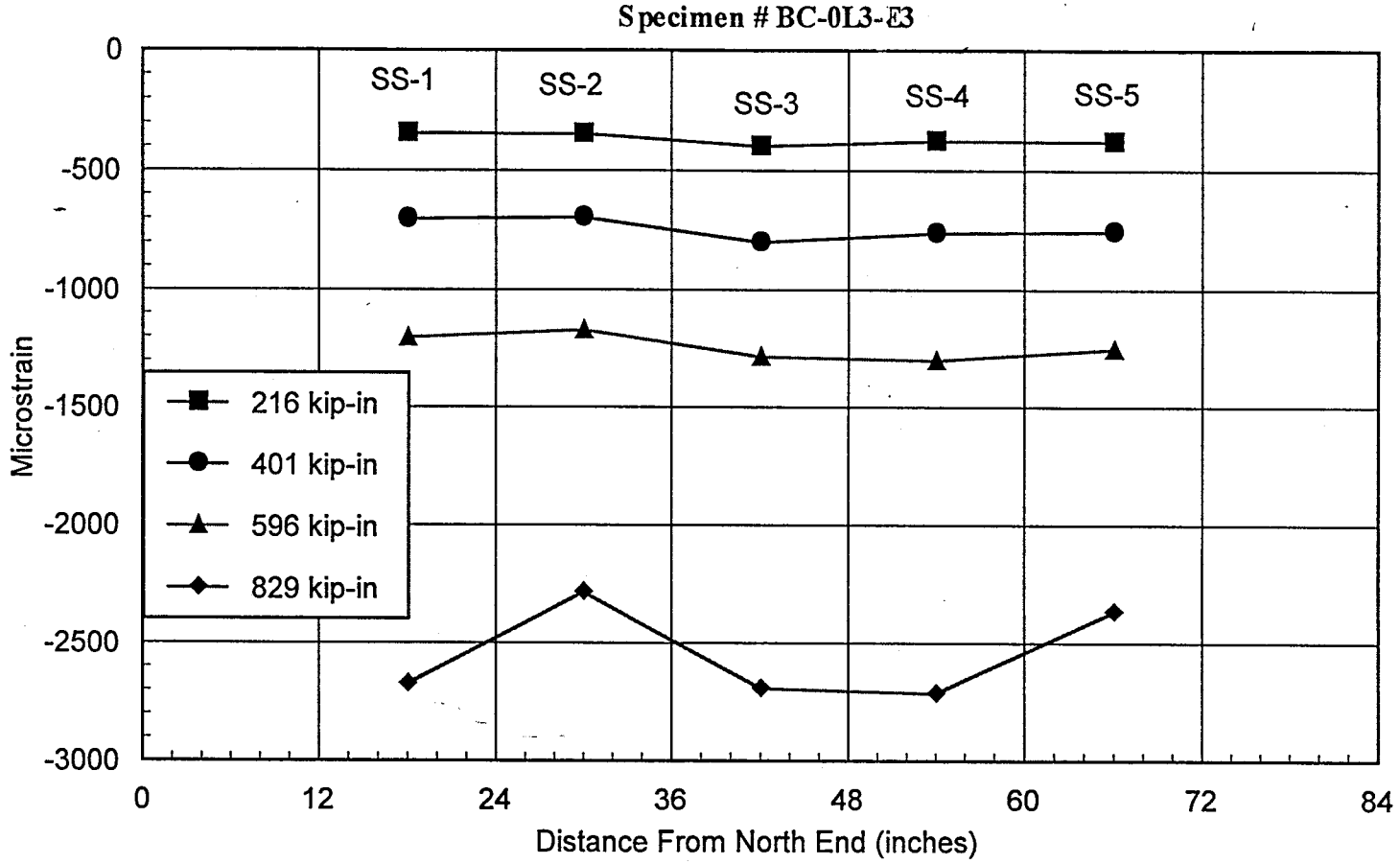

(Fig. 5.8b) Longitudinal Tension Strain Distribution Along Beam Length

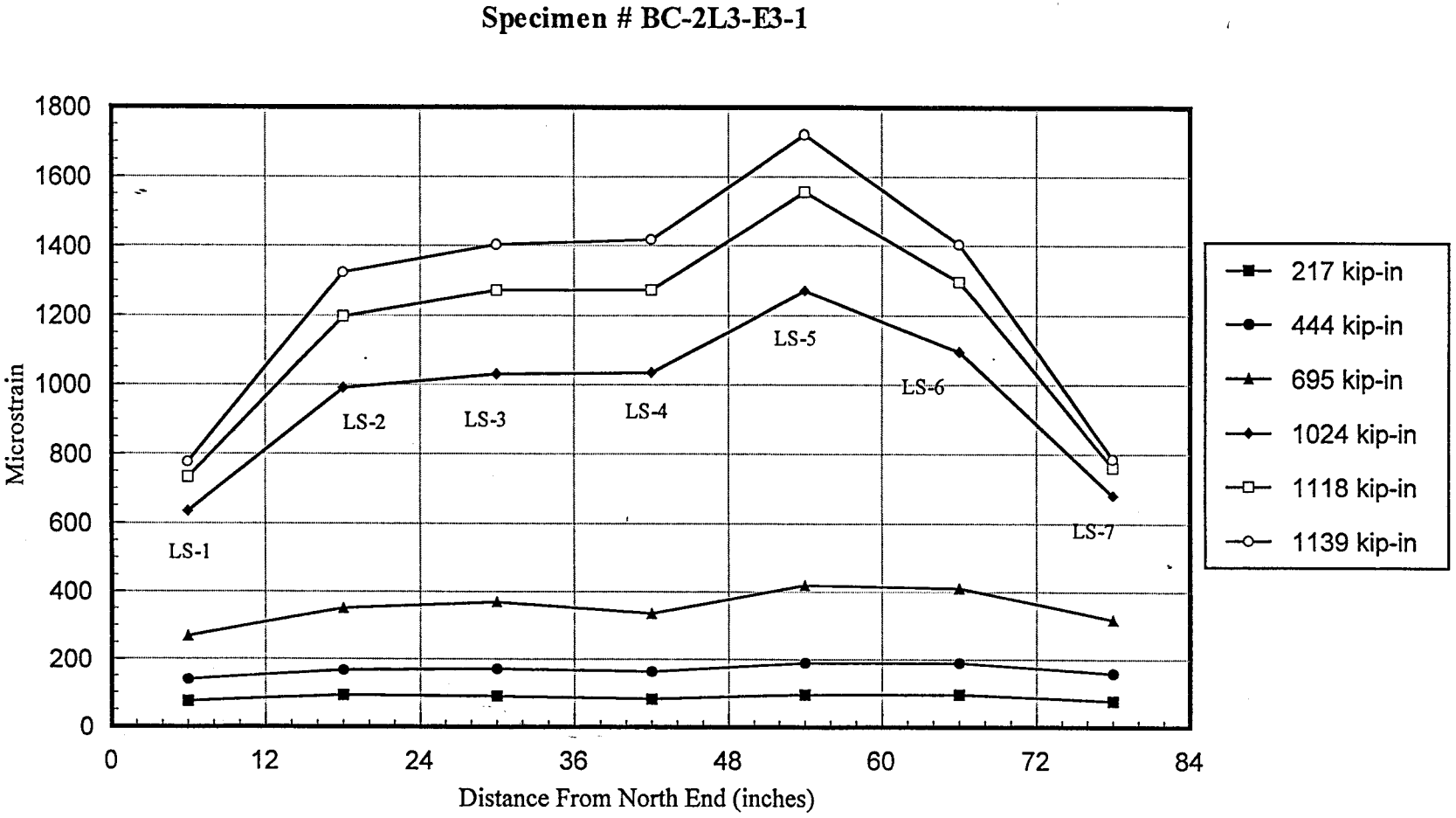

(Fig. 5.8b) Longitudinal Compressive Strain Distribution Along Beam Length

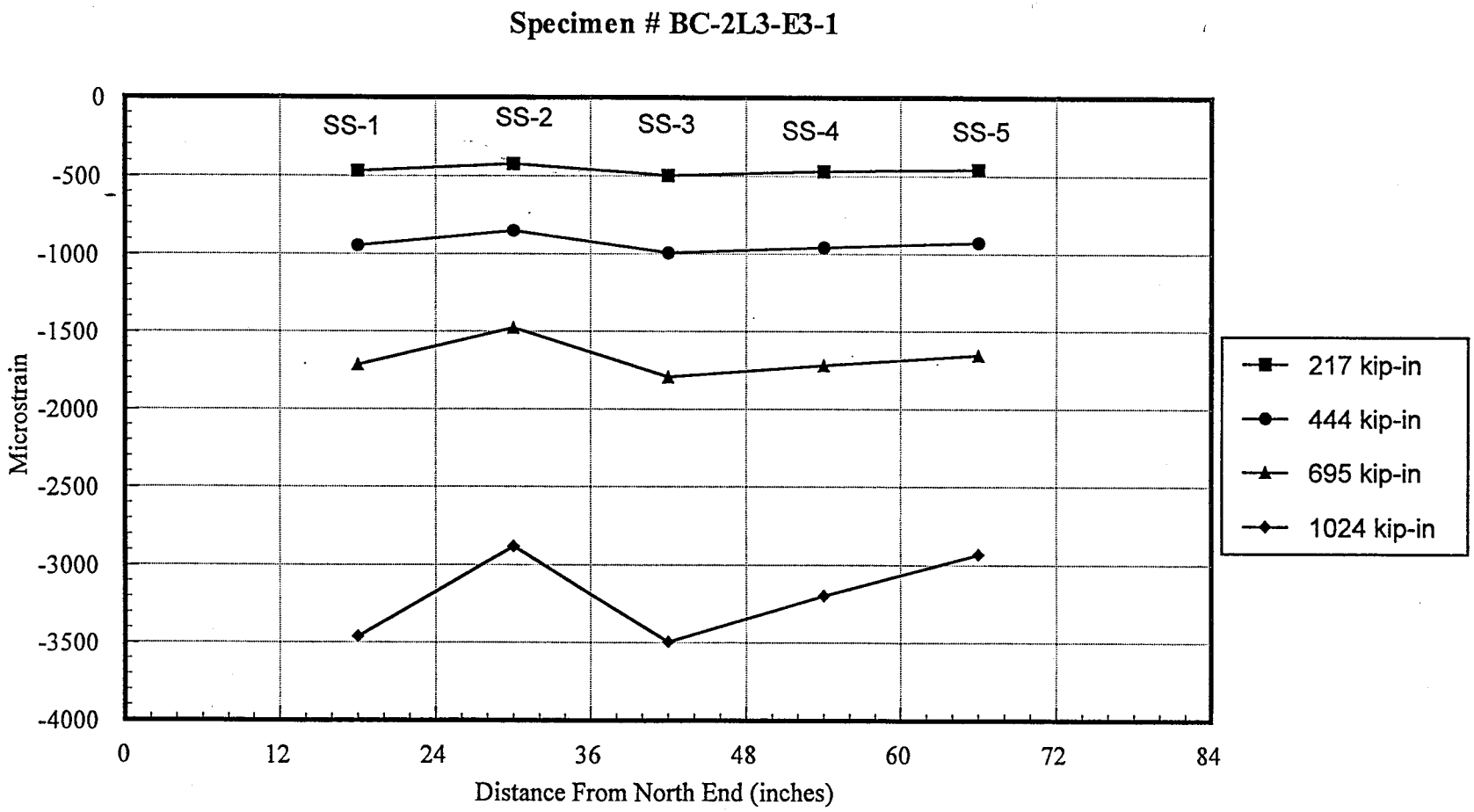

(Fig. 5.8c) Longitudinal Tension Strain Distribution Along Beam Length

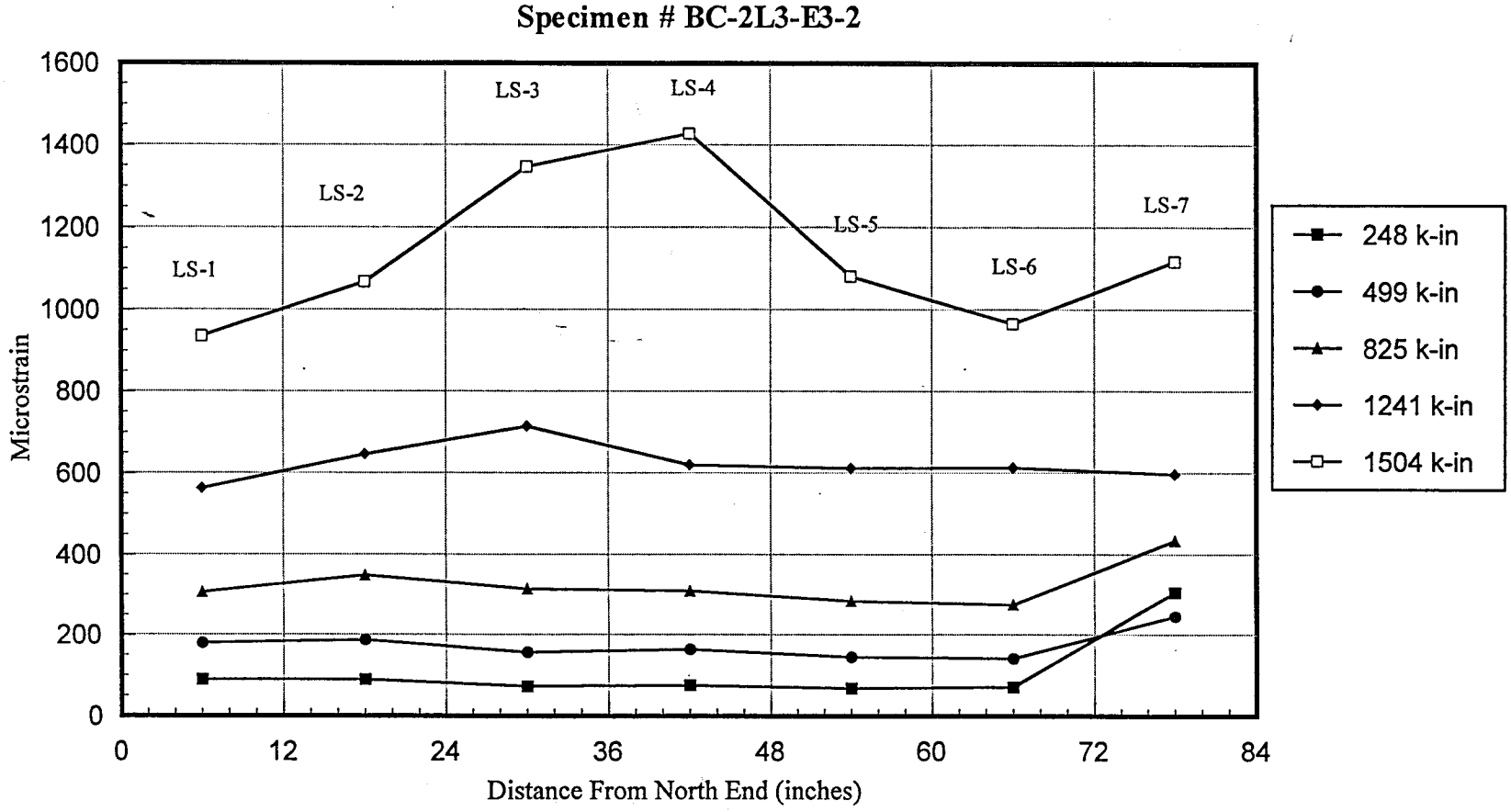

(Fig. 5.9b) Moment VS. Transverse Surface Strain Around Beam Center Line

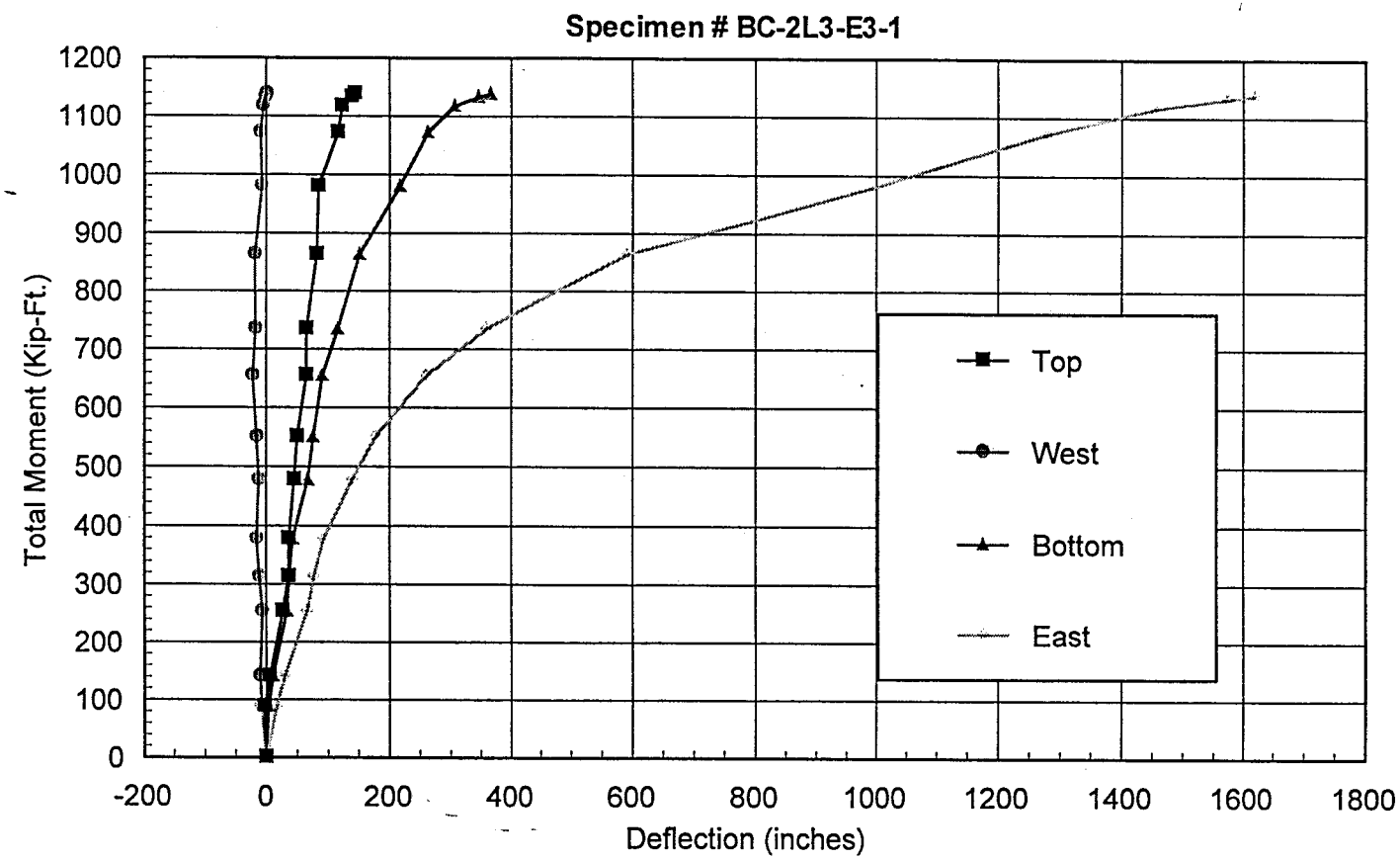

(Fig. 5.9c) Moment VS. TRansverse Surface Strain Around Beam Center Line

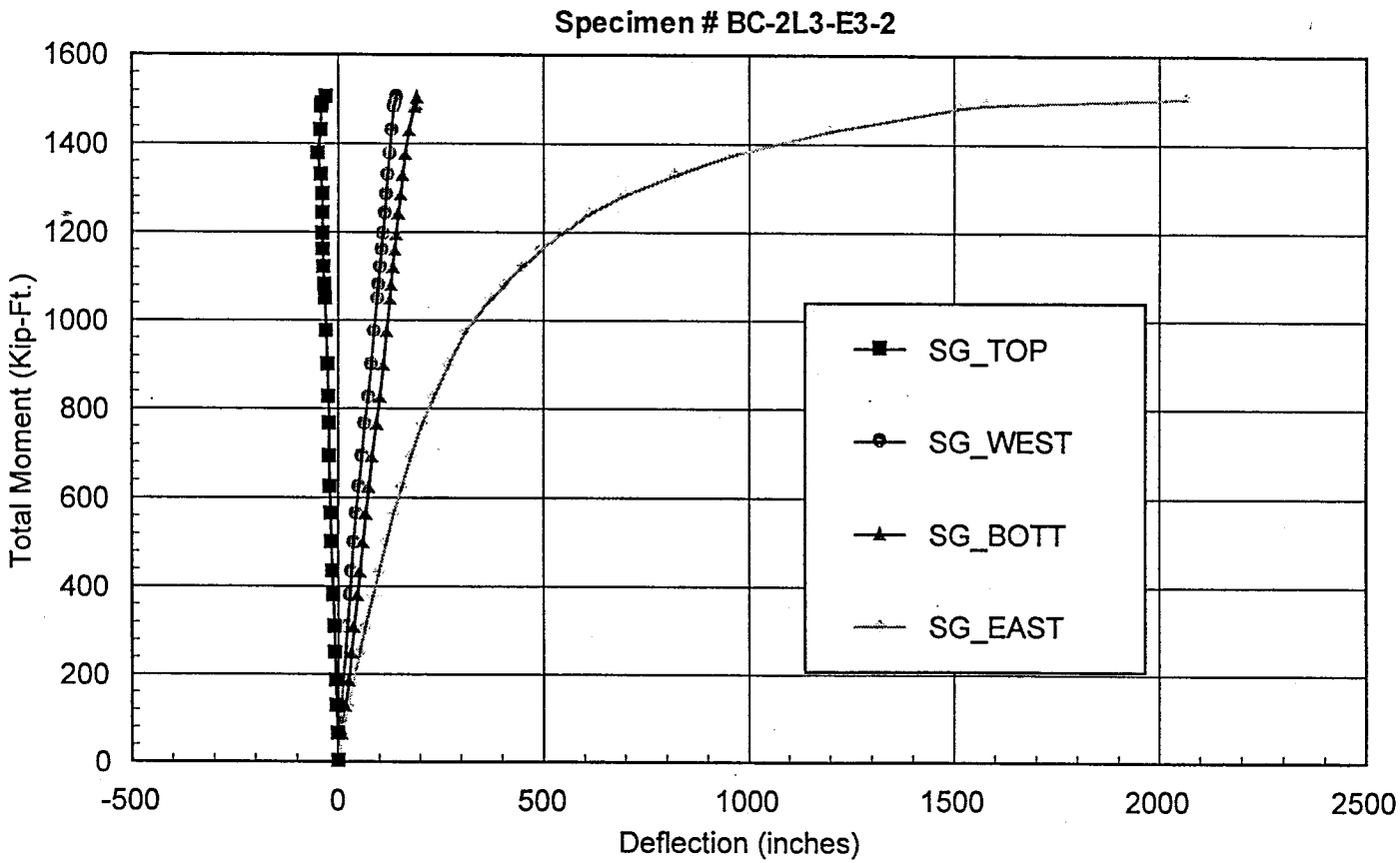

(Fig. 5.10a) Moment vs. Deflection At Center Line
Specimen # BC-0L3-E6

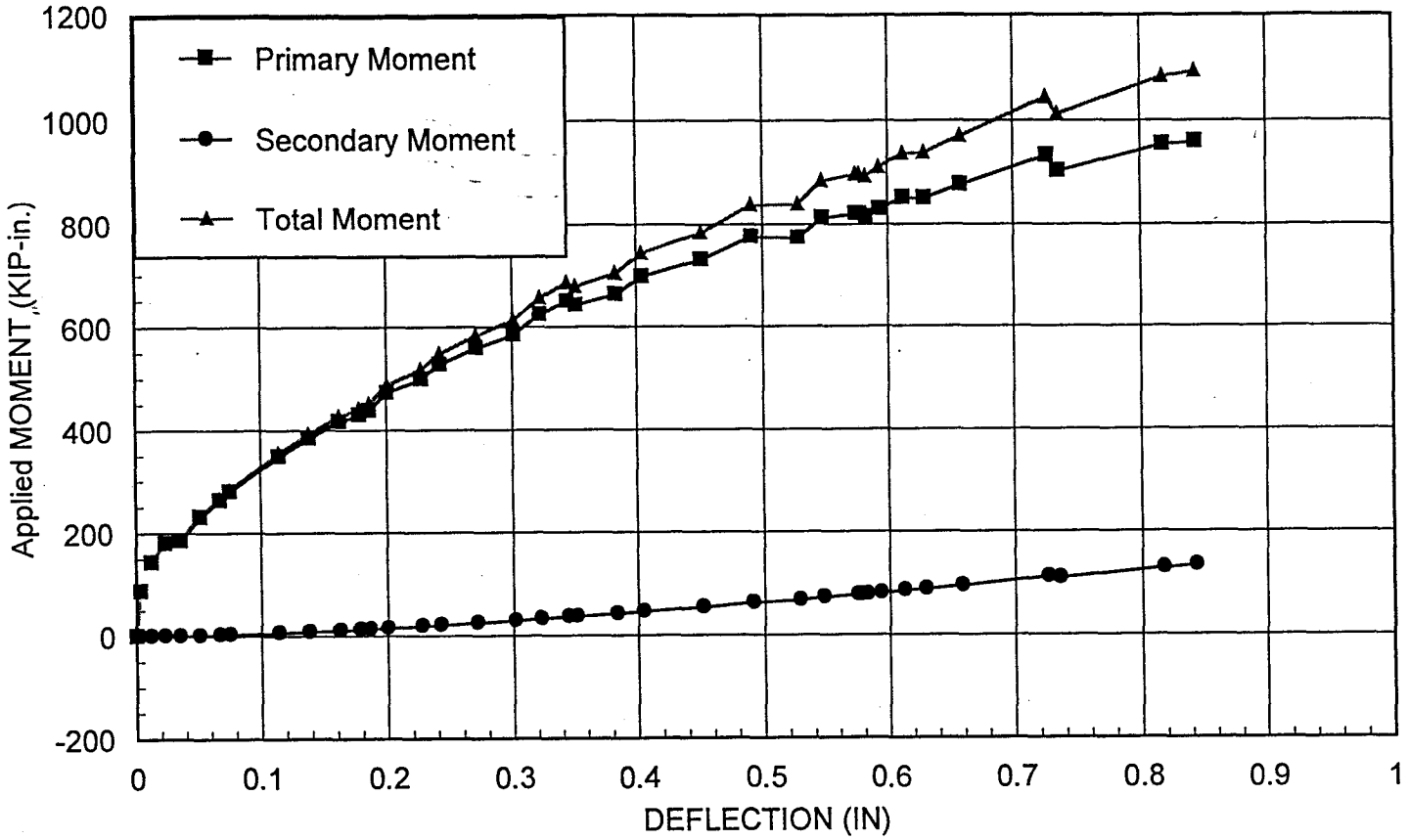

(Fig. 5.11b)Strain Distribution at Specimen Center Line

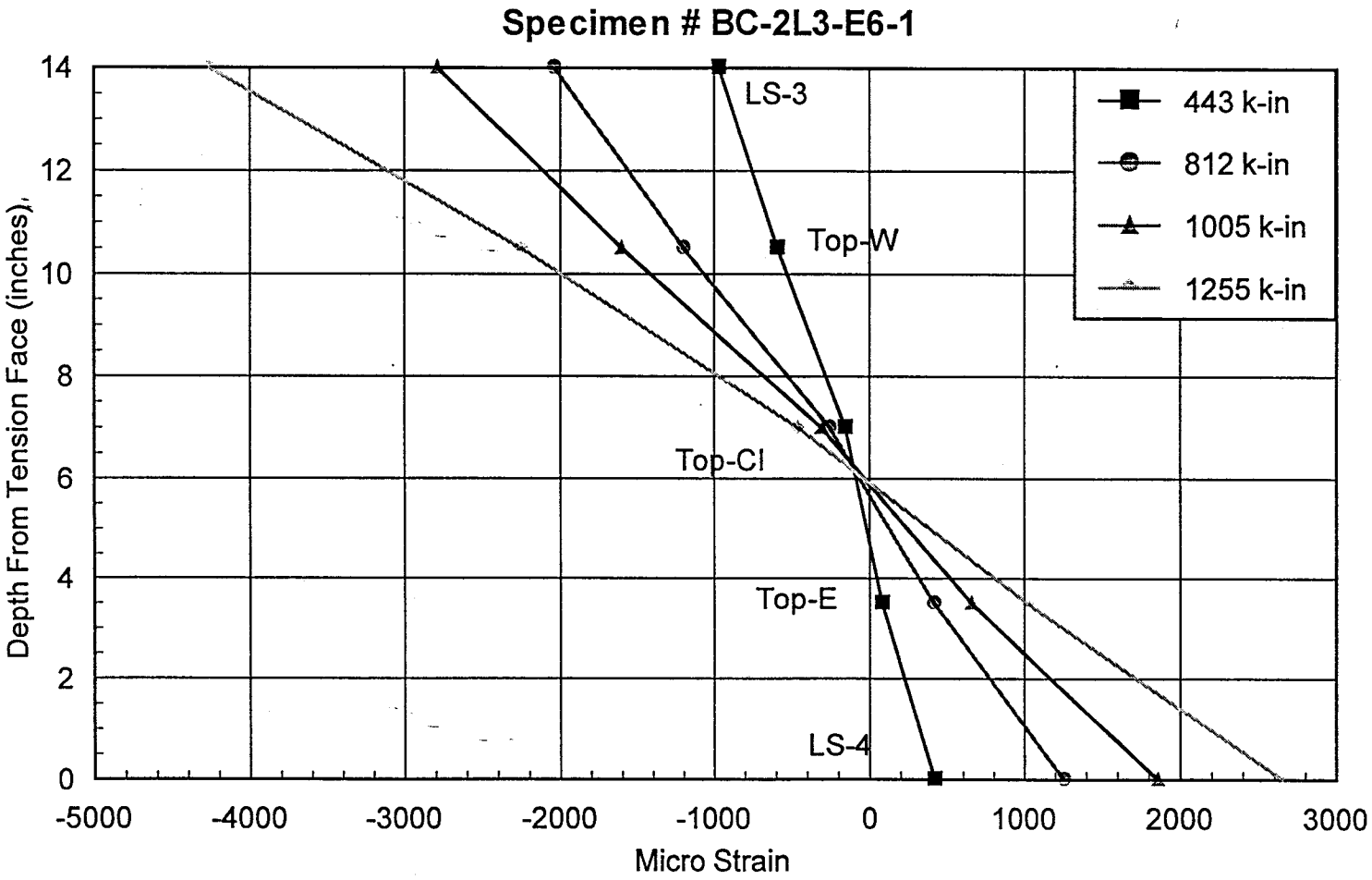

(Fig. 5.12a) LONGITUDINAL TENSION STRAIN DISTRIBUTION ALONG BEAM LENGTH
Specimen # BC-0L3-E6

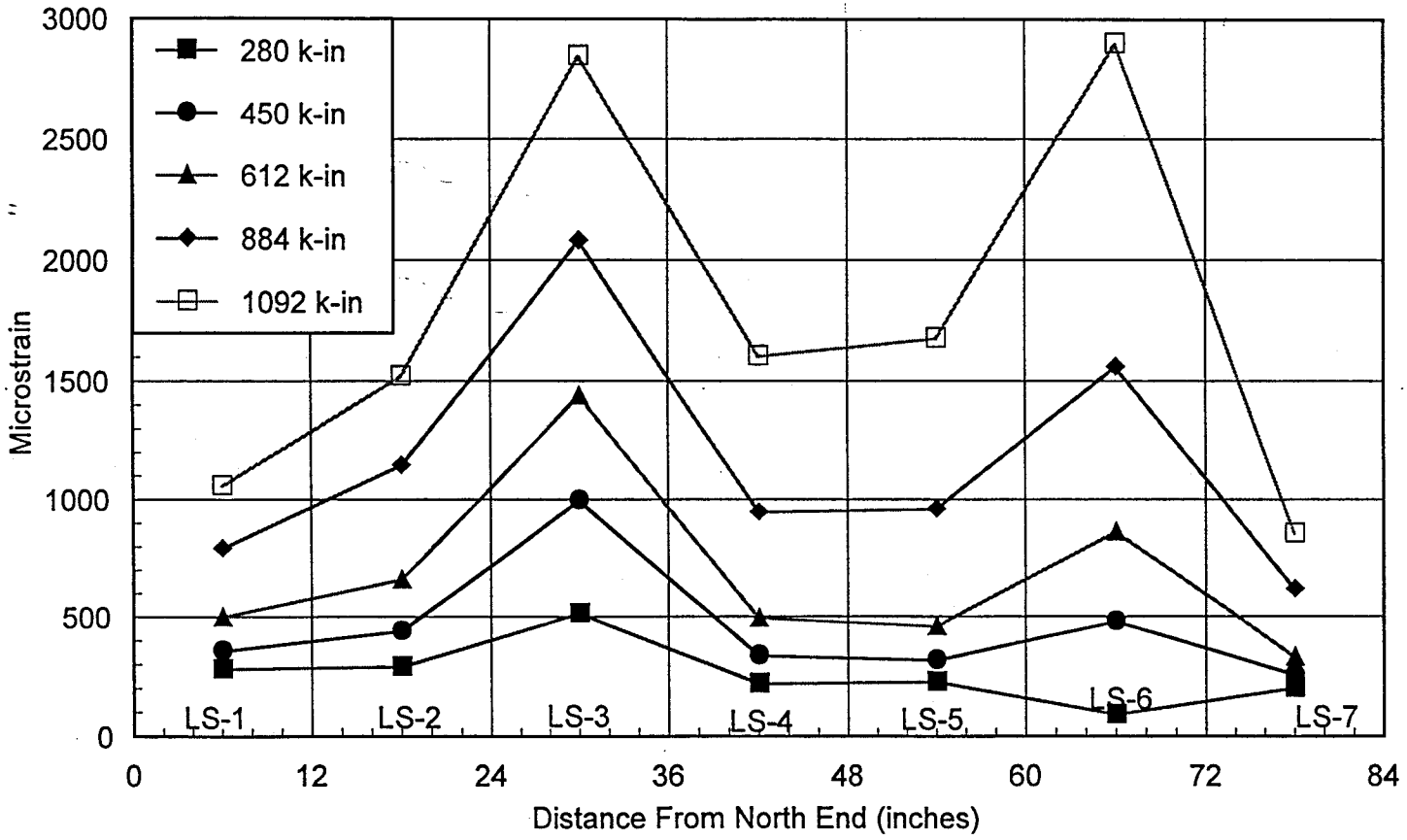

(Fig.5.12b) LONGITUDINAL TENSION STRAIN DISTRIBUTION ALONG BEAM LENGTH

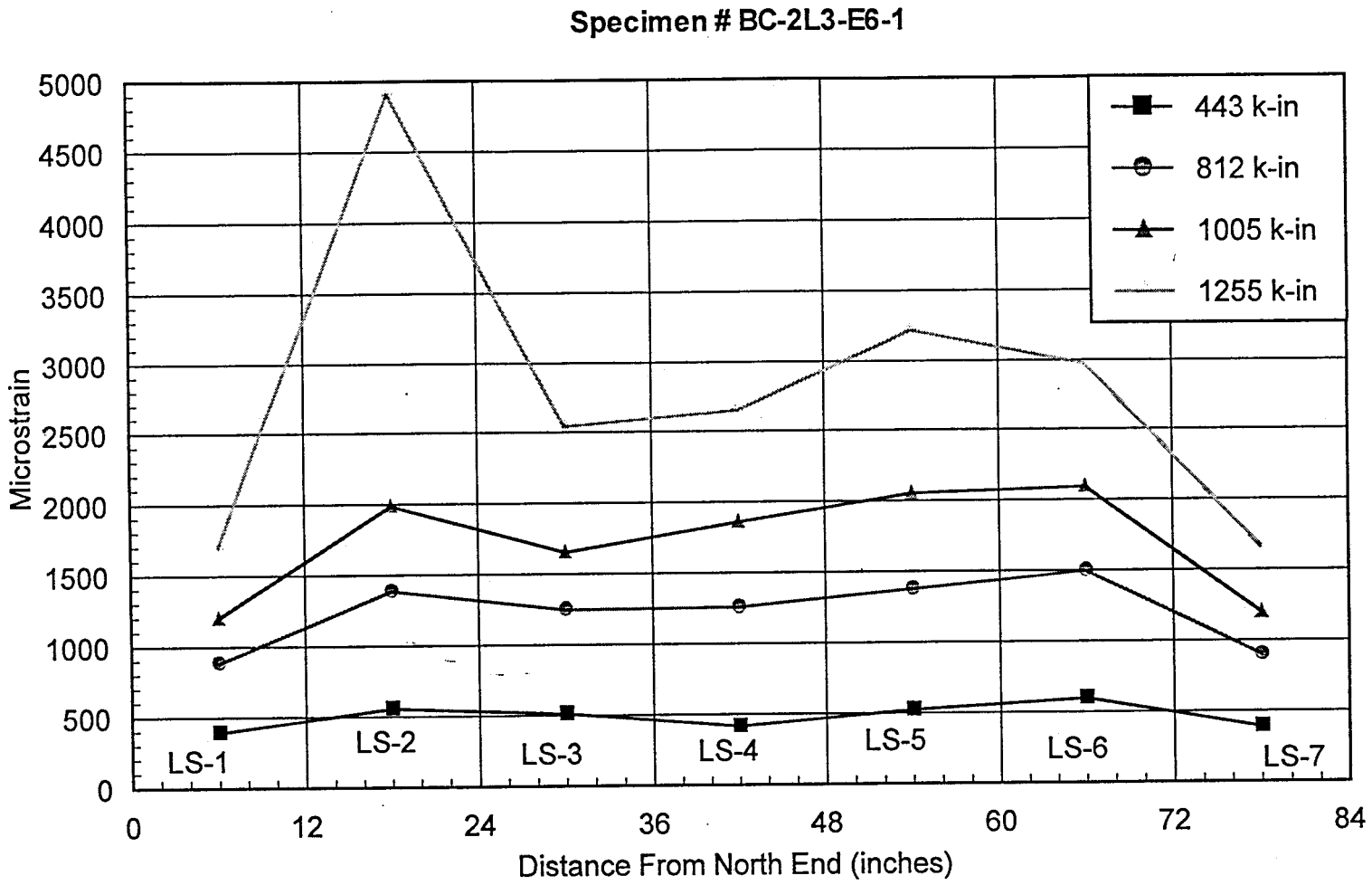

(Fig. 5.12c) Longitudinal Compressive Strain Distribution Along Beam Length

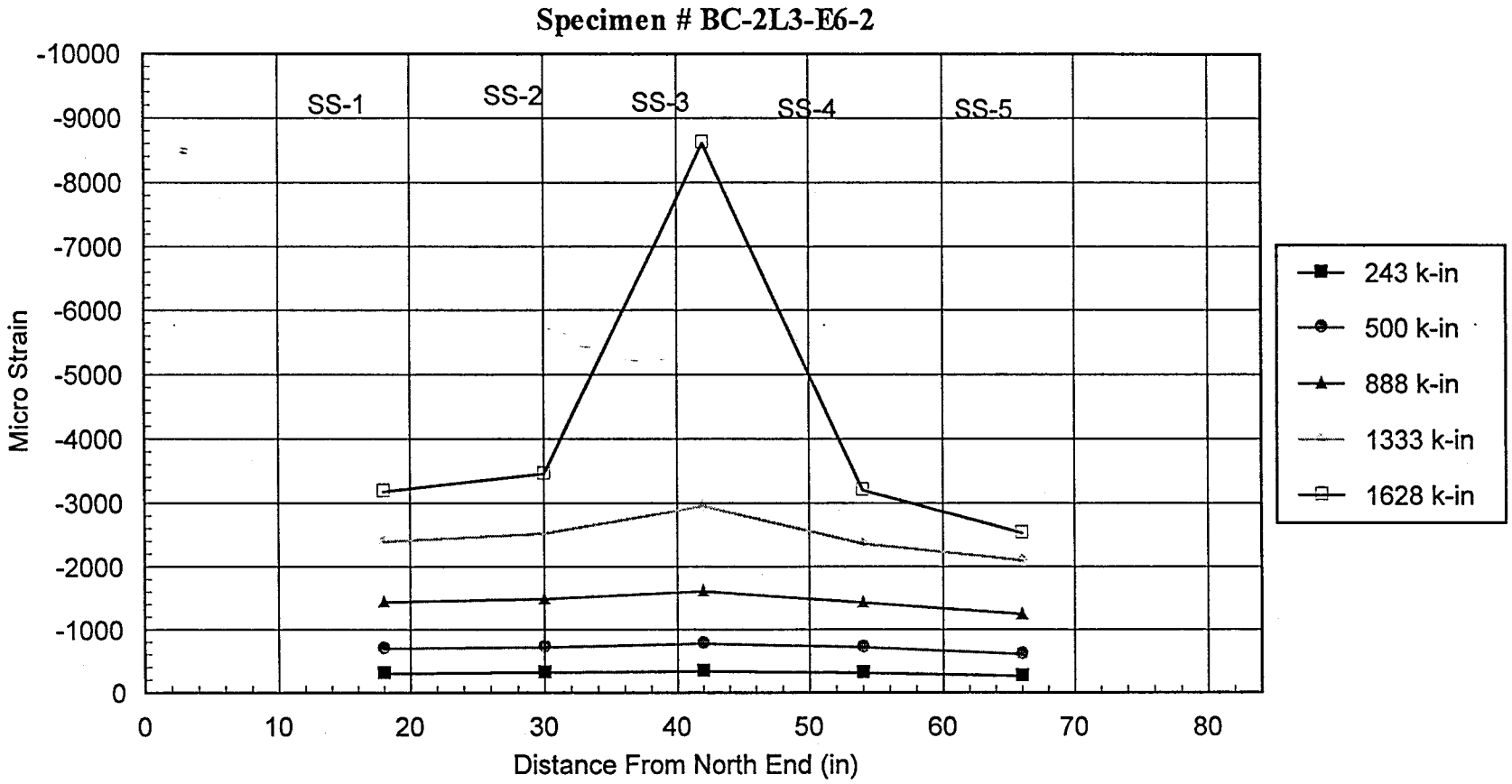

(Fig. 5.13b) Moment vs.Transverse Strain
Specimen # BC-2L3-E6-1

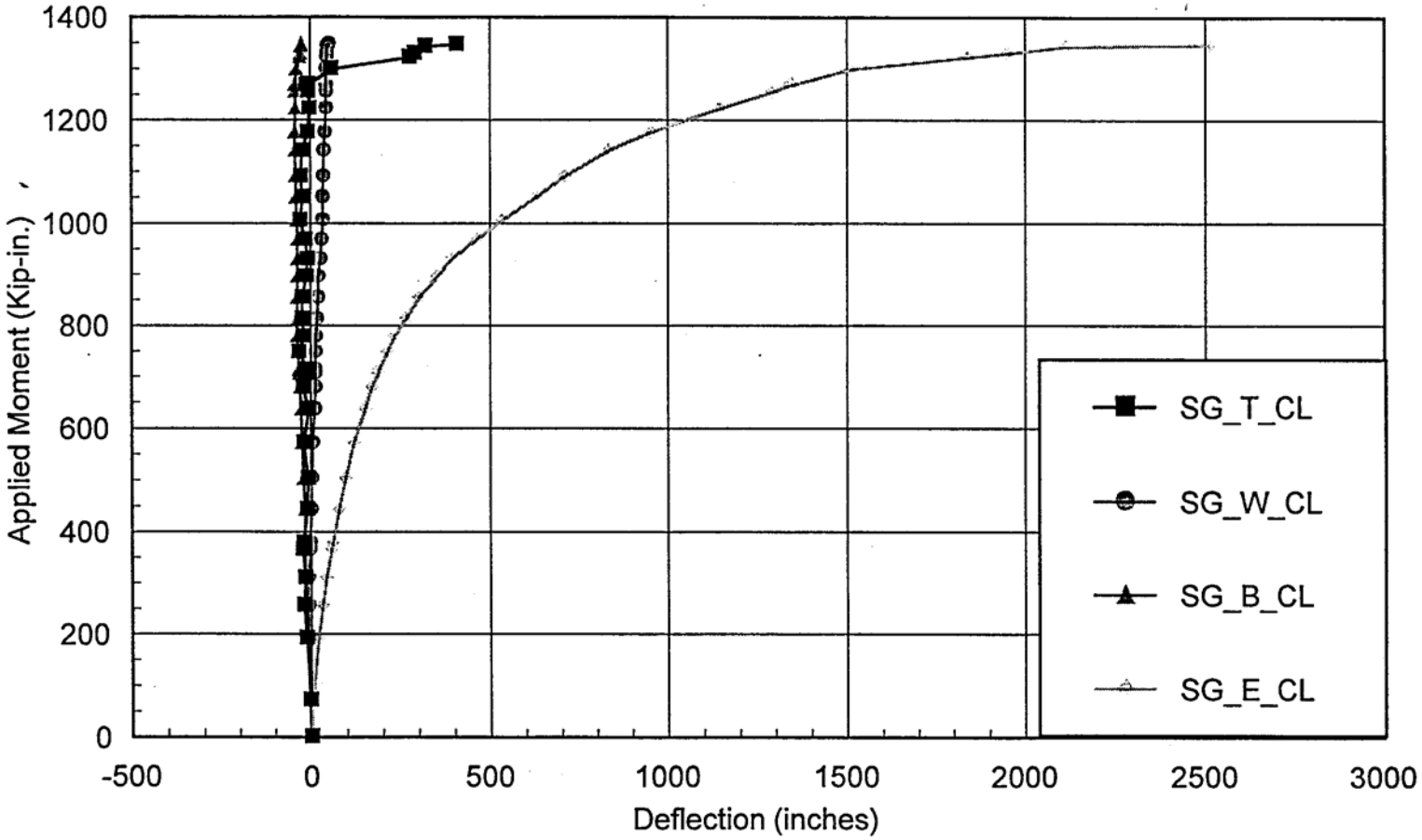

(Fig. 5.13c) Moment VS. TRansverse Surface Strain Around Beam Center Line

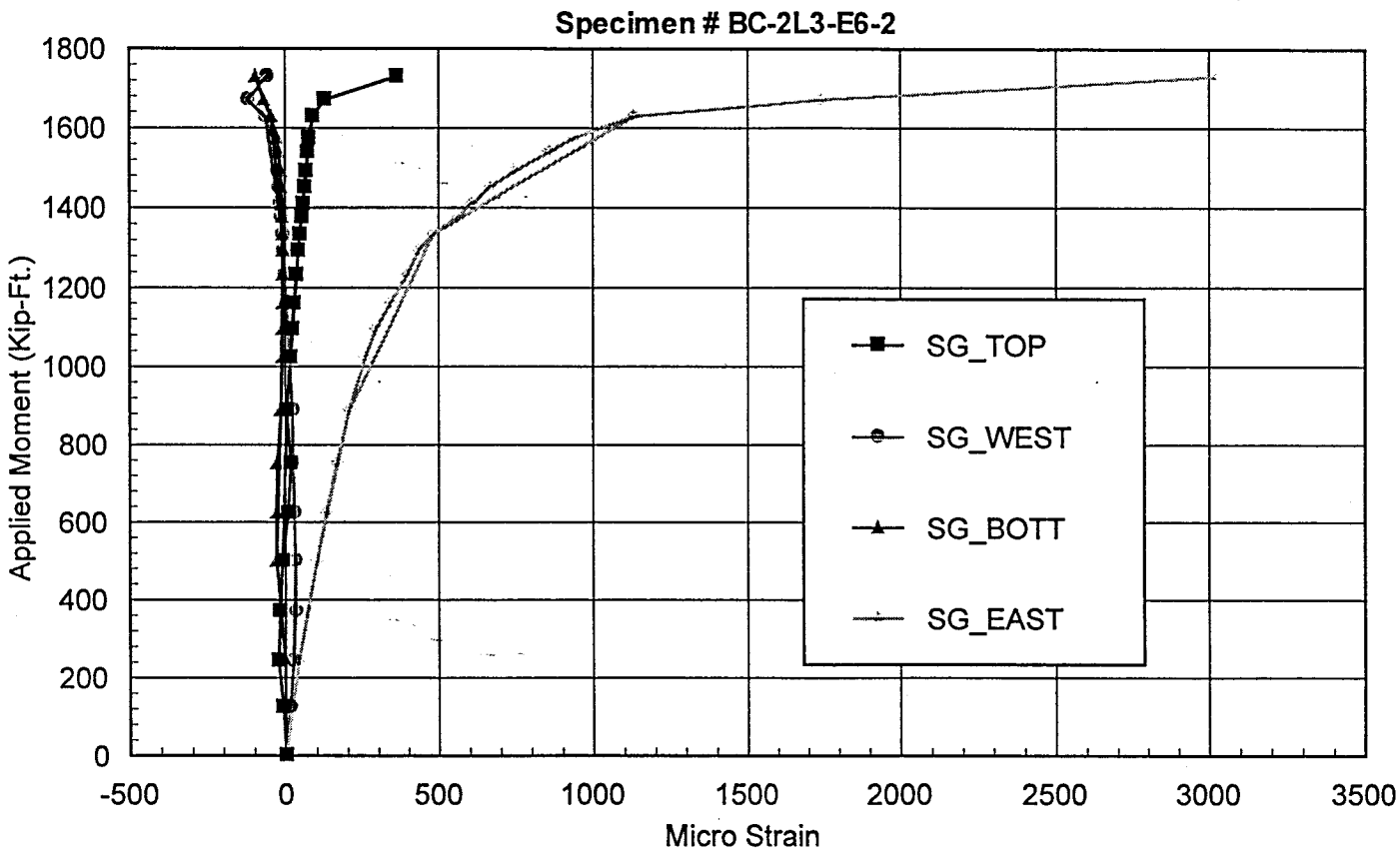

(Fig. 5.14a) Moment vs. Deflection At Center Line

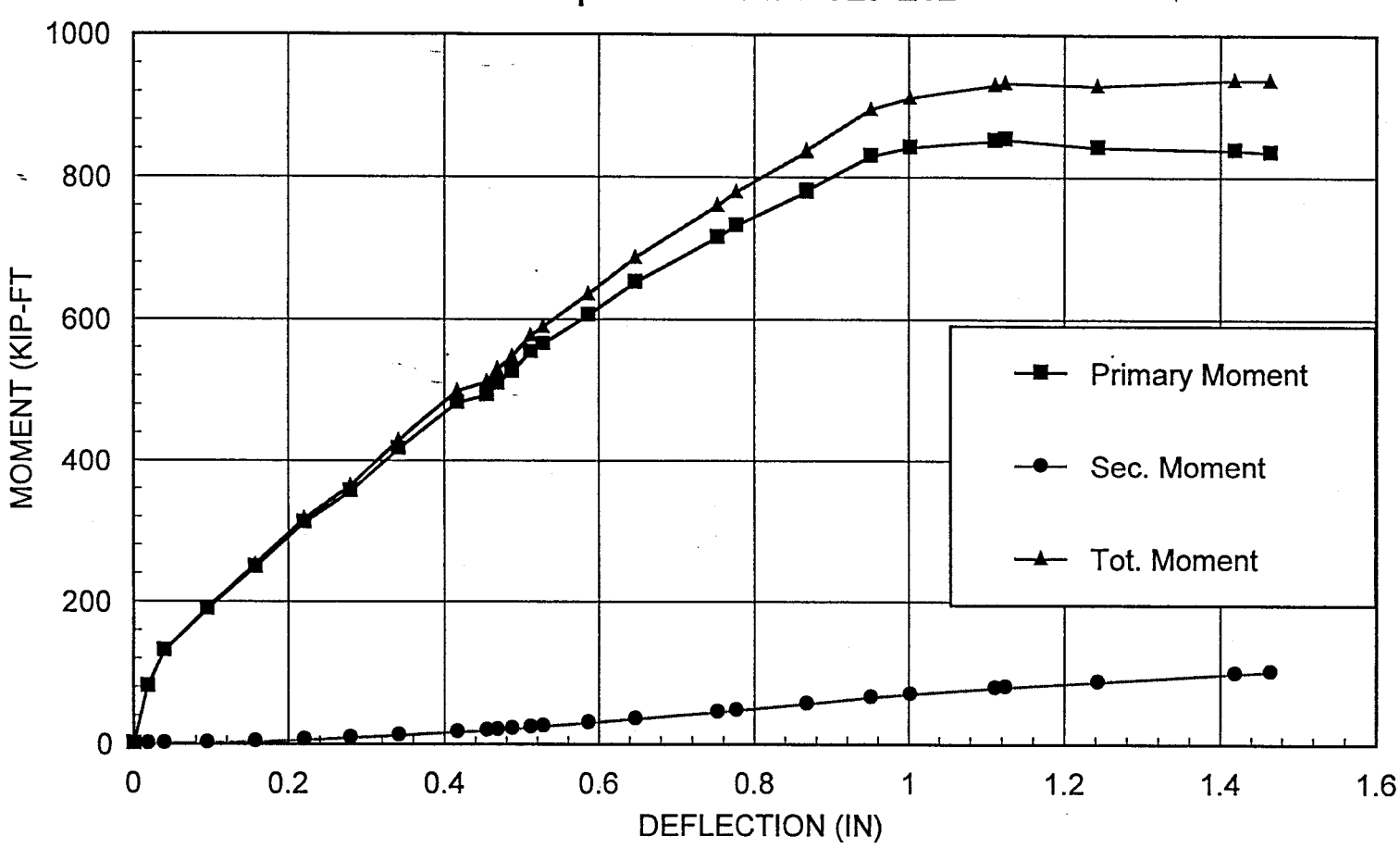

(Fig. 5.14b) Moment vs. Deflection At Center Line

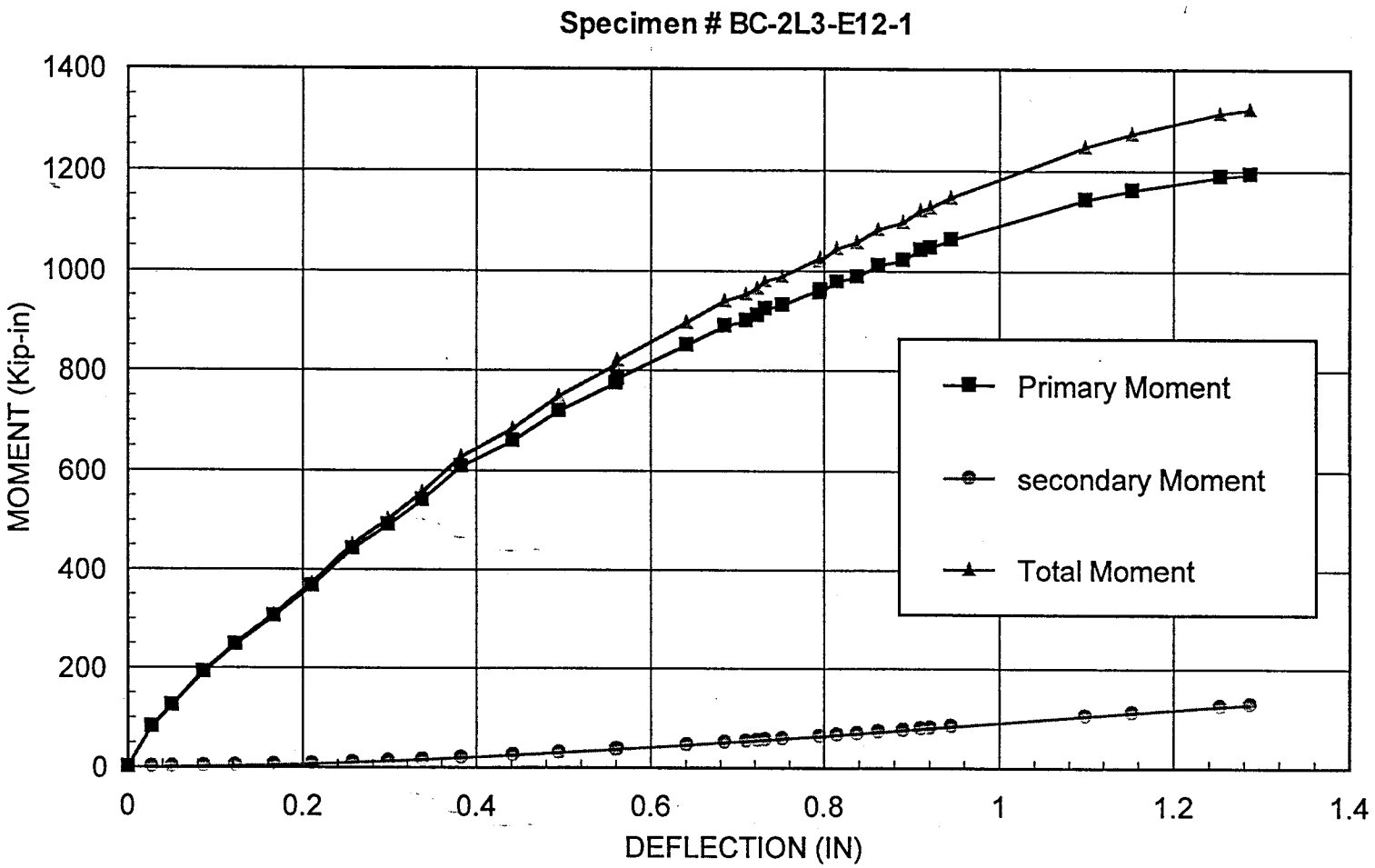

(Fig. 5.14c)Moment vs. Deflection Along Beam Length

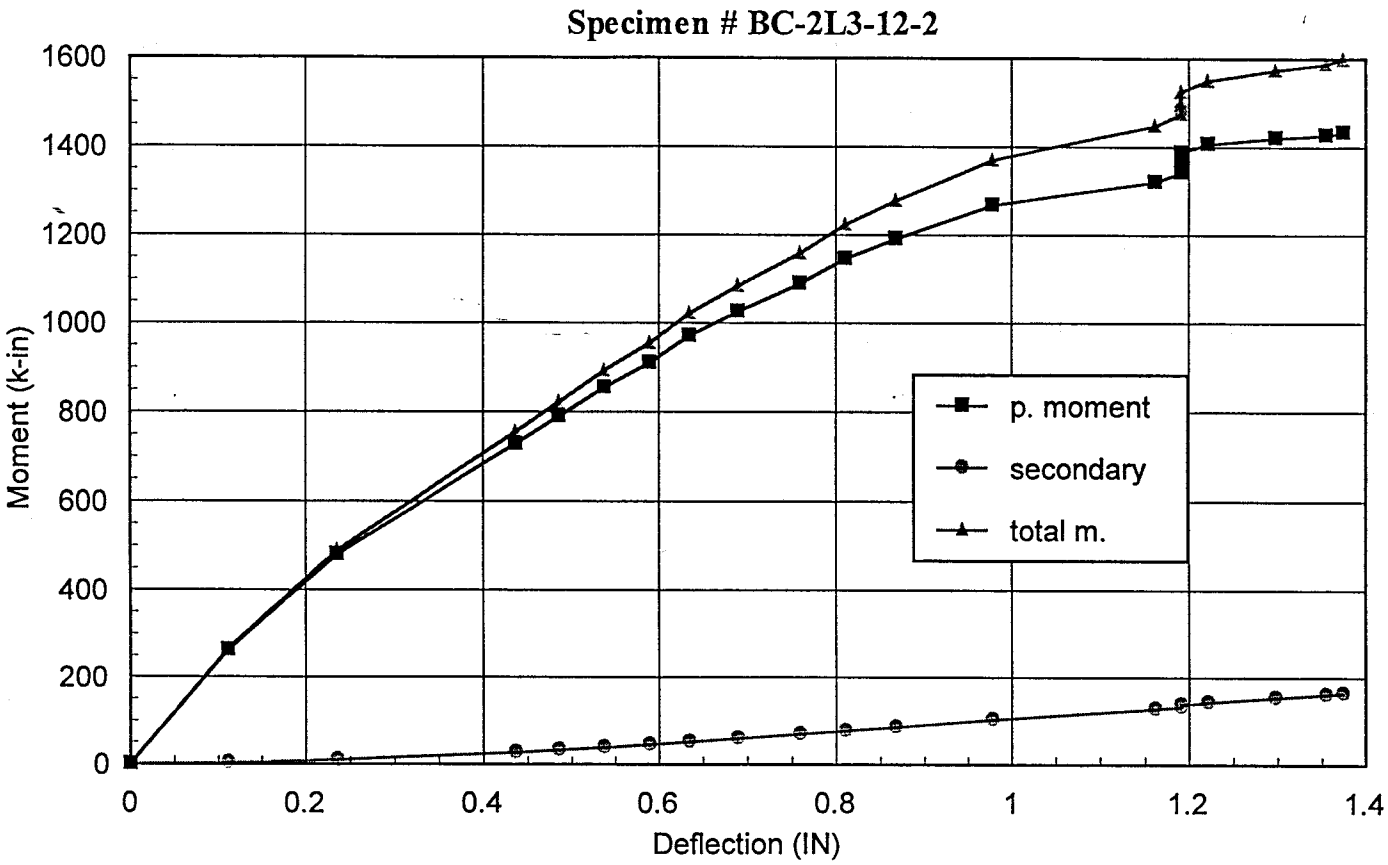

(Fig. 5.14d) Moment vs. Deflection At Center Line

Specimen # BC-0L3-E12-RL2

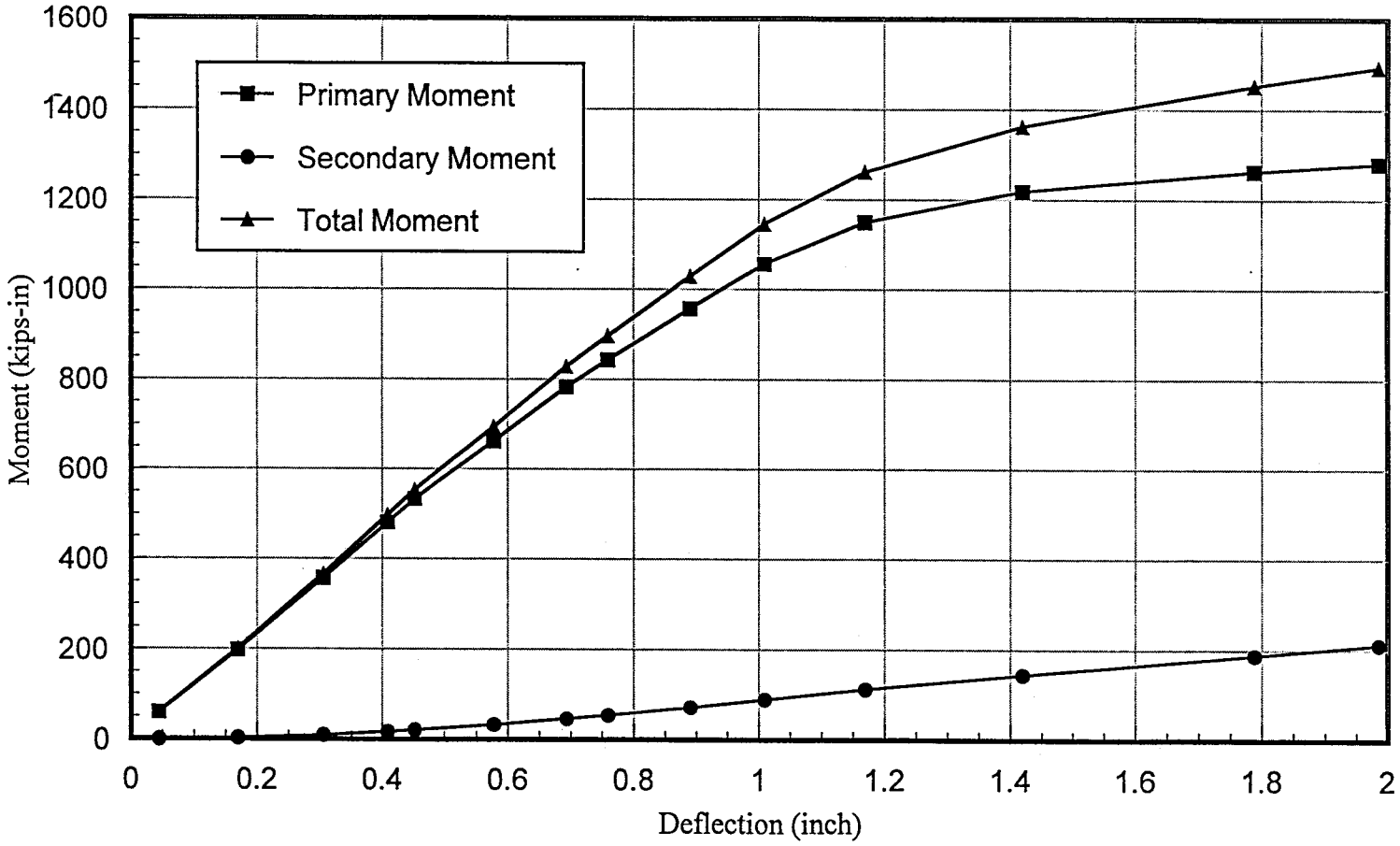

(Fig. 5.15a) Strain Distribution at Specimen Center Line

Specimen # BC-0L3-E12

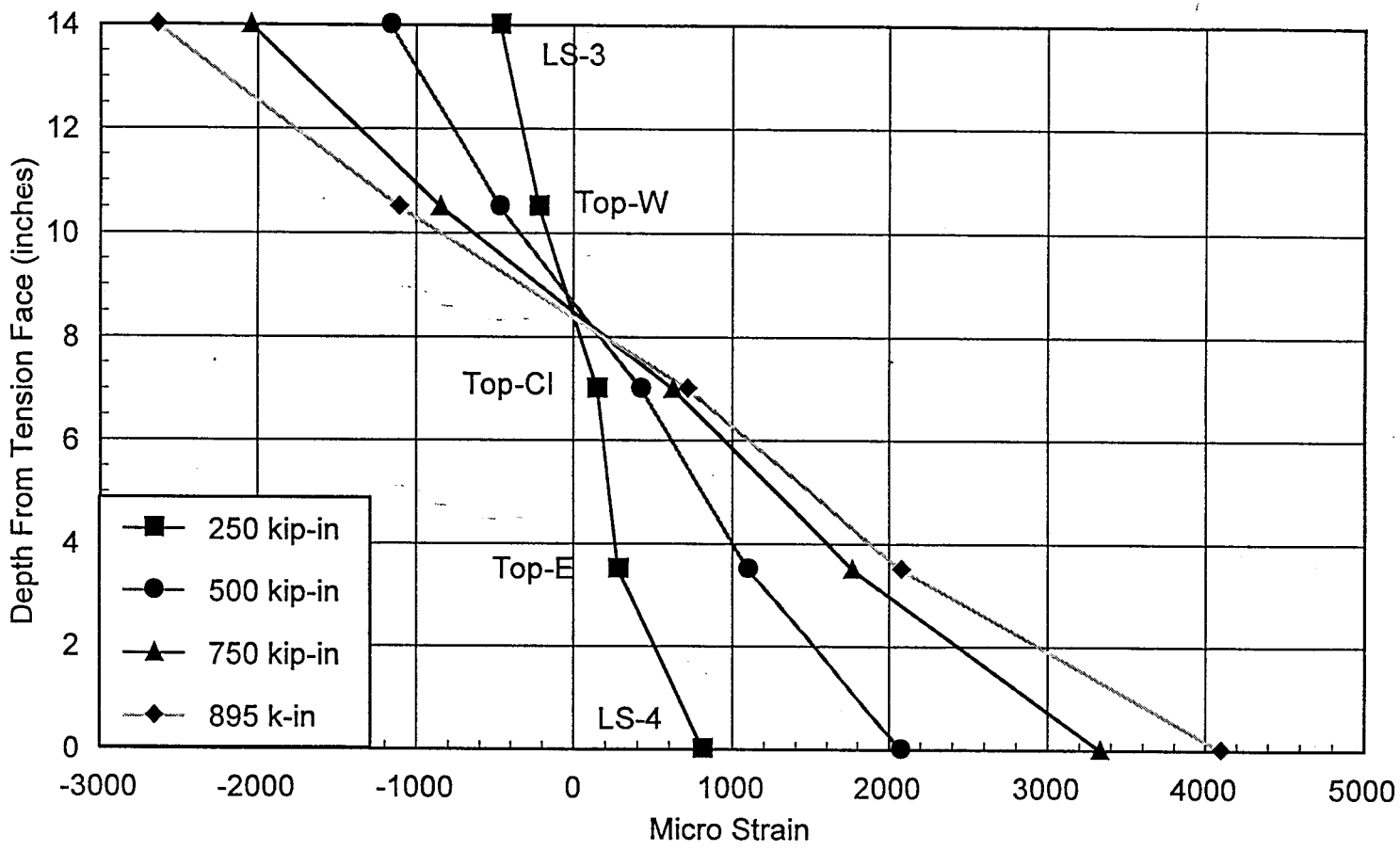

(Fig. 5.15b) Strain Distribution at Specimen Center Line

Specimen # BC-2L3-E12-1

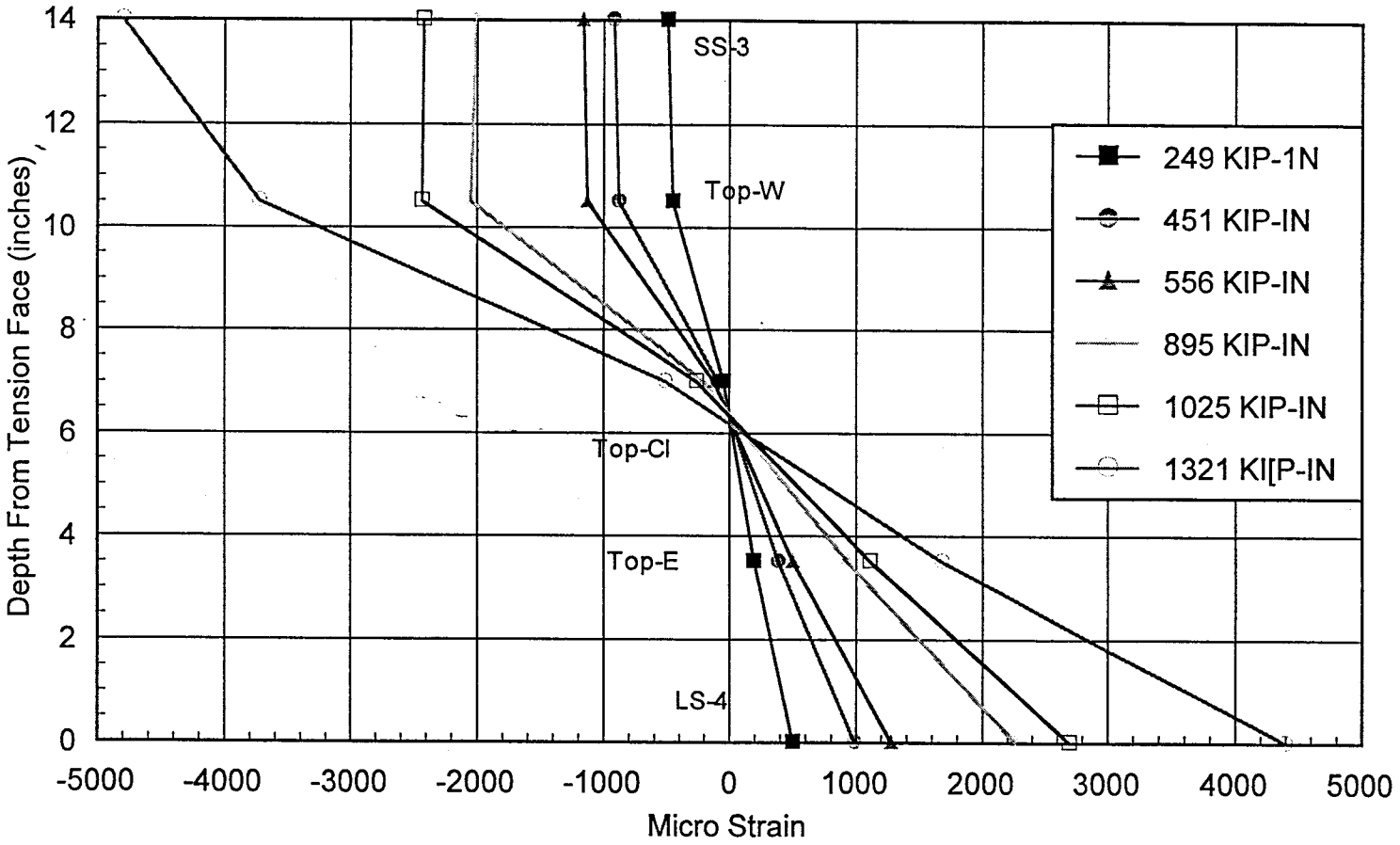

(Fig. 5.15c) Centerline Strain Distribution

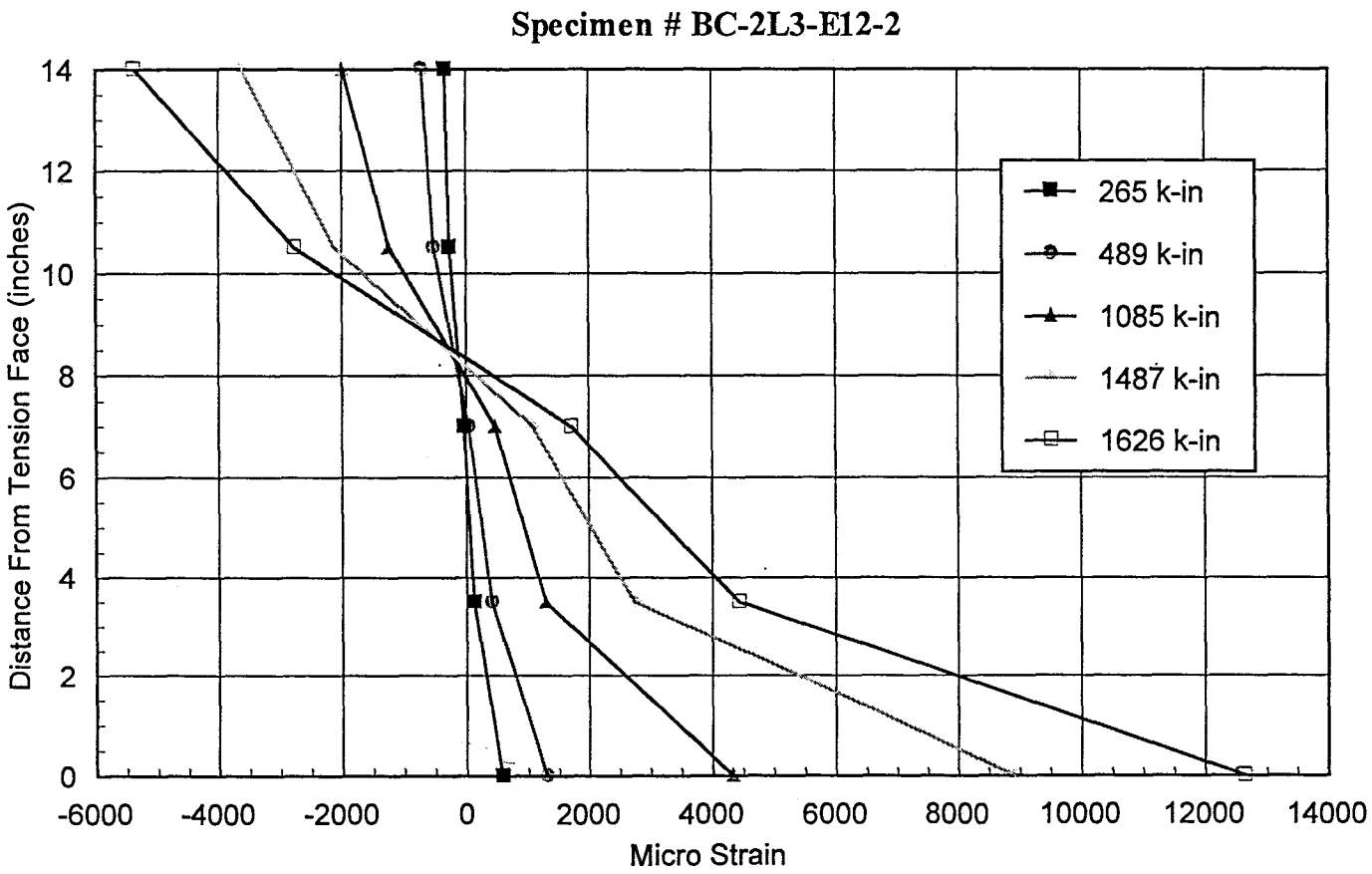

(Fig.5.15d) Centerline Strain Distribution

Specimen # BC-0L3-E12-RL2

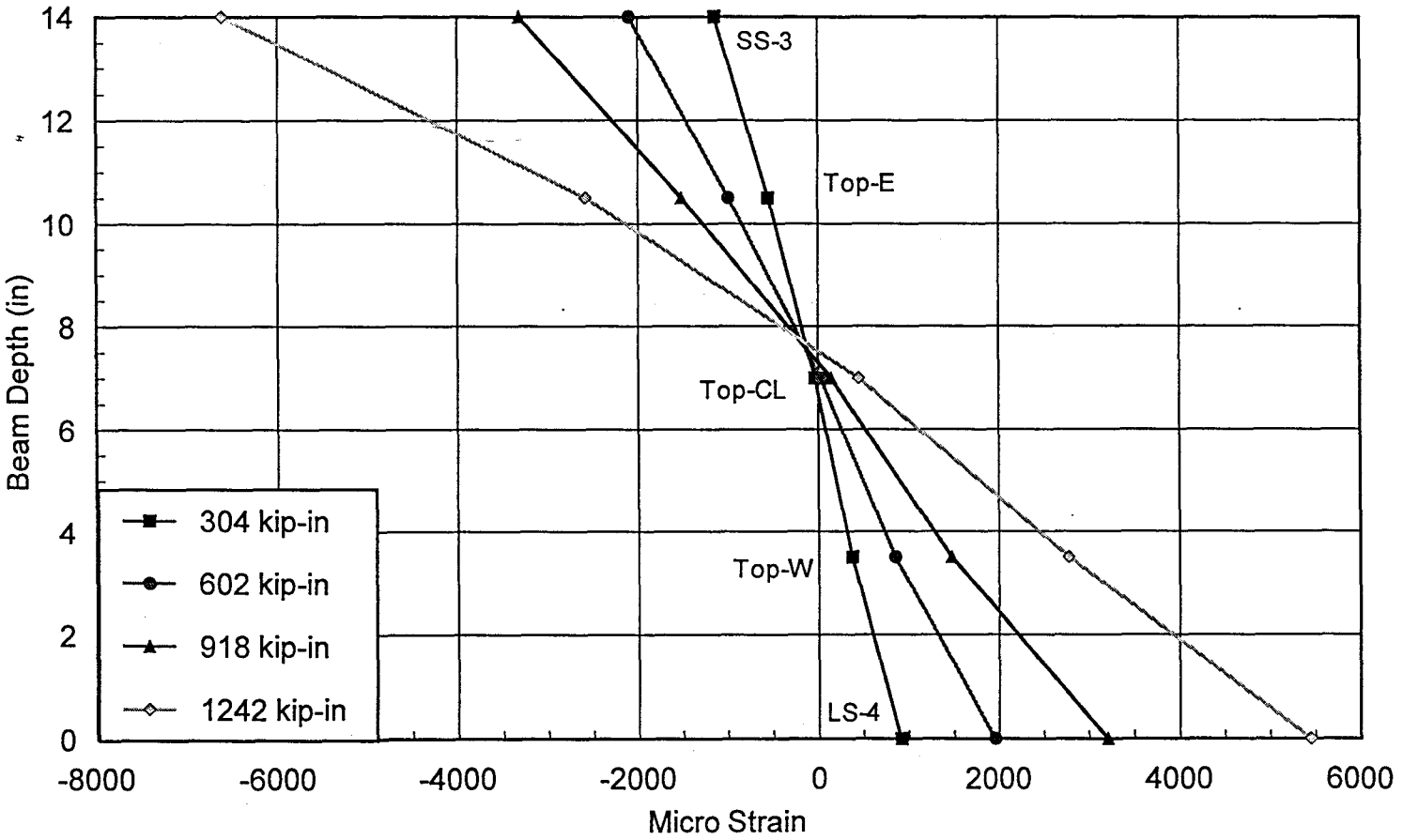

(Fig. 5.16a) LONGITUDINAL TENSION STRAIN DISTRIBUTION ALONG BEAM LENGTH

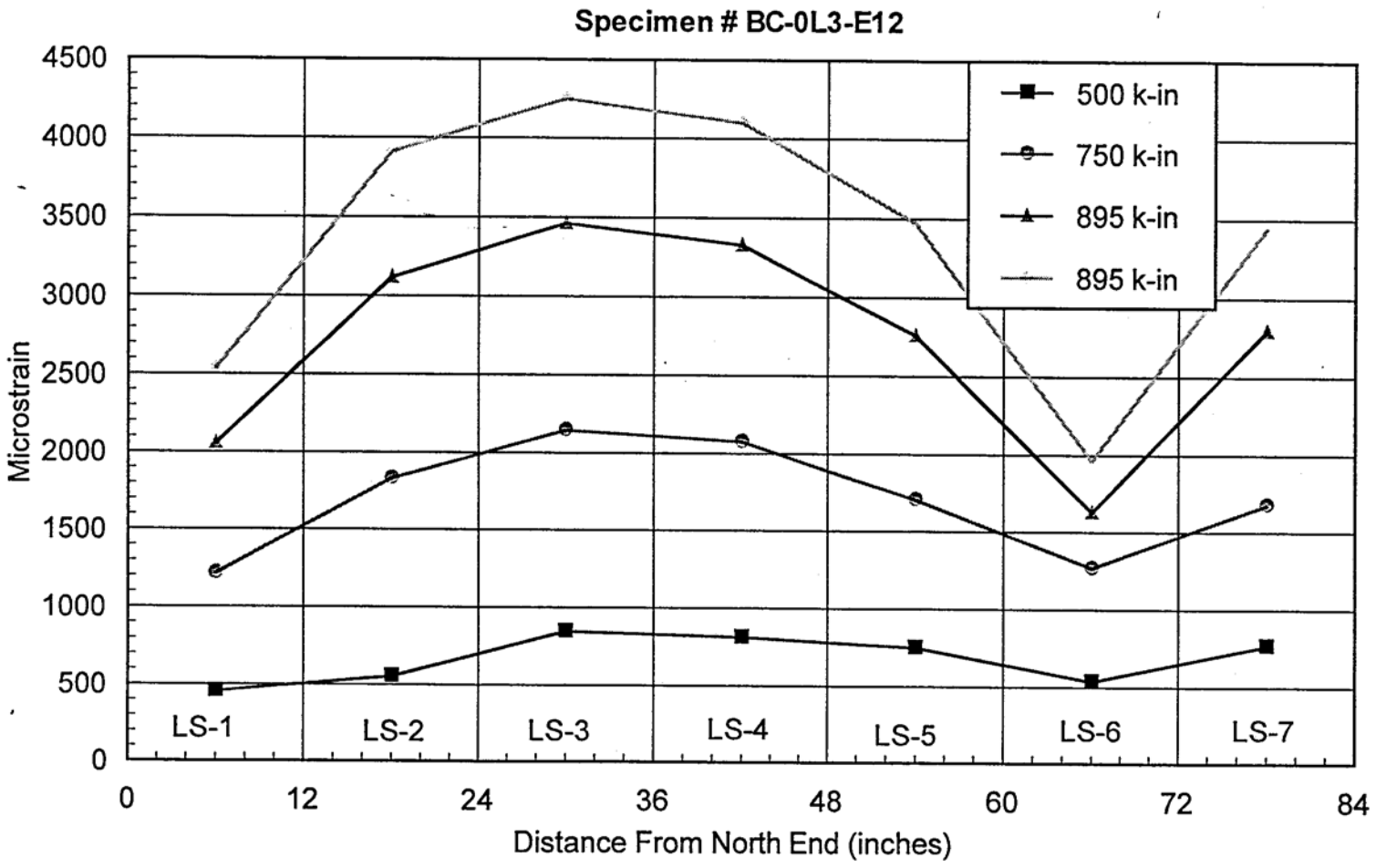

(Fig. 5.16a) LONGITUDINAL COMPRESSIVE STRAIN DISTRIBUTION ALONG BEAM LENGTH

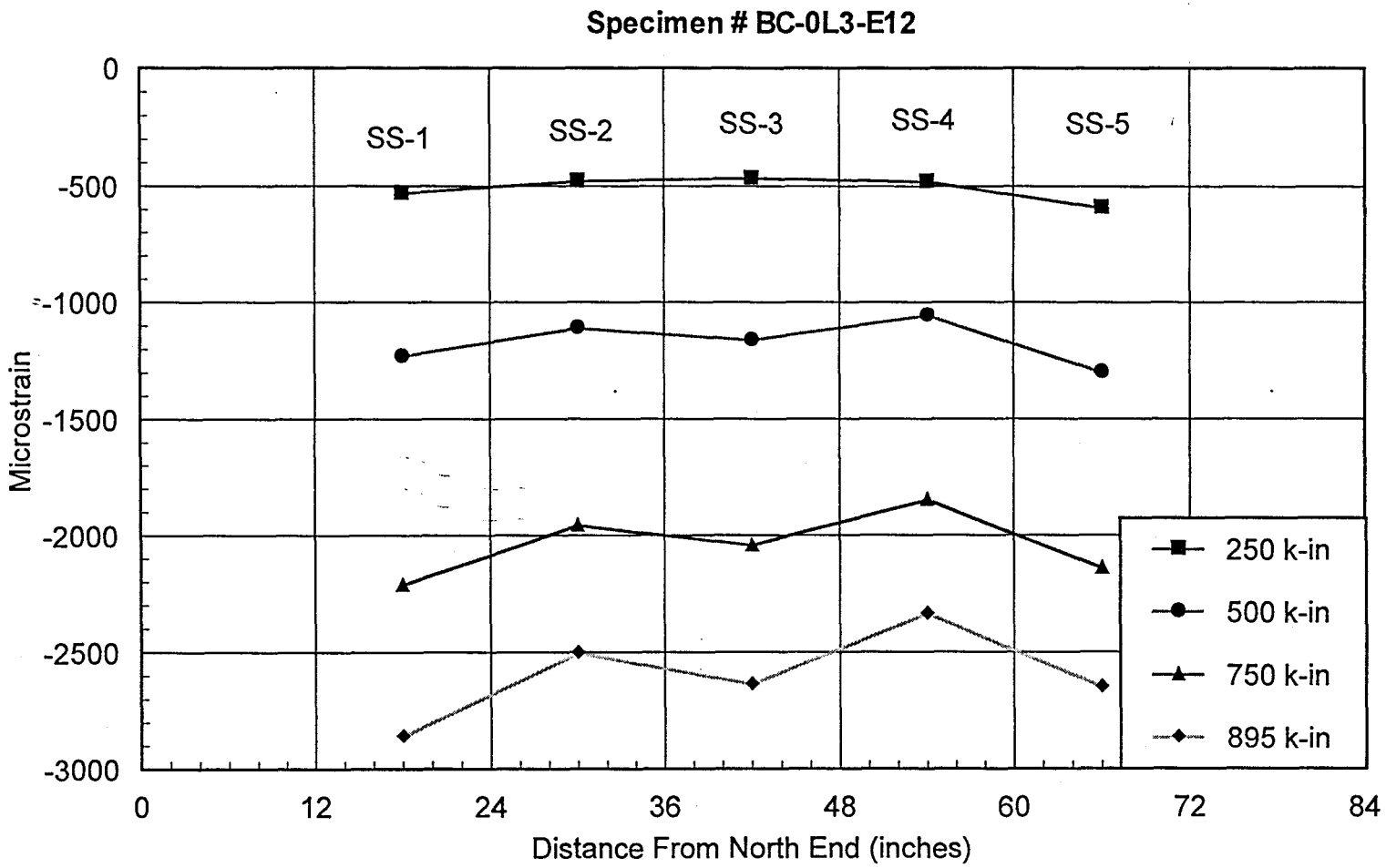

(Fig. 5.16d) Longitudinal Tension Strain Distribution Along Beam Length

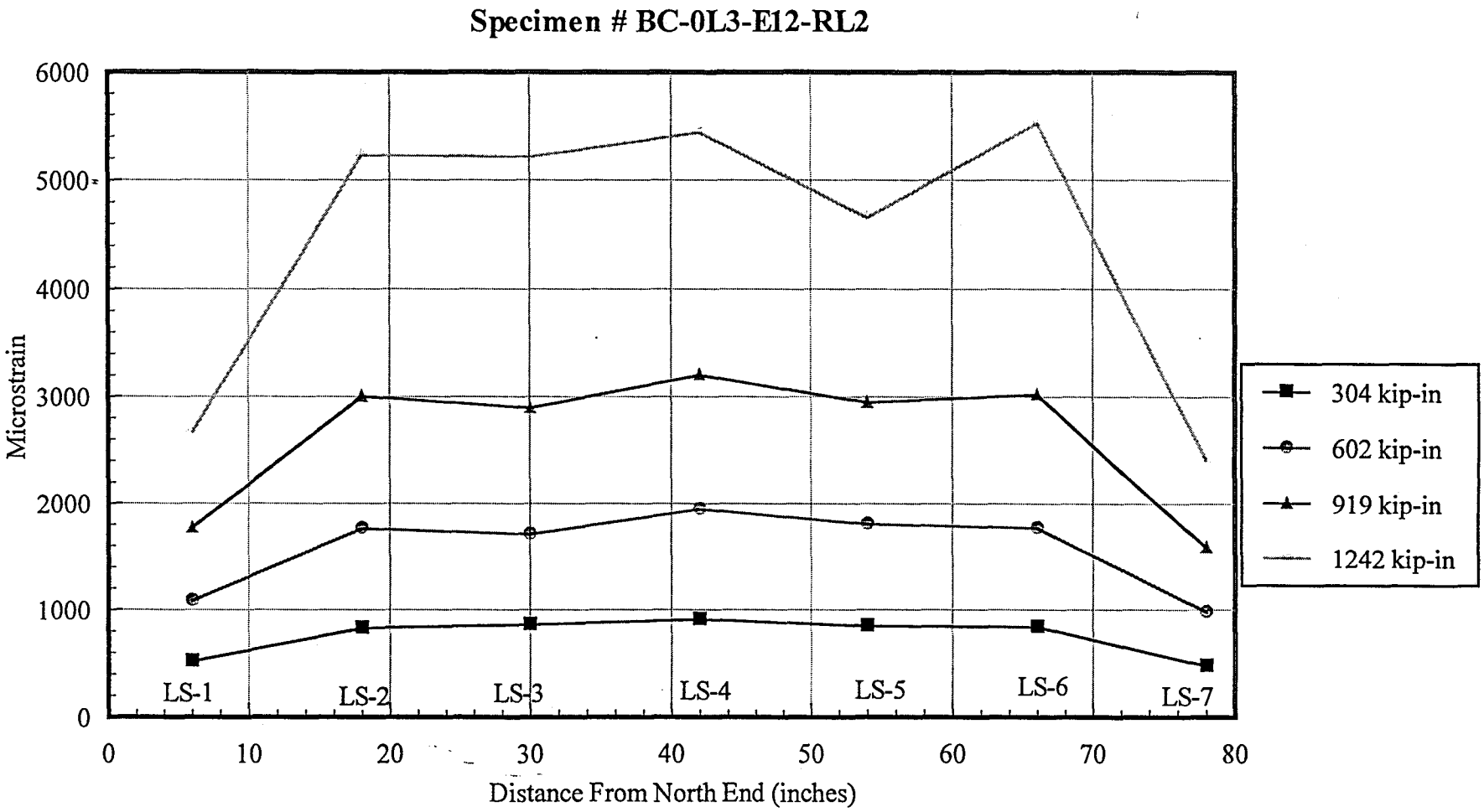

(Fig.5.16d) Longitudinal Compressive Strain Distribution Along Beam Length

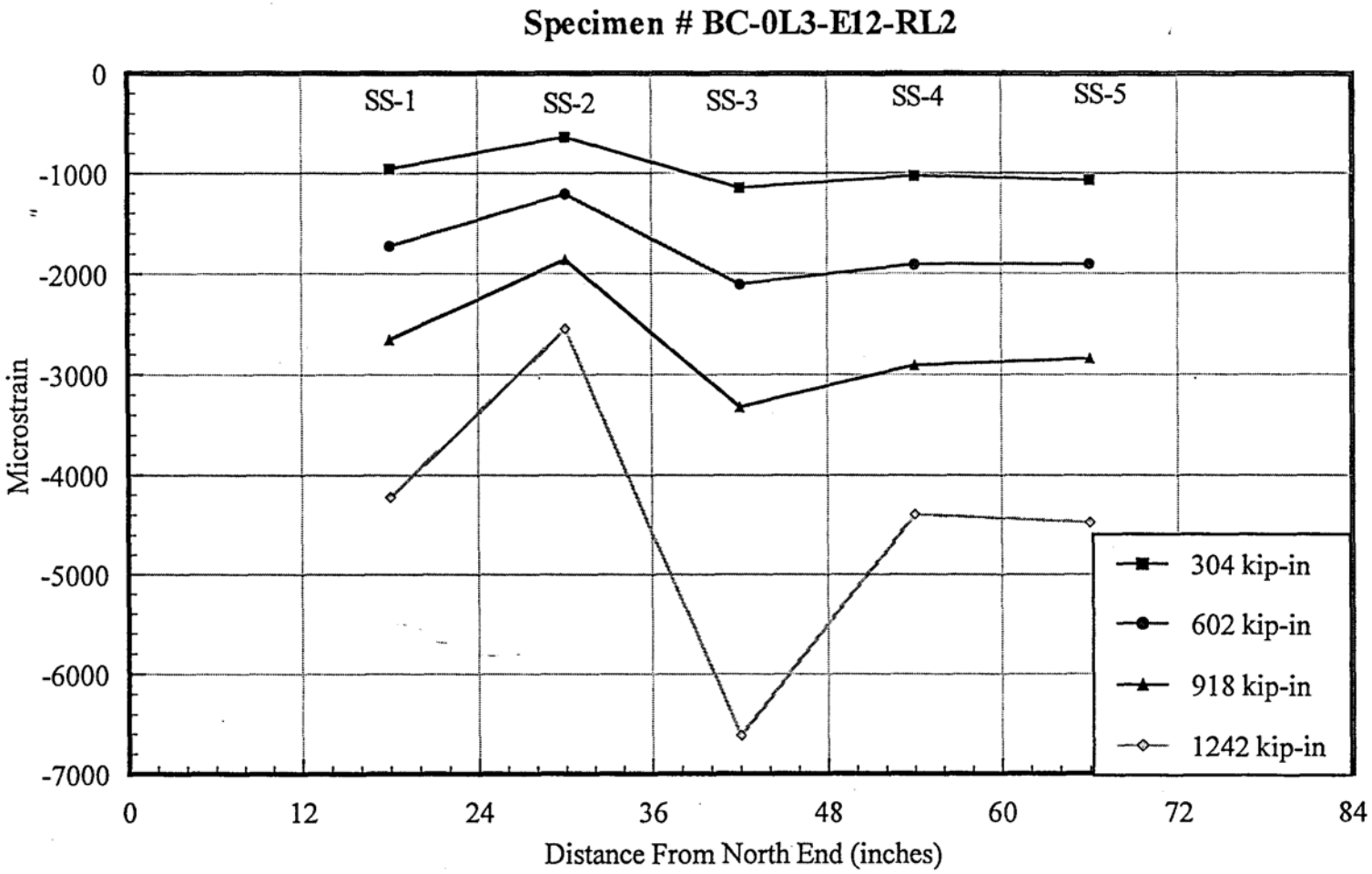

(Fig.5.17b) Moment VS. Transverse Strain Around Beam Center Line

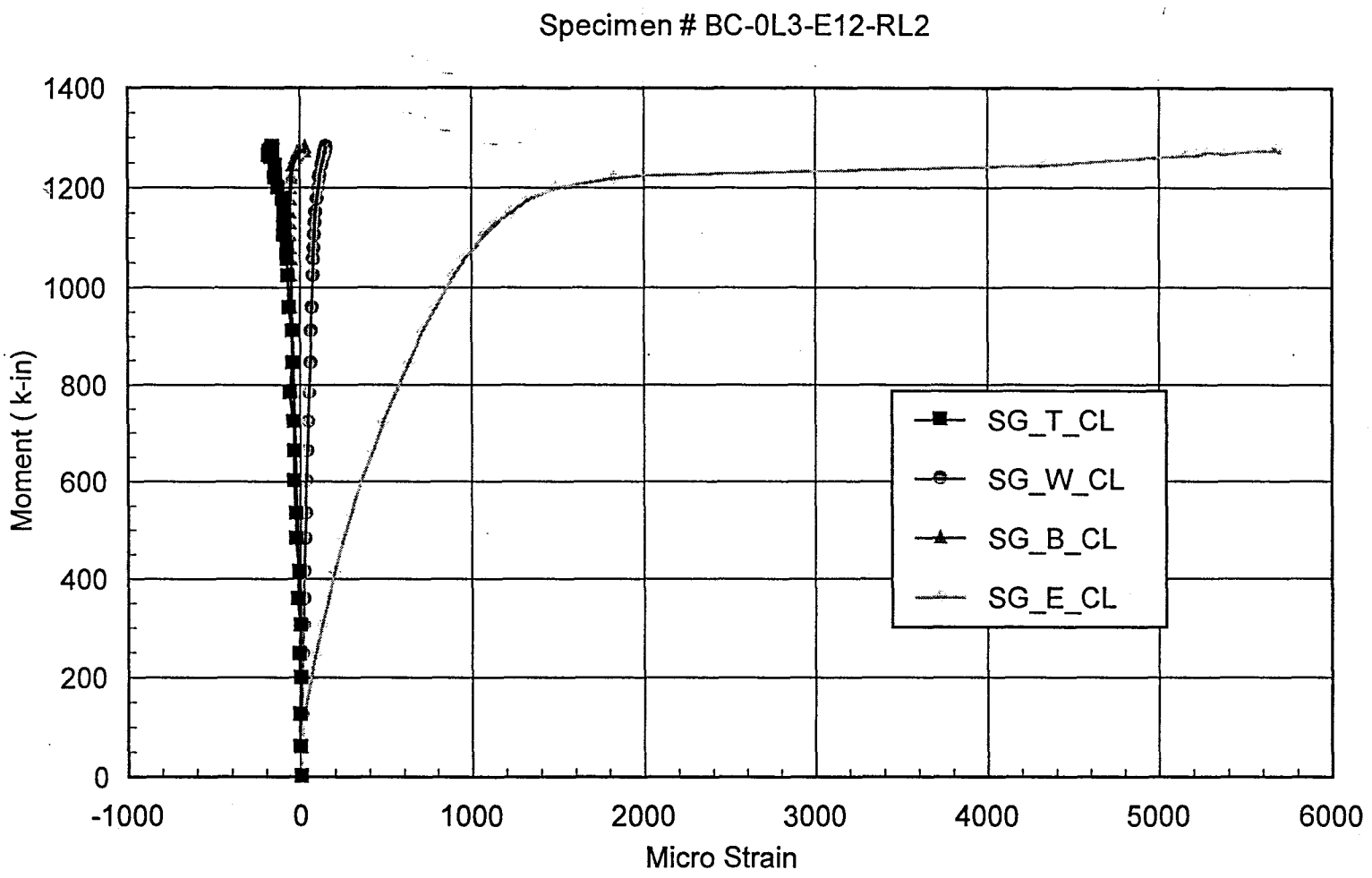

(Fig. 5.17c) Moment VS. TRansverse Surface Strain Around Beam Center Line

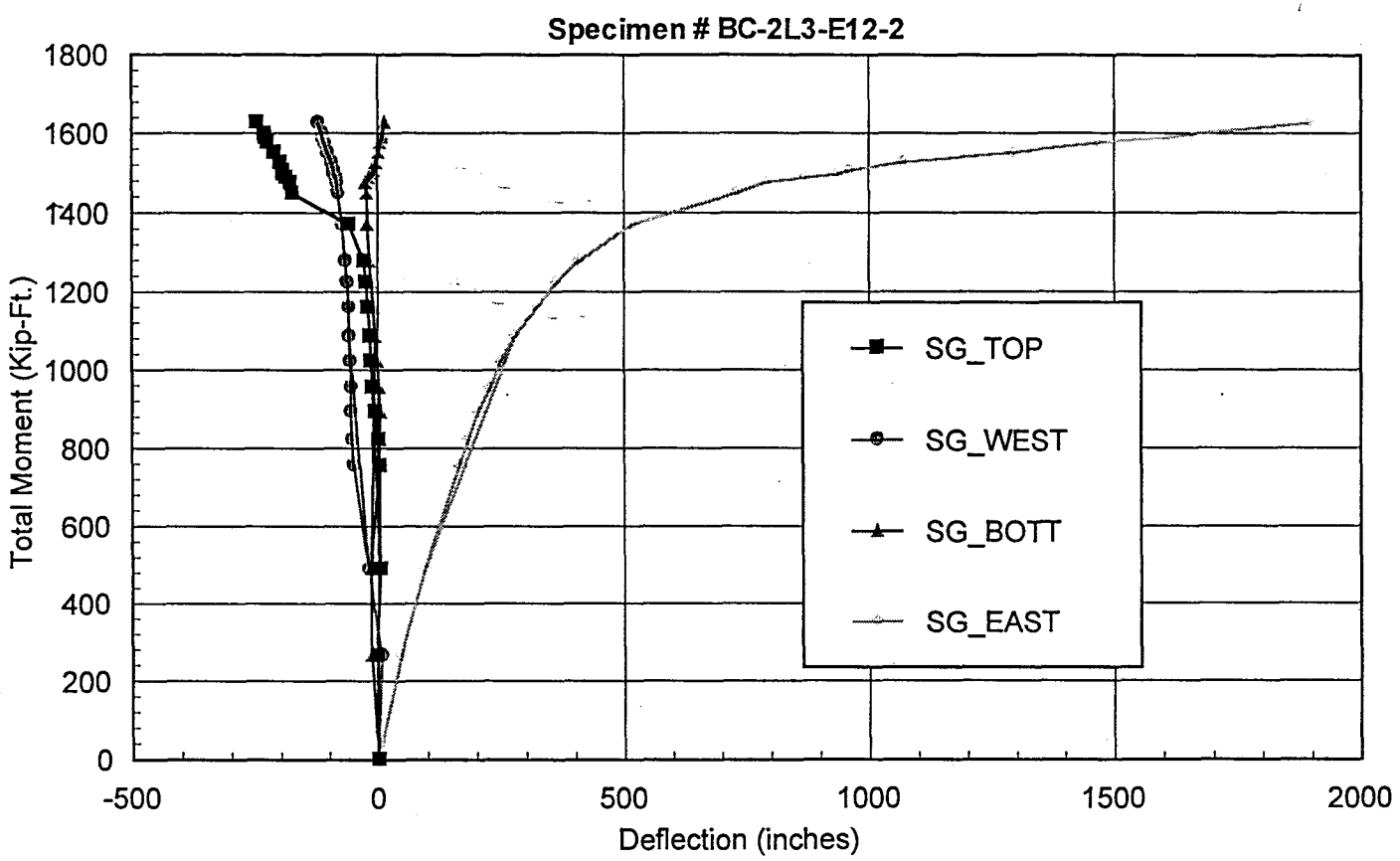

(Fig 5.18a) Moment vs. Deflection At Center line

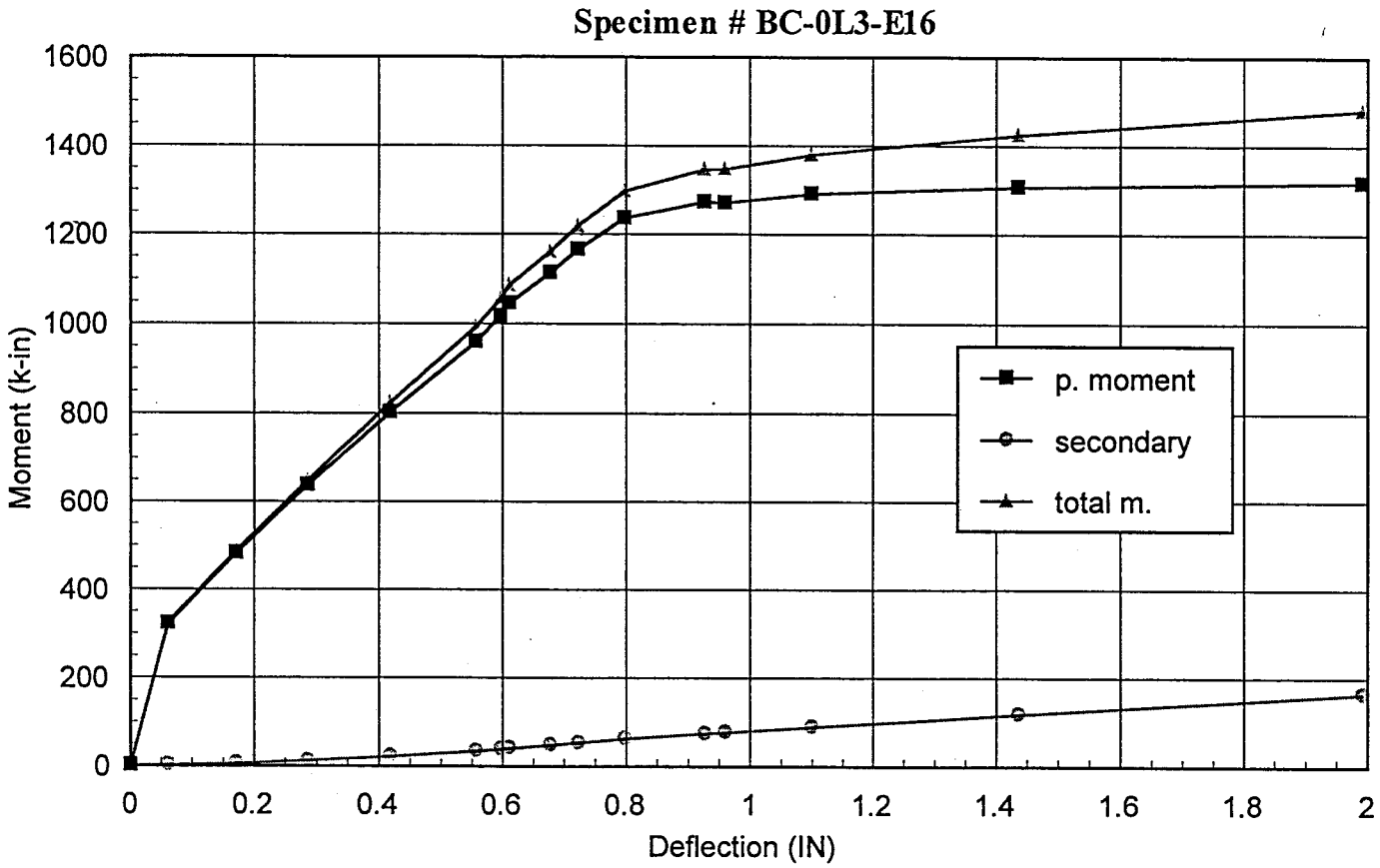

(Fig. 5.18b) Moment VS. Deflection At Center Line

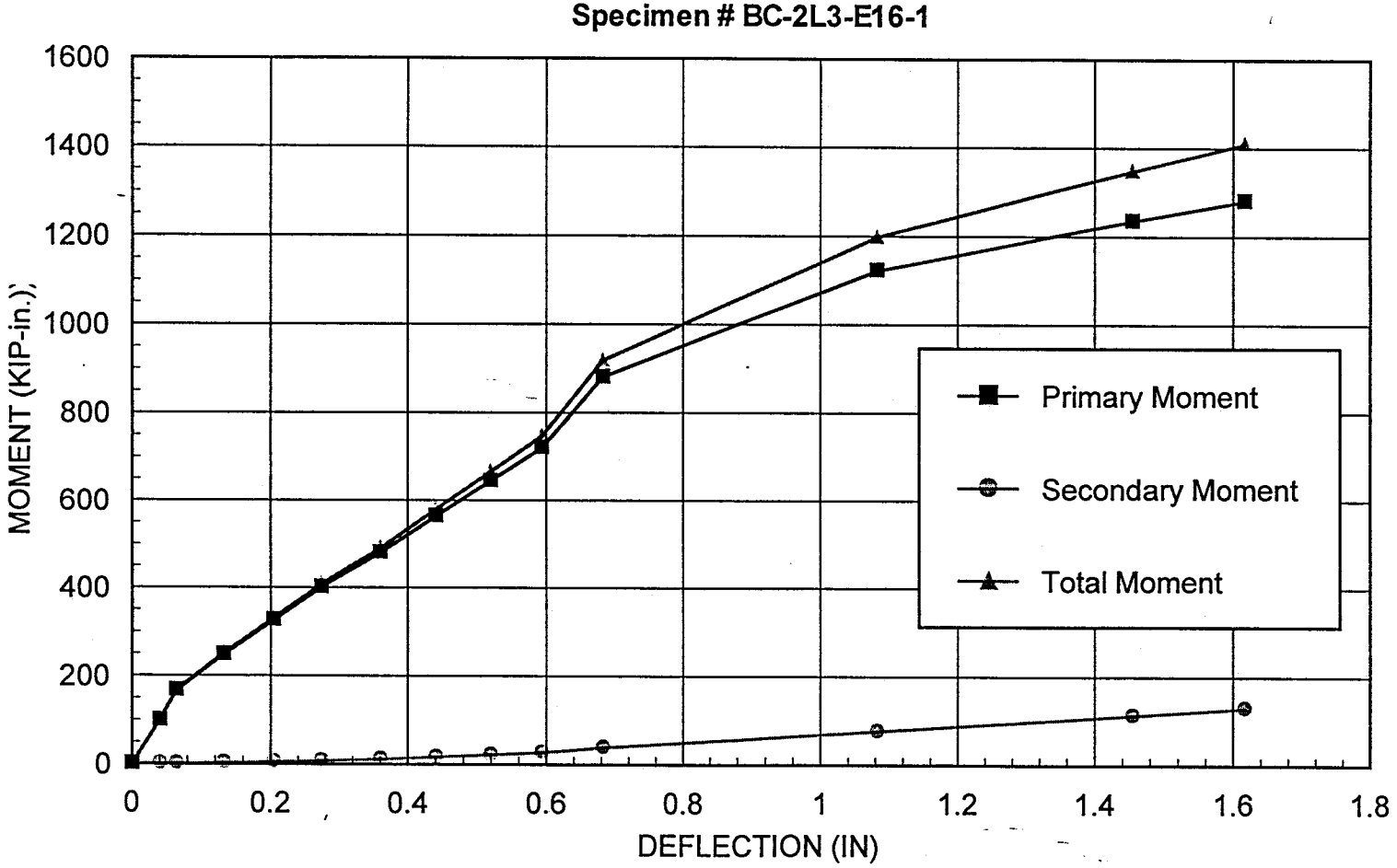

(Fig 5.18c) Moment vs. Deflection At Center line

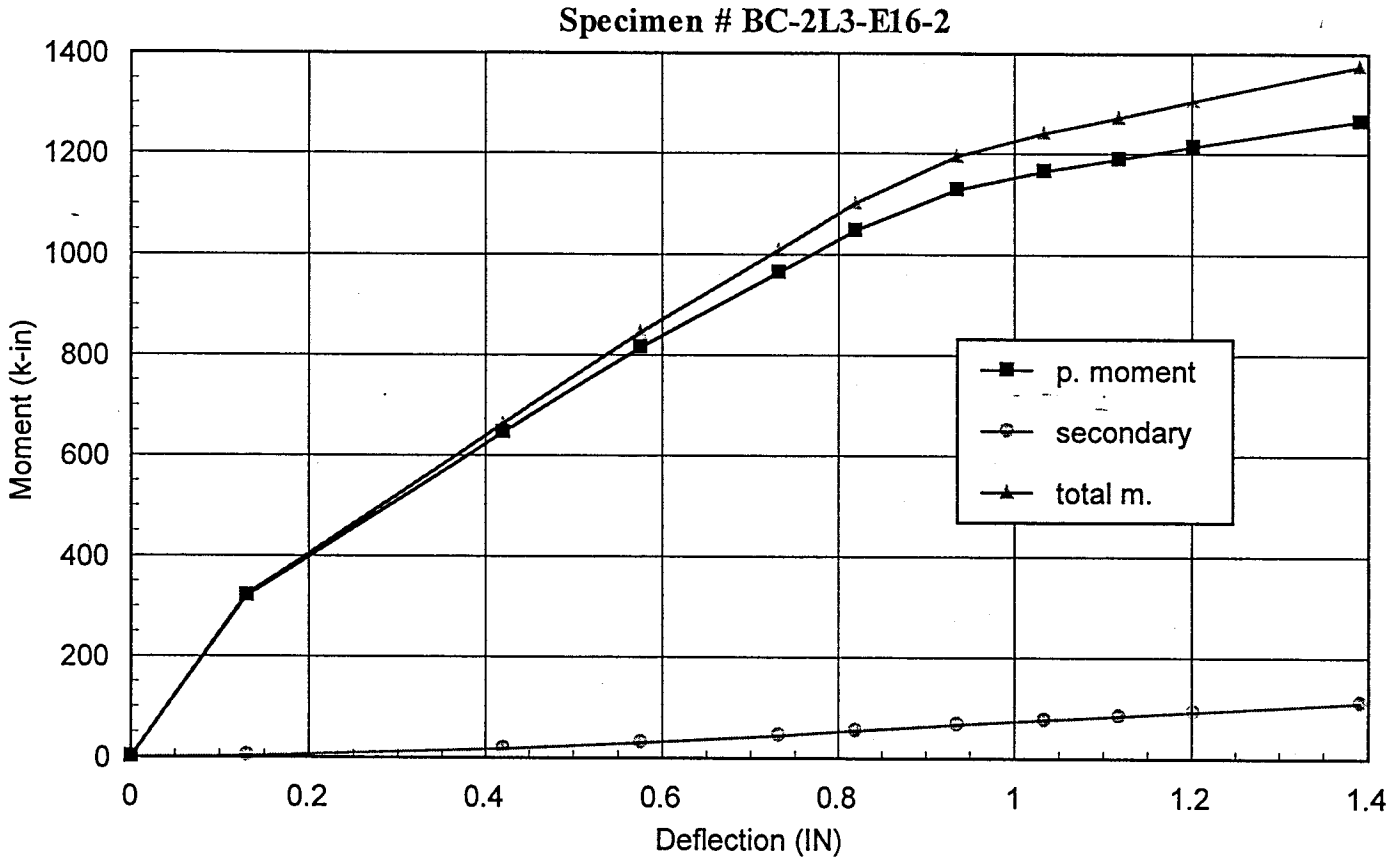

(Fig. 5.19a) Centerline Strain Distribution

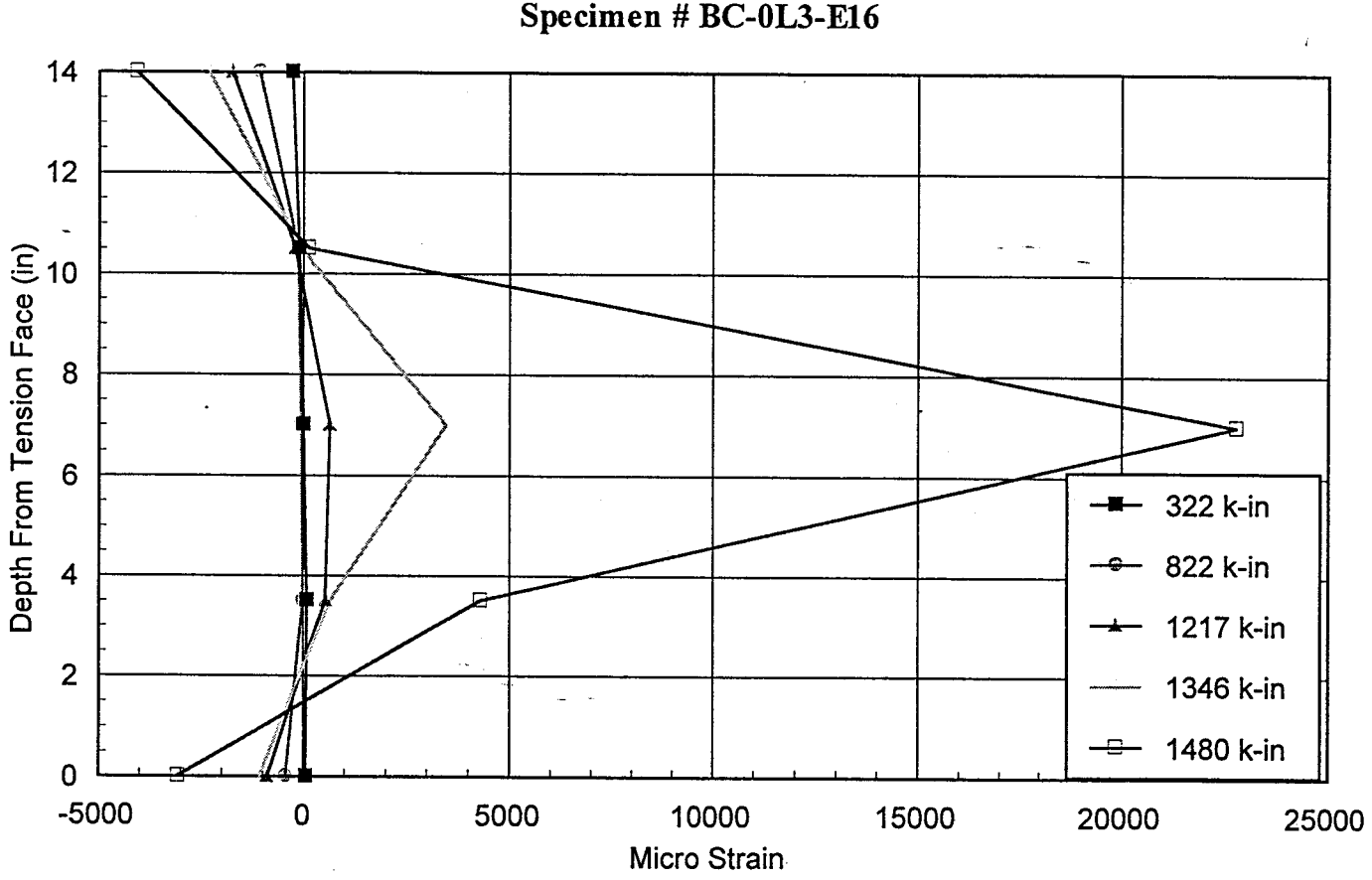

(Fig. 5.19b) Center line Strain Distribution

Specimen # BC-2L3-E16-1

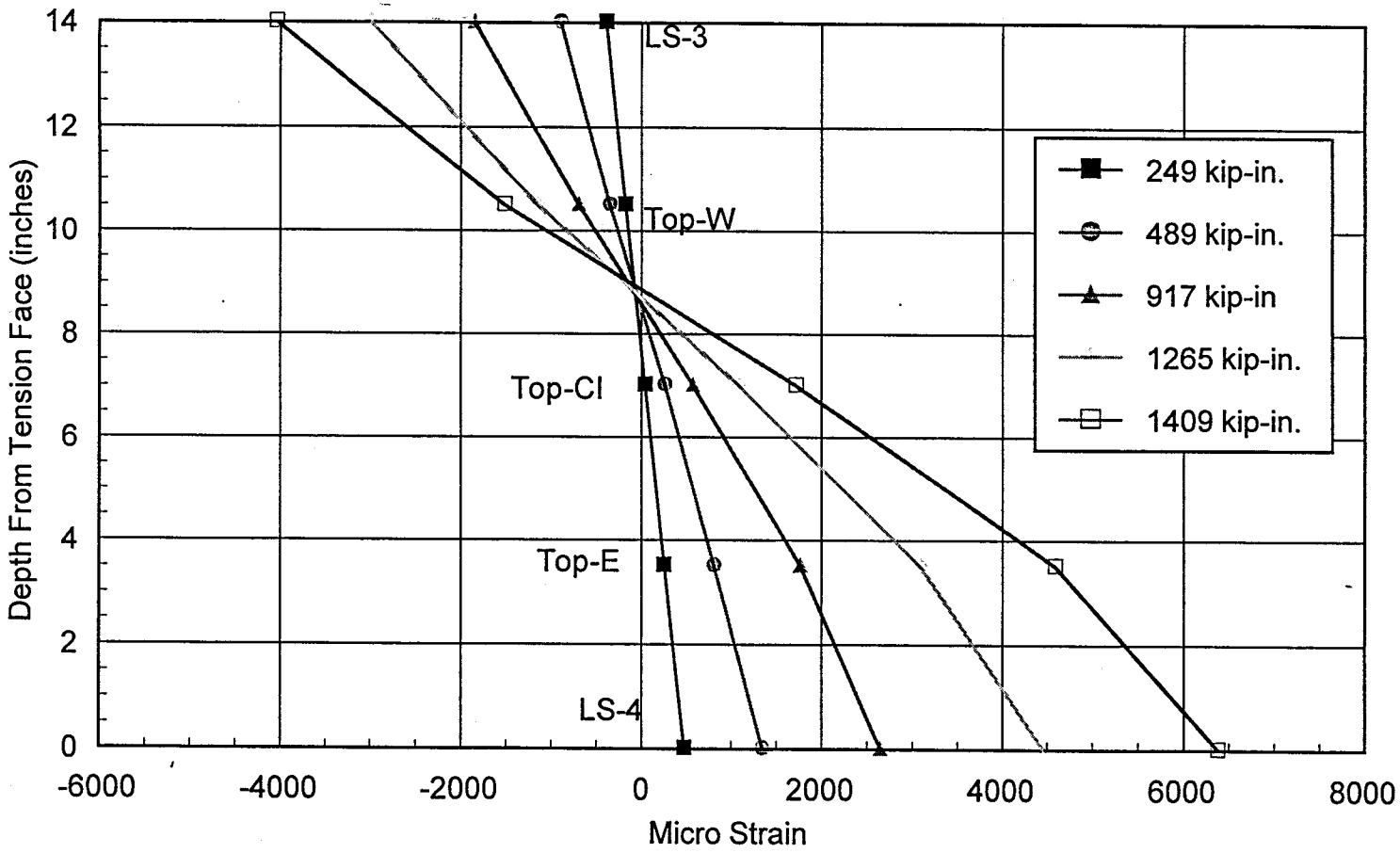

(Fig. 5.19c) Centerline Strain Distribution

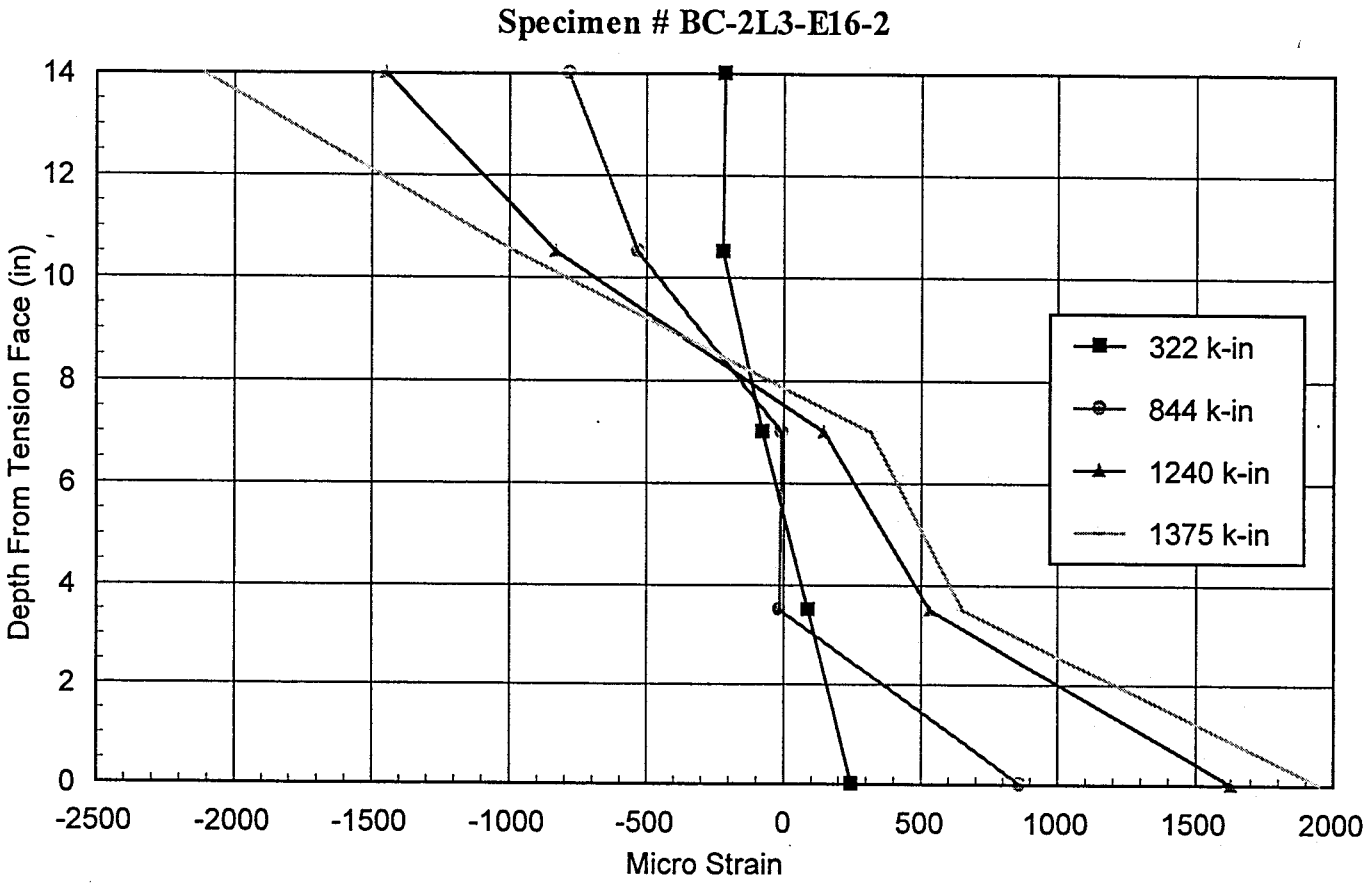

(Fig. 5.20a) Longitudinal Tension Strain Distribution Along Beam Length

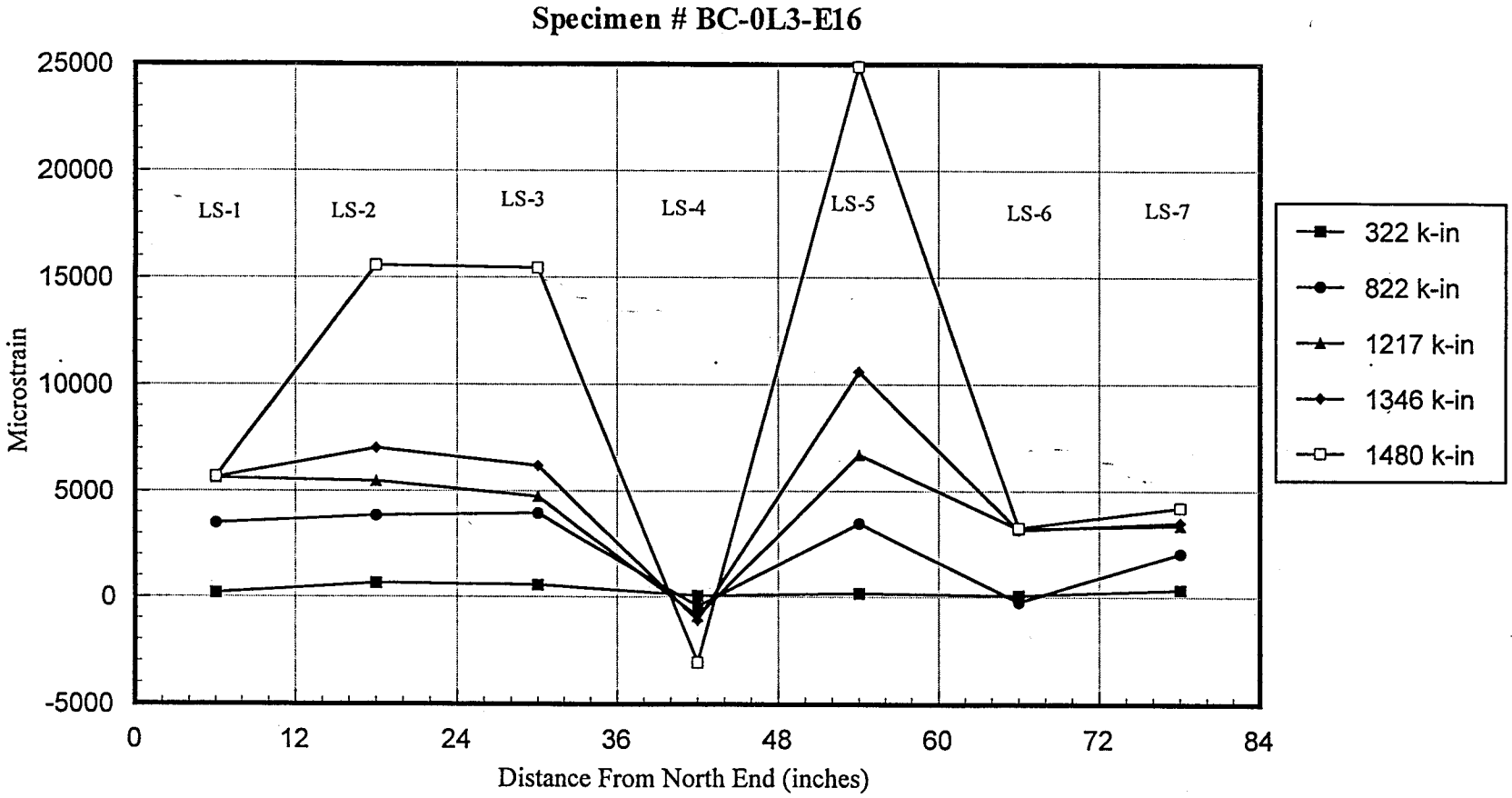

(Fig. 5.20a) Longitudinal Compressive Strain Distribution Along Beam Length

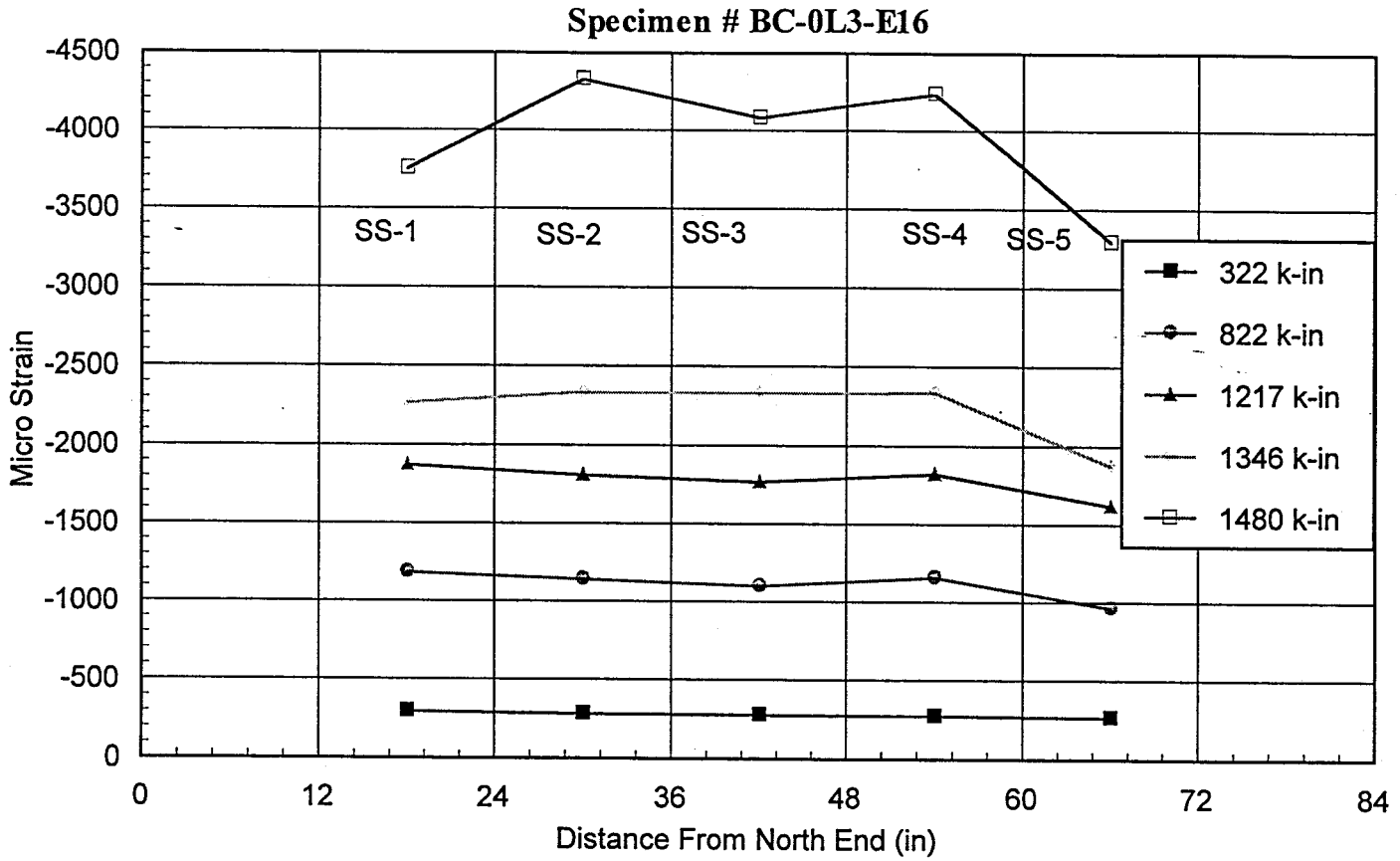

(Fig. 5.20b) LONGITUDINAL COMPRESSIVE STRAIN DISTRIBUTION ALONG BEAM LENGTH

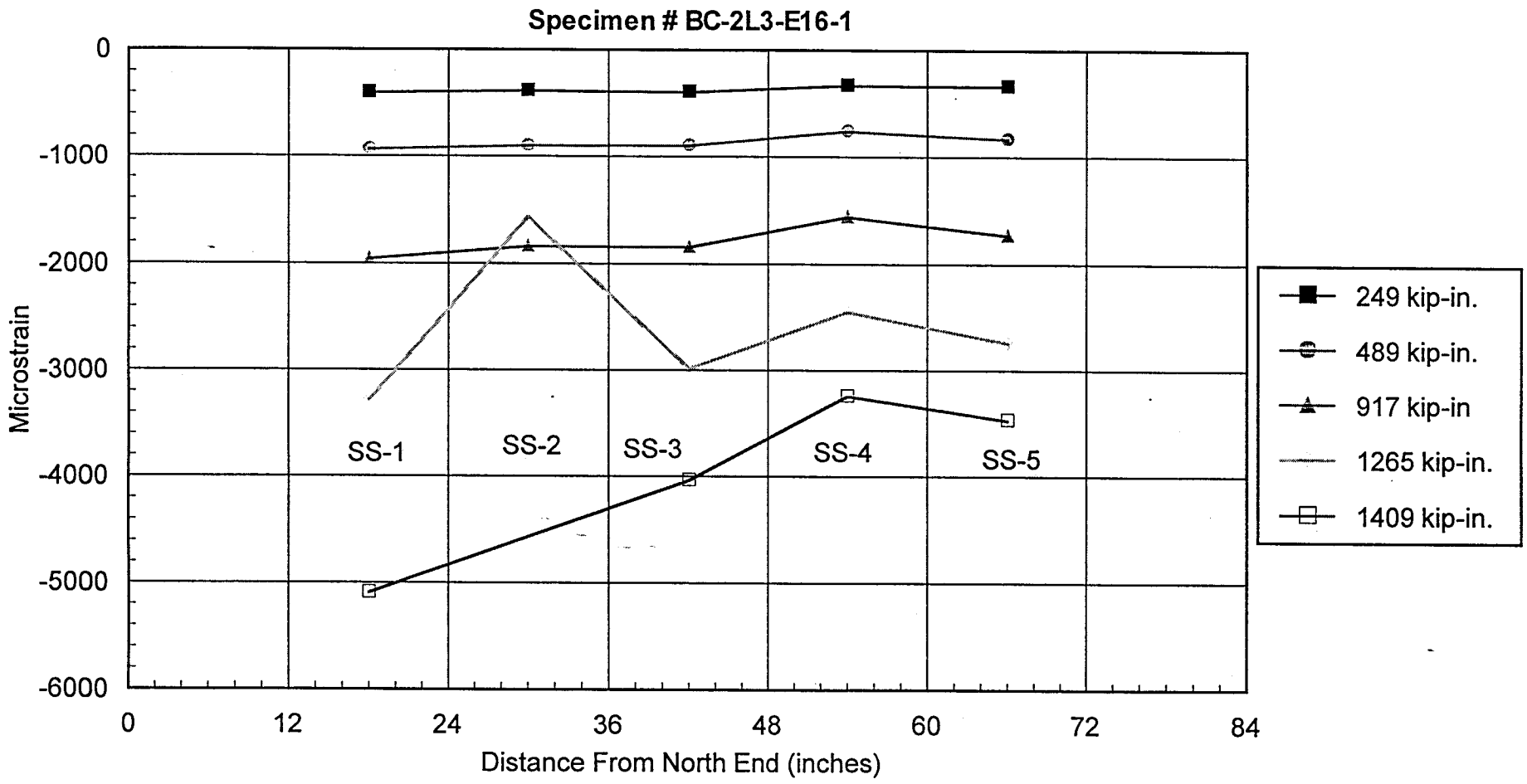

(Fig. 5.20b) LONGITUDINAL TENSION STRAIN DISTRIBUTION ALONG BEAM LENGTH

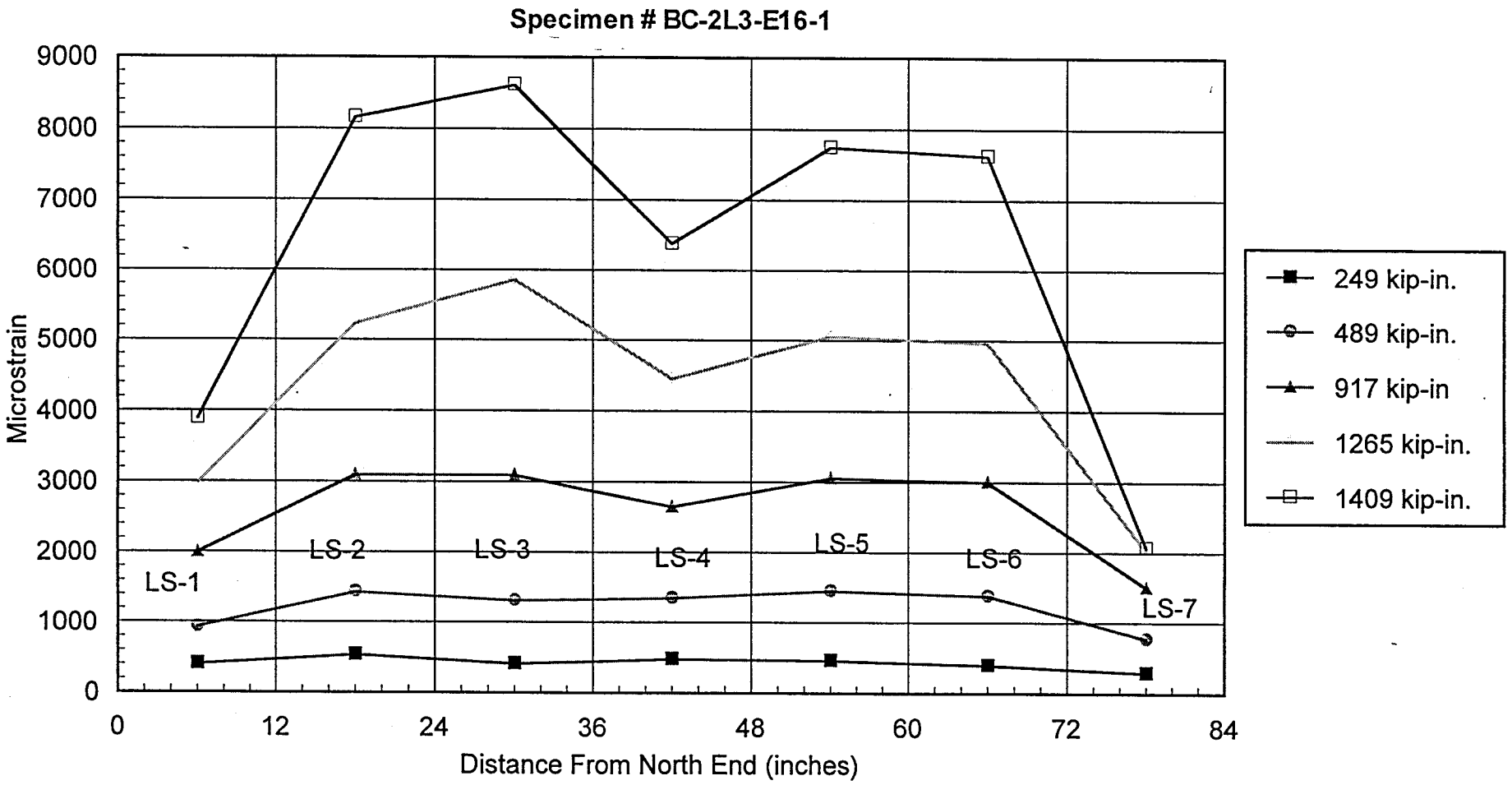

(Fig. 5.20c) Longitudinal Tension Strain Distribution Along Beam Length

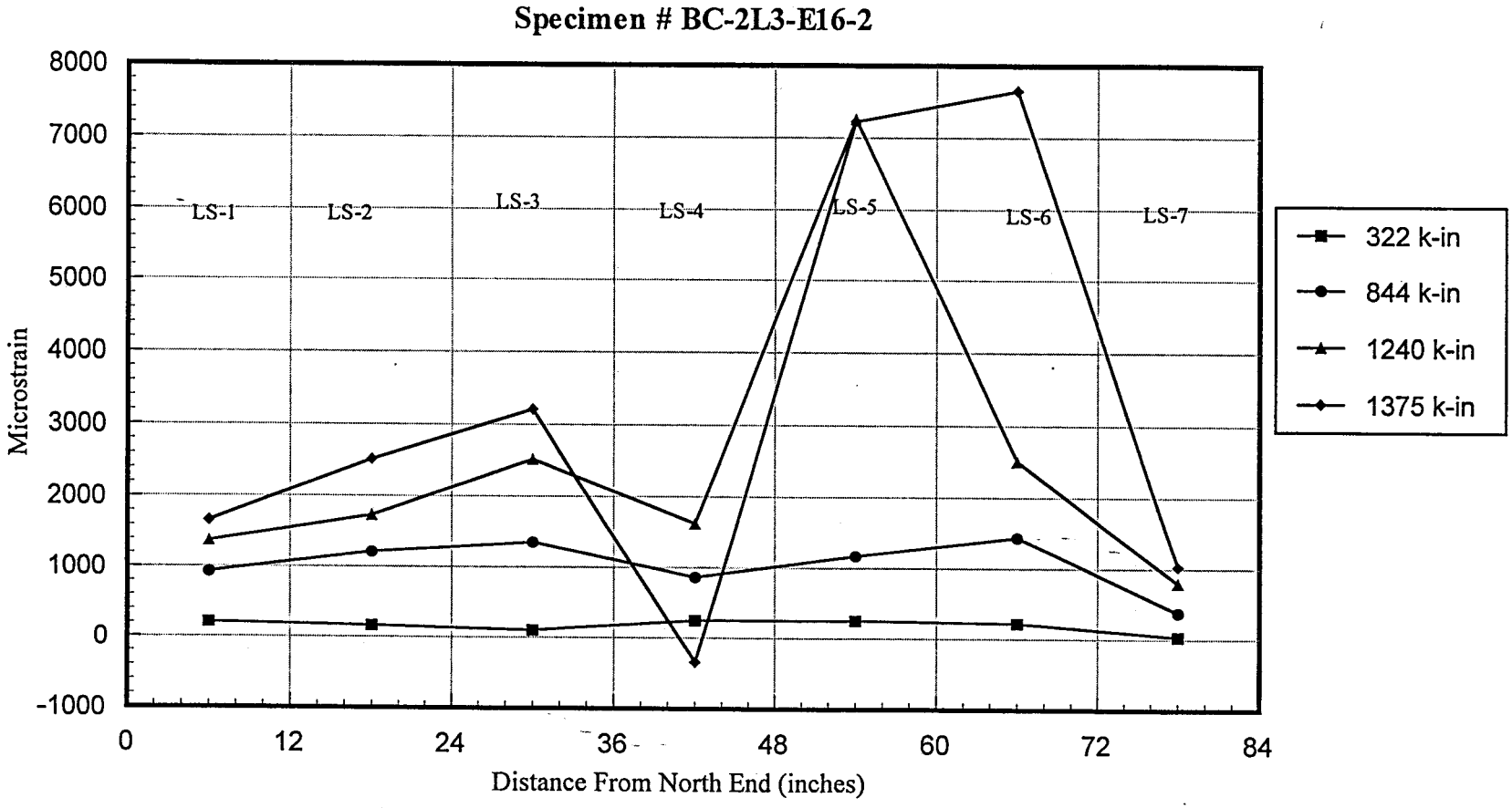

(Fig. 5.20c) Longitudinal Compressive Strain Distribution Along Beam Length

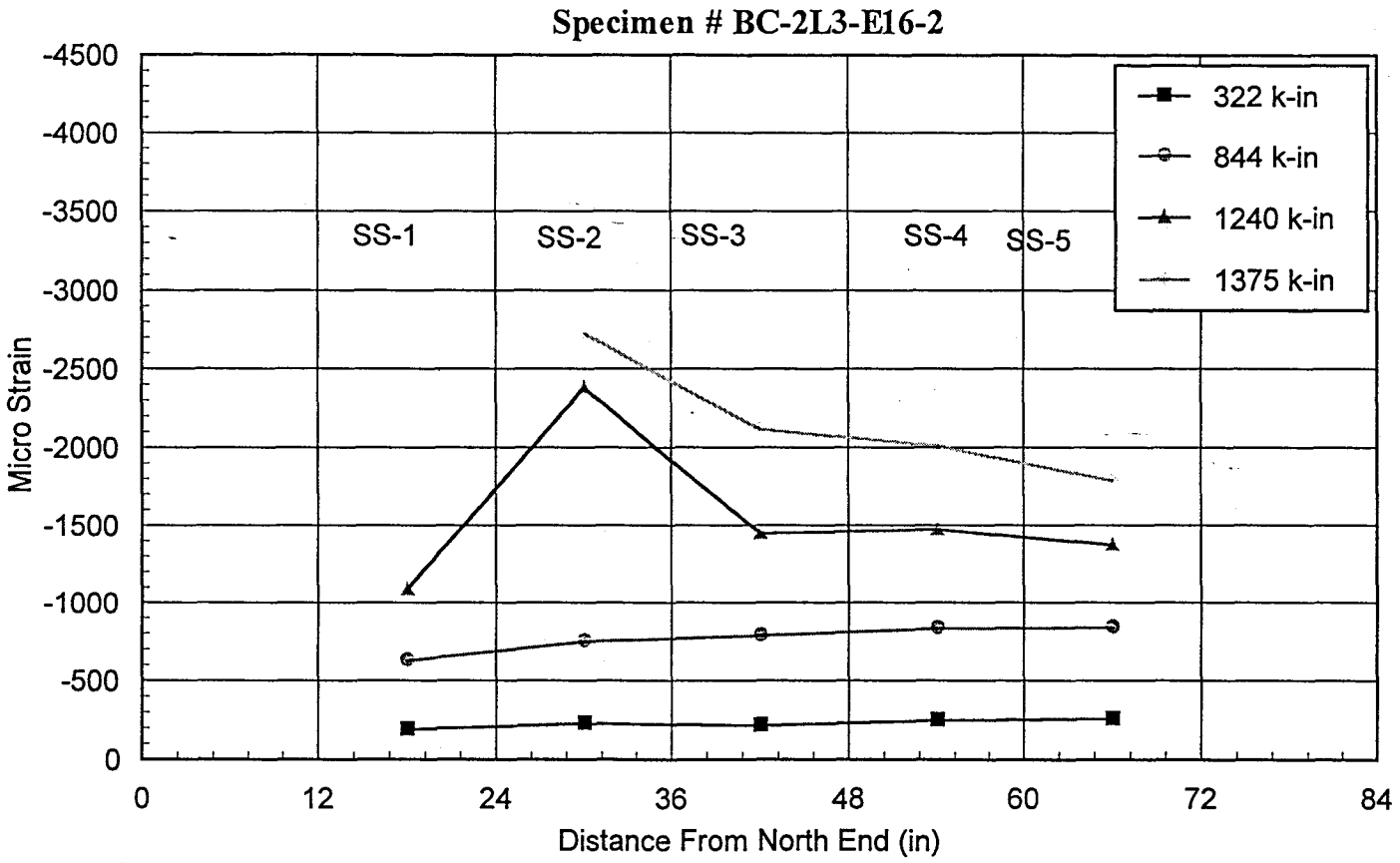

(Fig. 5.21a) Moment VS. TRansverse Surface Strain Around Beam Center Line

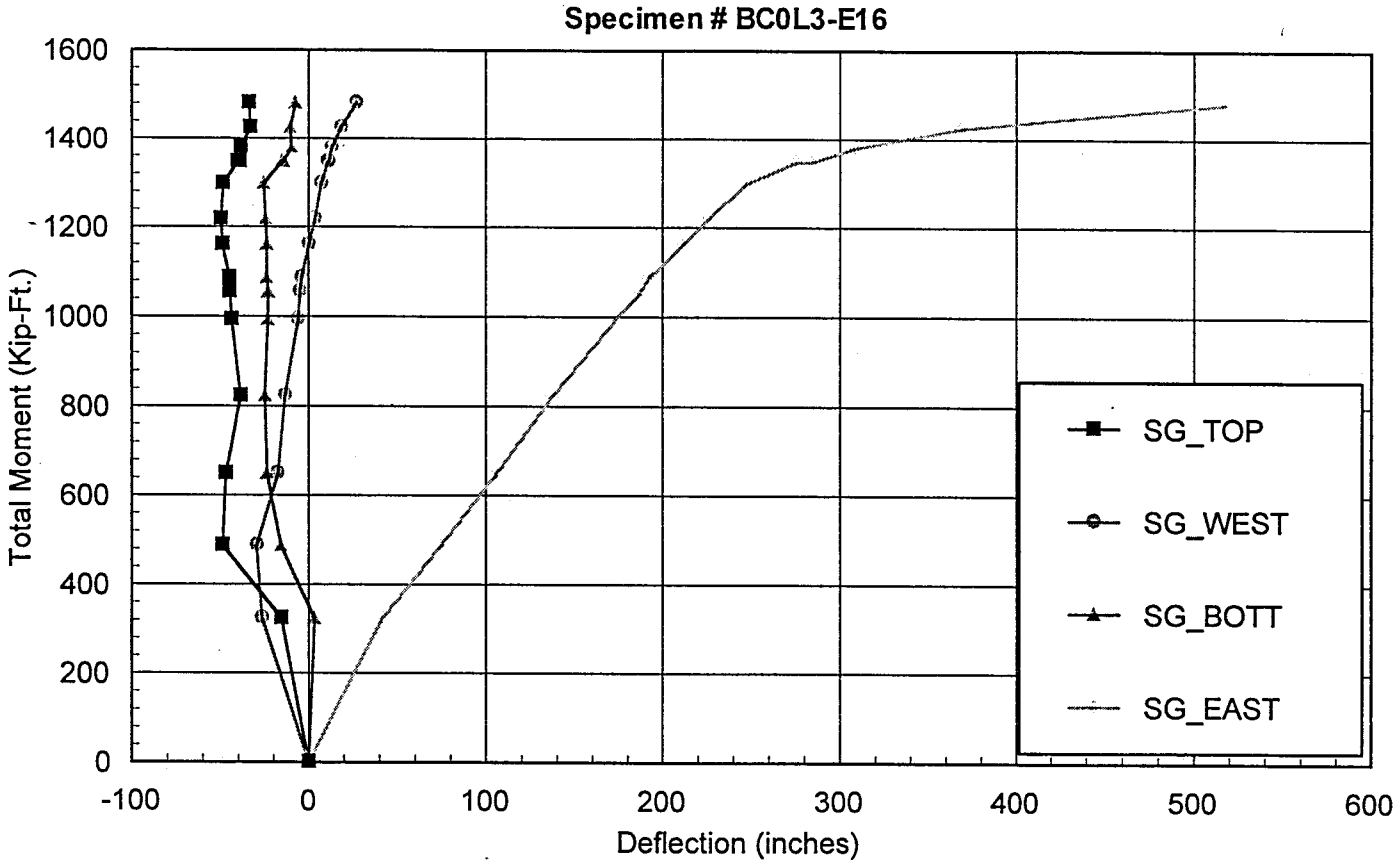

(Fig. 5.21b) Moment vs.Transverse Strain Around Beam Centerline
Specimen # BC-2L3-E16-1

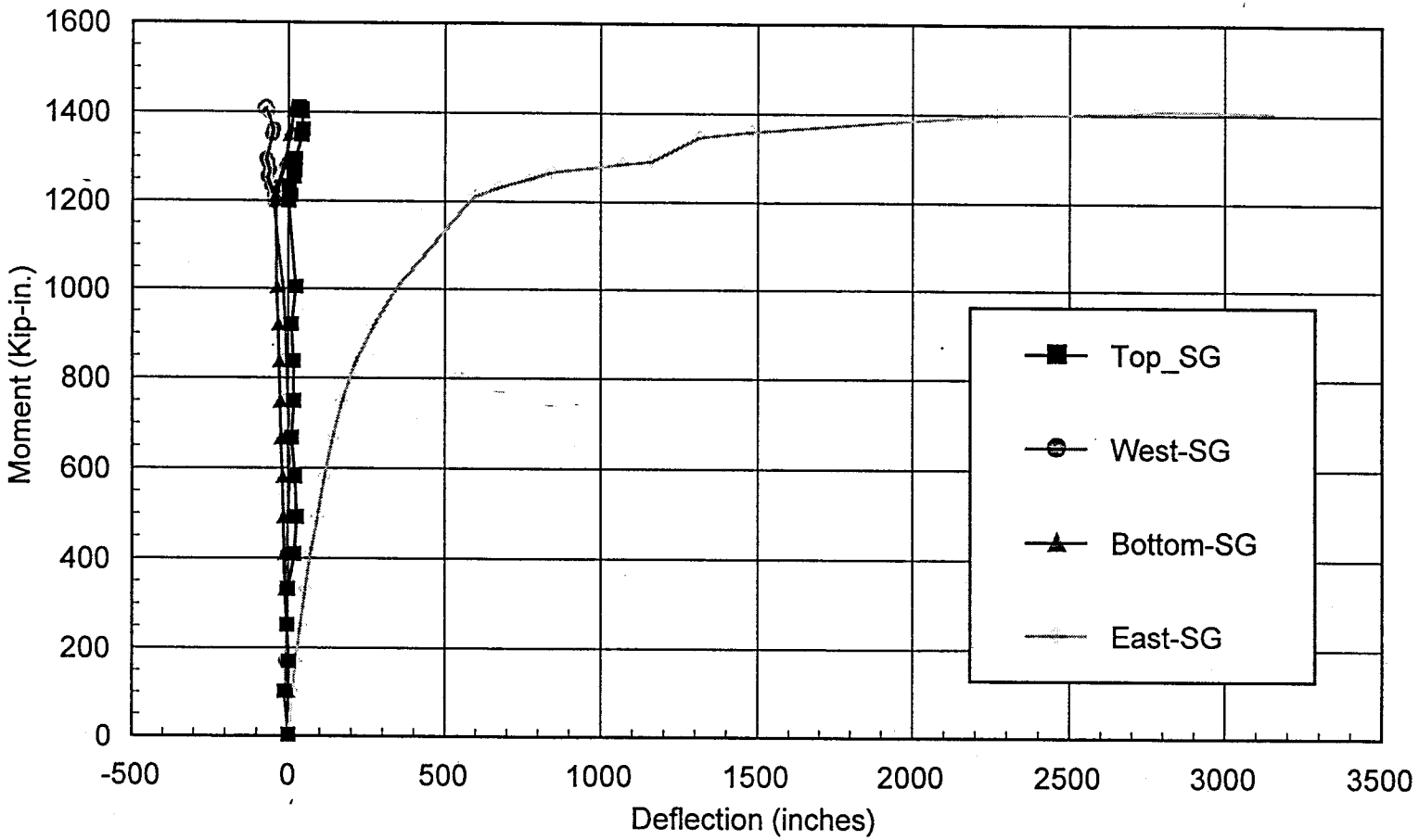

(Fig. 5.21c) Moment VS. TRansverse Surface Strain Around Beam Center Line

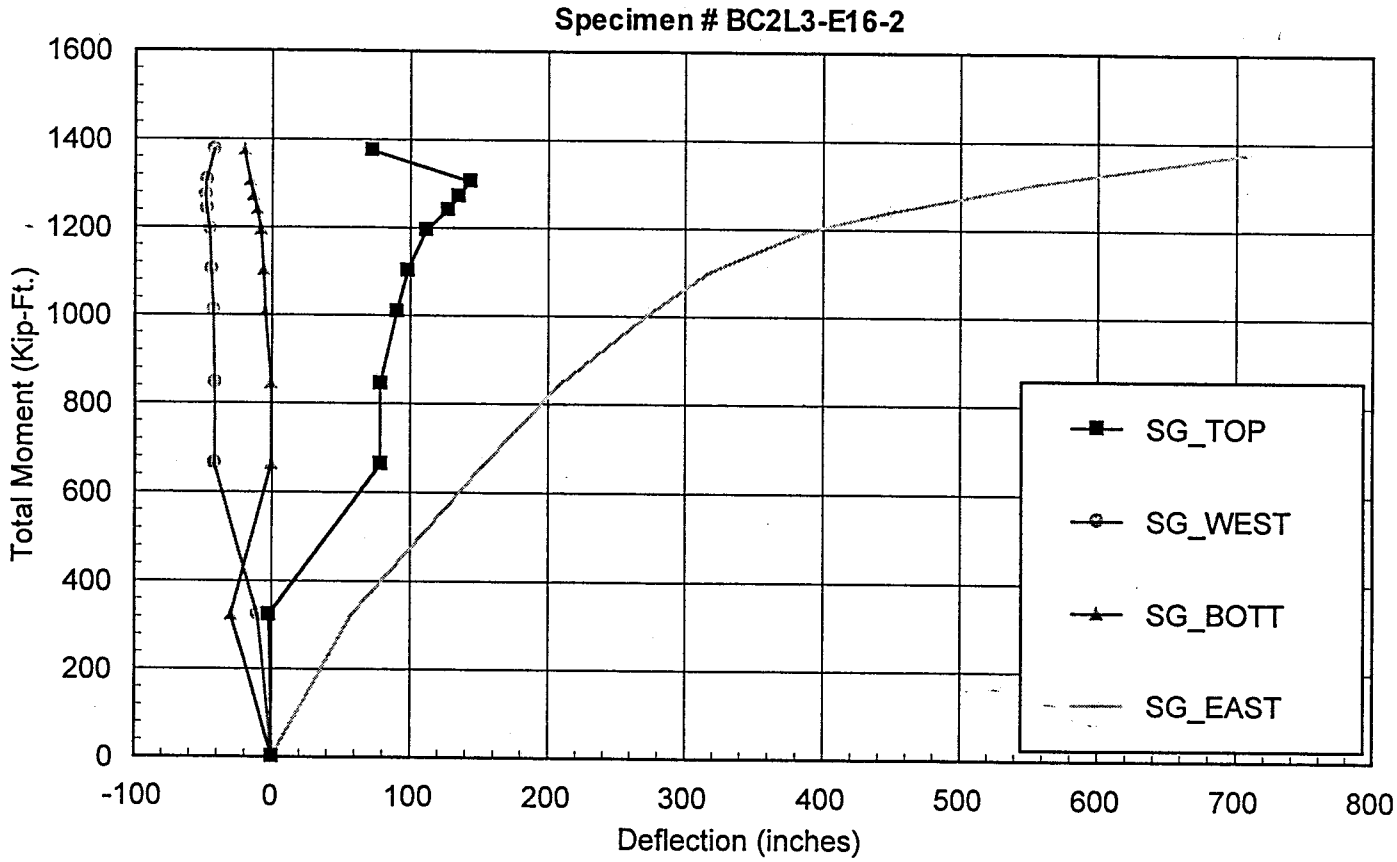

(Fig. 5.22a) Moment VS. Mid-Span Deflection

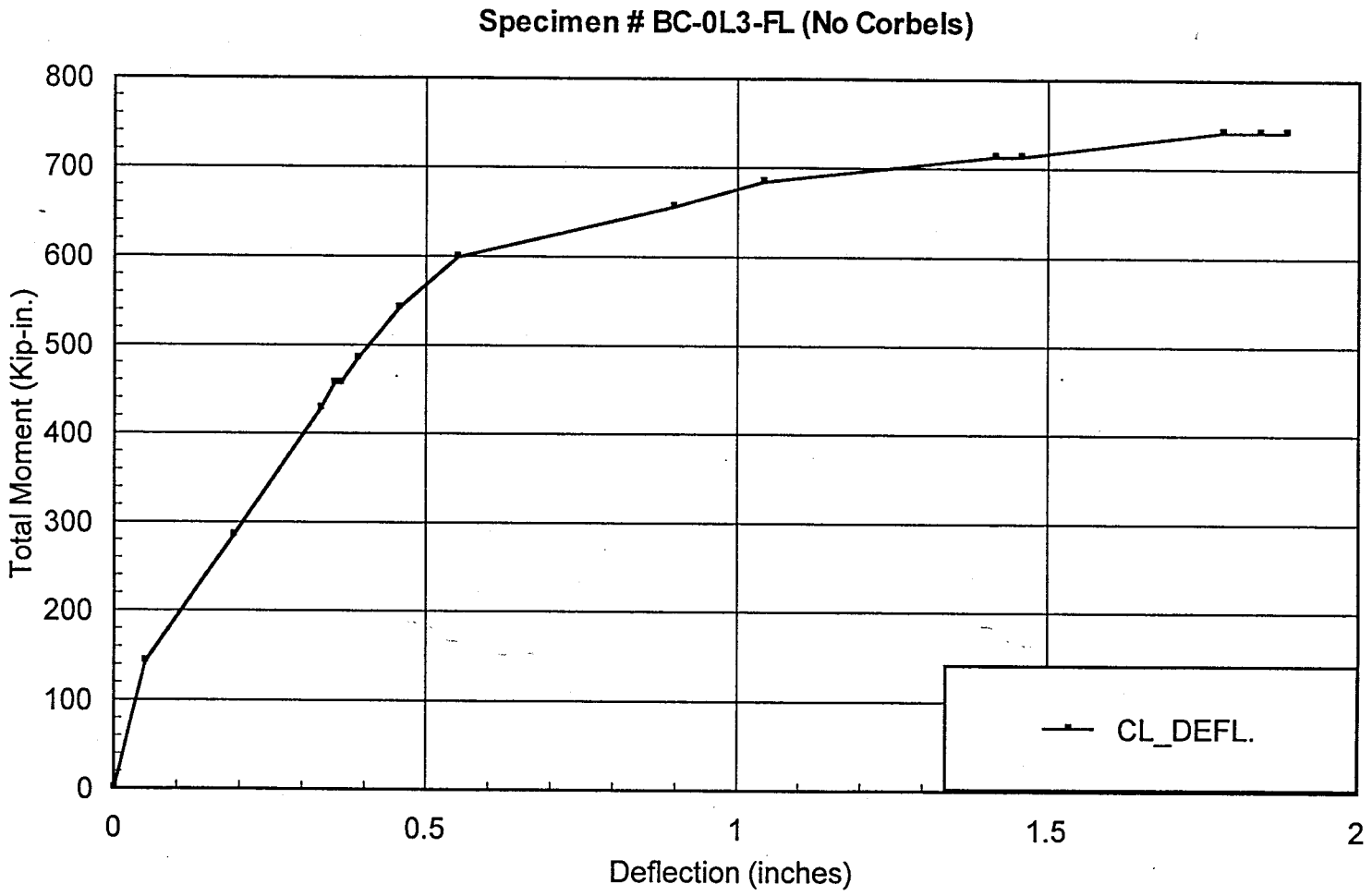

(Fig. 5.22b) Moment VS. Mid-Span Deflection

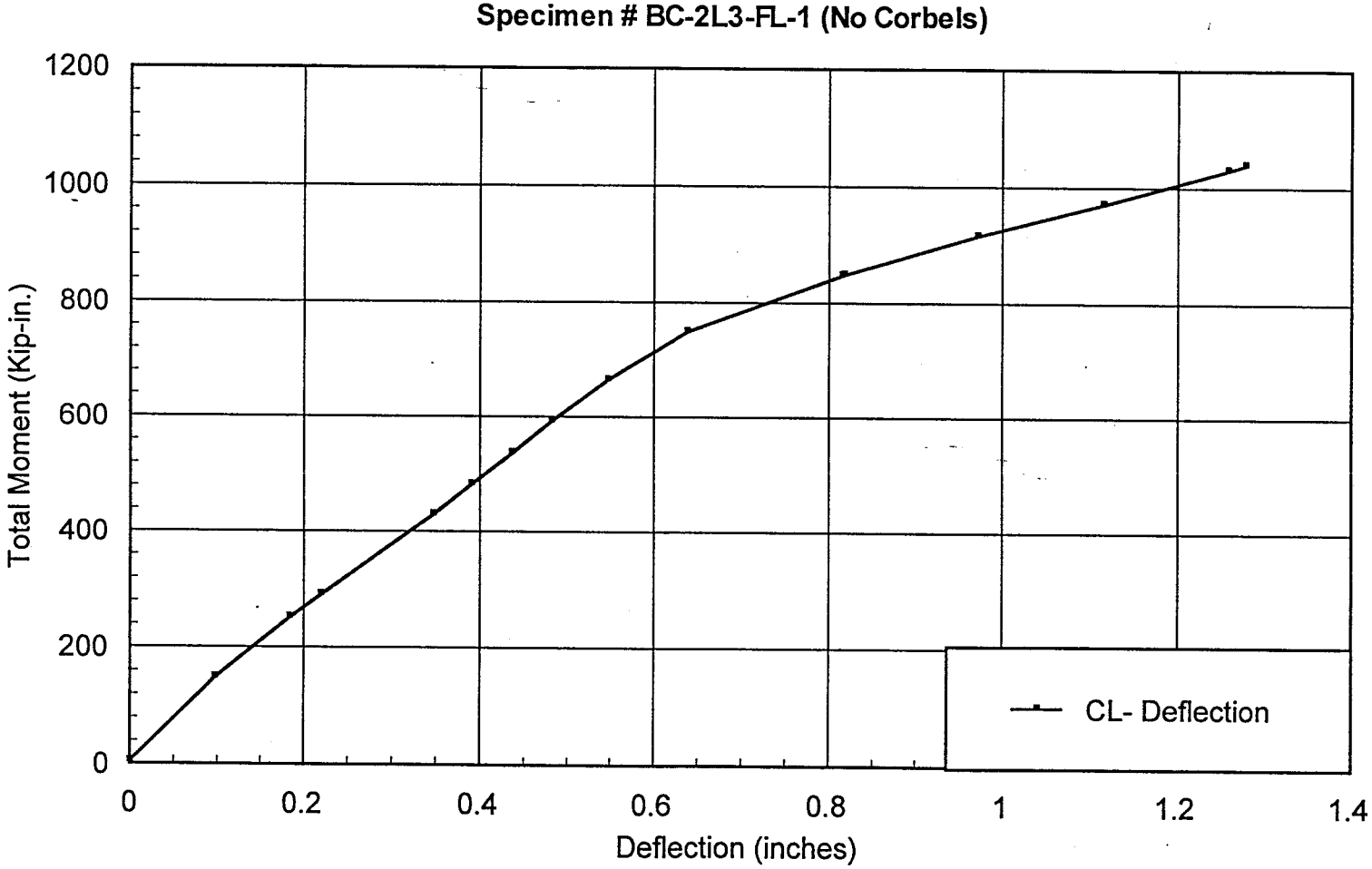

(Fig. 5.22c) Moment VS. Mid-Span Deflection

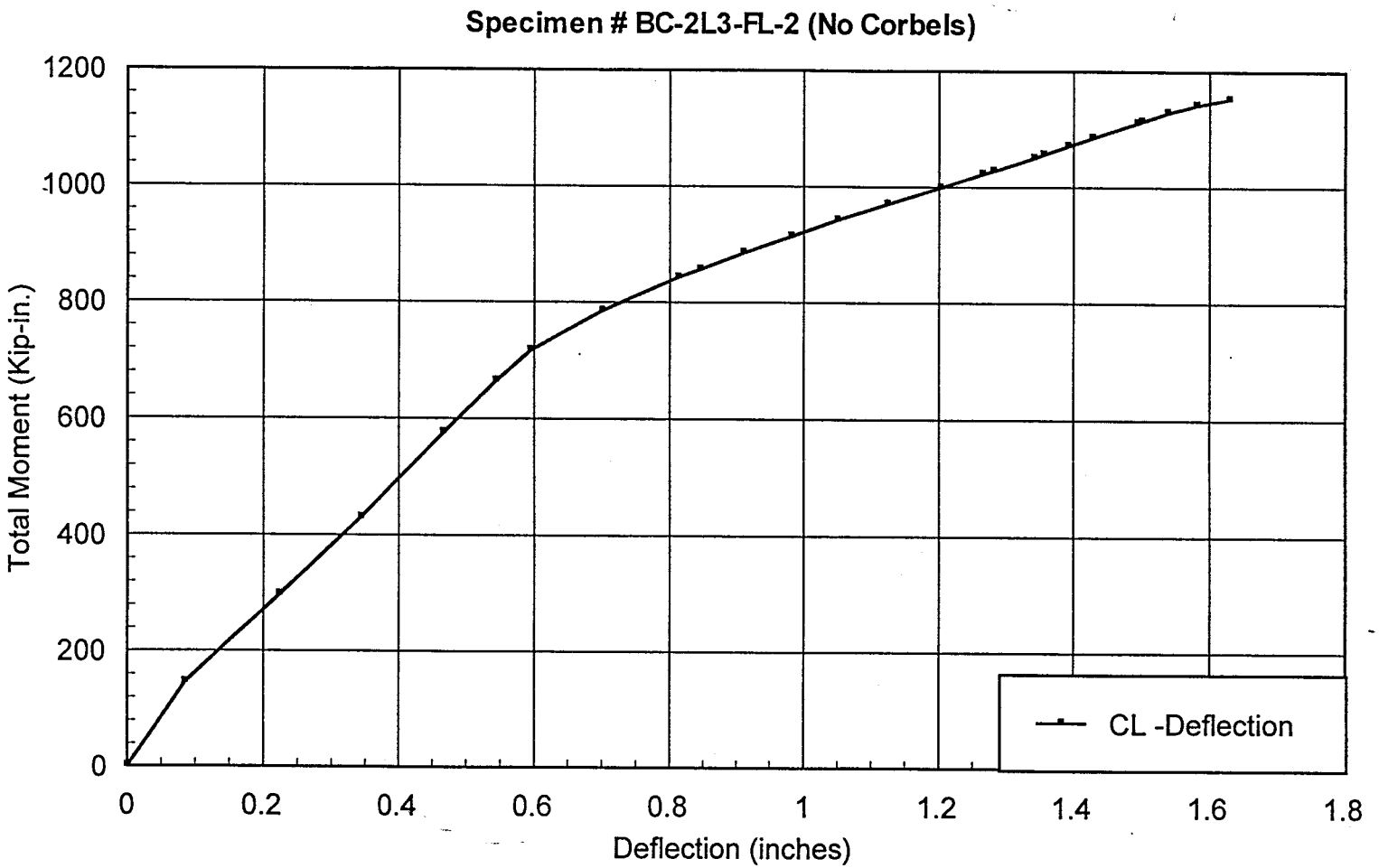

(Fig. 5.22d) Moment VS. Mid-Span Deflection

Specimen # BC-2L3-FL-3 (No Corbels)

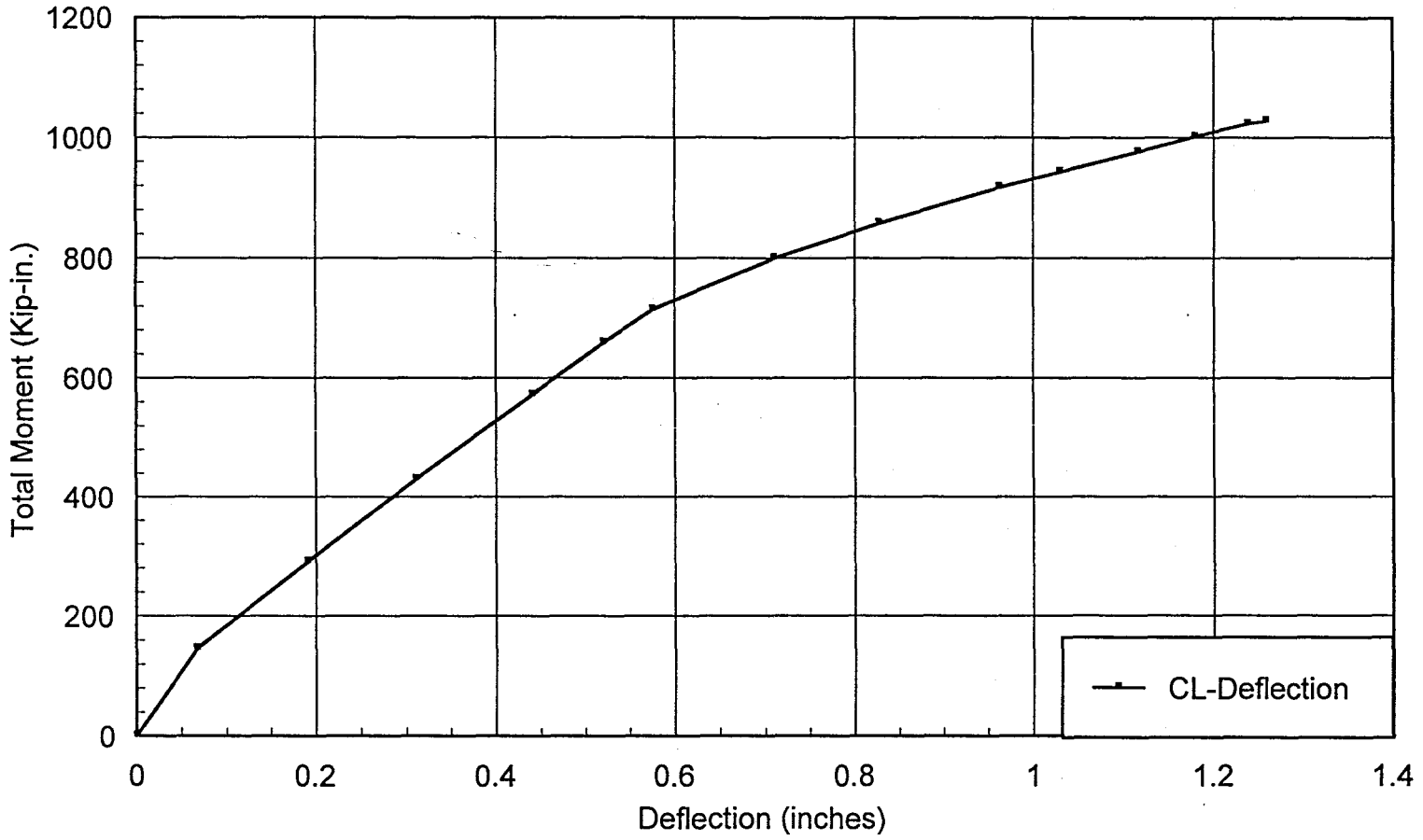

(Fig. 5.22e) Moment VS. Mid-Span Deflection

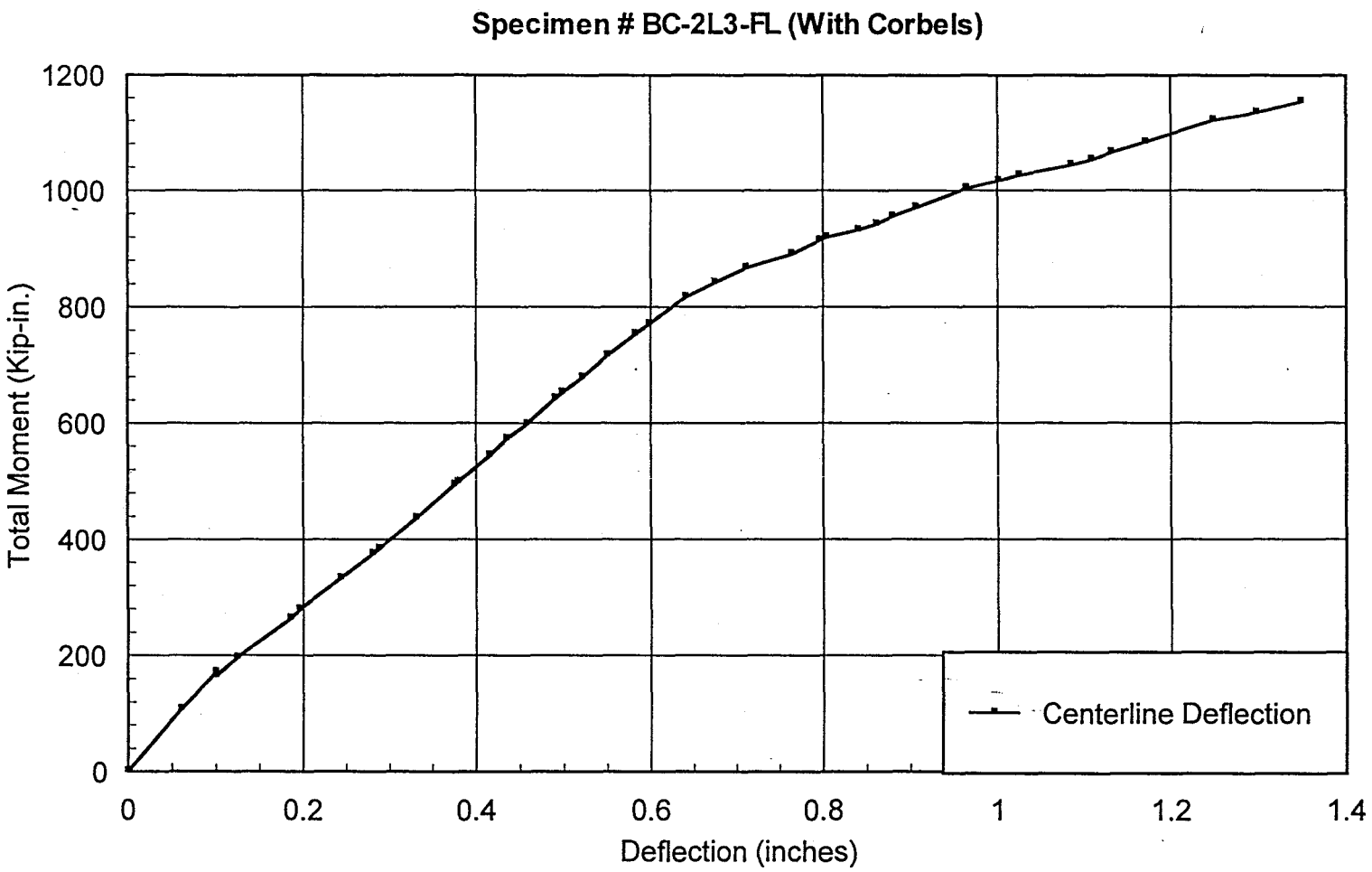

(Fig. 5.23a) Strain Distribution at Specimen Midspan

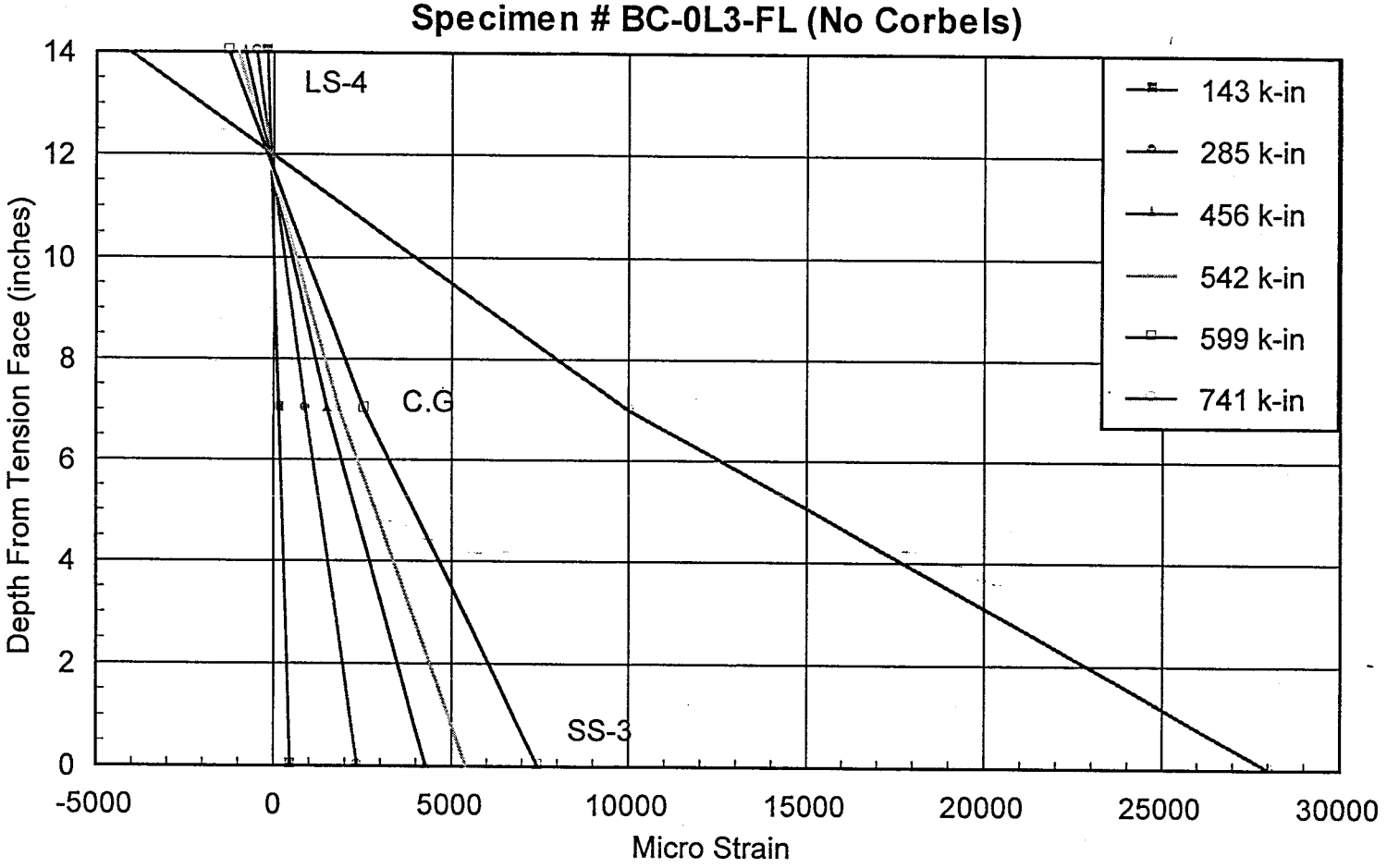

(Fig 5.23b) Strain Distribution at Specimen Midspan

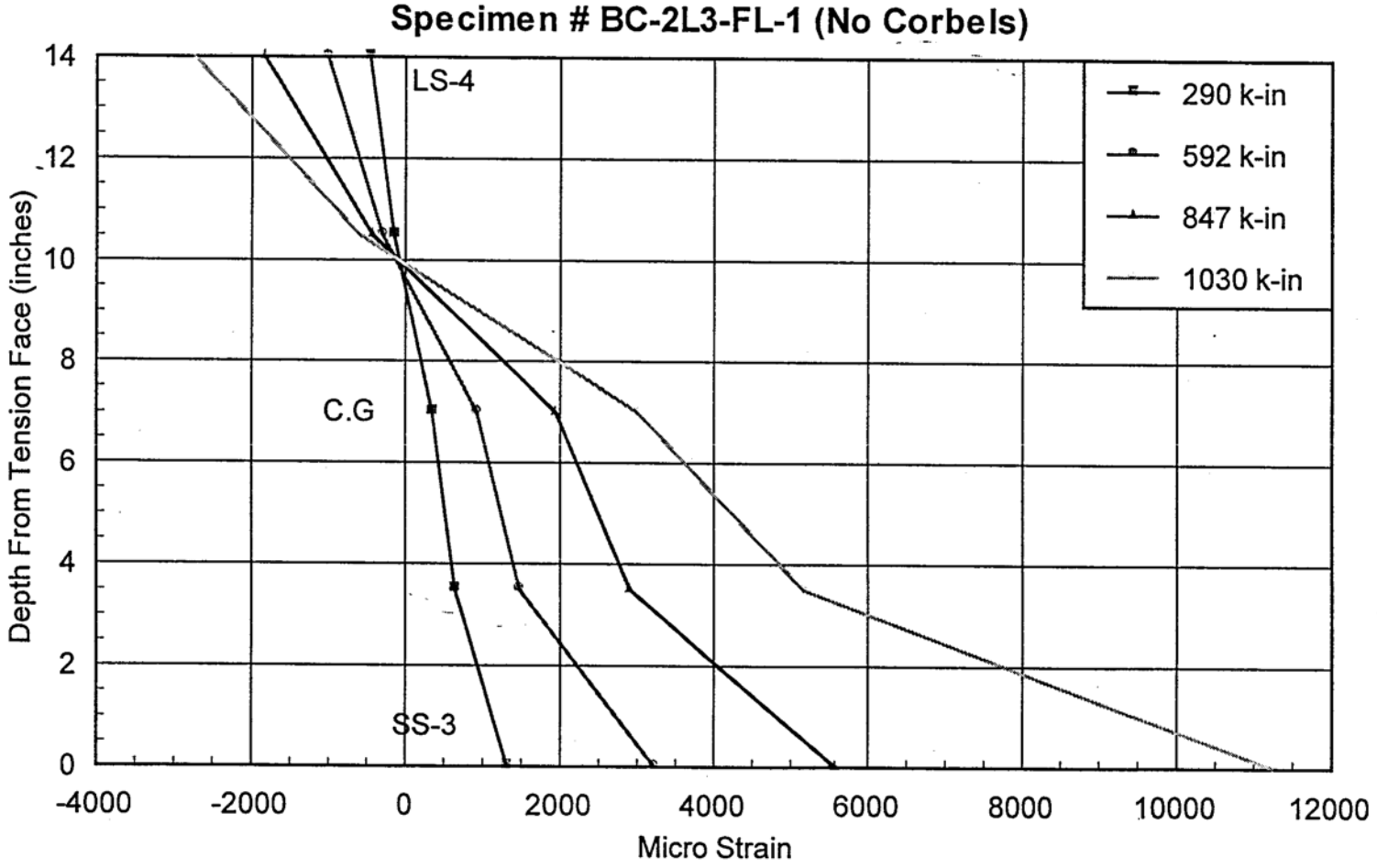

(Fig. 5.23c) Strain Distribution at Specimen Midspan

Specimen # BC-2L3-FL-2 (No Corbels)

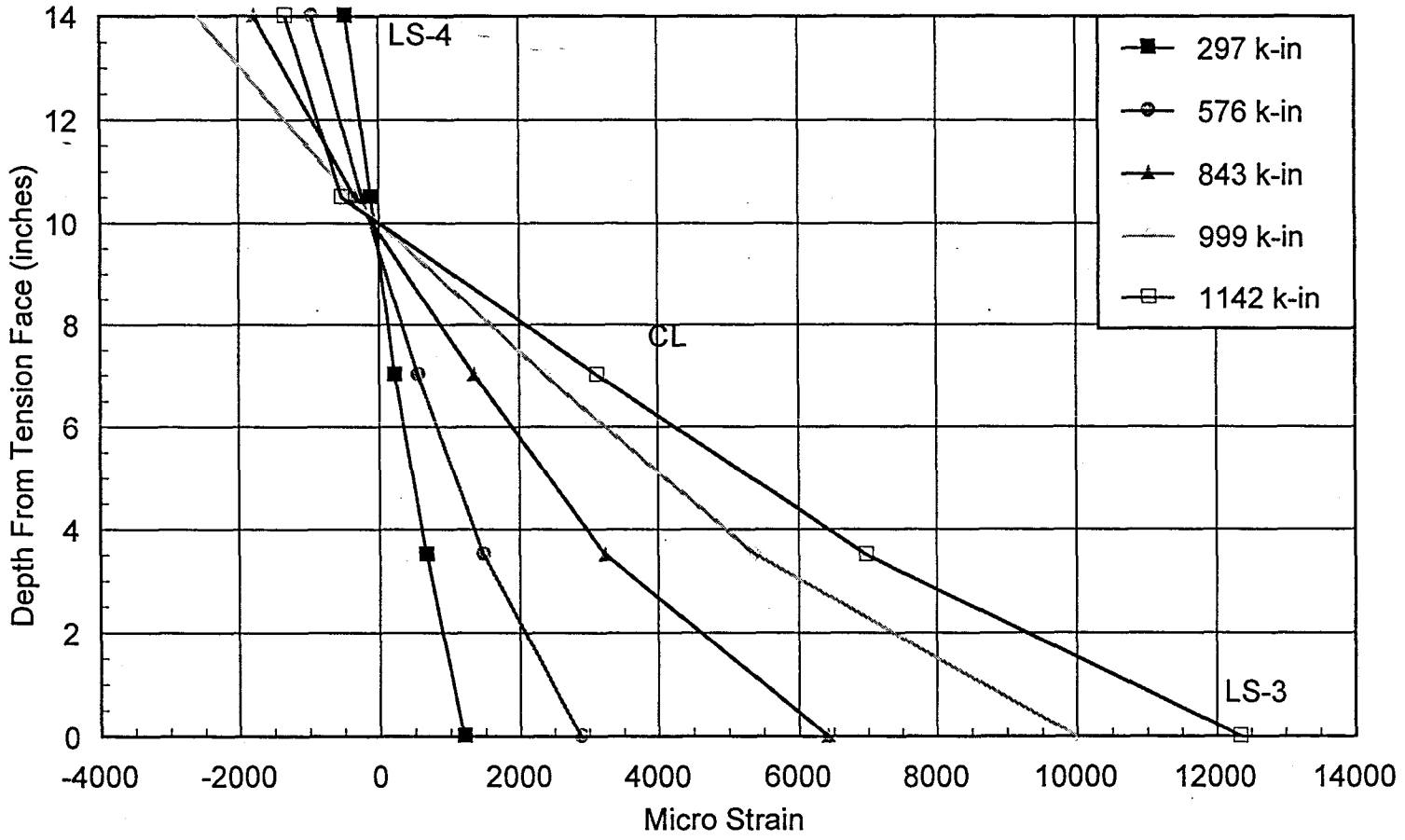

(Fig. 5.23d) Strain Distribution at Specimen Midspan

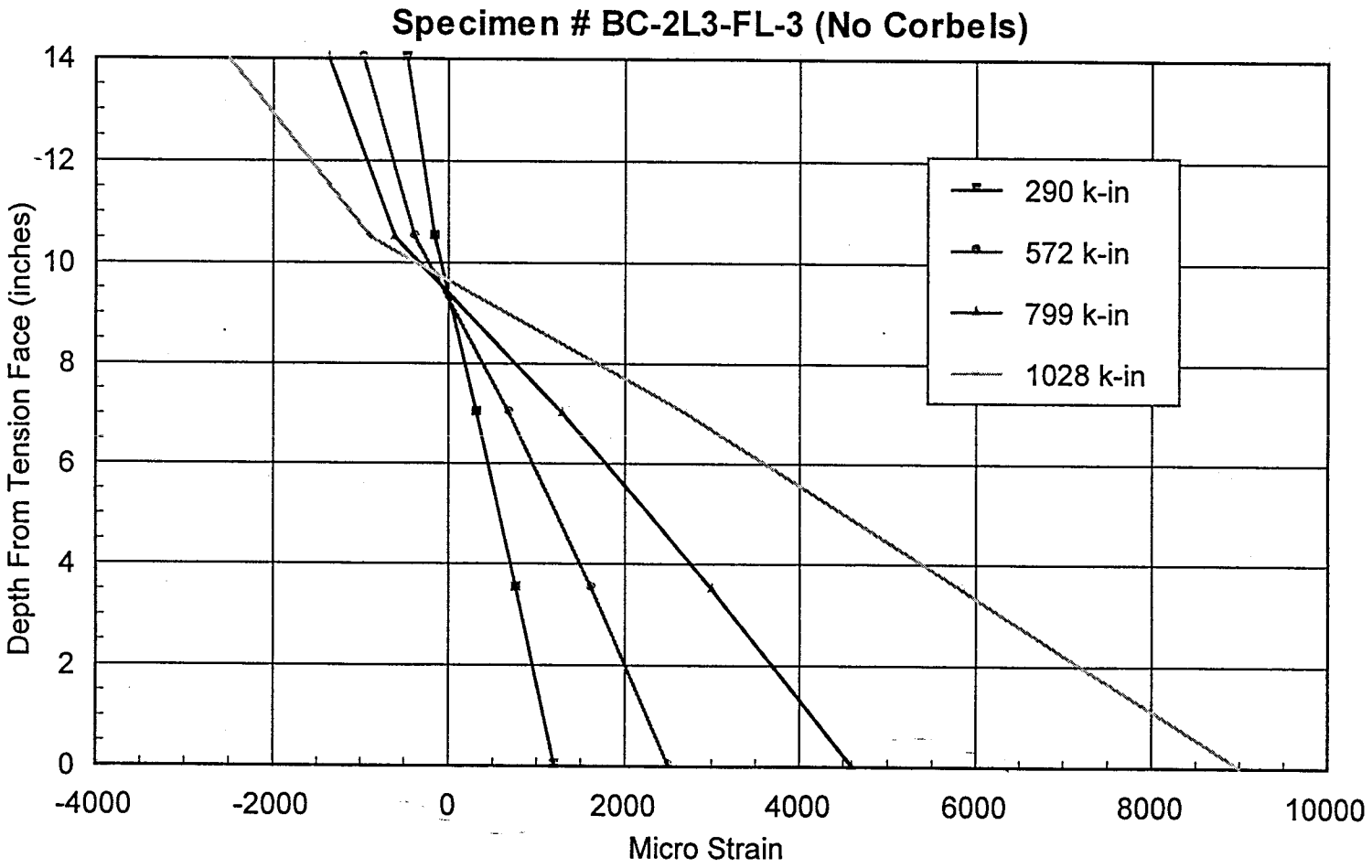

(Fig. 5.23e) Strain Distribution at Specimen Midspan

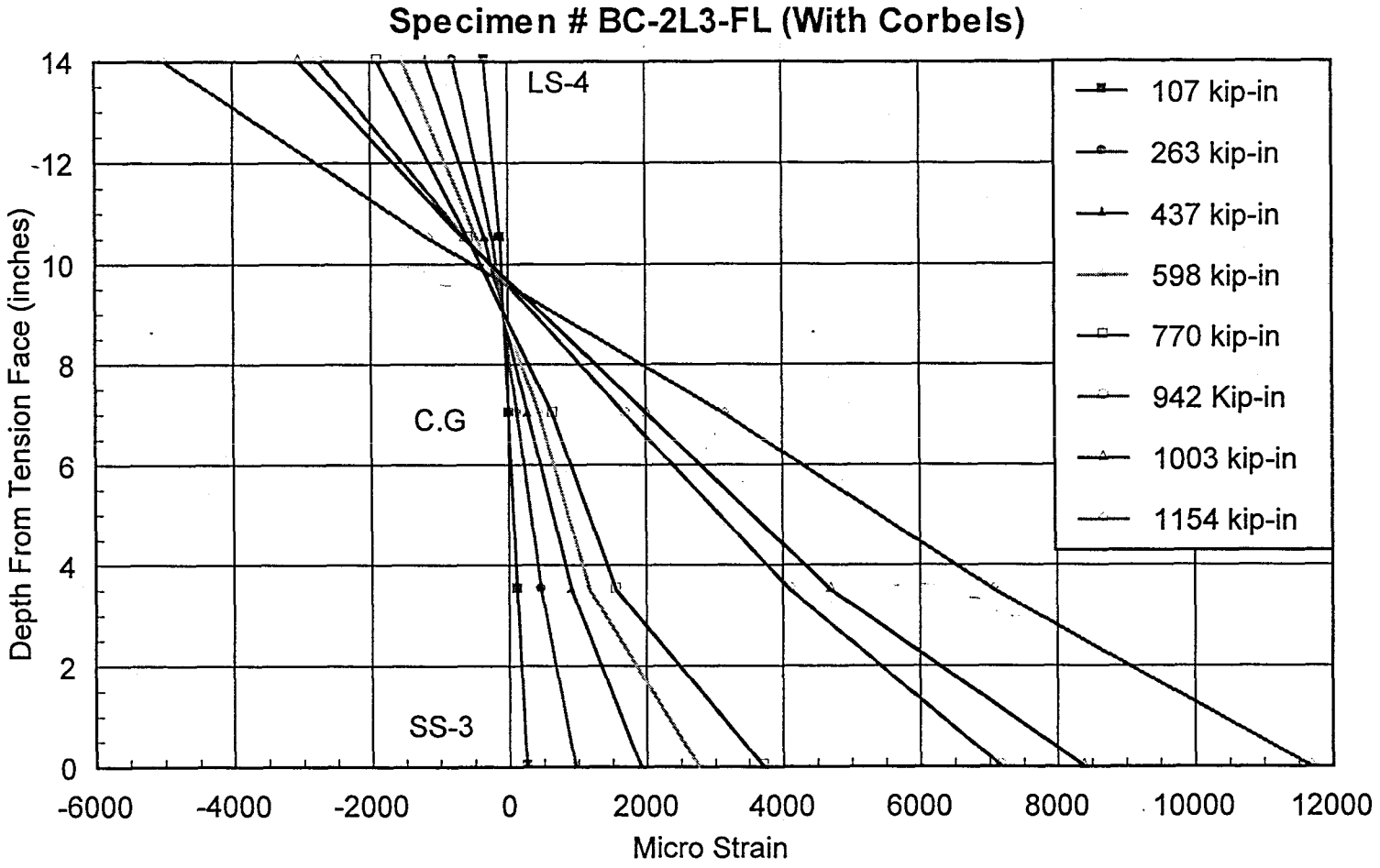

(Fig. 5.24a) Moment VS. Strain At Midspan

Specimen # BC-0L3-FL (No Corbels)

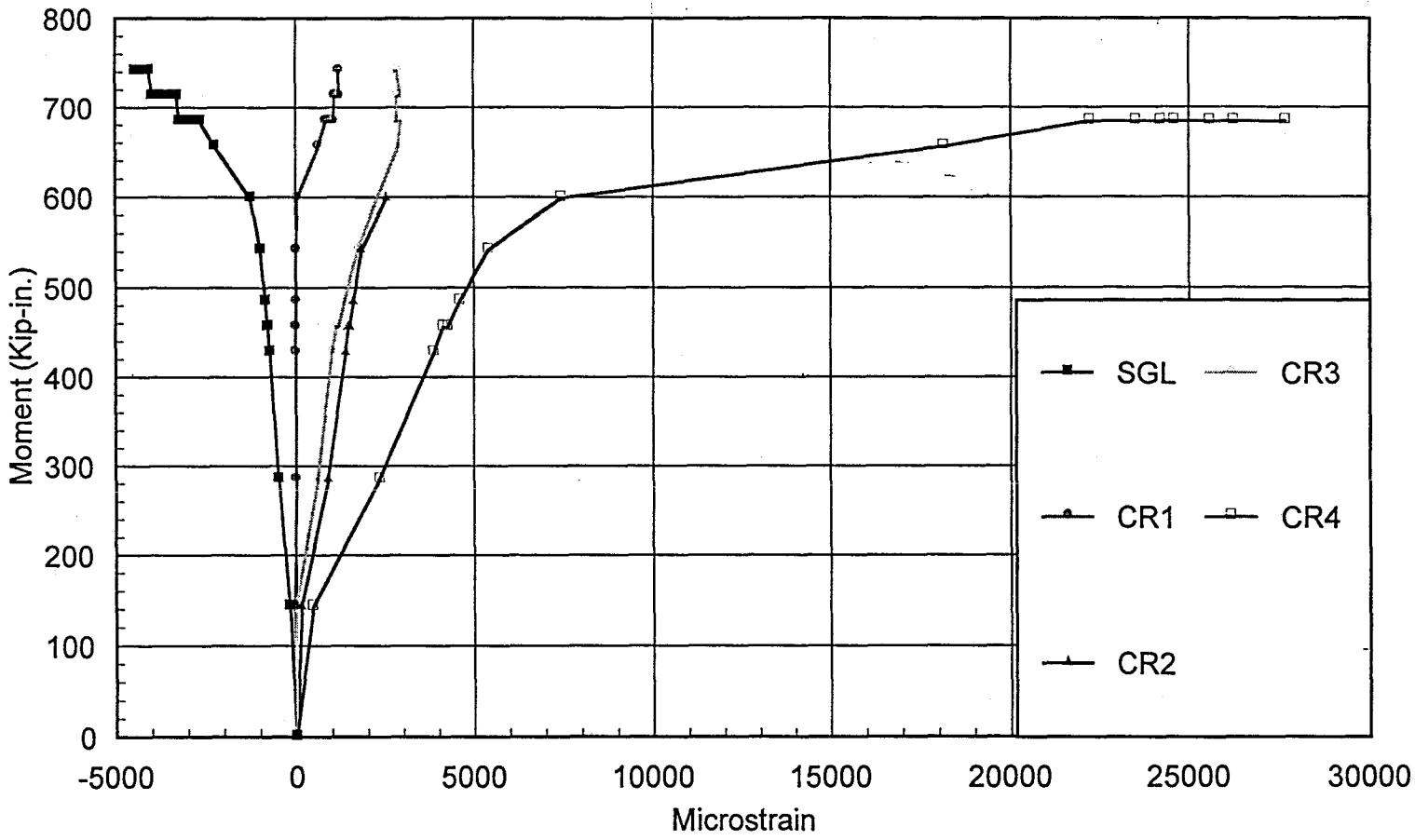

(Fig 5.24b) Moment VS. Strain At Midspan

Specimen # BC-2L3-FL-1 (No Corbels)

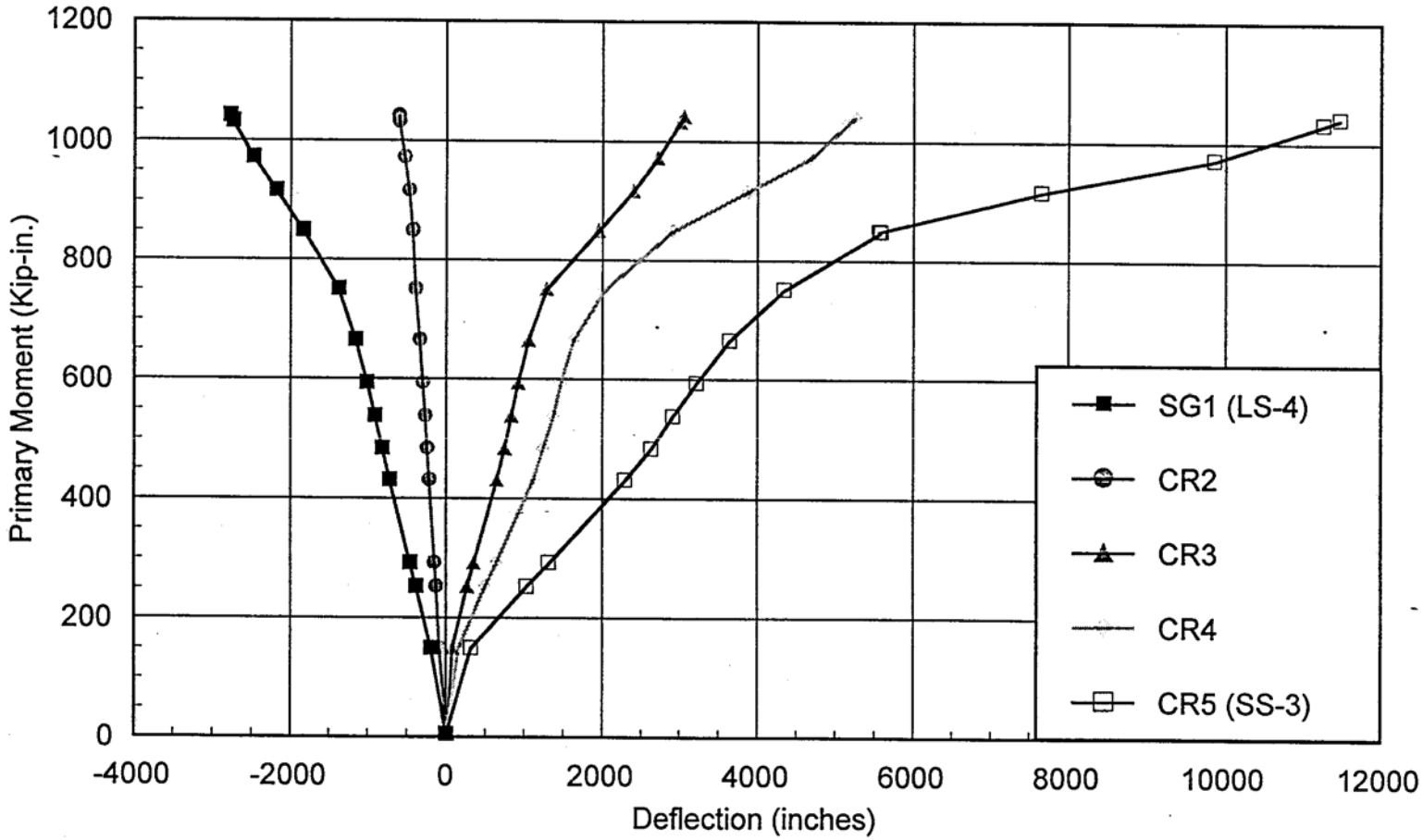

(Fig. 5.24c) Moment VS. Strain At Midspan

Specimen # BC-2L3-FL-2 (No Corbels)

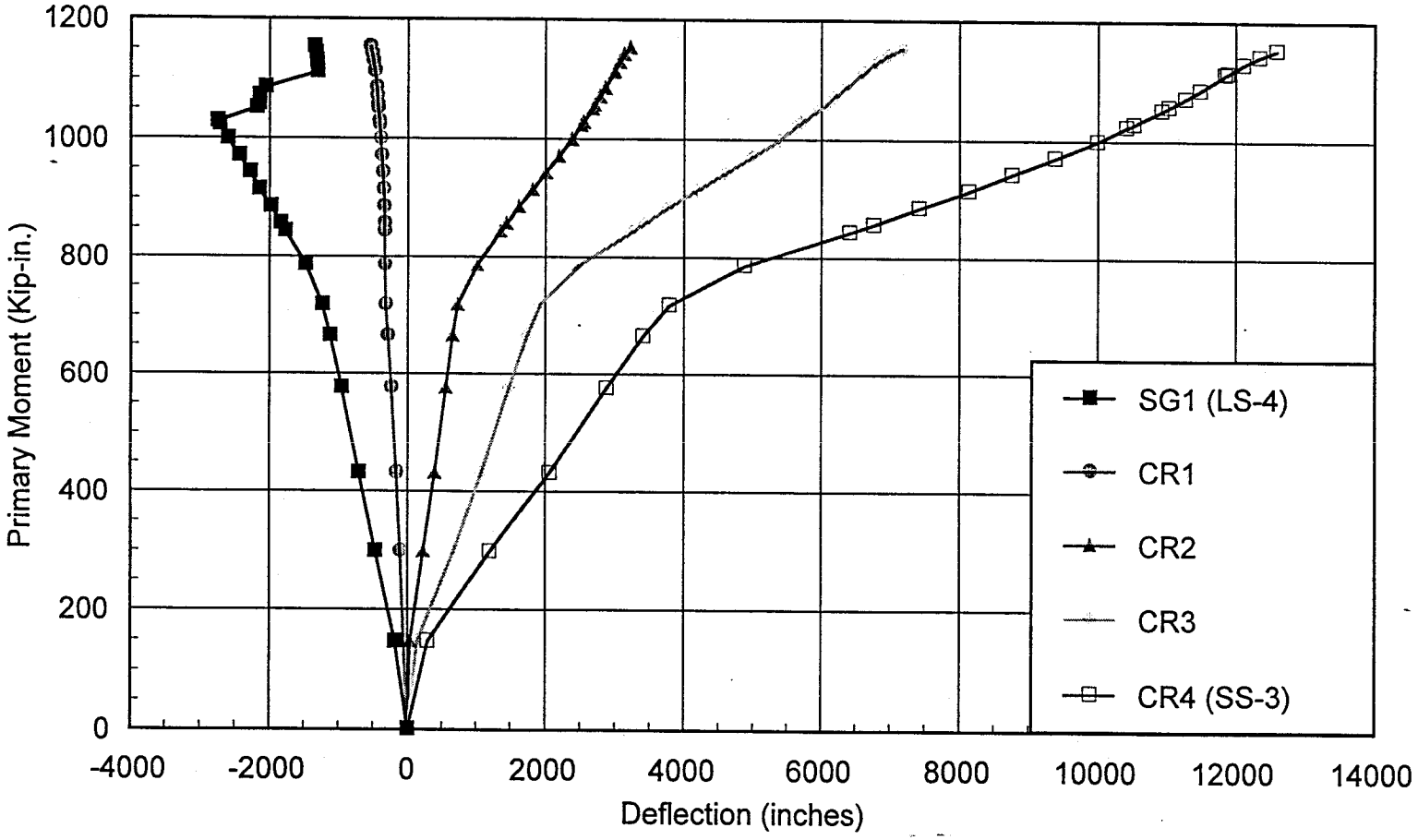

(Fig. 5.24d) Moment VS. Strain At Midspan

Specimen # BC-2L3-FL-3 (No Corbels)

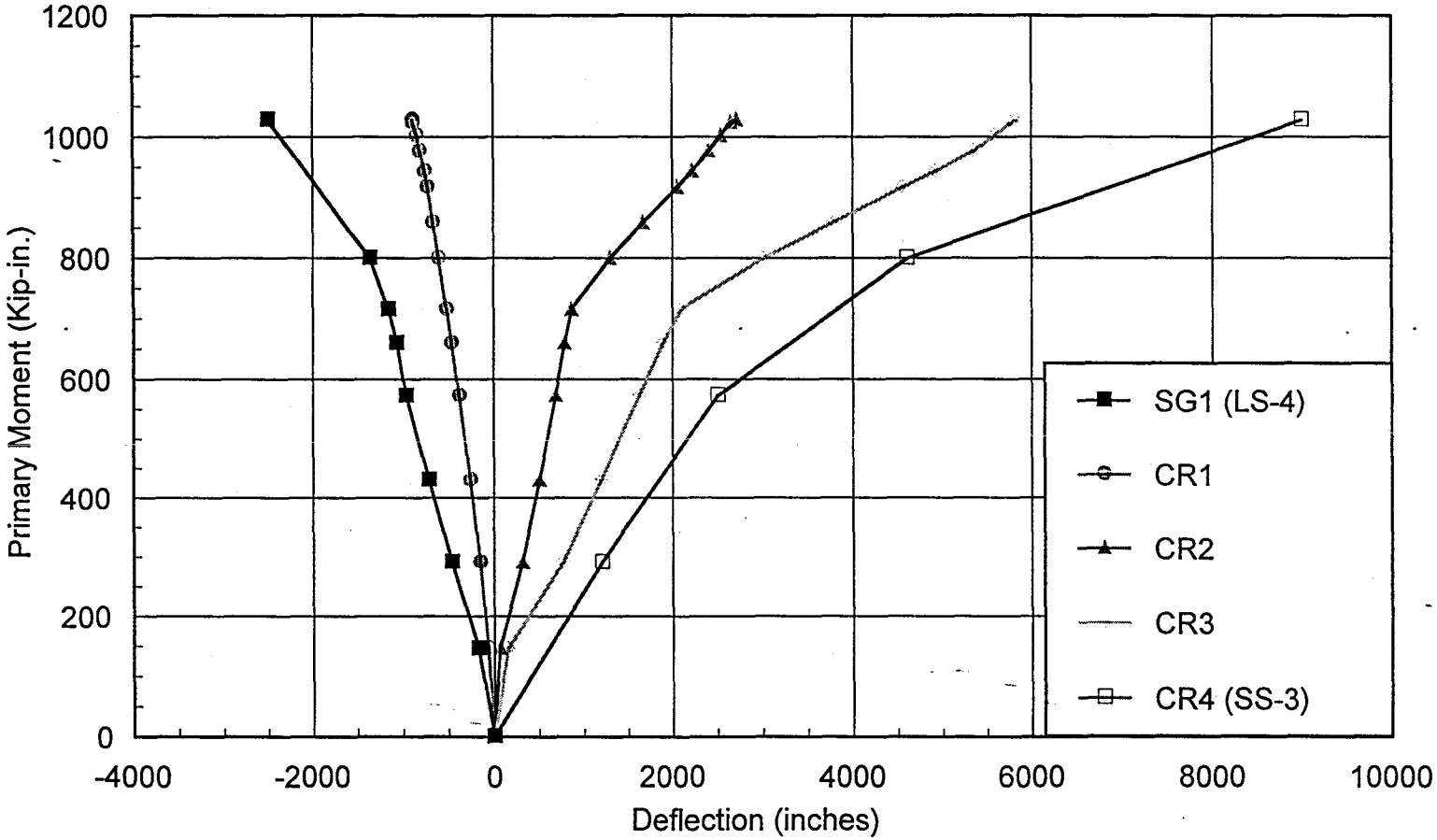

(Fig. 5.24e) Moment VS. Strain At Midspan

Specimen # BC-2L3-FL (With Corbels)

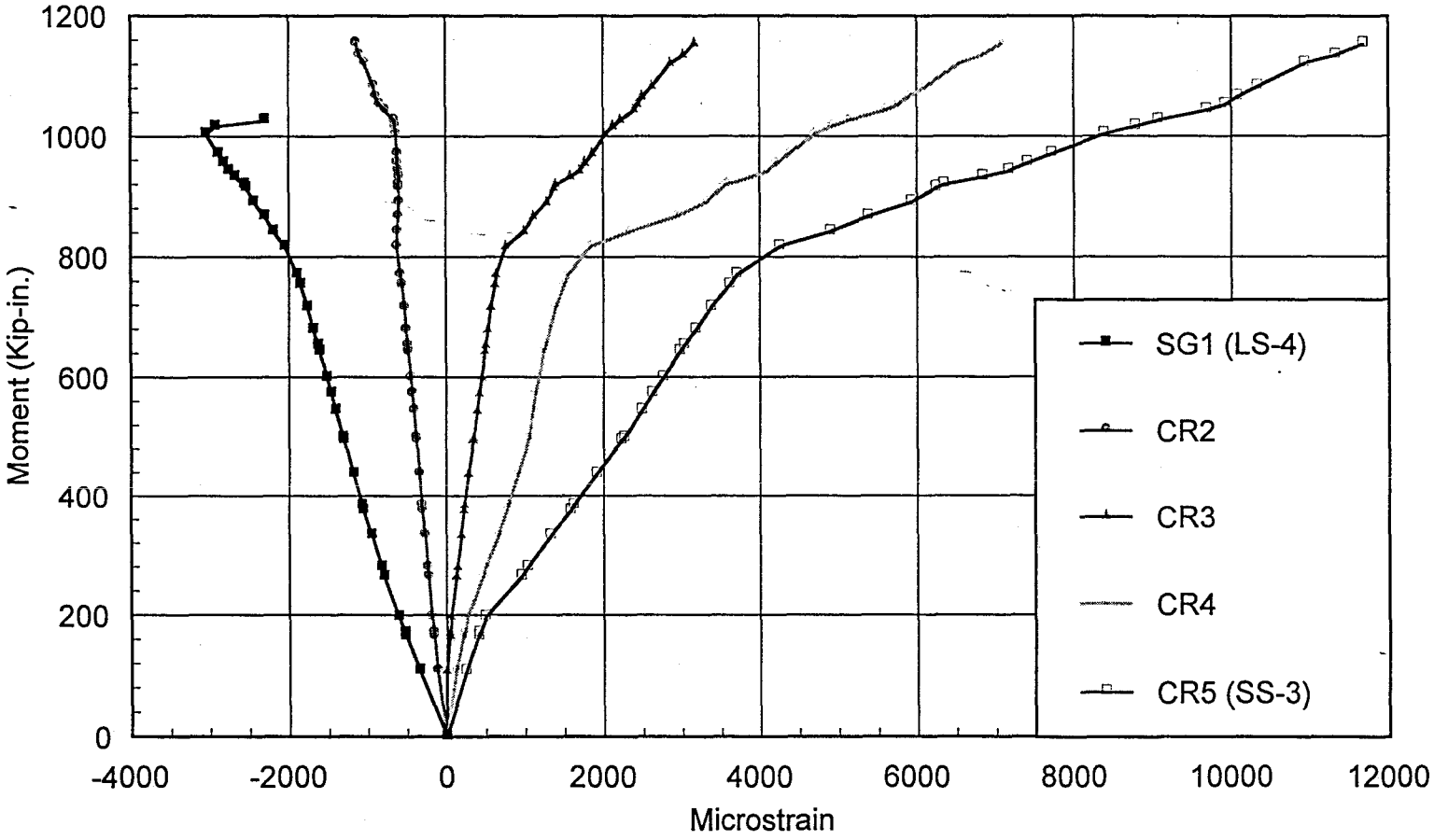

(Fig. 5.25a) Moment VS.Transverse Strain At Midspan

Specimen # BC-0L3-FL (No Corbels)

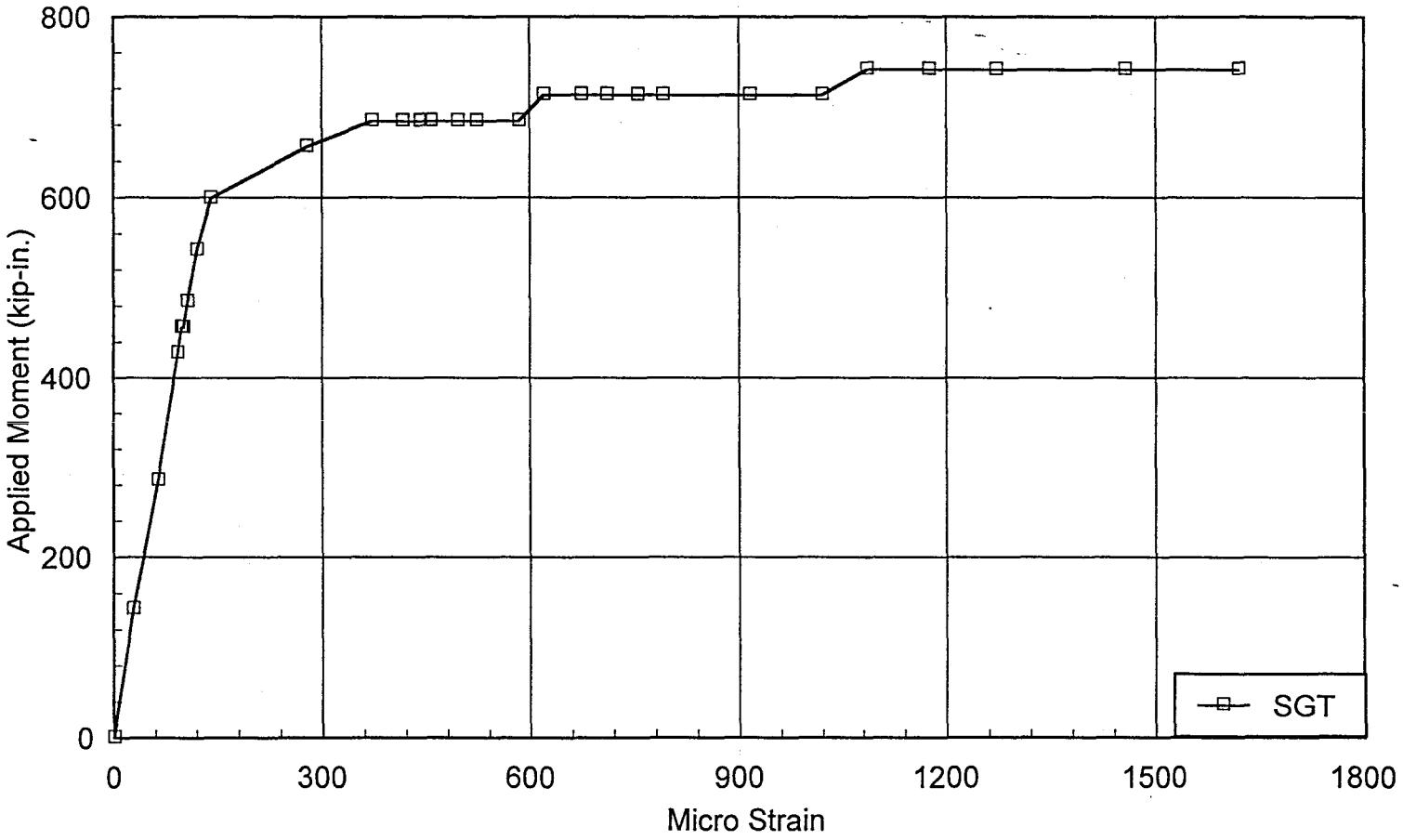

(Fig. 5.25b) Moment vs.Transverse Strain At Mid-Span

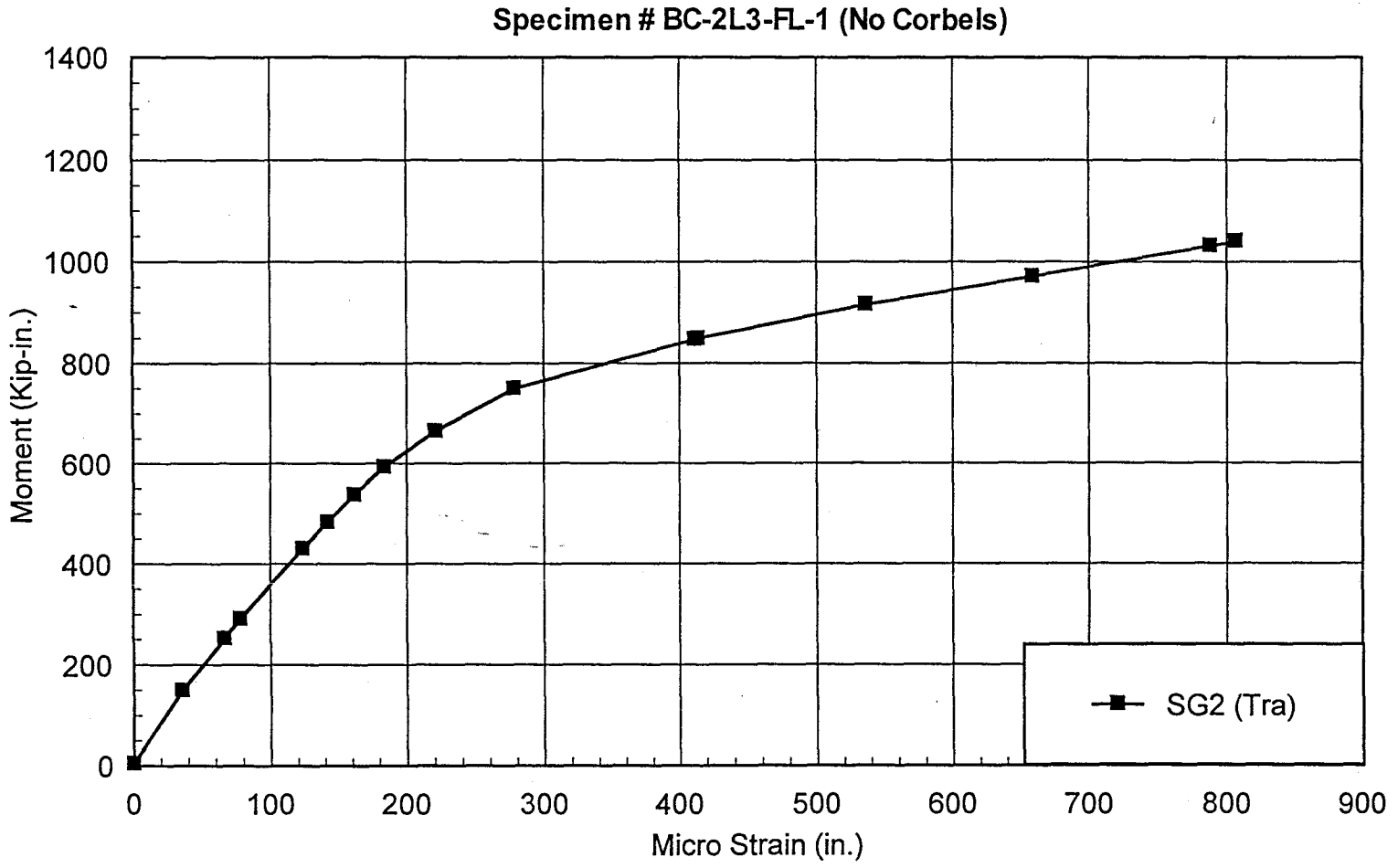

(Fig. 5.25c) Moment vs.Transverse Strain At Mid-Span

Specimen # BC-2L3-2FL-2 (No Corbels)

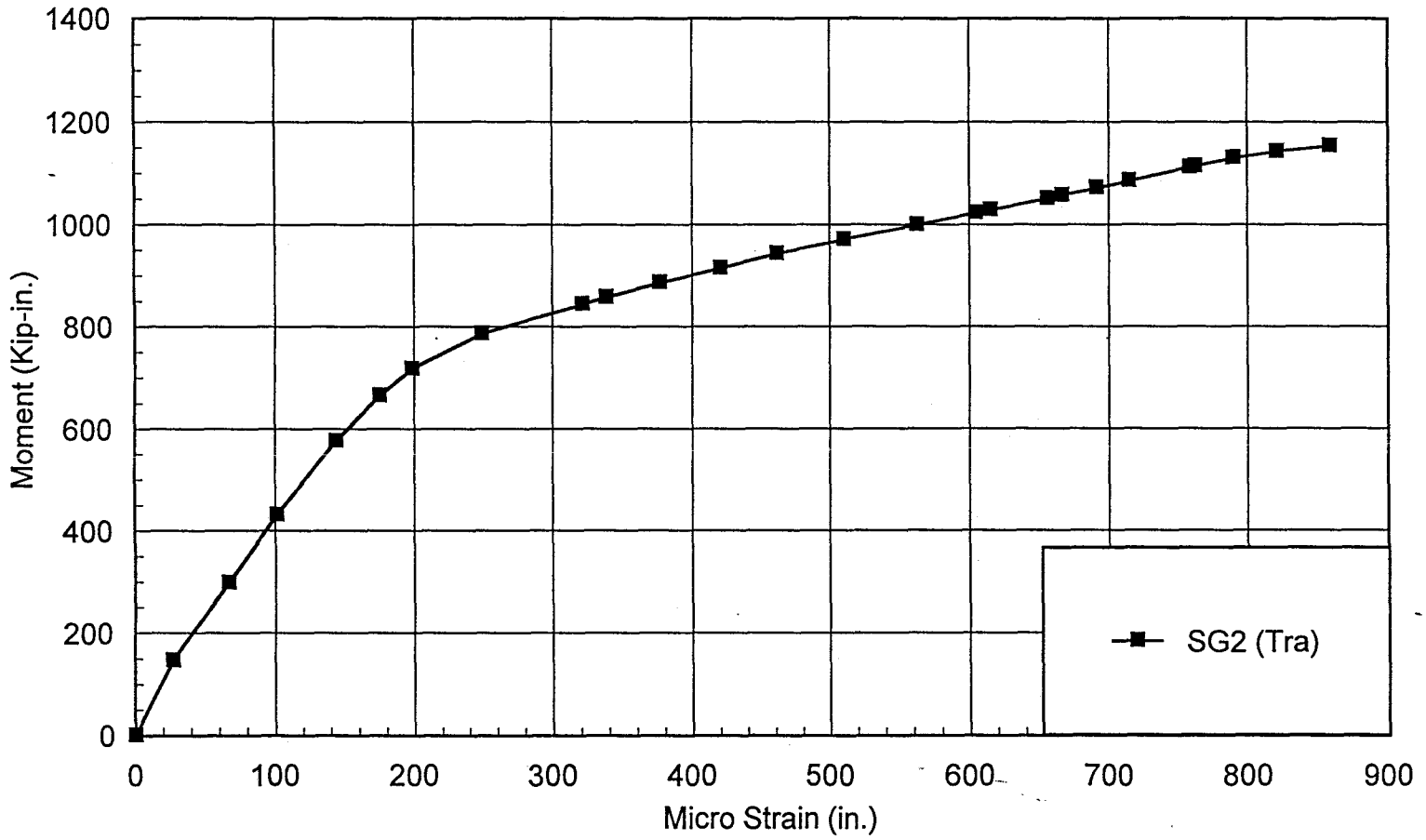

(Fig. 5.25d) Moment vs.Transverse Strain At Mid-Span

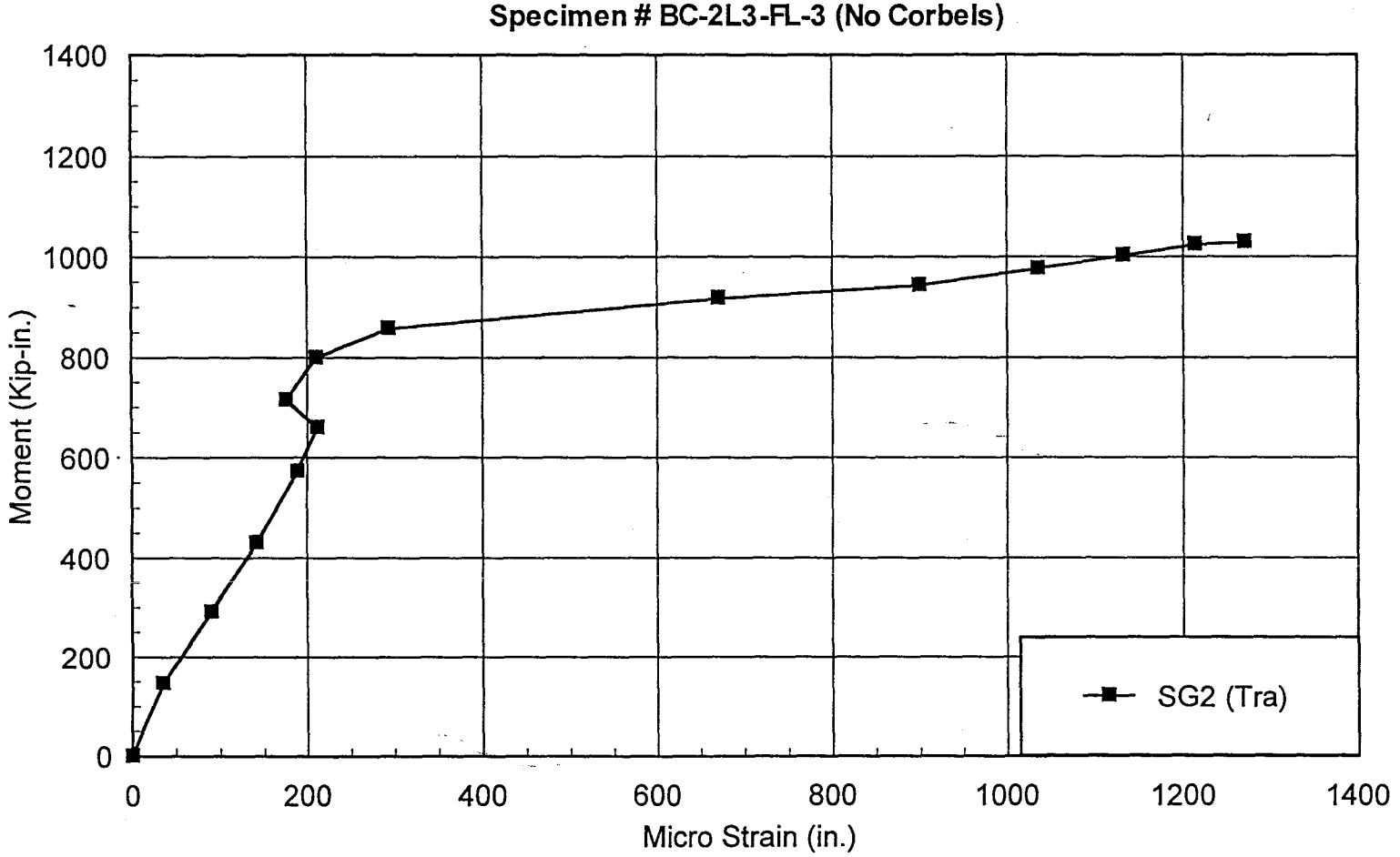

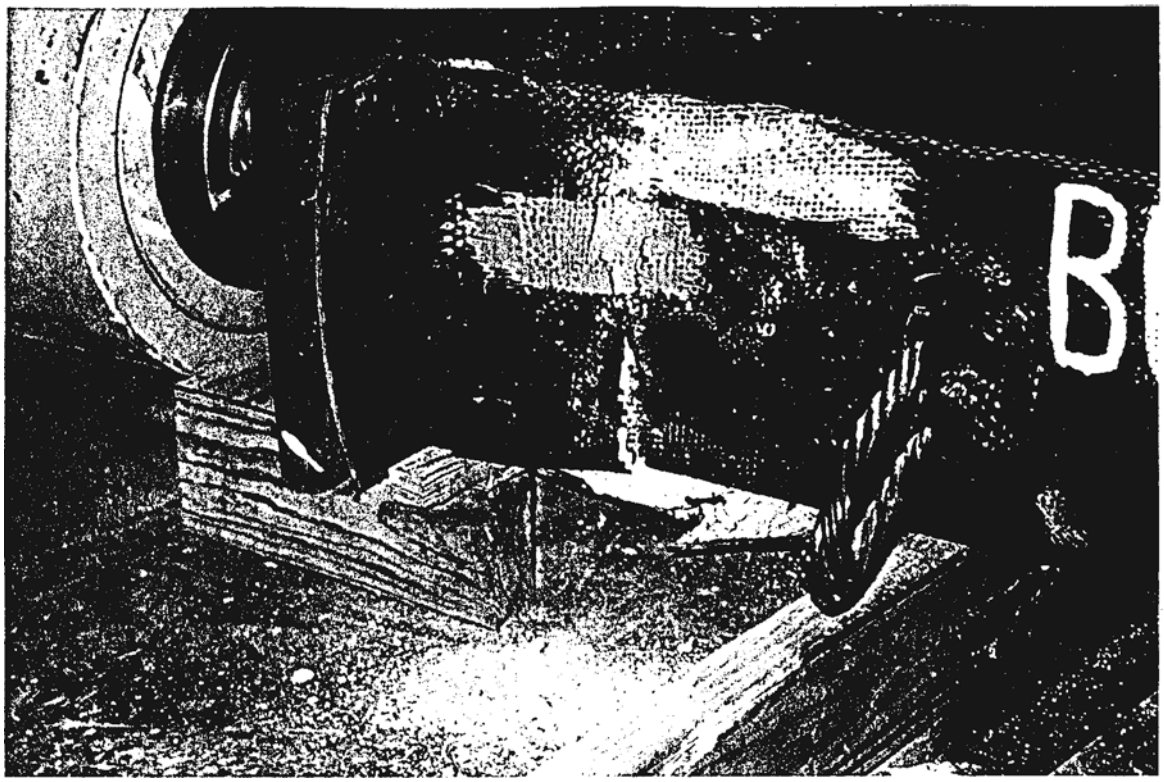

(a) Eccentricity=0"

(b) Eccentricity=3"

Fig. 6.1 Typical Views of Specimens After Tests
(a) Eccentricity=0" and (b) Eccentricity=3"

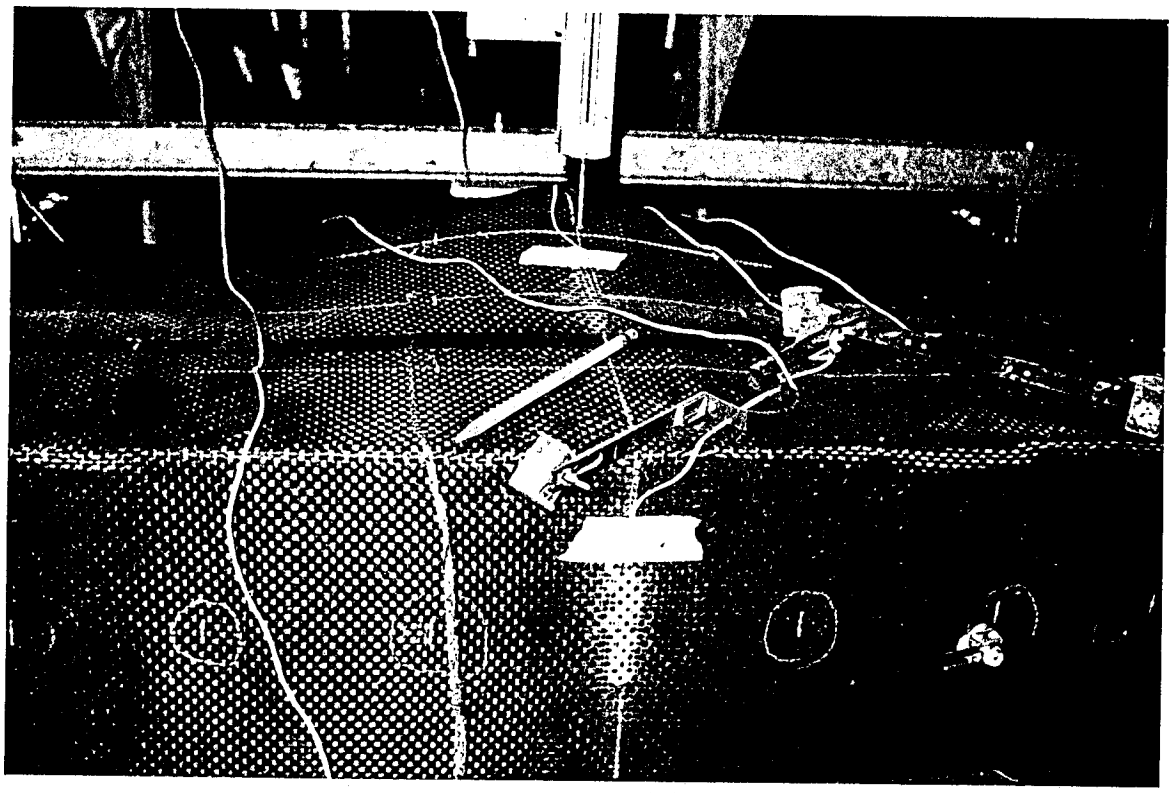

c) Eccentricity=6"

Fig. 6.1 Typical Views of Specimens After Tests
(c) Eccentricity=6"

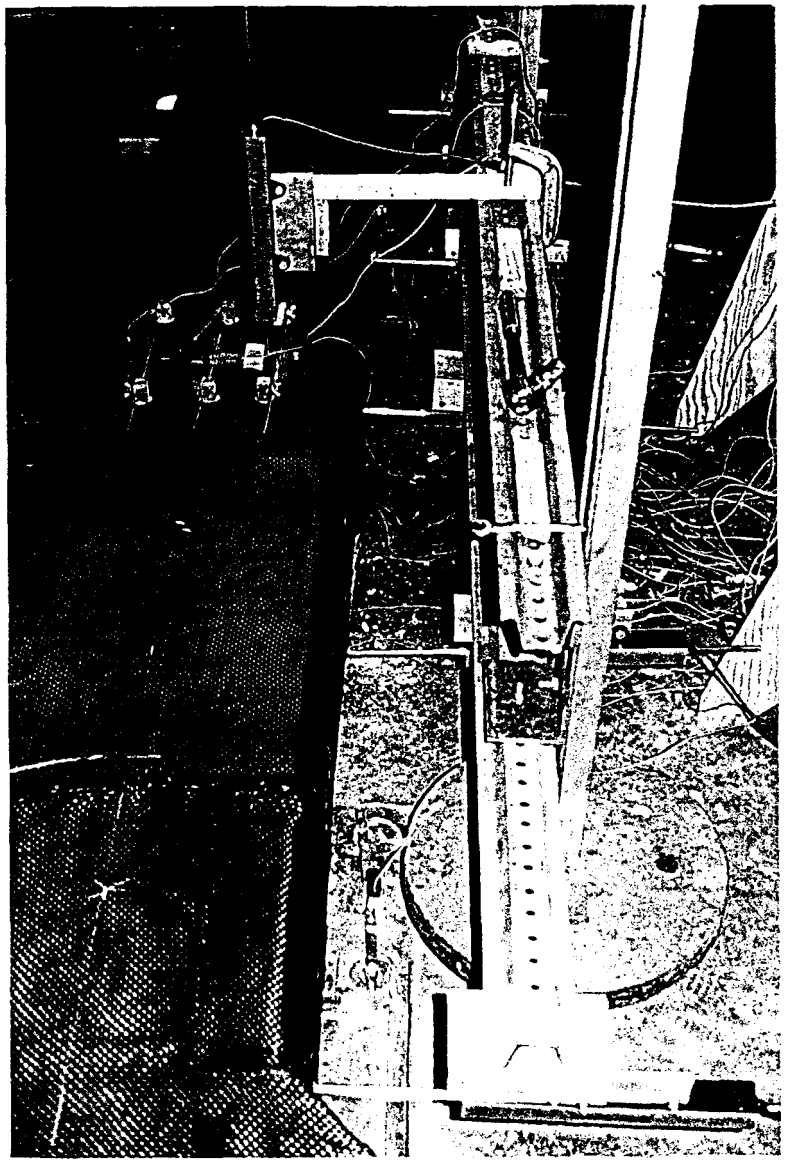

(d) Eccentricity=12"

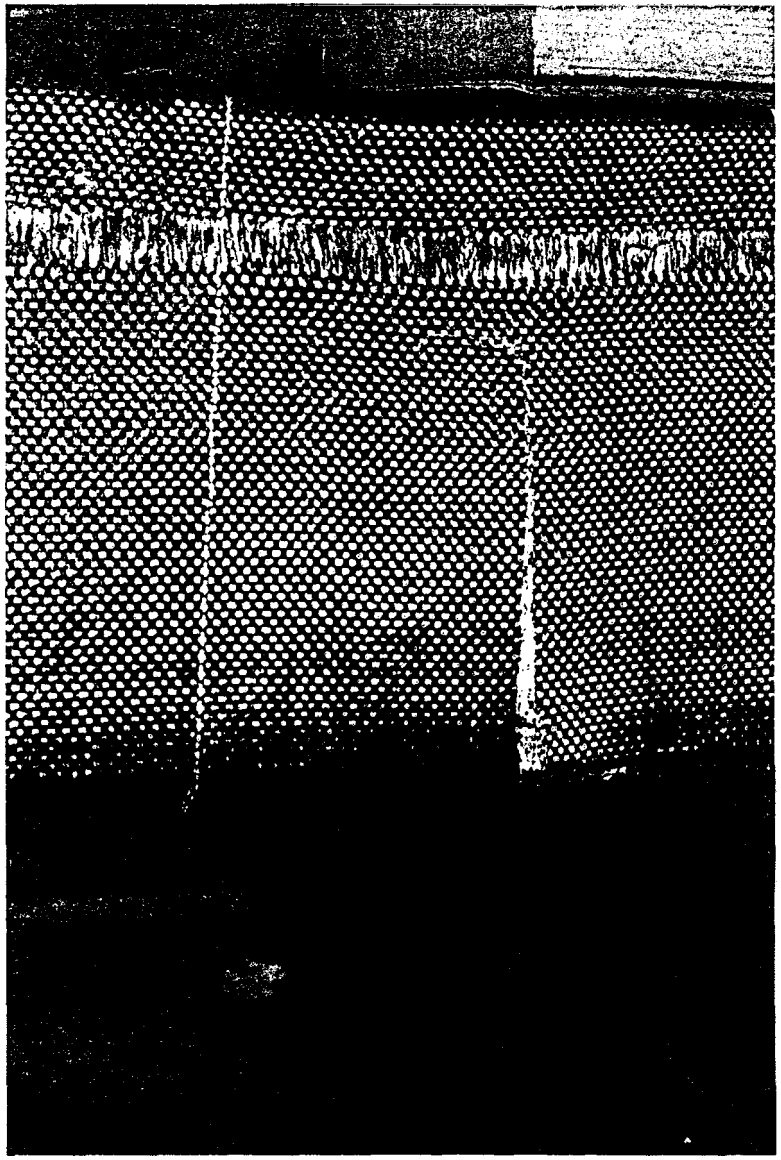

(e) Pure bending

Fig. 6.1 Typical Views of Specimens After Tests
(d) Eccentricity=12" and (e) Pure Bending

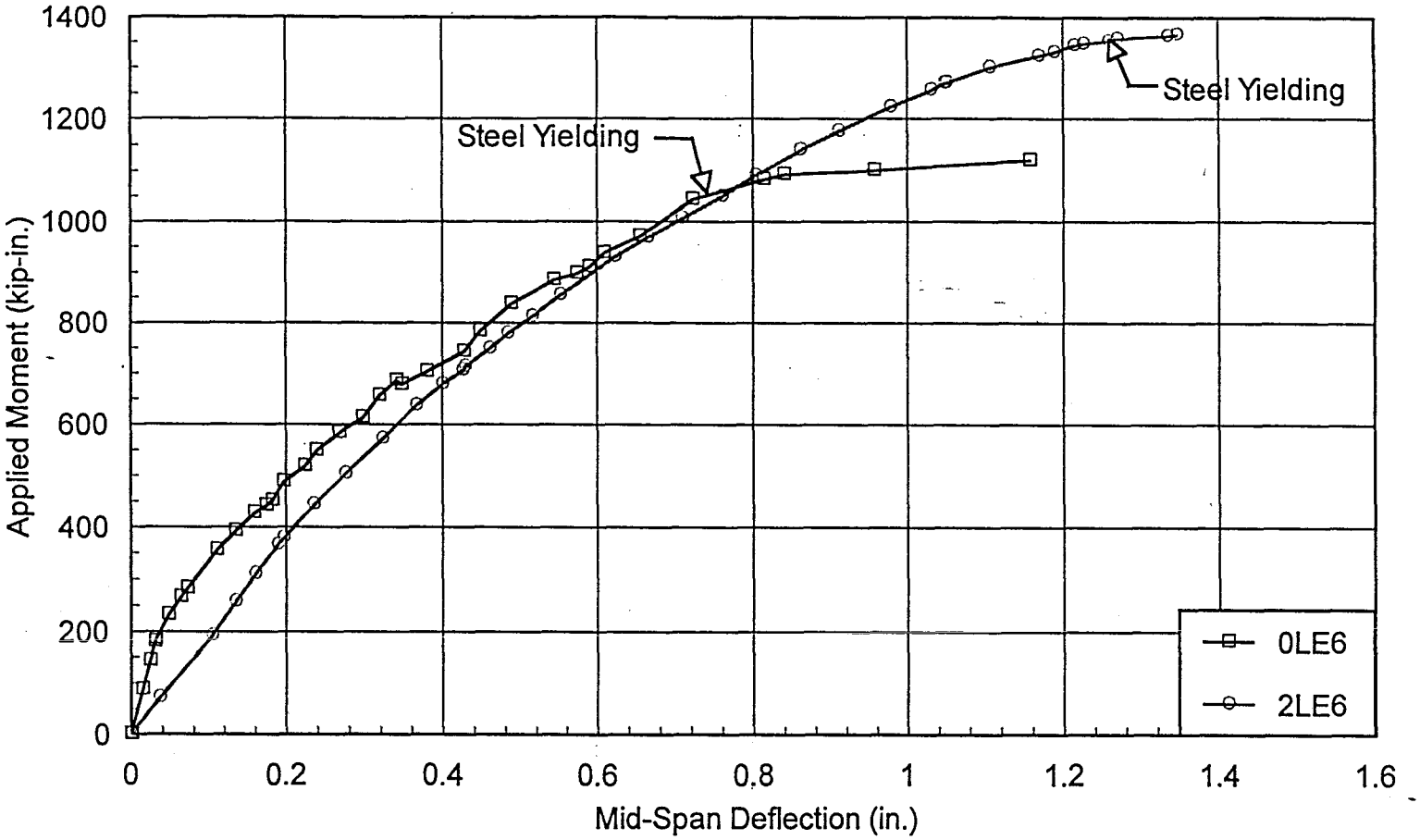

Fig. 6.2 Applied Moment versus Mid-Span Deflection
(a) Eccentricity=6"

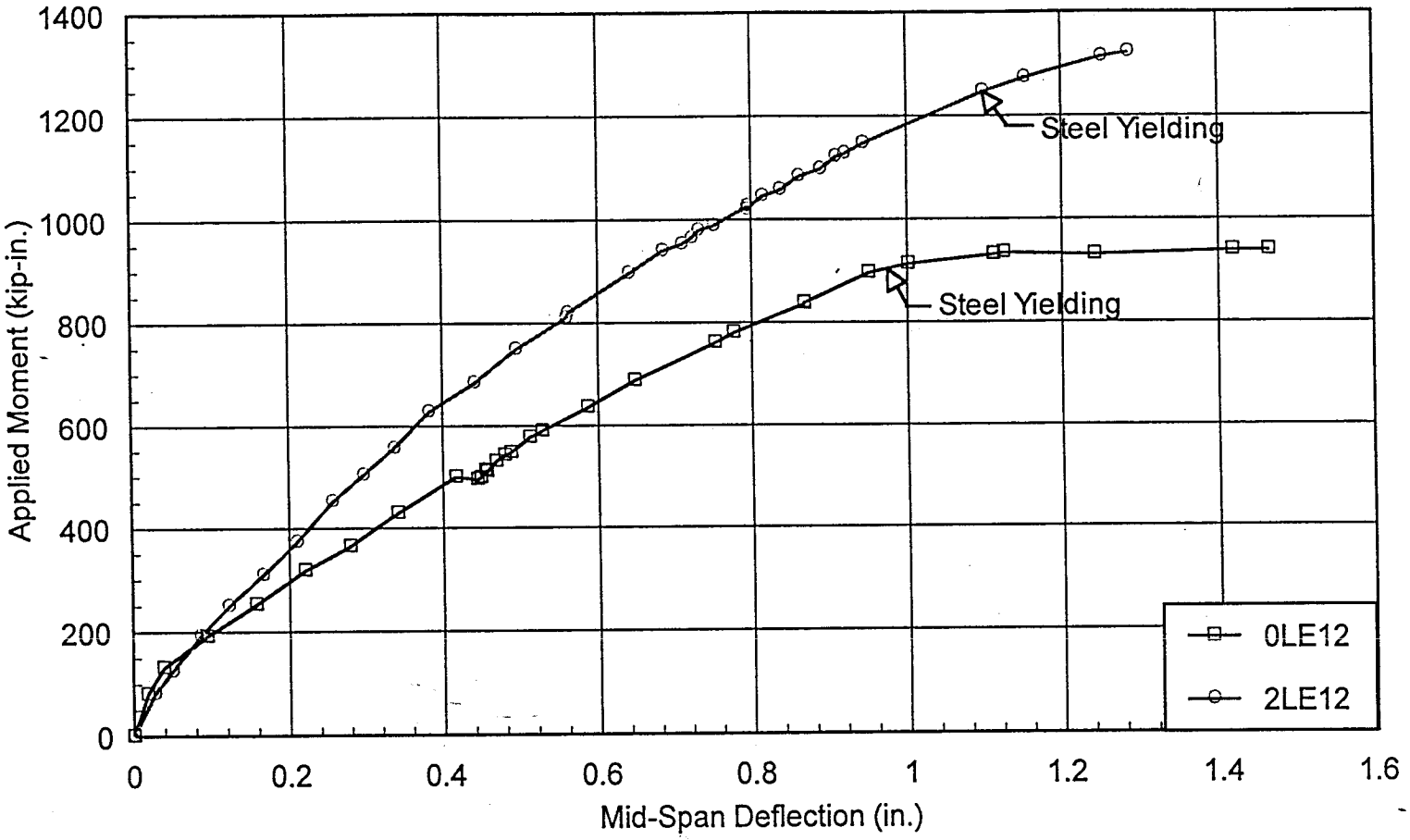

Fig. 6.2 Applied Moment versus Mid-Span Deflection
(b) Eccentricity=12"

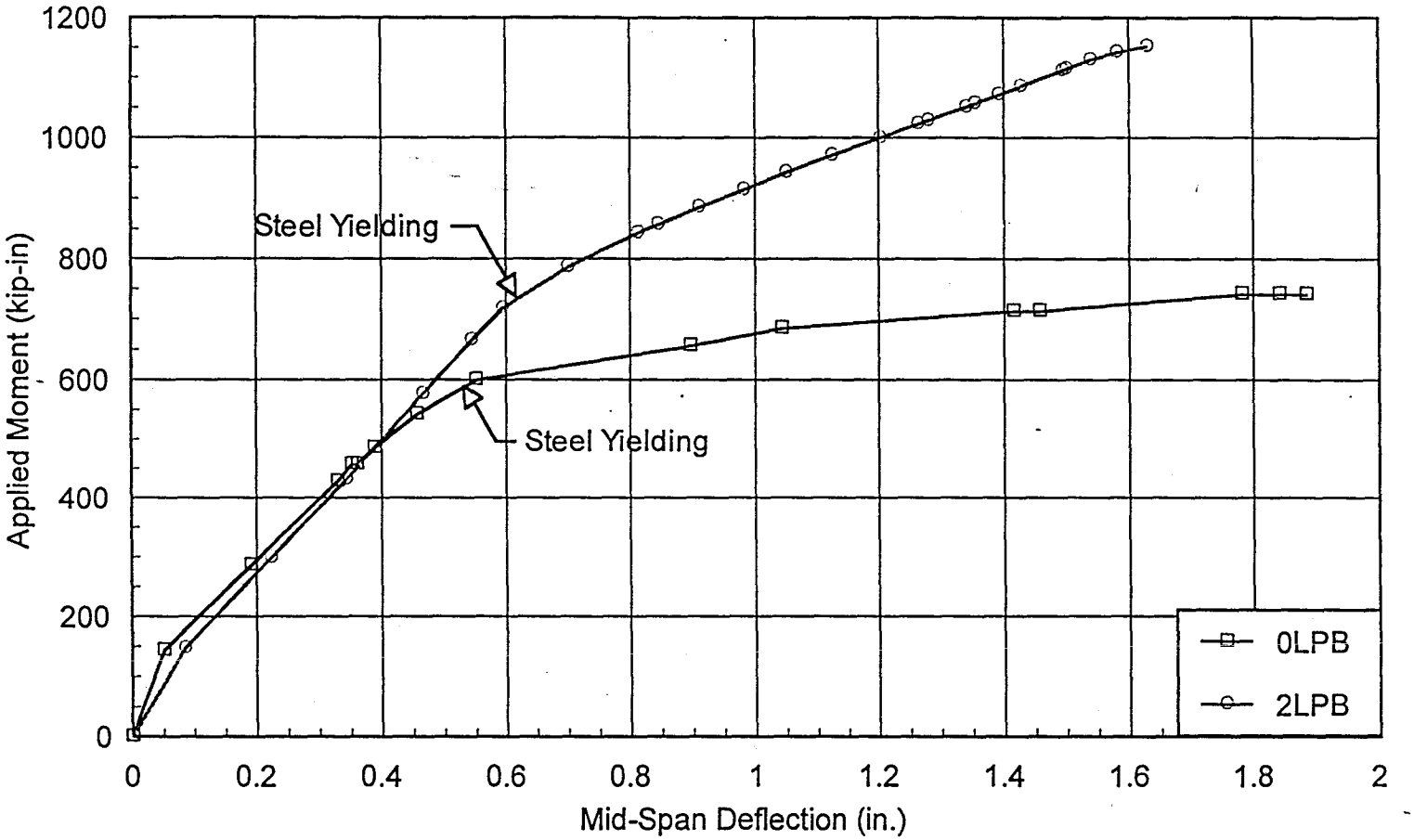

Fig. 6.2 Applied Moment versus Mid-Span Deflection

(c) Pure Bending

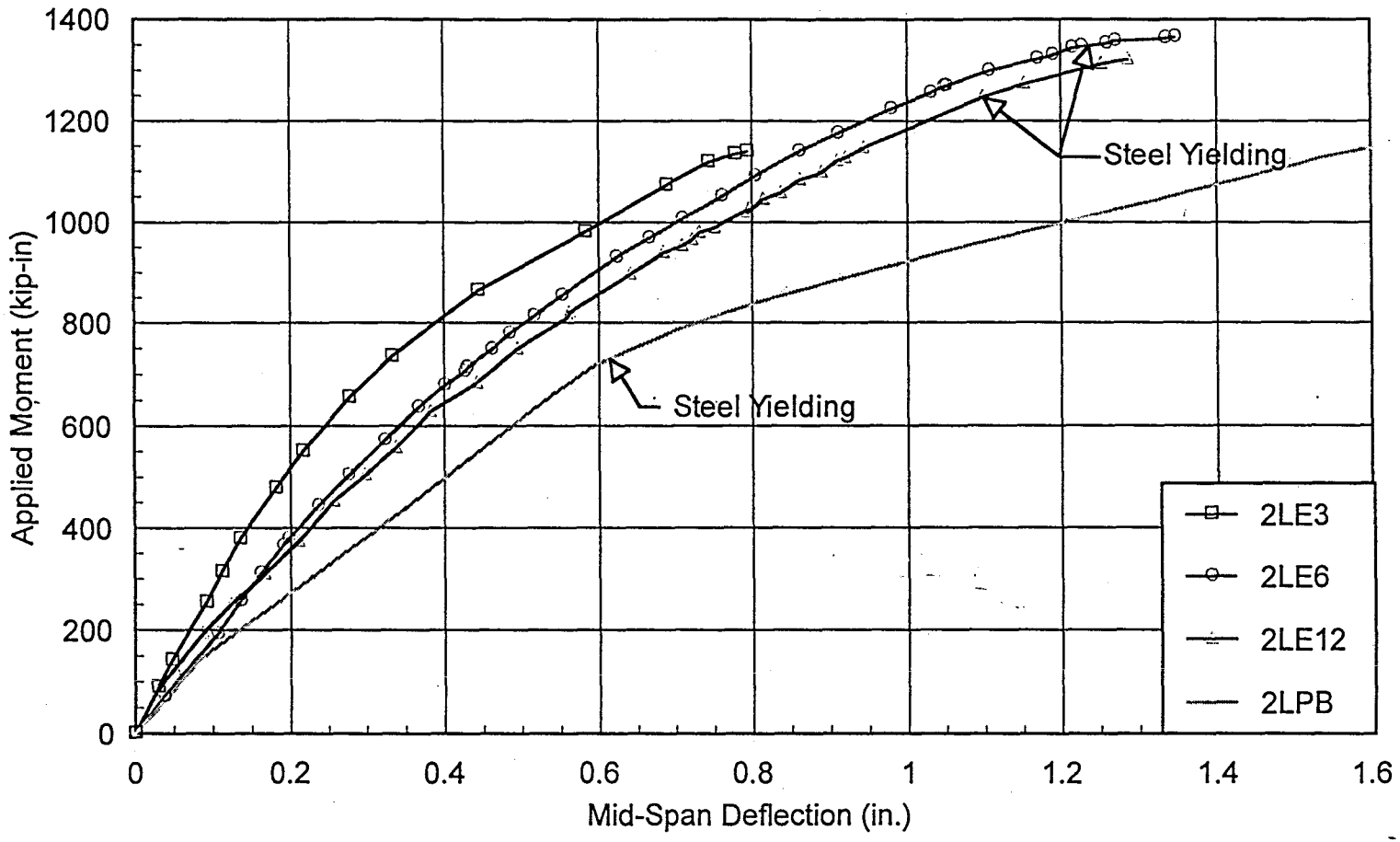

Fig. 6.3 Effect of Eccentricity on Moment-Deflection Curves of Wrapped Columns

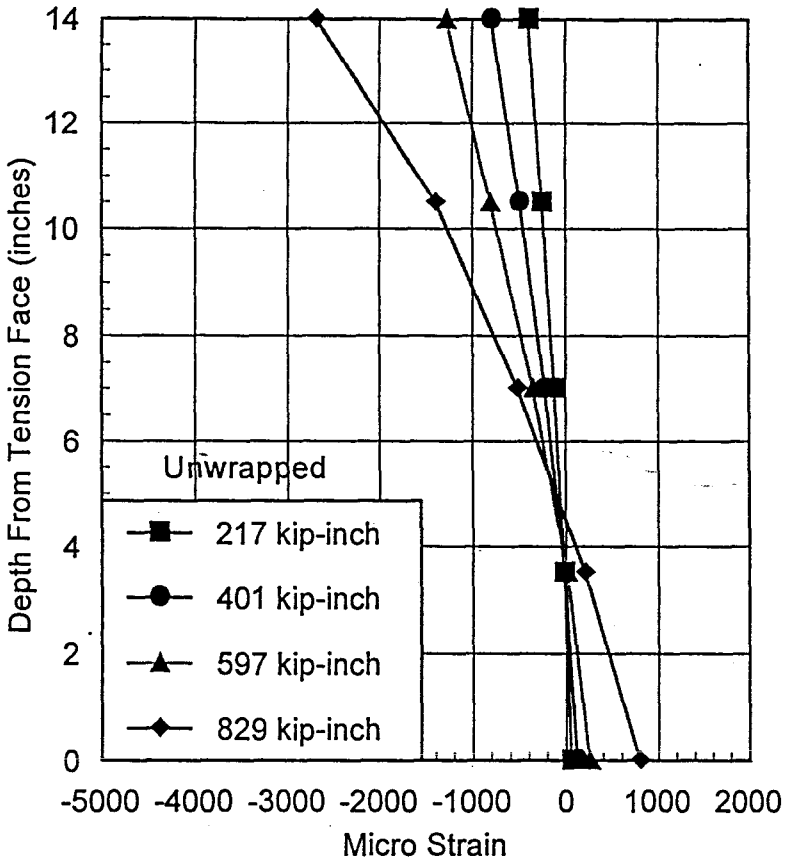

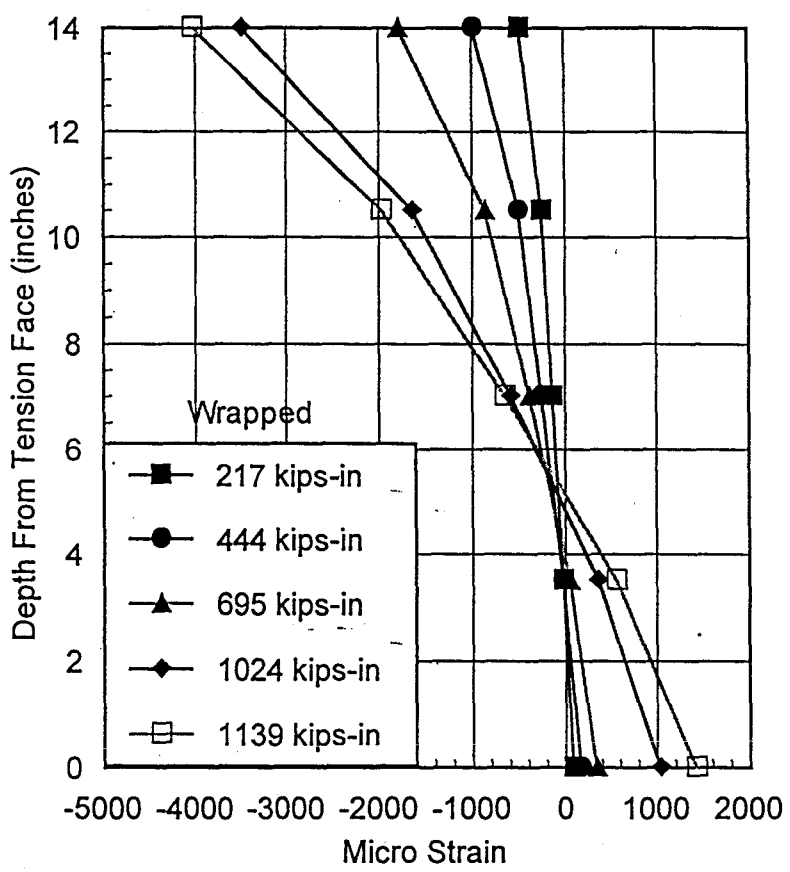

(a)

Fig. 6.4 Longitudinal Strain distribution at Mid-Span (a)
Eccentricity=3"

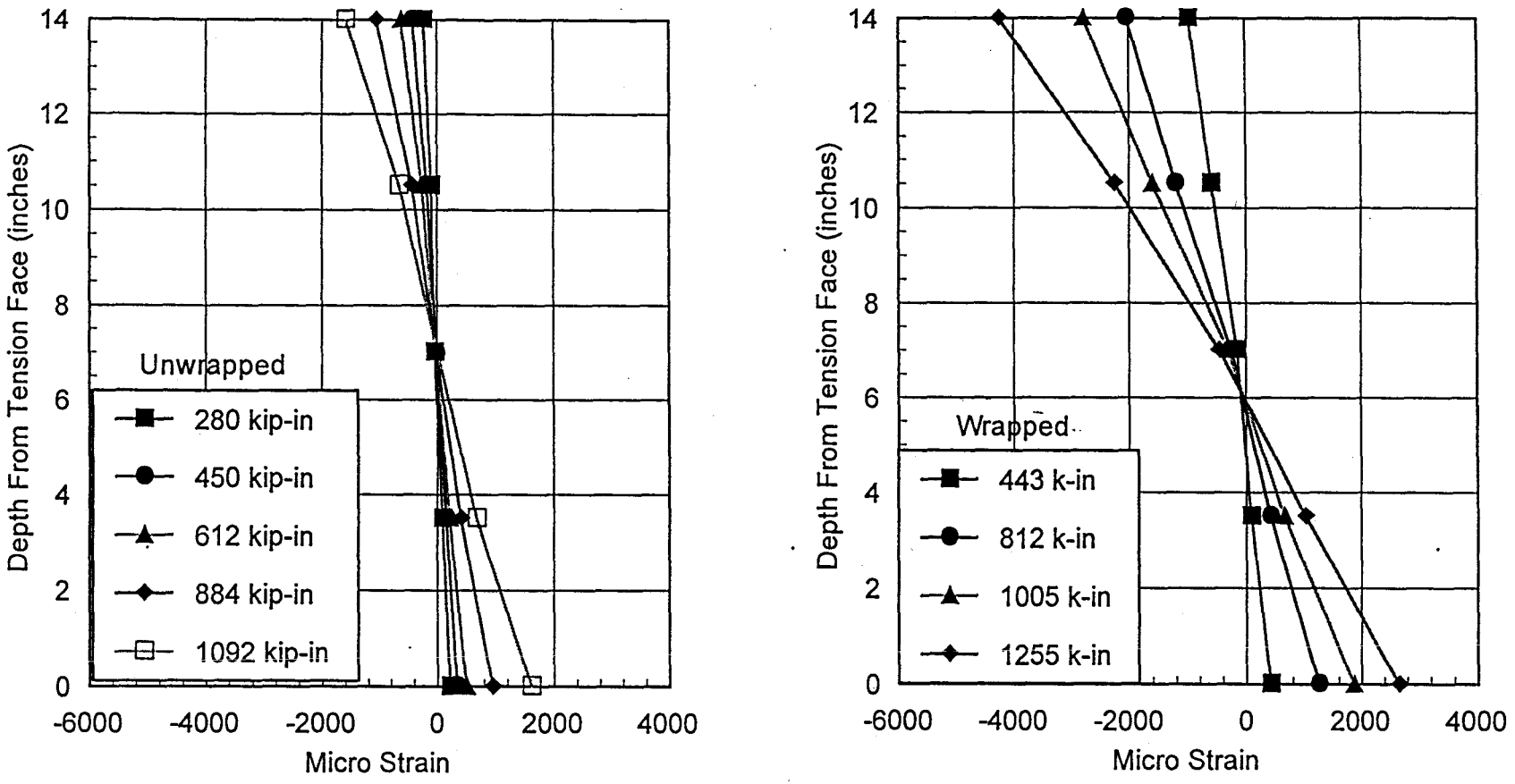

(b)

Fig. 6.4 Longitudinal Strain distribution at Mid-Span (b)
Eccentricity=6"

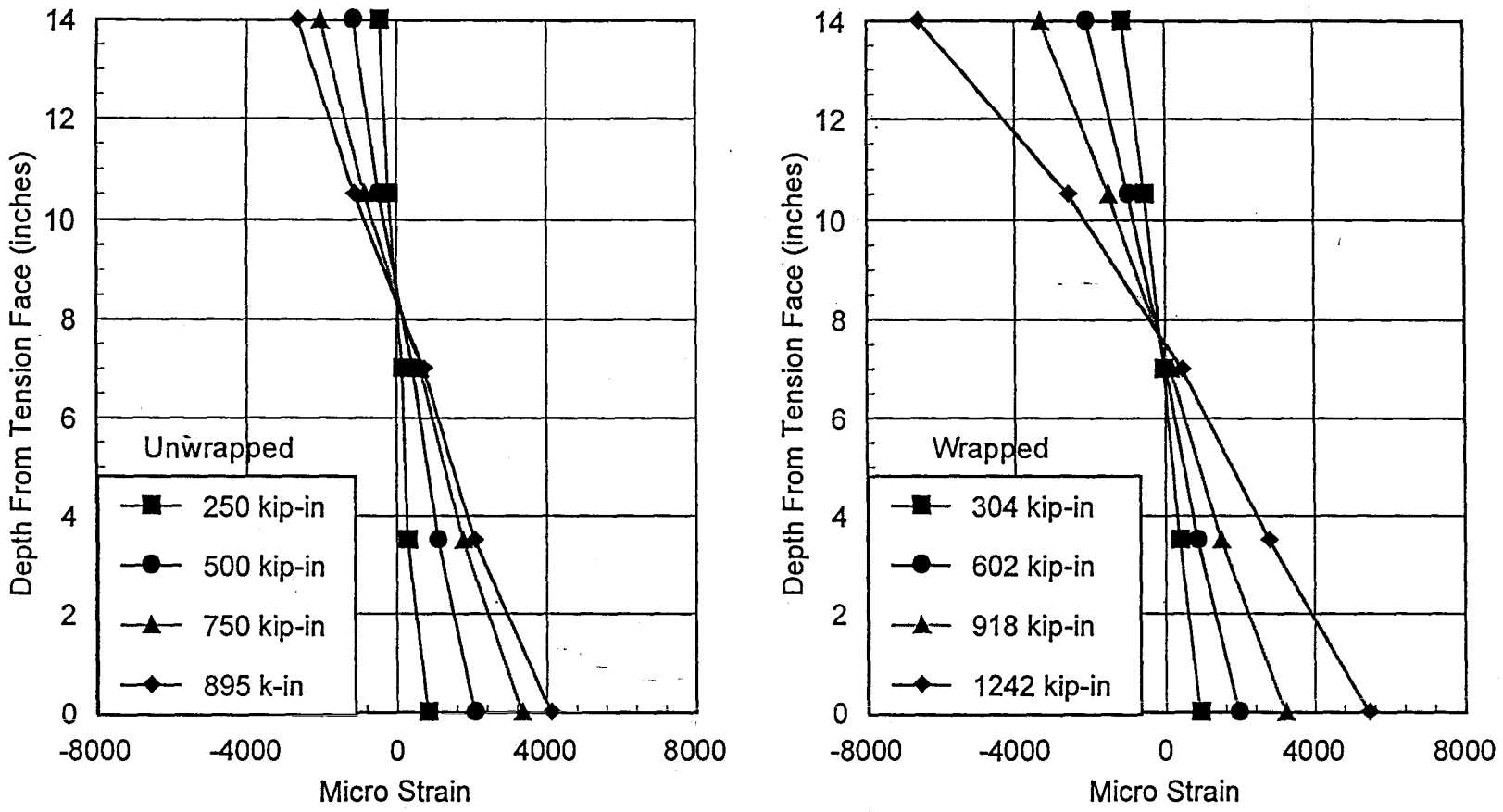

(c)

Fig. 6.4 Longitudinal Strain distribution at Mid-Span (c) Eccentricity=12"

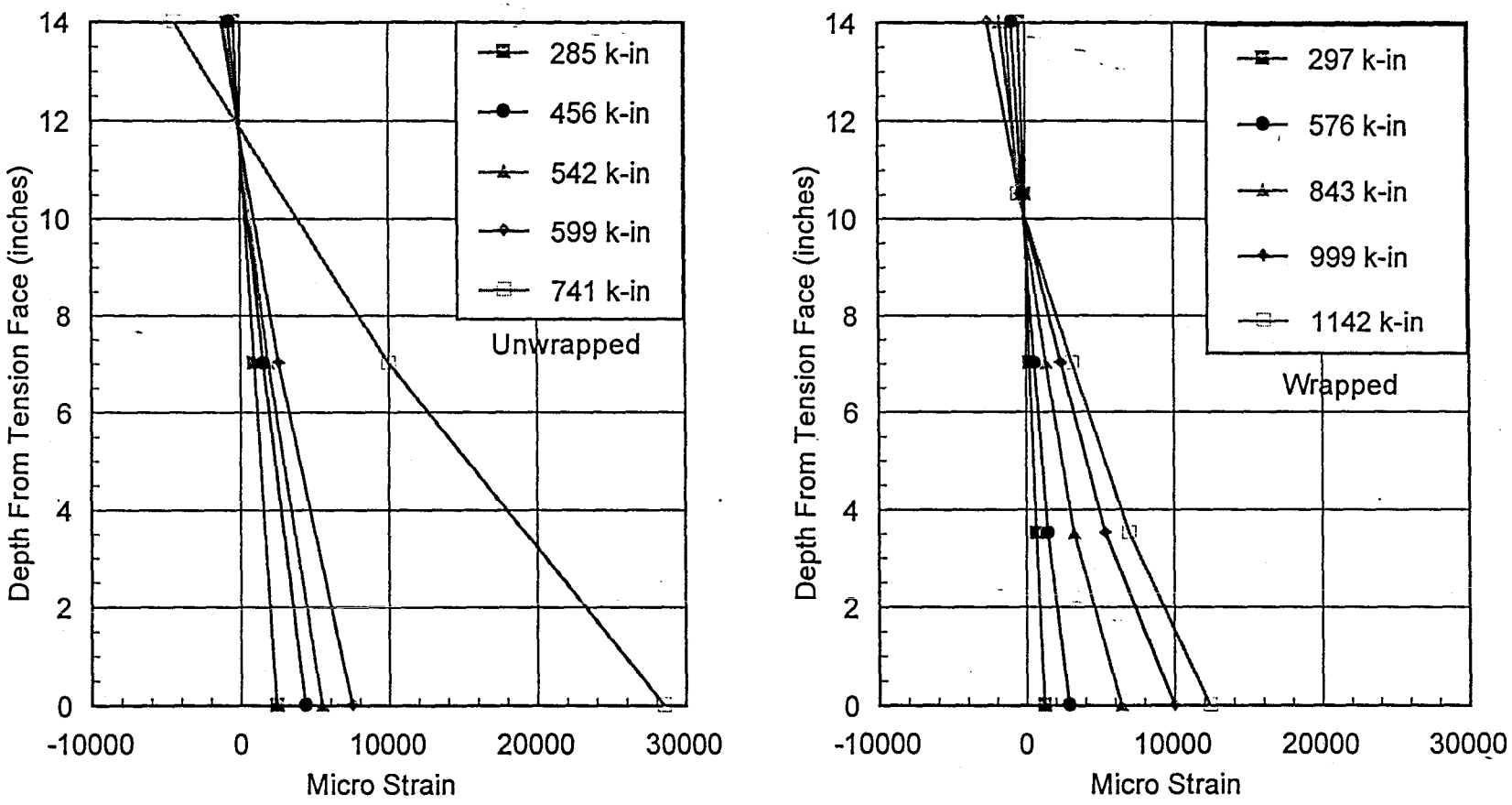

(d)

Fig. 6.4 Longitudinal Strain distribution at Mid-Span (d)
Pure Bending

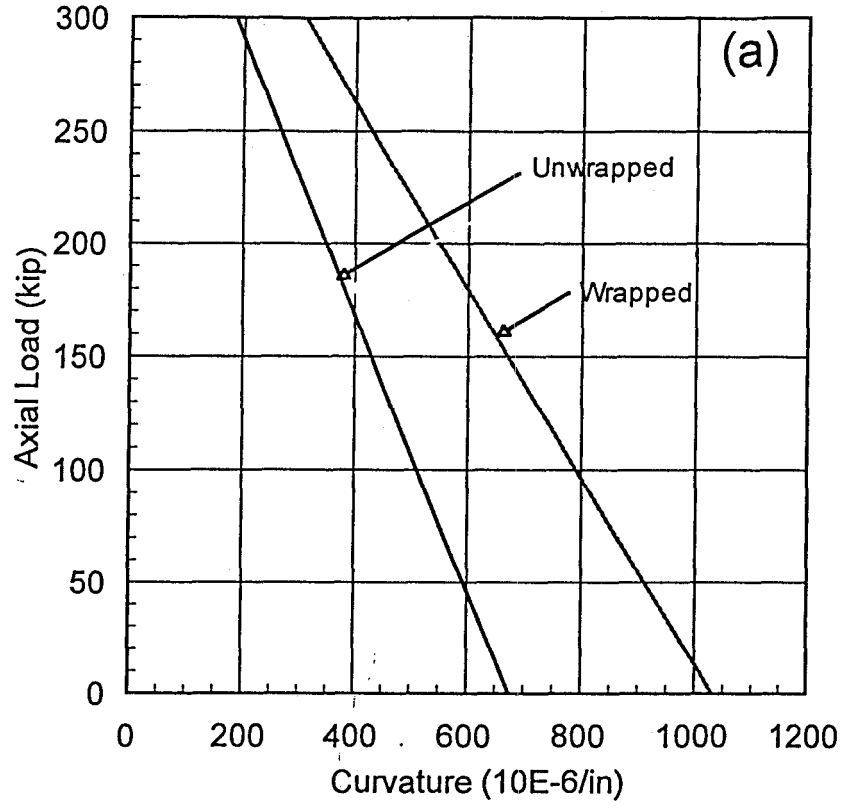

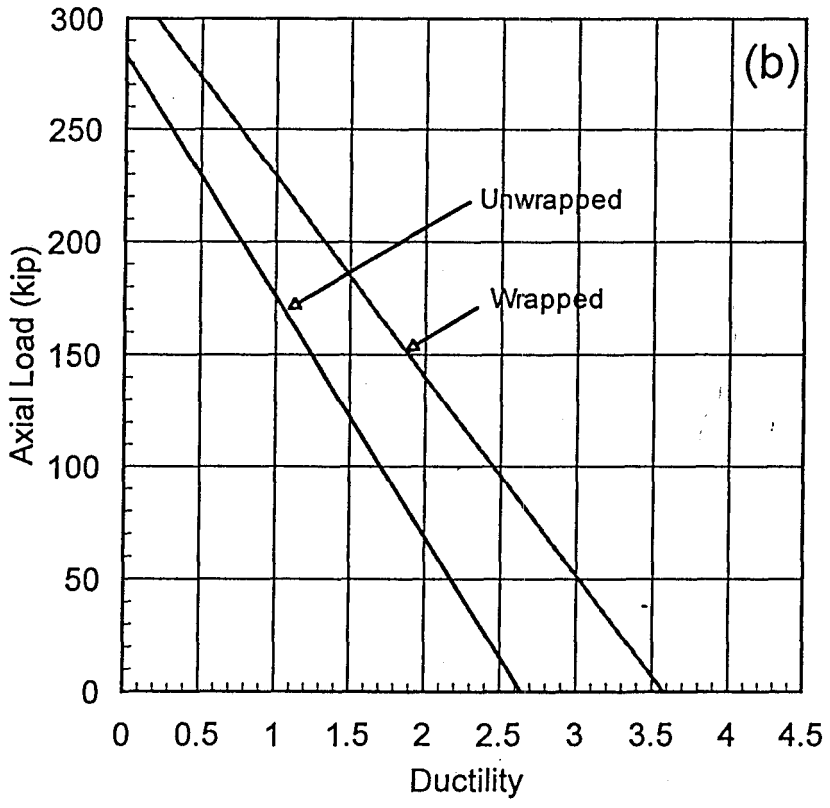

Fig. 6.5 Axial Load versus Curvature (a) and Ductility (b)

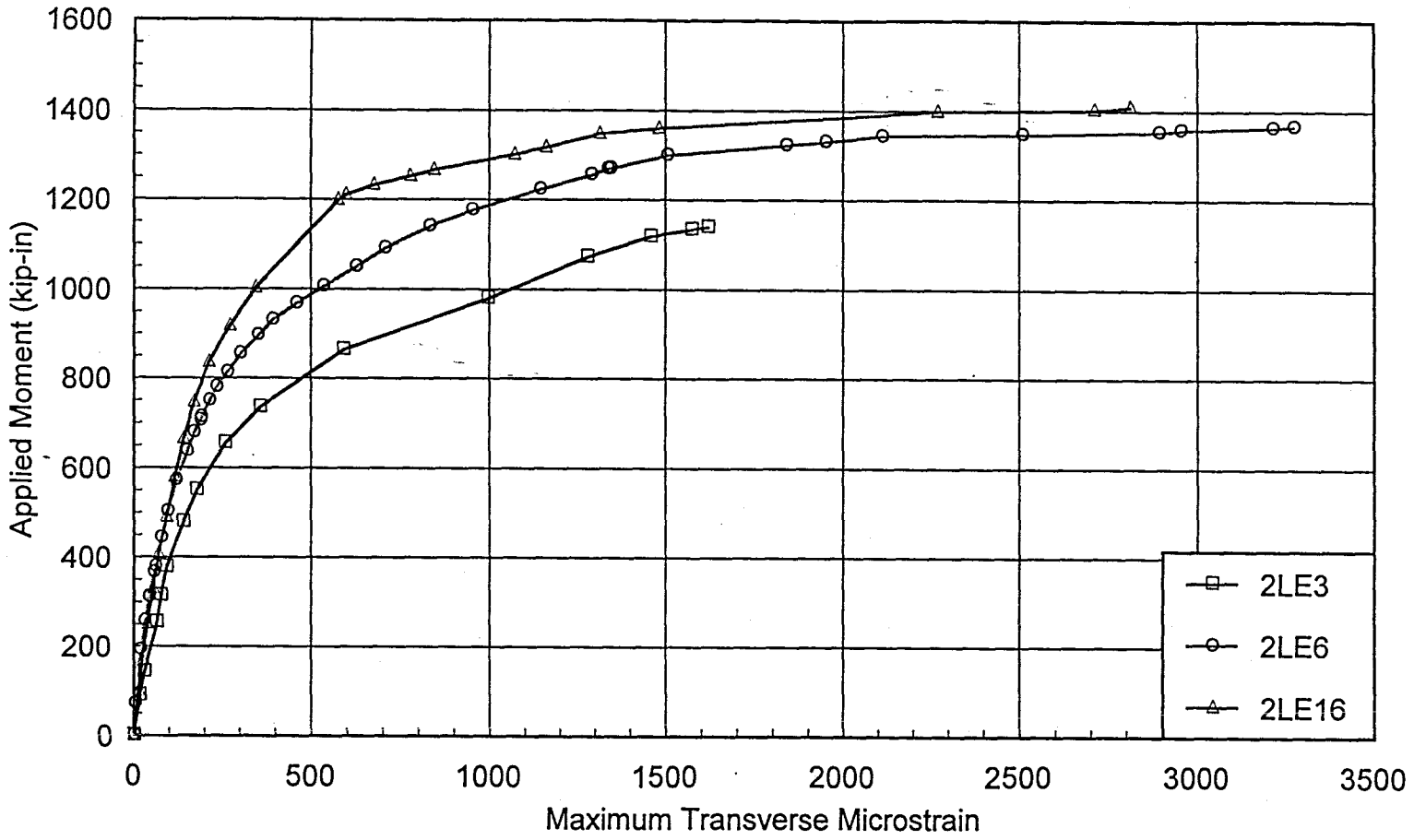

Fig. 6.6 Applied Moment versus Mid-Span Transverse Strain

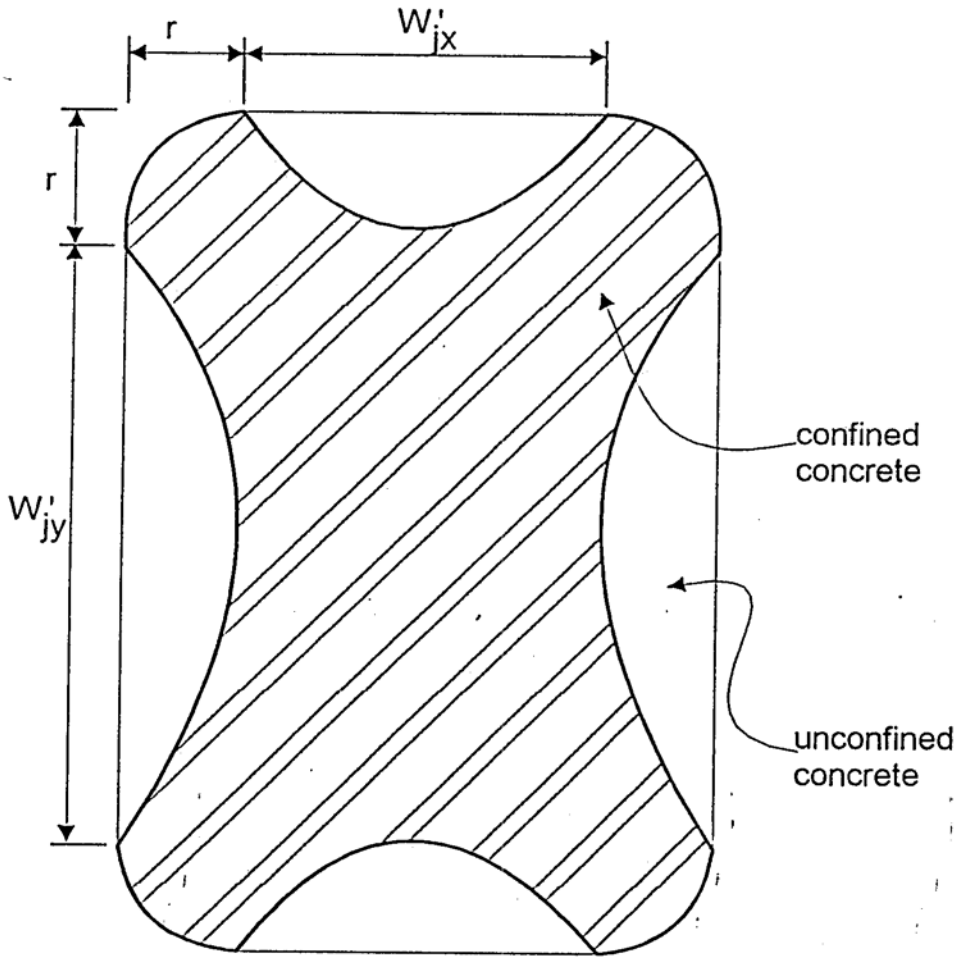

Fig. 7.1 Effective Wrap Confinement of a Rectangular Section

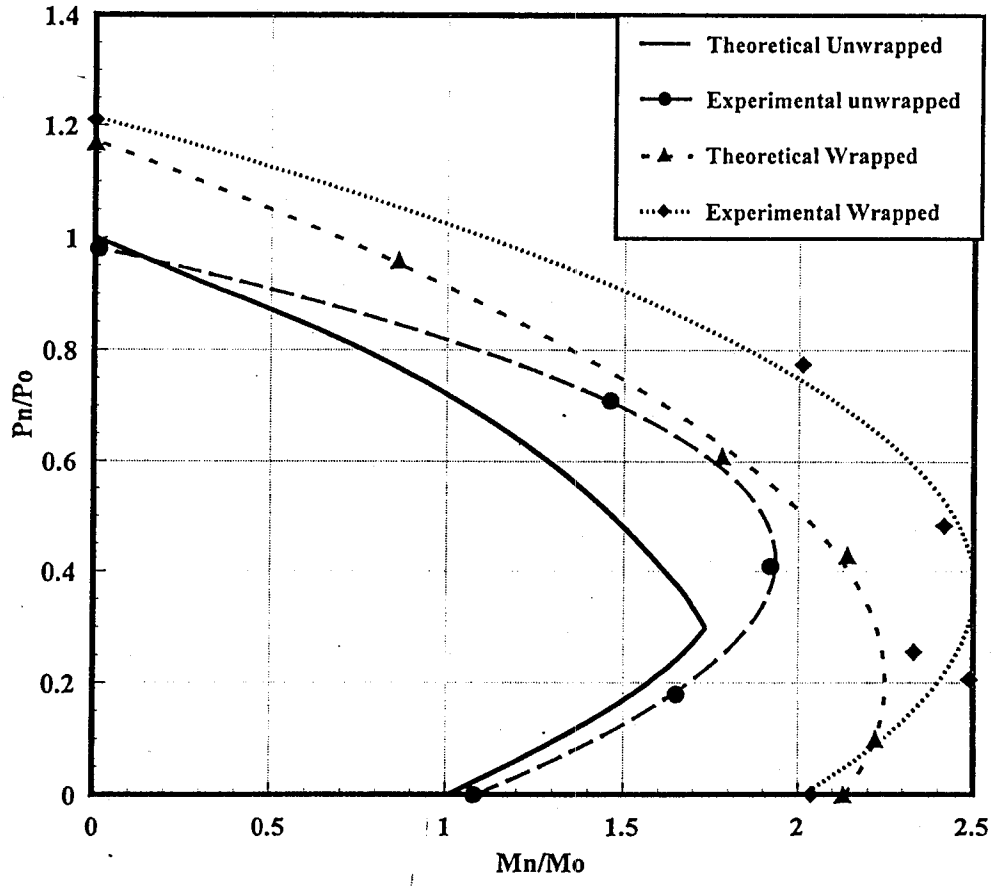

Fig. 7.2 Interaction Diagrams For Wrapped and Unwrapped Specimens